METAMORPHISM AND STRUCTURE OF THE CAMBRIAN-ORDOVICIAN SEDIMENTS IN SOUTHWEST NELSON DISTRICT

A thesis
submitted in partial fulfilment
of the requirements for the Degree
of
Master of Science in Geology
in the
University of Canterbury

by
S. W. Quek

University of Canterbury
1976

Frontispiece

I know a place, where no one ever goes,
There's peace and quiet, beauty and repose,
It's hidden in the valley, beside the mountain stream,
And lying there beside the stream, I find that I can dream,
Only of things of beauty to the eye,
Snow peaked mountains, tow'ring to the sky,
Now I know that there's a place in this world for me, for me .

- unknown author

OUTLINE OF CONTENTS

CHAPTER I

INTRODUCTION

I/1 LOCATION

I/2 PHYSIOGRAPHY

I/3 CLIMATE

I/4 FLORA AND FAUNA

I/5 ACCESS

I/6 PREVIOUS WORK

I/7 SCOPE OF PRESENT WORK

CHAPTER II

CHAPTER III

REGIONAL METAMORPHISM IN THE THOMPSON'S FLAT, SLUICE BOX, AND ALFRED FORMATIONS IN THE SPRINGS JUNCTION DISTRICT, WEST OF THE NEW ZEALAND ALPINE FAULT.

III/1 MAPPING OF METAMORPHIC ROCKS AND PROBLEMS ASSOCIATED WITH IT

III/2 LITHOLOGIES:

Pelite

Limestone

Marl

Sandstone

Quartzite

Volcanogenic sediment and conglomerate

Mafic intrusive

III/3 EFFECTS OF REGIONAL METAMORPHISM:

A. MINERALOGICAL CHANGES:

i) In pelite

ii) In limestone

iii) In marl

iv) In sandstone

v) In quartzite

vi) In volcanogenic sediment and conglomerate

vii) In mafic intrusive

B. TEXTURAL CHANGES:

i) In pelite

ii) Relationship of textural features to deformation in pelite

iii) In limestone

iv) In marl

v) In sandstone

vi) In quartzite

vii) In volcanogenic sediment and conglomerate

viii) In mafic intrusive

III/4 METAMORPHIC FACIES/GRADES - TEMPERATURE/PRESSURE OF METAMORPHISM:

A. STAUROLITE-ALMANDINE SURFACIES

B. QUARTZ-ALBITE-EPIDOTE-BIOTITE AND QUARTZ-ALBITE-EPIDOTE-ALMANDINE SURFACIES

C. QUARTZ-ALBITE-MUSCOVITE-CHLORITE SUBFACIES

D. CLASSIFICATION ACCORDING TO WINKLER 1974

III/5 EFFECTS OF RETROGRADE METAMORPHISM:

A. MINERALOGICAL CHANGES

B. TEXTURAL CHANGES

III/6 CORRELATION AND AGE OF REGIONAL METAMORPHISM

III/7 SUMMARY

CHAPTER IV

CONTACT OR THERMAL METAMORPHISM IN THE THOMPSON'S FLAT, SLUICE BOX, AND ALFRED FORMATIONS IN THE SPRINGS JUNCTION DISTRICT, WEST OF THE NEW ZEALAND ALPINE FAULT.

IV/1 MAPPING OF THE ROCKS AFFECTED BY CONTACT METAMORPHISM

IV/2 EFFECTS OF CONTACT METAMORPHISM:

A. MINERALOGICAL CHANGES:

i) In pelite of the Lower Brown Grey River

ii) In pelite, 2 km east of Thompson's Flat

iii) In sandstone, downstream from the Sluice Box bridge

B. TEXTURAL CHANGES:

i) In pelite of the Lower Brown Grey River

ii) In pelite, 2 km east of Thompson's Flat

iii) In sandstone, downstream from the Sluice Box bridge

IV/3 METAMORPHIC FACIES-TEMPERATURE/PRESSURE OF METAMORPHISM

IV/4 EFFECTS OF RETROGRADE METAMORPHISM:

A. MINERALOGICAL CHANGES

B. TEXTURAL CHANGES

IV/5 CORRELATION AND AGE OF CONTACT METAMORPHISM

IV/6 SUMMARY

CHAPTER V

FOLD STRUCTURES IN THE LOWER PALEOZOIC ROCKS BETWEEN THE ALPINE AND RAHU FAULTS

V/1 TERMINOLOGY

V/2 STRUCTURAL ELEMENTS:

- A. S0 STRUCTURE
- B. S1 STRUCTURES
- C. F2 MEGASCOPIC STRUCTURE
- D. F2 MESOSCOPIC STRUCTURES
- E. F2 AND S2 MICROSCOPIC STRUCTURES
- F. F3 AND S3 MICROSCOPIC STRUCTURES
- G. F4 AND S4 STRUCTURE
- H. RECONSTRUCTION OF THE F4 MEGASCOPIC STRUCTURE
- I. LINEATIONS

V/3 TIME RELATIONSHIP OF DEFORMATION AND REGIONAL METAMORPHISM

CHAPTER VI

THE KOURA AND RAHU FAULT ZONES

CHAPTER VII

METAMORPHISM IN THE ROCKS OF THE KOURA FORMATION

VII/1 LITHOLOGIES:

A. HORNBLENDE-BIOTITE ANDESITE

B. VOLCANOGENIC CONGLOMERATE

C. TURRACEOUS SEDIMENTS

VII/2 EFFECTS OF METAMORPHISM

A. MINERALOGICAL CHANGES:

i) In andesite

ii) In conglomerate

iii) In tuffaceous sediments

B. TEXTURAL CHANGES

i) In andesite

ii) In conglomerate

iii) In tuffaceous sediments

VII/3 METAMORPHIC FACIES/GRADES - TEMPERATURE/PRESSURE OF METAMORPHISM

VII/4 CORRELATION AND AGE OF METAMORPHISM

VII/5 SUMMARY

CHAPTER VIII

RE-APPRAISAL OF THE LOWER PALEOZOIC SEQUENCE IN SPRINGS JUNCTION DISTRICT

CHAPTER IX

CONTACT METAMORPHISM IN THE SEDIMENTS, WEST OF THE RAHU FAULT.

IX /1 MAPPING OF THE ROCKS AFFECTED BY CONTACT METAMORPHISM AND THE PROBLEMS ASSOCIATED WITH IT

IX /2 LITHOLOGIES
SEDIMENTARY STRUCTURES
DISTRIBUTION OF LITHOLOGIES

IX /3 EFFECTS OF CONTACT METAMORPHISM:

- A. MINERALOGICAL CHANGES IN SANDSTONE
- B. MINERALOGICAL CHANGES IN MUDSTONE
- C. TEXTURAL CHANGES IN SANDSTONE
- D. TEXTURAL CHANGES IN MUDSTONE

IX /4 METAMORPHIC FACIES - TEMPERATURE/PRESSURE OF METAMORPHISM:

- A. ALBITE-EPIDOTE-HORNFELS FACIES
- B. HORNBLENDE-HORNFELS FACIES

IX/5 EFFECTS OF RETROGRADE METAMORPHISM:

- A. MINERALOGICAL CHANGES IN THE SANDSTONE HORNFELS

CHAPTER X

DEFORMATION STRUCTURES IN THE VICTORIA RANGE META-SEDIMENTS

X/1 TERMINOLOGY

X/2 STEREO-ANALYSIS

X/3 STRUCTURAL ELEMENTS:

- A. S0 STRUCTURES
- B. S1 STRUCTURES
- C. S2 AND F2 STRUCTURES
- D. S3 AND F3 STRUCTURES
- E. S2 AND F2 MICROSCOPIC STRUCTURES
- F. LINEATIONS
- G. PLANAR STRUCTURE GENERATED BY LOCAL INTRUSIVE BODIES IN THE META-SEDIMENTS
- H. DEFORMATION OF S1 BY THE INTRUSIVES

X/4 THE PROBABLE CAUSES OF S1, S2, F2, S3, AND F3 STRUCTURES AND CORRELATIONS

CHAPTER XI

TERTIARY SEDIMENTS

XI/ INTRODUCTION

XI/2 LITHOLOGIES

XI/3 FAUNAS

XI/4 AGE AND CORRELATION

XI/5 INFERRED PALEO-ENVIRONMENT

CHAPTER XII

MESOZOIC SEDIMENTS

CHAPTER XIII

SUMMARY OF CONCLUSIONS OF THE GEOLOGICAL HISTORY PRESENTED IN CHRONOLOGICAL ORDER

ACKNOWLEDGEMENTS

APPENDIX 1

APPENDIX 2

REFERENCES

LIST OF FIGURES

PAGE

LIST OF TABLES

ABSTRACT

The geology of the Victoria Range and the Maruia-Upper Grey depression in Springs Junction district has been examined with particular emphasis on metamorphisms and structures.

The 'Z?' sediments in the Victoria Range are correlated with the Aorere Group of NW Nelson on the basis of their consistency with Cooper's (1975) Lower Paleozoic sedimentary model, and Shelley's (1975) paired metamorphic belt model. These sediments have been deformed and metamorphosed twice; the first regional metamorphism is considered to be related to an Upper Ordovician Orogeny, and the second metamorphism is thought to be associated with the Tuhua Orogeny. The latter metamorphism was at temperatures ranging from 400° to 550° C, and pressures not exceeding 2 to 3 kb.

The volcanics and volcanogenic sediments of the Koura Formation are correlated with the Haupiri Group of NW Nelson also on the basis of their consistency with Cooper's (1975) sedimentary and Shelley's (1975) paired metamorphic belt models. These rocks have been metamorphosed under P-T conditions of 350° to 450° C, and moderate to high pressure. This metamorphism is considered to be related to the Upper Ordovician Orogeny.

The Lower Paleozoic (Cambrian? - Upper Ordovician) deposits in the Maruia-Upper Grey depression are correlated with the Mt. Arthur Group of NW Nelson. These rocks were regionally metamorphosed during the Tuhua

Orogeny under conditions of 350° to 640° C, and not less than 4 to 6 kb. The deformation accompanying this metamorphism has generated three orders of folds; a) a NE-trending, gently plunging, and inclined major anticline, b) mesoscopic folds whose attitudes are similar to that of the major anticline, and c) microscopic crenulations whose axial planes are oriented parallel to the axial plane of the major anticline. The Koura Volcanics, the Victoria Range rocks, and the Lower Paleozoic sediments of the Maruia-Upper Grey depression were juxtaposed by movement(s) of the Koura Fault- a proposed Tuhuan major structure which coincided with the Tuhuan median boundary.

The Lower Paleozoic rocks of the Maruia-Upper Grey Valley were again metamorphosed during the Rangitata Orogeny. The thermal metamorphism at 500° to 580° C, and 1.5 to 2.5 kb was accompanied by an episode of deformation which resulted in the microscopic folding of one limb of the microscopic crenulations produced during the Tuhua Orogeny. The Rangitatan event was closely followed by dextral movement(s) along the Koura Fracture System which resulted in the folding about a vertical axis of the Victoria Range meta-sediments and the Lower Paleozoic sequence bordering the major fracture. The deformed Victoria Range rocks were subsequently refolded about a gently plunging or horizontal axis.

The formation of the Rahu Fault and sinistral movement(s) along this major structure during or subsequent to the Rangitata Orogeny has displaced the Mesozoic rocks in the Brown Grey Valley.

The Lower Paleozoic sediments in the Maruia-Upper Grey depression were refolded about a gently plunging, N-S trending axis during the Kaikoura Orogeny. In addition, renewed activities of the Rahu Fault have displaced the Lower (?) Tertiary rocks west of Springs Junction.

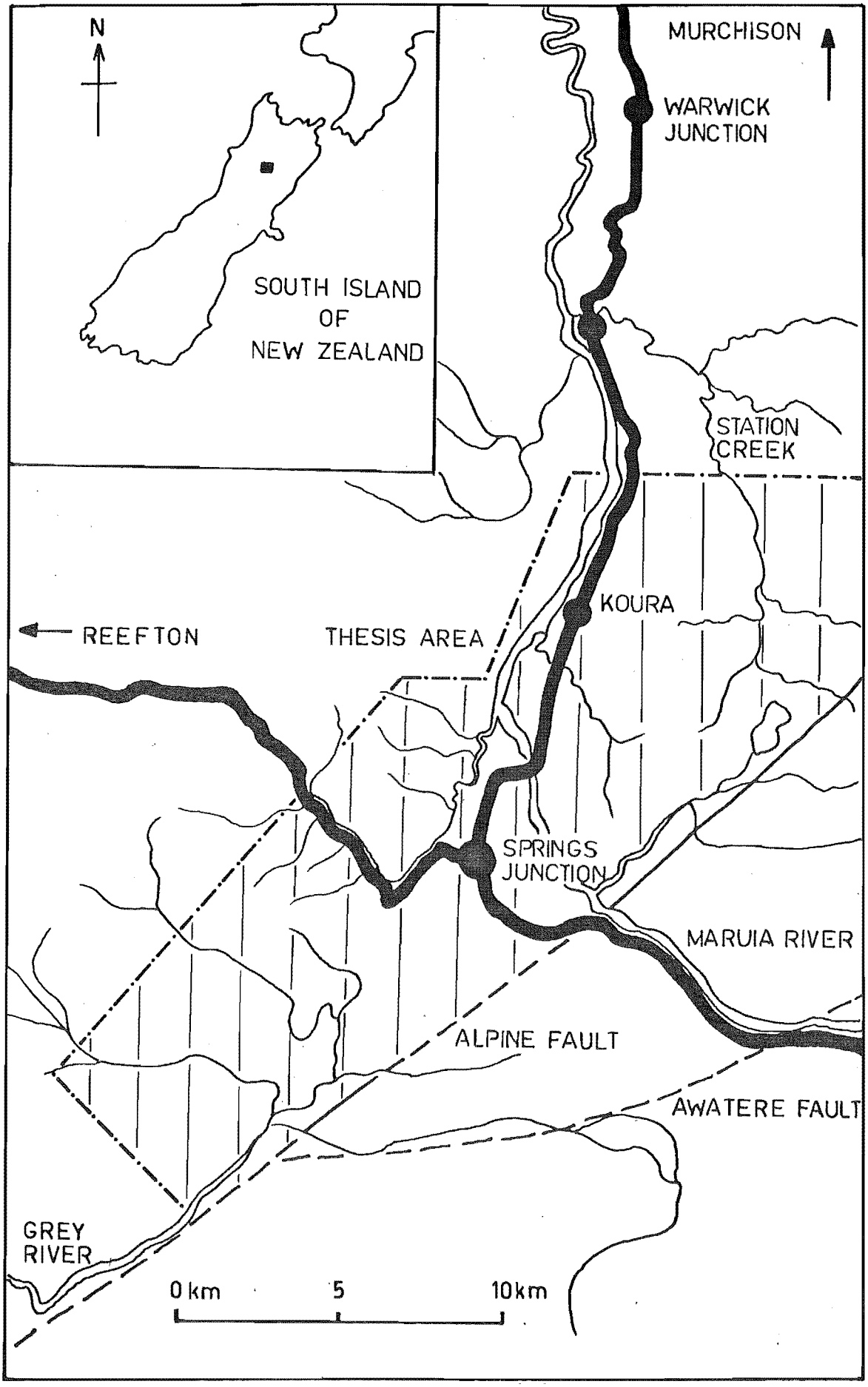

FIG. 1 Location diagram showing the geographic position and size of thesis area .

CHAPTER I

INTRODUCTION

I/1 LOCATION

The area chosen for study is 225 km from Christchurch by way of the Lewis Pass highway. It consists of two parts; 1) the wedge-shaped area bounded by the Rahu and Alpine Faults extending from the vicinity of Palmer's Flat to Trig. GA, and 2) the eastern slope of the Victoria Range between Ellis Creek and the unnamed stream west south-west of Koura. The former is nearly 130 sq. km, and the latter is approximately 80 sq. km. The location diagram in Fig. (1) gives a rough outline of the thesis area.

I/2 PHYSIOGRAPHY

The eastern slope of the Victoria Range is characterised by a steep front. The area is rugged, densely bushed, and dissected by four major streams; the Ellis Creek, the May Creek, the Brown Grey River, and the Rahu River. All these streams flow eastwards into the Upper Grey-Maruia Valley. Many short steeply graded creeks join the four main drainage channels, giving rise to trellise drainage patterns in this part of the thesis area.

The open elongate depression between the eastern slope of the Victoria Range, and the western slopes of the Main Divide and Freyberg Range is less rugged and

densely bushed. The Upper Grey River drains southwards and is separated from the northwards flowing Maruia River by the Bog Saddle. In the vicinity of Lake Daniells, the country is densely bushed, and generally mountainous.

The occurence of cirques, U-shaped valleys, truncated spurs, glacial lakes, lateral moraine in the thesis area indicates that Pleistocene glaciation was extensive in this part of the South Island of New Zealand.

I/3 CLIMATE

The thesis area is doubly sheltered from the north-westerly rain bearing wind by the Paparoa Range, and the Victoria-Brunner mountains. In spite of this, the annual rainfall remains high - averaging nearly 2,000 mm per year. Because of the high annual rainfall, humidity is high through out the year except during the dry season from February to March. Snow on tussock-clad ridges, and heavy frosts (up to -15° C) in the valleys occur during June or later. The true winter snow line is at about 1,200 m. However, there are periods when the snow line descends to as low as 700 m. Like rain, snow is brought to the thesis area by southerly winds.

I/4 FLORA AND FAUNA

The vegetation predominantly consists of Red and Silver beech up to an altitude of 1,200 m. Above this height, the beech forests give way rapidly to sub-alpine

woody scrubs and herbs e. g. mountain daisies and flax, speargrass, snowgrass, etc. At lower altitudes, moss and shrubs occupy the forest floors and bogs. In the Grey and Maruia Valleys, much of the bush has been cleared for agriculture.

Native birds are the main inhabitants of the beech forests. At least five species have been observed. South Island Robin, Wood Pigeons, and Fantails are very common. Tuis, Rifleman, wild ducks, and Blue Ducks are also present, but rarely seen. Paradise ducks and keas are known to frequent the major river flats. Red deer, Chamois, and less commonly, wild pigs have been observed on higher altitude river flats. The beech forest on the Rahu Saddle is occupied by a large population of opossums.

I/5 ACCESS

The Lewis Pass - Reefton highway, Palmers road, and the Springs Junction - Murchison highway form a 'cross-shaped' network of roads in the thesis area. This has allowed easy access to the main rivers and streams which contain the majority of outcrops in the thesis area. Exposures on ridges and peaks are reached by following known tracks or routes 'pioneered' by the writer.

I/6 PREVIOUS WORK

The earliest visit by a geologist to the Upper Maruia Valley was that made by Julius Haast in 1860.

He reported that the Victoria Range is composed of granites, pegmatites, hornblendic granites, and gneissic-granites, and is separated from the Main Divide and Freyberg Range whose rocks are schists and slates by the Maruia plains and Upper Grey River Valley. Haast also mentioned some glacial features in his 1860 field report.

S. H. Cox - another geologist explored the Upper Maruia country for a short period in 1883. He confirmed Haast's report on the Victoria Range Granites and suggested that the Lake Daniells Granites are members of that major intrusive. In addition, Cox introduced three formations which he briefly described as 1) Metamorphic crystalline rocks, 2) Lower Devonian or Upper Silurian crystalline limestone, slate, and schist, and 3) Lower Carboniferous slates and sandstones of the Matai Series.

A. Mackay made a geological study on the rocks in the vicinity of Lake Cristable, and the Upper Grey Valley in 1895. Like the previous geologists, he noted the schist terrain on the east, and granite mountains on the west. He also reported that the sandstones and slates at the source of the Maruia River are Carboniferous, and continuous with the present Alpine schists, and the Springs Junction Lower Paleozoic sediments. In addition he assigned a Cretaceous age to the conglomerates and sandstones in Station Creek.

Between 1928 and 1929, H. E. Fyfe mapped the Maruia district in preparation for a Geological Survey Bulletin. He concentrated his effort on mapping the sediments and structures in the area between the Rahu and Alpine

Faults. The limestone, slate, and schist were correlated with the Mt. Arthur Series of NW Nelson. He also briefly mentioned the presence of hornfels, schists, phyllites, and injection gneiss in the vicinity of the Rahu Saddle. He considered the meta-sediments in the Victoria Range to be the equivalent of the Aorere Series, and that they were intruded and metamorphosed by the Victoria Range Granites. Fyfe pointed out that the Victoria Range Granites and the Rotorua igneous rocks are unrelated 'formations'.

The next major study of the rocks between the Rahu and Alpine Faults was that conducted by R. T. Farmer in 1967. He reported that the Ordovician sediments were folded into a major NE-trending anticline which was refolded some time during the Permian period. The lithologies and their inferred depositional environment are mentioned in his unpublished thesis (1967- lodged with Canterbury University). Farmer suggested that the Lake Daniells Granite is a sliver of fault-emplaced Victoria Range Granite and that the meta-sediments west of the Rahu Fault are possibly continuous with the Ordovician sediments in the Upper Grey-Maruia depression.

Besides the studies carried out by the five geologists mentioned above, minor investigations have also been conducted by other workers. The following briefly accounts for the studies of these people.

H. W. Wellman (1941, 1942) - examination and chemical analyses of the talc-magnesite bodies in Springs Junction district.

H. W. Wellman (1948) - discovery of fossils in the Sluice Box Formation (crinoid stem).

H. W. Wellman (1952) - investigation of the Alpine Fault near Springs Junction.

R. P. Suggate and F. E. Bowen (1952) - casual examination of the rocks along the Lower Brown Grey River. They reported the presence of hornfels, quartzites, granites, and less metamorphosed greywackes.

R. P. Suggate, F. E. Bowen, B. D. Webby, and E. T. Annear (1959) - examination of the rocks along May Creek, Ellis Creek, parts of the Rahu River, and the ridge east of Pinnacle Peak. They reported the presence of weakly schistose meta-sediments, pegmatites, biotite granites, porphyritic granites, and gneisses. Their unpublished field map shows that the Victoria Range meta-sediments form an 'enclave' with interfingering boundaries at the northern and southern end of the structure. The fault contact between the meta-sediments and the granites previously shown in Fyfe's (1928-1929) map has been deleted.

R. P. Suggate (1965) - study and mapping of the late Pleistocene rocks. He recorded the presence of lateral moraines, glacial terraces, outwash deposits, moraine loops, and a pre-existing glacial lake.

R. P. Suggate and N. T. Moar (1960-1966) - pollen analyses and radiocarbon dating of the material from the bog at the junction of Upper Grey and Crooked Mary Rivers.

R. P. Suggate, H. S. Gair, and D. R. Gregg (1961) - mapping of the Awatere and Alpine Faults; the latter was shown separating the Alpine garnet schist from the Ordovician sediments.

H. W. Wellman (1962) - discovery of graptolites in the Ordovician sediments near the Alfred River.

J. J. Reed (1964) - description of the effects of movements along the Alpine Fault on the rocks near Pell Stream, Alfred River, and on Palmer's road 0.5 ml north of Clear Grey River.

F. E. Bowen (1964) - extension of Fyfe's (1928-1929) mapping, and interpretation of the major structure as a NE-trending anticline. His map (Buller - Sheet 15) shows the Victoria Range meta-sediments as a gigantic 'enclave' in the Tuhuan Granites.

M. G. Laird (1964) - examination of the major fault along the Rahu River previously mapped by Fyfe (1928-1929). He concluded that the structure is a 0.5 km wide fault zone. He also reported no evidence of a fault contact between the meta-sediments and granites on the Rahu Saddle that was formerly mentioned by Fyfe.

J. L. Aronson (1966) - radiometric studies on the Rahu Adamellites. He concluded that they have been metamorphosed about 110 m. y. ago or afterwards.

S. Nathan and J. Foster (1968) - examination of the rocks along the Springs Junction - Reefton highway, 6 km west of the thesis area. They recognised the Waiuta Group meta-sediments, and a variety of intrusive rocks.

I/7 SCOPE OF PRESENT WORK

This project has three objectives.

1) To study the effects of metamorphisms and deve-

lopment of structures in the rocks previously mapped by Bowen (1964) as 'Z?' on the eastern slope of the Victoria Range west of Springs Junction. In addition, the writer hoped to improve the formation boundaries seen in the present 4 mile series map (NZGS 1:250,000 - Buller Sheet 15), and to establish more positively the correlation for the Victoria Range meta-sediments.

2) To study the effects of regional and thermal metamorphisms, and development of structures in the rocks mapped by Farmer (1967) as the Thompson's Flat, Sluice Box, Alfred, and Koura Formations.

3) To investigate and record any new geological formations and features not previously recognised or mapped by geologists.

Field work was carried out during the winter and summer of 1974 and 1975. Laboratory work involved examination of thin sections from both the writer's and Farmer's collection, identification of Tertiary Foraminifera, chemical analyses of garnets using the microprobe analyser, atomic absorption analyser, and X-Ray Fluorescence equipment, and identification of minerals using the X-Ray diffraction equipment.

CHAPTER II

GARNETS

II/1 INTRODUCTION AND DESCRIPTION

Garnets constitute about 5% of the schist of the Thompson's Flat Formation. They range in size from 0.5 to 6.0 mm, and are usually euhedral, always in the form of a rhombdodecahedron combining with a trapezohedron (Fig. 3). Some crystals are less well developed and occur as anhedral porphyroblasts, these garnets being restricted to quartzitic beds (Fig. 4).

Optical examination shows that all the garnets are zoned. A large core containing quartz and opaque inclusions is surrounded by a narrow rim of relatively clear garnet. Many such porphyroblasts are coated with a veneer of dusty material, usually consisting of carbonaceous matter and fine-grained opaques. In Fig. (5) , garnets show evidence of being deformed after crystallization, displaying strain features like fractures and pressure shadows. In addition to such strain effects, the crystals at locality B6 also display a texture suggesting that the growth of rim garnet (late syntectonic) was stress controlled (Fig. 6).

II/2 SPECIAL TEXTURE

The garnet contains a set of discontinuous internal S-surfaces which are composed of elongated quartz, rutile,

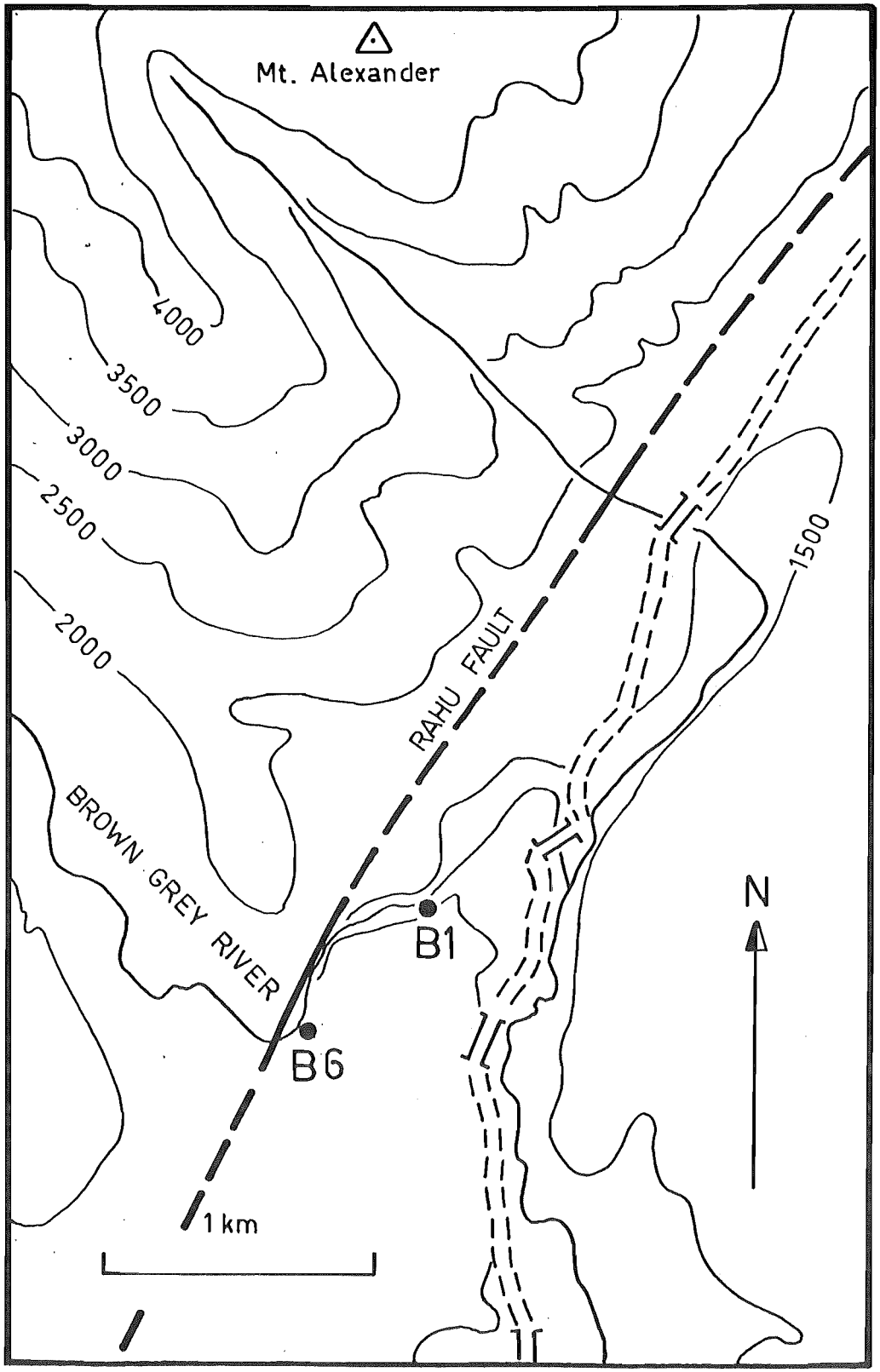

FIG. 2 Map showing localities B1 and B6 mentioned in this chapter . The specimen number of schist sample collected at B1 and B6 is UC 7651a and UC 7654 respectively .

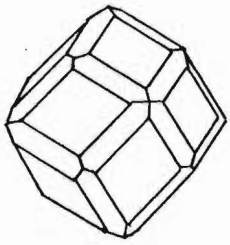

FIG. 3 Diagram illustrating the shape of almandine i.e. rhombdodecahedron combining with trapezohedron .

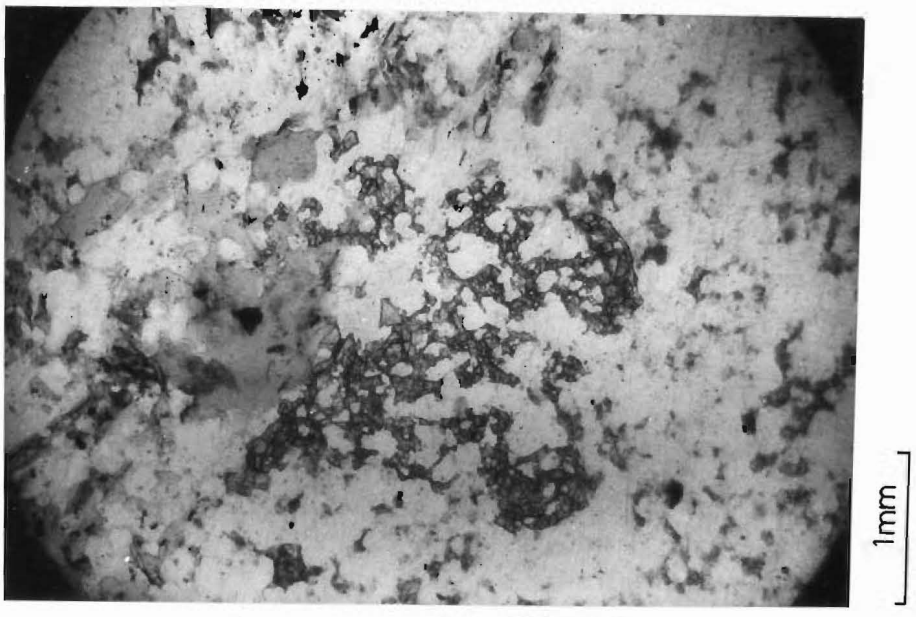

S46 563964

FIG. 4 The high relief mineral in the centre of the photograph is a crystal of anhedral almandine .

pyrite, and possibly ilmenite grains (Fig. 5). The surfaces are slightly curved at the edge of the crystal and are usually continuous with the crenulated schistosity outside the garnet (Fig. 6). In Fig. (7), the axial planes of the crenulated schistosity are deformed around the porphyroblasts generating pressure shadows which are subsequently filled by coarser-grained quartz and biotite. These secondary minerals show no signs of being deformed and their boundaries with the rim garnets are straight and distinct (Fig. 5). The described garnet texture and the relation between garnets and secondary minerals strongly suggest that the porphyroblasts are the result of syntectonic crystallization.

II/3 REFRACTIVE INDEX AND CELL PARAMETER

The R. I. (n) of garnets determined by the immersion method at room temperature is approximately 1.8. Microscope examination shows that there are no sharp changes in refractive index from centre to edge.

The cell parameter values calculated from X-ray diffraction analyses of garnets are around 11.554 Å (Table 1). Two methods of cell parameter calculations were used. The first method involves solving a_o from the formula:

$$d_{h\,k\,l} = \frac{a_o}{(h^2 + k^2 + l^2)}$$ (Jenkins & de Vries 1970)

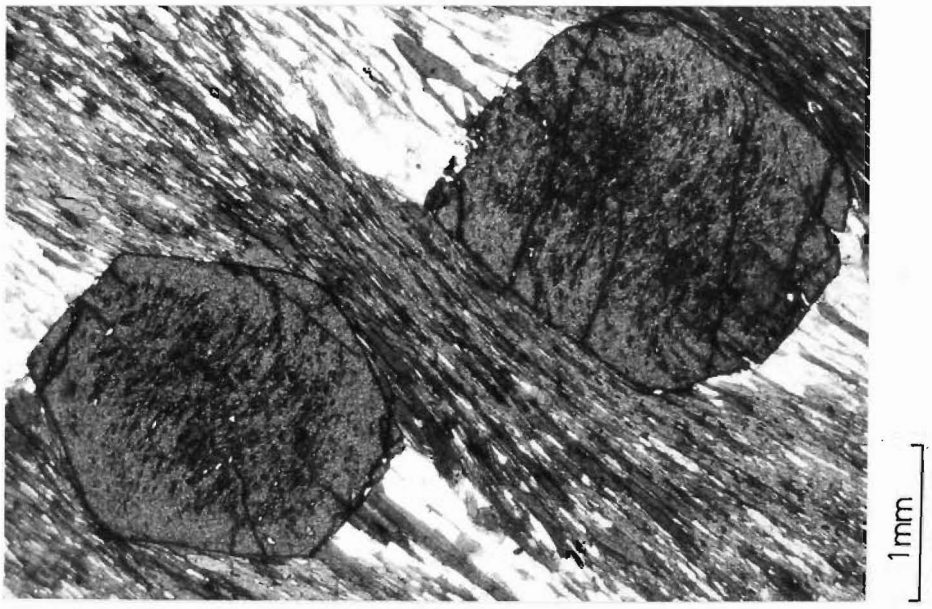

S46 563964

FIG. 5 Garnets displaying strain features - pressure shadows and fractures . Note that the dominant fracture planes are oriented perpendicular to the schistosity (S1) .

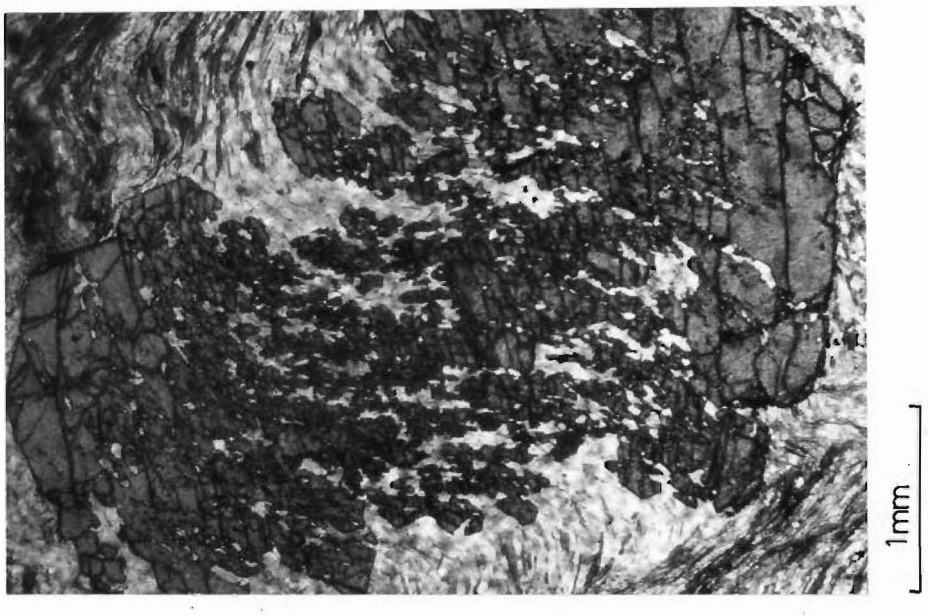

S46 557959

FIG. 6a Trail inclusions (S1) in almandine photographed in plain polarised light . Note that the included S-surfaces are slightly bend towards the crystal edge . Such texture indicates that almandine is syn-tectonic, probably early syn-tectonic as suggested by the large portion of undeformed included S-surface .

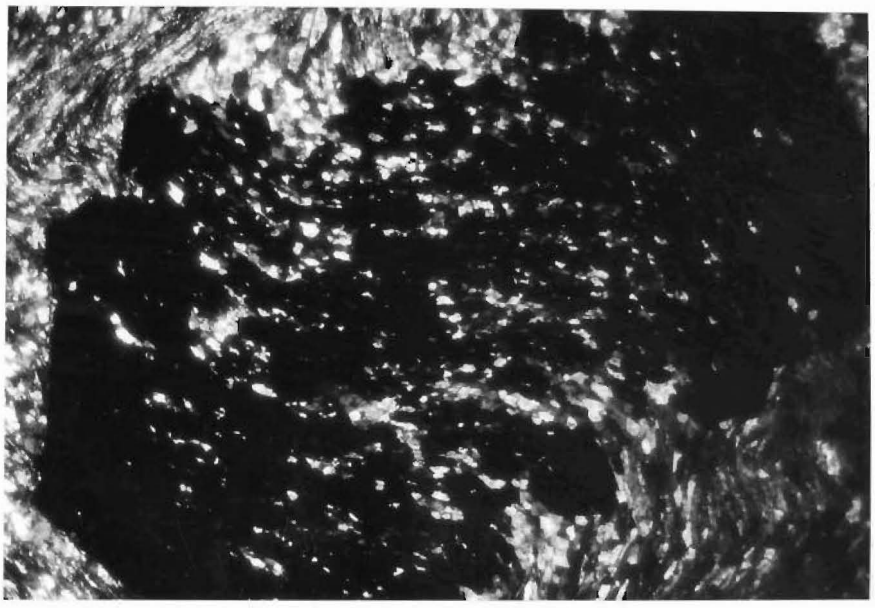

S46 557959

FIG. 6b Same crystal as in Fig. 6a photographed in cross-polarised light .

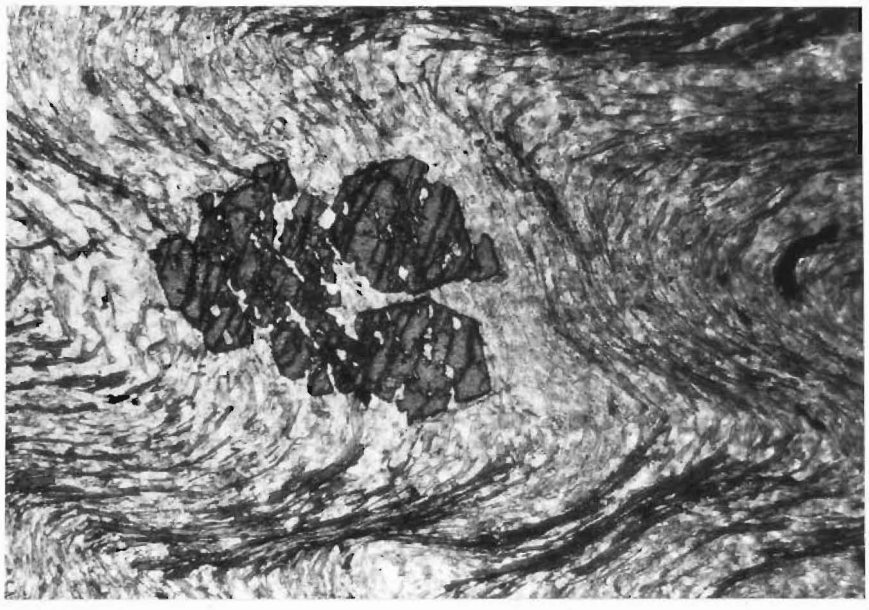

S46 557959

FIG. 7 The axial planes (S2) are 'wrapped' round the almandine porphyroblast .

SPECIMEN No:	METHOD OF CALCULATION	No: OF READINGS USED	CELL PARAMETER (a_o)
B 1	Used the formula	1	11.557 *
B 1	$d_{hkl} = \frac{a_o}{\sqrt{(h^2+ k^2+ l^2)}}$	1	11.555 *
B 6		1	11.559 *
B 6		1	11.555 *
B 6	Used the modified	8	11.555 *
B 6	cell refinement	10	11.554 *
B 6	computer programme	10	11.552
MEAN a_o	11.554	AVERAGE a_o	11.555

OPERATING CONDITIONS FOR THE XRD ANALYSES

Radiation CuK $\bar{a}$ at 1.5405	Scan Speed 1/8° per minute
Std. used NaCl * or Quartz	Current 20 mA
Scan Range 15° to 80°	Accelerating voltage 40 kV

TABLE 1 Cell parameter values for garnets (B1 & B6)

where $d_{h\ k\ l}$ is the lattice spacing on the h k l plane,

h k l are the Miller indices whose value is 4 0 0,

and a_o is the cell parameter of garnet. The second method uses a modified cell refinement computer programme to calculate a_o.

II/4 CHEMICAL COMPOSITION

Nine complete chemical analyses were performed on three specimens of garnets using a JXA-A5 electron microprobe operating at 15 kV acceleration potential and 1.5×10^{-8} amp. sample current. The results of the analyses are given in Table (2), and plotted in Fig. (8) as a function of distance from the crystal centre.

The analysed garnets are predominantly almandine (Table 2), with an average end-member composition of $Alm_{72.95}Py_{11.04}Sp_{5.04}Gr_{10.58}$. Fig.(9b) show that the garnet cores consist of nearly equal proportions of pyrope, sparssartite, and grossular, and are surrounded by rims enriched in pyrope and almandine. Such compositional trends are thought to reflect changing metamorphic conditions during crystallization.

Detailed microprobe step-scans reveal that the garnets are concentrically zoned, even when the crystals are very closely spaced. The cores of the mineral are enriched in Mn and Ca, and slightly depleted in Mg and Fe^{2+} relative to the rims. Figs. (10a and 10b) show

SPECIMEN No: B 1	1 C	1 T	1 R	2 C	2 T	2 R	3 C	3 T	3 R
SiO_2	37.664	37.837	38.379	36.609	37.135	37.094	37.518	37.567	38.049
Al_2O_3	21.111	21.014	20.595	20.890	20.854	21.151	20.033	21.765	21.940
TiO_2	0.071	0.013	0.000	0.056	0.031	0.006	0.166	0.030	0.022
FeO	31.199	34.162	33.895	30.974	33.549	35.055	29.740	32.841	35.252
MnO	3.605	1.307	0.344	4.571	1.743	0.365	6.222	2.787	0.392
MgO	2.404	3.128	2.910	2.306	2.784	3.571	1.059	2.454	3.256
CaO	4.117	3.560	3.435	3.991	3.840	2.867	4.355	3.795	3.033
TOTAL Wt. %	100.170	101.021	99.558	99.398	99.935	100.109	101.875	101.239	101.944
Number of cations calculated on the basis of 12 oxygens:									
Si	6.030	6.014	6.148	5.948	5.982	5.950	5.933	5.963	5.975
Al	3.984	3.936	3.888	4.000	3.959	3.999	4.085	4.071	4.061
Ti	0.009	0.002	0.000	0.007	0.004	0.001	0.020	0.004	0.003
Fe	4.178	4.541	4.541	4.209	4.520	4.703	3.934	4.359	4.630
Mn	0.489	0.176	0.047	0.629	0.238	0.050	0.833	0.375	0.052
Mg	0.574	0.741	0.695	0.559	0.669	0.854	0.462	0.581	0.762
Ca	0.706	0.606	0.590	0.695	0.663	0.493	0.738	0.645	0.510
TOTAL	15.969	16.016	15.908	16.045	16.034	16.049	16.005	15.999	15.992
Composition in terms of end-members:									
Alm	70.252	74.196	77.106	68.307	73.543	76.537	65.703	73.116	77.773
Py	9.630	12.553	11.908	9.406	11.264	14.341	7.790	9.732	12.799
Sp	8.233	2.986	0.830	10.577	4.007	0.833	14.050	6.299	0.875
Gr	11.886	10.265	10.106	11.711	11.186	8.289	12.458	10.853	8.553
Average end-member composition: $Alm_{72.95}$ $Py_{11.04}$ $Sp_{5.04}$ $Gr_{10.58}$									

TABLE 2 Electron microprobe analyses of almandine (B1) from Springs Junction . Computer programmes used for processing the microprobe data are a) Nakamura's version of Bence and Albee (1968) data reduction programme, and b) Y. Kawachi's version of Rickwood (1968) garnet end-member calculation .

Notation : C=core ; T=transition zone ; R=rim .

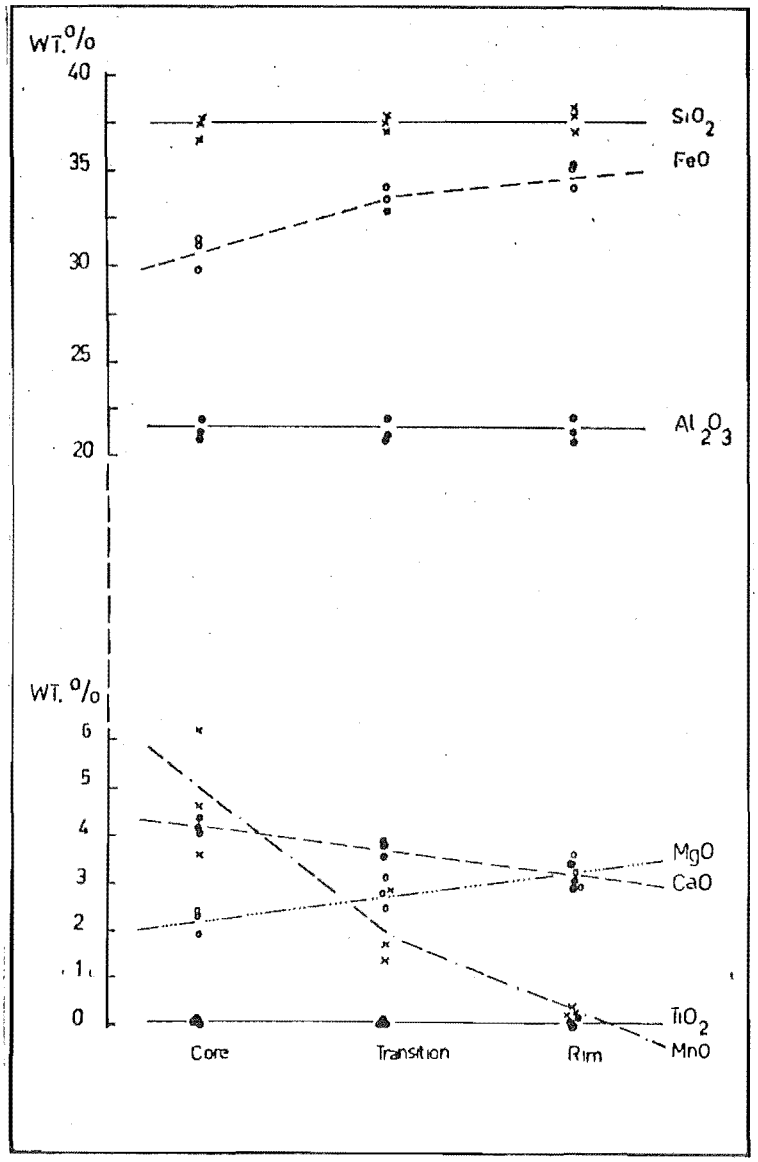

CHEMICAL COMPOSITION OF GARNET

FIG. 8 Diagram shows the concentration of seven elements at the core, transition zone and rim of almandine from locality B1 .

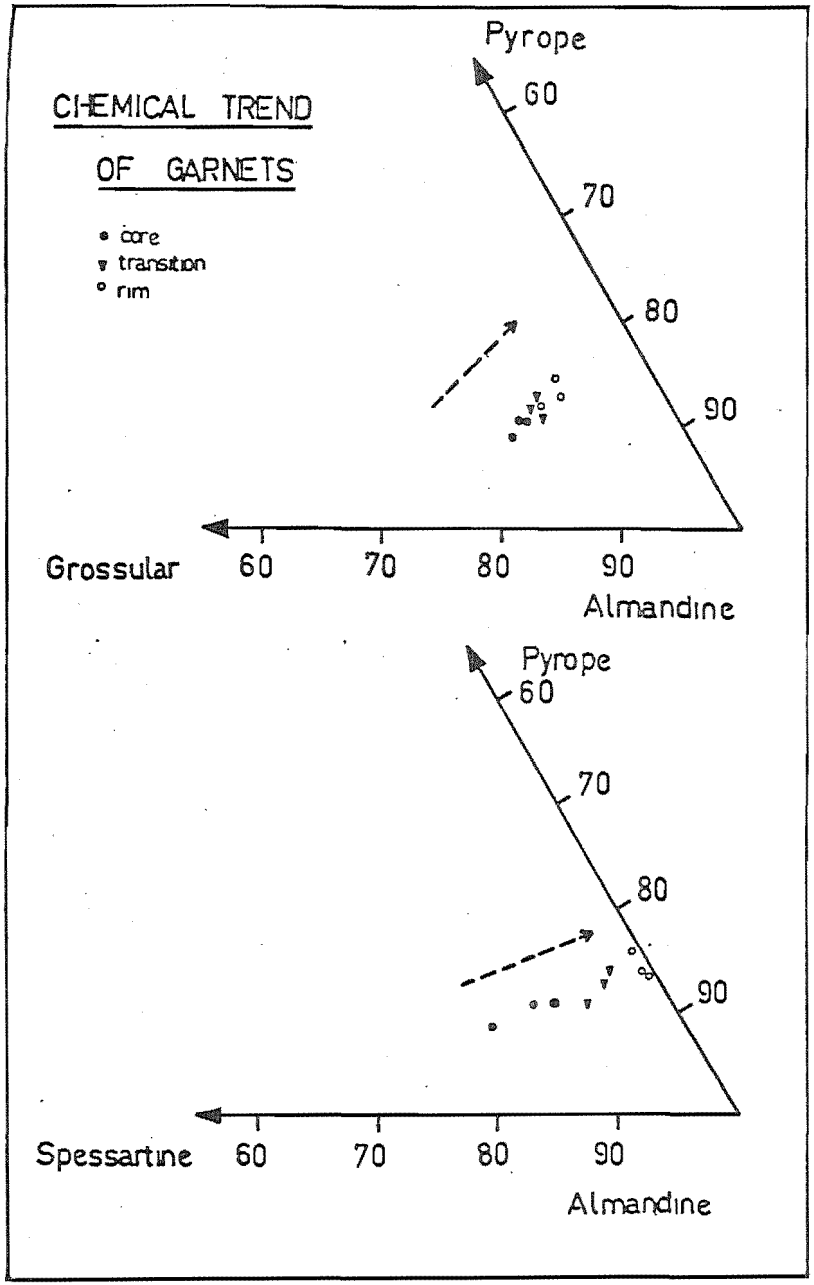

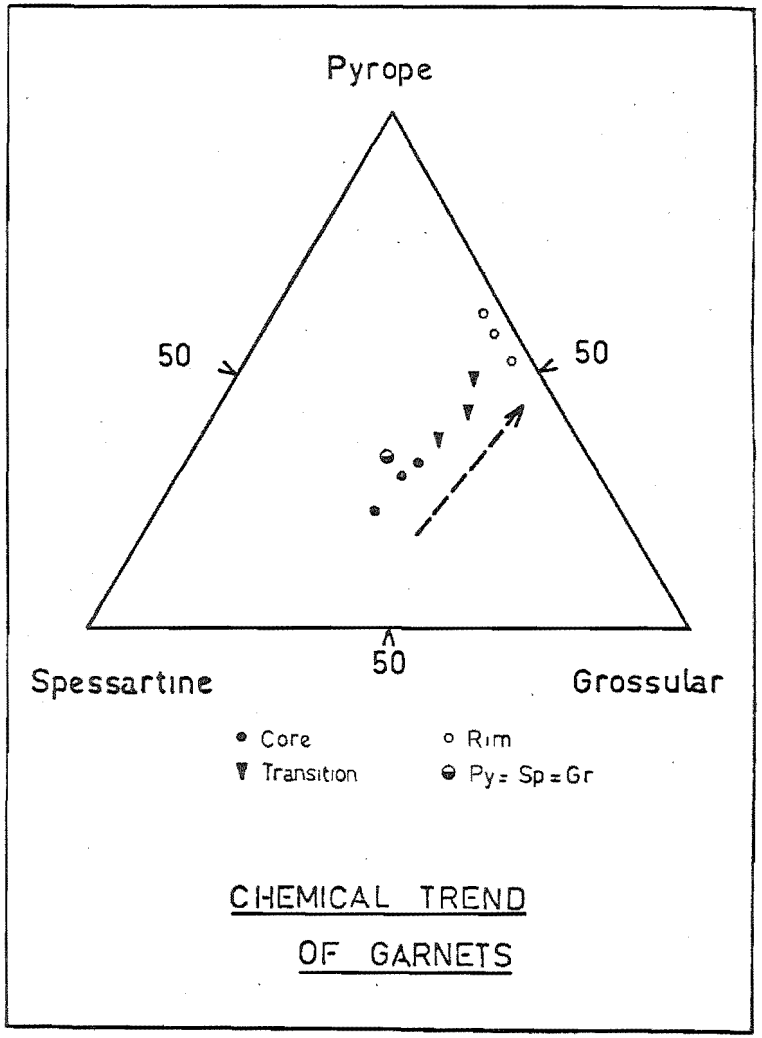

FIGS 9a (Left) 9b (Right) 7a shows the chemical trend of garnets (B1) towards Almandine and Pyrope. 7b shows equal proportions of Pyrope, Sparssartite, and Grossular in the cores of garnets (B1).

that the distribution of these four elements are unaffected by textural changes in the garnet.

The data given in Table (3) compares the average chemical composition of garnets in different host rocks at different localities. The garnets from xenoliths in pegmatitic veins have the highest content of Mn and Ca, nearly twice the amount of that in garnets occurring in schists at the same locality. Such chemical variation suggests different bulk chemical composition of the host rocks, or different P-T conditions. Garnets rich in Mn content are normally considered to indicate a lower temperature of formation.

The garnets in the schists at localities B1 and B6 also display different Mn, Ca, Fe^{2+} and Mg contents. All chemical analyses show that the latter garnets are richer in Mn content. The implied difference in bulk chemical composition between the two localities could be due to either a real variation in the chemical composition of Thompson's Flat Formation, or contamination of the chemical environment by pegmatitic veins at locality B6. Detailed investigations by the writer show that both suggestions are possible (See section on interpretation of grain size distribution).

II/5 GROWTH RATE

Growth rate of a mineral, expressed as dr/dt or da/dt or dv/dt, is proportional to temperature, pressure, water content in the system, concentration of reactants, and

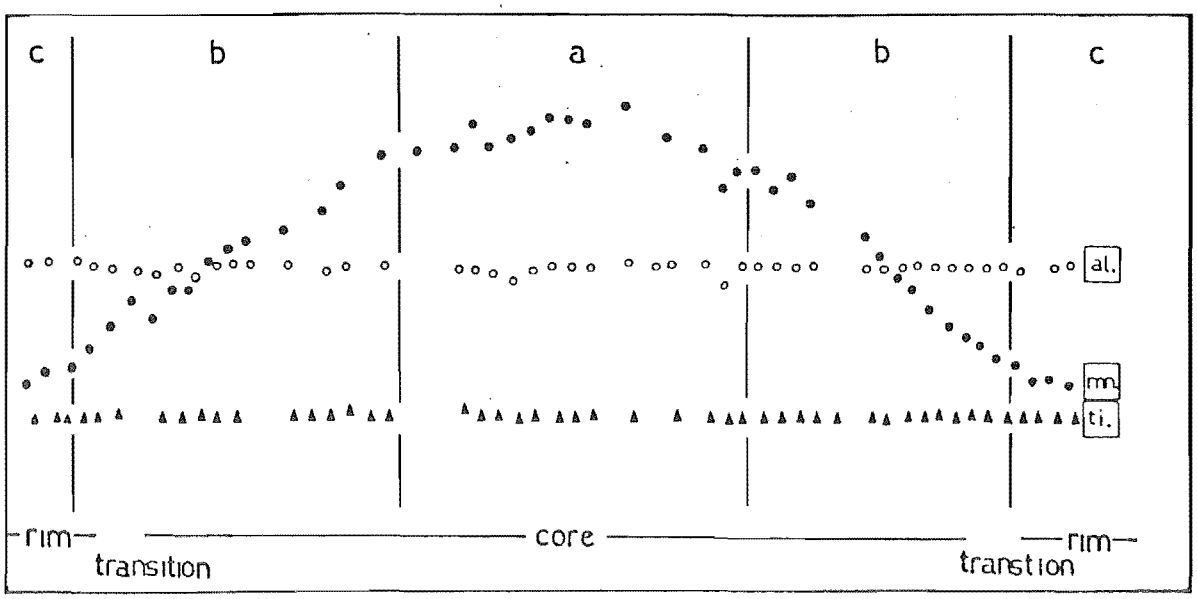

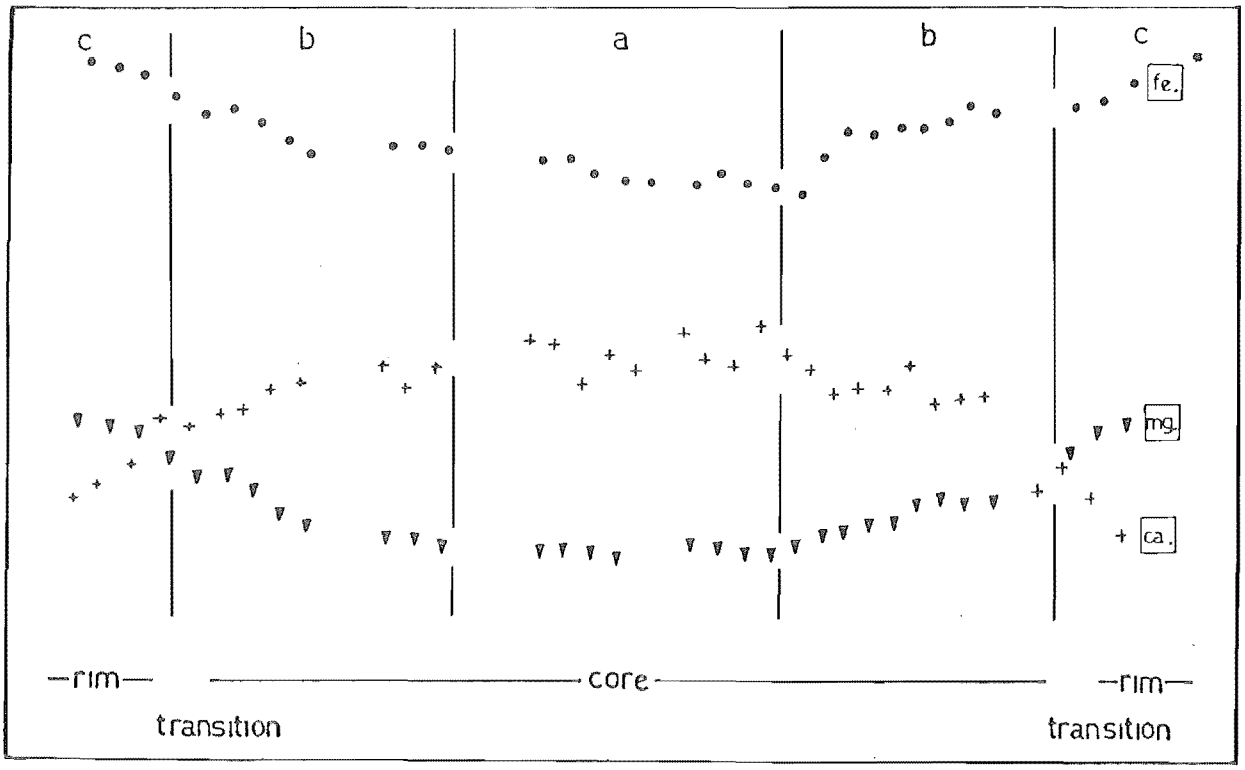

DISTRIBUTION OF ELEMENTS * total iron

FIGS. 10a (Above)
10b (Below)

Edge to edge microprobe step scan across garnet (B1). All the analysed almandine show similar zonation patterns. Note that the trends of elemental distribution are unaffected by textural change in the transition zone. A microprobe analysis of Si which is not included in this diagram shows homogeneous distribution.

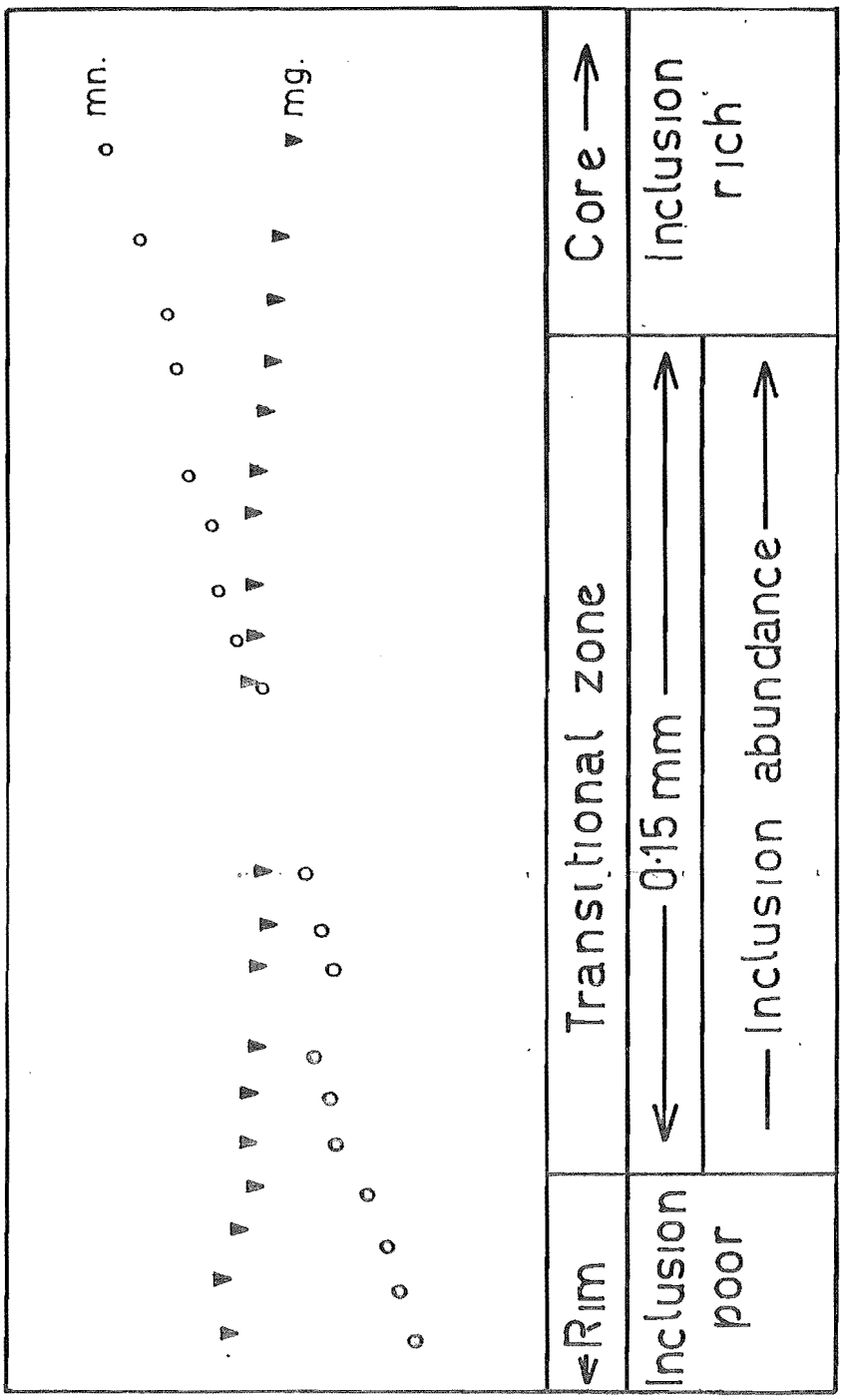

FIG. 10c Closely spaced microprobe analyses show that the zonation of elements are independent of textural change . Almandine analysed from locality B1 .

ANALYTICAL METHOD	Microprobe	AA	XRF	AA	AA	XRF
HOST ROCK & LOCALITY	Schist at B 1	Schist at B 1	Schist at B 6	Schist at B 6	Schist at B 6	Xenoliths in veins at B 6
SiO_2	38.10*	NA	39.57	NA	NA	42.84
Al_2O_3	22.00*	NA	18.91	NA	NA	18.64
FeO	32.97*	29.68	29.15	29.96	29.92	24.14
CaO	3.66*	3.38	2.45	NA	1.82	4.31
TiO_2	0.10*	NA	0.45	NA	NA	0.34
MnO	2.37*	2.39	3.53	4.09	4.85	7.18
MgO	2.75*	2.67	NA	NA	3. 8	NA
Total Wt.%	101.95		94.06			97.45

* - Average value of the nine analyses in Table 2

NA - Not analysed

AA - Atomic absorption

XRF - X-ray flourescense

TABLE 3 Average chemical composition of garnets from localities B1 and B6. Except for the values in the microprobe column, all the values in the table are corrected for the quartz inclusions. For correction factor, see appendix .

concentration of impurities which depress or catalyse reaction(s).

According to Kretz (1966), the growth rate of garnet may be deduced from information on a) the relationship between size of garnet grains and distance to nearest neighbour garnet, or/and b) the previous experimental results on garnet growth in solids. Although the relationship between size of garnet grains and distance to nearest neighbour garnet has not been sought after by the writer, it is conceivable, in view of the rate of garnet growth is commonly constant in experimental situations, that the growth rate of almandine is steady. Assuming that this is true, and that the chemical composition of garnet which is in the process of crystallizing at numerous points in the small volume of rock is everywhere the same, as well as that the composition gradients within the crystals remained unchanged since the time of crystallization, the growth rate model for almandine may be considered to be that between those expressed by $dr/dt = k$ and $da/dt = k_2$ (refer Kretz 1974, p. 125 and Figs. 11 & 12).

II/6 GRAIN SIZE DISTRIBUTION

Because the specimens UC 7651a and UC 7654d are relatively friable rocks, it was possible to extract all the garnets as complete crystals. The sizes of randomly selected crystals were determined with a micrometer objective.

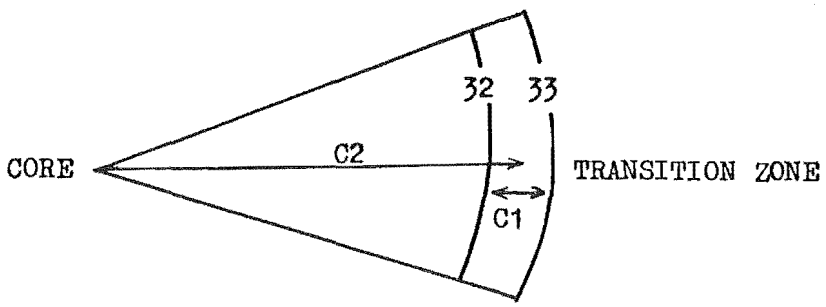

Section through the centre of garnet crystal, showing location of 32.0% and 33.0% 'FeO' contours .

SPECIMEN NO. B1	1	2	3
C1 (mm)	0.150	0.170	0.140
C1* (relative to largest crystal)	1.07	1.21	1.0
C2 (mm)	0.270	0.345	0.456
C2* (relative to largest crystal)	0.59	0.76	1.0

FIG. 11 Distance between composition contours (C1) and distance from crystal centre to mid-point between contours (C2) for the crystals of specimen B1 .

FORM OF GROWTH-RATE EQUATION FROM DATA
ON COMPOSITIONAL ZONING

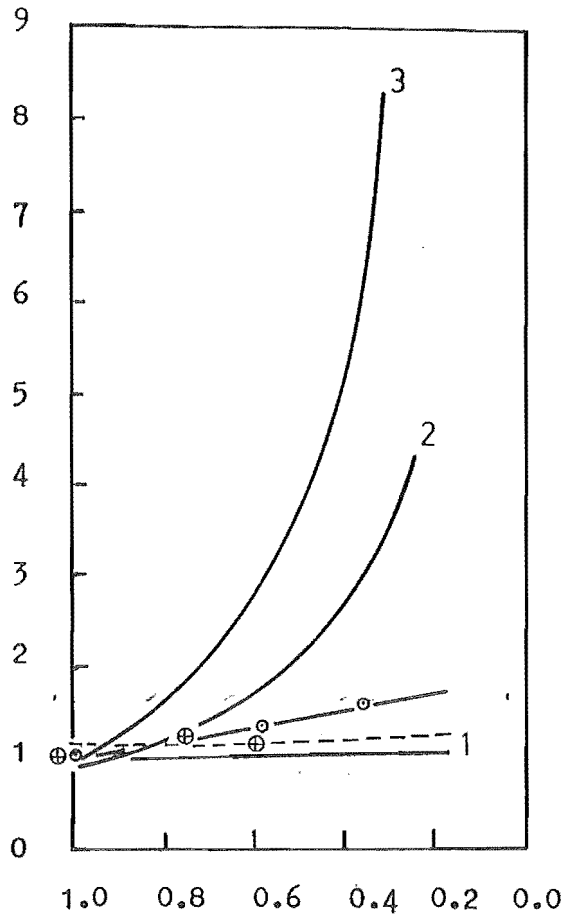

FIG. 12 Relation between $C1^*$ and $C2^*$ for growth models 1 ($dr/dt=k1$); 2 ($da/dt=k2$); and 3 ($dv/dt=k3$). Circled dots and crosses are data from specimens 285 of Kretz (1974) and B1 of the writer.

The diameter of garnets ranges from 0.75 to 3.75 mm, and each grain size distribution is bimodal with a slightly developed skew (Fig. 13). The bimodal nature of garnet distribution may be considered as real because the mineral grains are randomly selected and there are no significant number of broken crystals to bias the plots.

Fig. (15)features the cumulative area curves which are characteristic of bimodal distribution. With reference to garnets 8 to 16 sq. mm in area, the cumulative curves are straight lines, thus indicating that those portions of garnet distribution are normal.

II/7 INTERPRETATION OF GRAIN SIZE DISTRIBUTION PATTERNS

The discontinuities in size distribution is pronounced, as revealed by the bimodal distribution patterns and by the irregular cumulative curves. According to Kretz (1966) such distribution is the result of a discontinuity in nucleation rate, possibly accompanied by a discontinuity in growth rate.

If it is accepted that garnets at the two localities (B1 & B6) were grown in similar metamorphic conditions, which is likely to be the case especially since B1 and B6 are less than 0.5 km apart and are within the same metamorphic grade, then the distribution pattern for B1 should resemble that of B6. Fig.(14) features nearly similar patterns for B1 and B6 in the size range of 1.50 to 2.50 mm, thus suggesting that the rocks at both

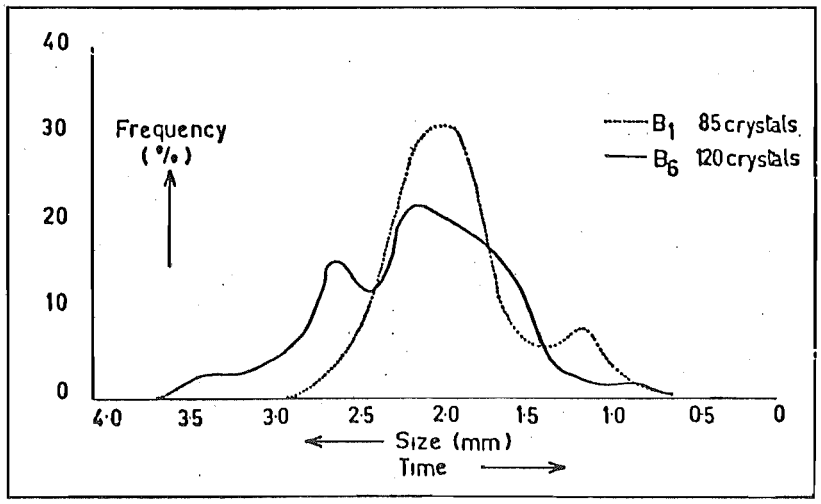

SIZE DISTRIBUTION OF GARNETS FROM B1 AND B6

FIG. 13 Diagram shows a bimodal distribution for B1 and B6, and three generations of almandine . The highest frequency of crystal size is in the range of 1.50 to 2.50 mm .

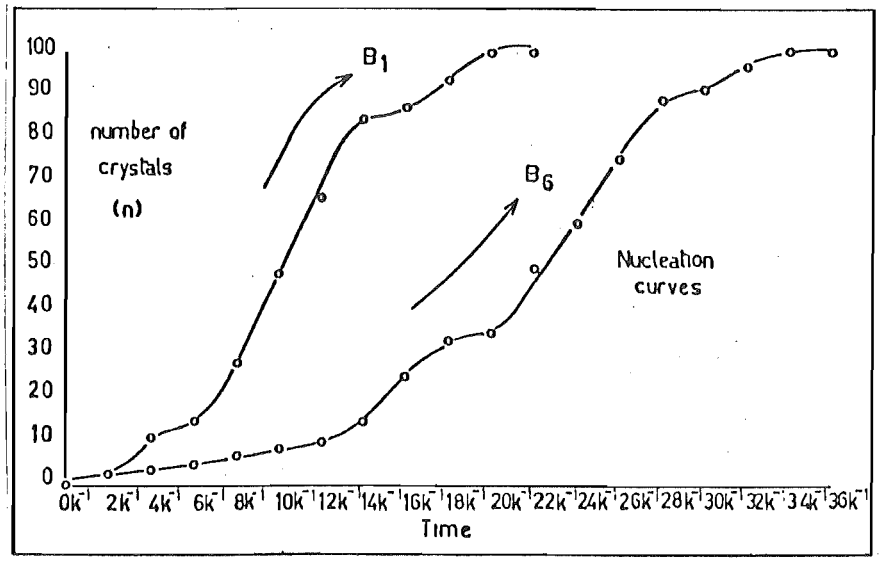

FIG. 14 The nucleation curves for B1 and B6 garnets if the rate of growth is constant .

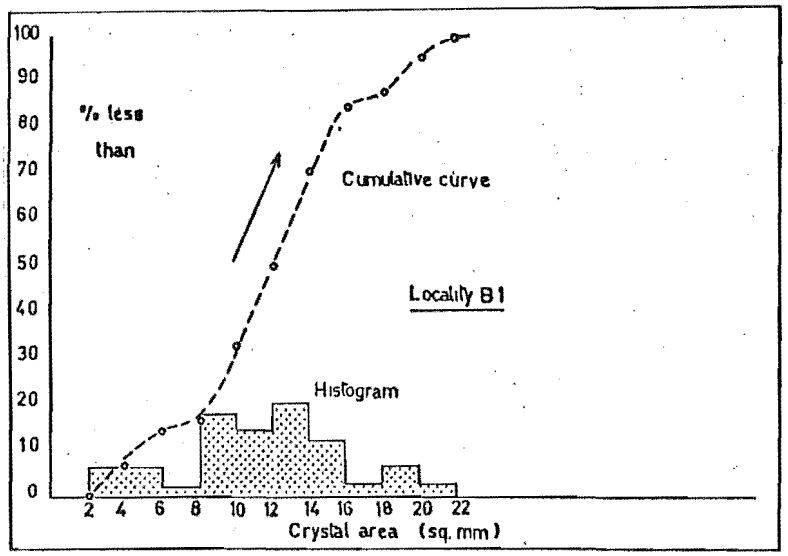

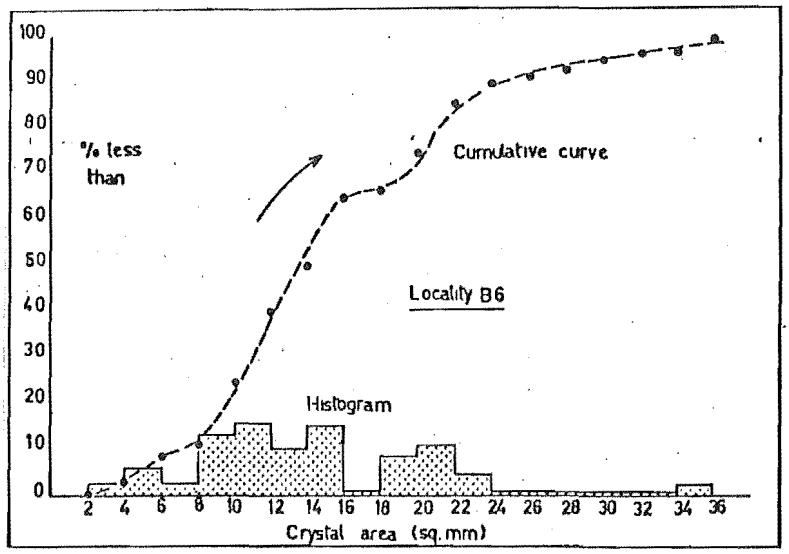

FIG. 15 Diagrams show the histograms of garnet crystal-area, and the cumulative curves for localities B1 and B6 .

localities experienced nearly similar metamorphic conditions.

Outside the size range of 1.50 to 2.50 mm, the distribution patterns are unique for B1 and B6. According to Fig.(13) an appreciable quantity of garnets were formed at an earlier period at B6. Since it has been mentioned that rocks at both localities suffered similiar metamorphism, the earliest generation of garnets is likely to be the result of crystallization caused by catalytic factors eg. presence of water, 'seeds', and elements which promote nucleation or/and lower the stability field of garnet. Analyses of garnets show that the mineral consistently contains higher Mn content at locality B6 (Table 3). In such a case, it is conceivable that the earliest generation garnets result from a high Mn content in the host rock because Mn is known to produce easier nucleation (Spry 1969) and to lower the stability field of garnets (Miyashiro 1953), or in other words the difference may possibly be a reflection of variations in the bulk chemical composition of Thompson's Flat Formation.

In the size range less than 1.5 mm, only graph B1 shows the last generation of garnets. The difference in distribution patterns between B1 and B6 may be due to the following.

1) An exclusive increase of total rock pressure at B1 causing an increase in nucleation and growth rates which resulted in an extra generation of garnets.

2) Competition of Al and Fe^{2+} in the diffusional system at B6 from the formation of staurolite, thereby

suppressing the production of the last generation of garnets.

In 1) the last generation of nucleation is confined to locality B1 whereas in 2) the last generation of nucleation is widespread.

Textural studies show that the crenulation cleavage is better developed at B1, and it is frequently deformed around fractured garnets to produce pressure shadows. Such observations suggest that the directed pressure is more intense at B1, and hence supports possibility 1). Conversely, mineralogical studies reveal that staurolite formation is confined to B6, and hence supports possibility 2). However, one may argue that since staurolite is always restricted to aluminous rocks, the depletion of Al and Fe^{2+} in the system is unlikely, and therefore possibility 1) should be preferred. A combination of 1) and 2) will account for the textural and mineralogical observations given above.

II/8 DETERMINATION OF NUCLEATION CURVES FROM CRYSTAL SIZE DATA ON ASSUMPTION OF CONSTANT GROWTH

The form of nucleation-rate equation may be deduced from information concerning crystal size distribution together with information or an assumption on the form of the growth rate-equation as described by Kretz (1966, 1973,1974). The procedure is illustrated in Tables (4a , 4b).

Area (r^2) in sq. mm	Class Mid-point	No. of crystals	% of crystals	% less than	Duration of growth	Time scale	n, of crystals
0				0		22/k	100.00
	1	0	0		1/k		
2				0		20/k	100.00
	3	5	6.17		3/k		
4				6.17		18/k	93.83
	5	5	6.17		5/k		
6				12.34		16/k	87.66
	7	2	2.47		7/k		
8				14.81		14/k	85.19
	9	15	18.52		9/k		
10				33.33		12/k	66.67
	11	14	17.28		11/k		
12				50.61		10/k	49.39
	13	17	21.00		13/k		
14				71.61		8/k	28.39
	15	11	13.58		15/k		
16				85.19		6/k	14.81
	17	3	3.70		17/k		
18				88.89		4/k	11.11
	19	6	7.41		19/k		
20				96.30		2/k	3.7
	21	3	3.70		21/k		
22				100.00		0/k	0

TABLE 4a Determination of the relationship between number of crystals and time from crystal-size data (B6 almandine) Columns 1 and 5 - cumulative curves . Columns 7 and 8 - nucleation curves .

Area (r^2) in sq. mm	Class mid-point	No. of crystals	% of crystals	% less than	Duration of growth	Time scale	n, no. of crystal
0				0		36/k	100
	1	0	0		1/k		
2				0		34/k	100
	3	3	2.50		3/k		
4				2.50		32/k	97.5
	5	7	5.83		5/k		
6				8.33		30/k	91.67
	7	3	2.50		7/k		
8				10.83		28/k	89.17
	9	16	13.33		9/k		
10				24.16		26/k	75.84
	11	19	15.83		11/k		
12				40.00		24/k	60.0
	13	12	10.00		13/k		
14				50.00		22/k	50.0
	15	18	15.00		15/k		
16				65.00		20/k	35.0
	17	2	1.67		17/k		
18				66.66		18/k	33.34
	19	10	8.33		19/k		
20				75.00		16/k	25.0
	21	13	10.83		21/k		
22				85.82		14/k	14.18
	23	5	4.17		23/k		
24				90.00		12/k	10.0
	25	2	1.67		25/k		
26				91.66		10/k	8.34
	27	2	1.67		27/k		
28				93.33		8/k	6.67
	29	2	1.67		29/k		
30				95.00		6/k	5.0
	31	2	1.67		31/k		
32				96.67		4/k	3.33
	33	1	0.83		33/k		
34				97.50		2/k	2.5
	35	3	2.50		35/k		
36				100.00		0/k	0

TABLE 4b Determination of the relationship between number of crystals and time from crystal-size data (B1 almandine). Columns 1 and 5 - cumulative curves. Columns 7 and 8 - nucleation curves.

The crystal area histograms (Fig. 15) show that the nucleation rate is a combination of two models depicted in Fig (16 after Kretz 1974), and is therefore irregular. Although the nucleation curves in Fig.(14) are not representative, they indicate that B6 has a longer nucleation history which is consistent with the suggestion that garnets crystallized at an earlier period at this locality (see preceeding section). The nucleation curves for B1 and B6 are strikingly similar. They perhaps imply that the two localities experienced similar nucleation history.

II/9 DISCUSSION OF TEXTURAL AND CHEMICAL ZONATIONS

The discussion in this section is based on two possible models for the behaviour of water in rocks undergoing metamorphic recrystallization.

1) When pelitic sediments are mixed with calcareous deposits and metamorphic reactions produce an intergranular fluid containing both H_2O and CO_2. In this model, $P_s = P_{fluid} = P_{H_2O} + P_{CO_2}$, and the chemical potential of water and P_{H_2O} decreases with a decreasing proportion of the component in the mixture (refer Miyashiro's (1973) model 2, p. 44).

2) When an intergranular fluid phase is not necessary for metamorphic reactions to take place. Prolonged metamorphism at relatively high temperatures may cause a virtually complete disappearance of the intergranular fluid phase though discrete water or/and CO_2 molecules are present in an adsorbed state along the intergranular

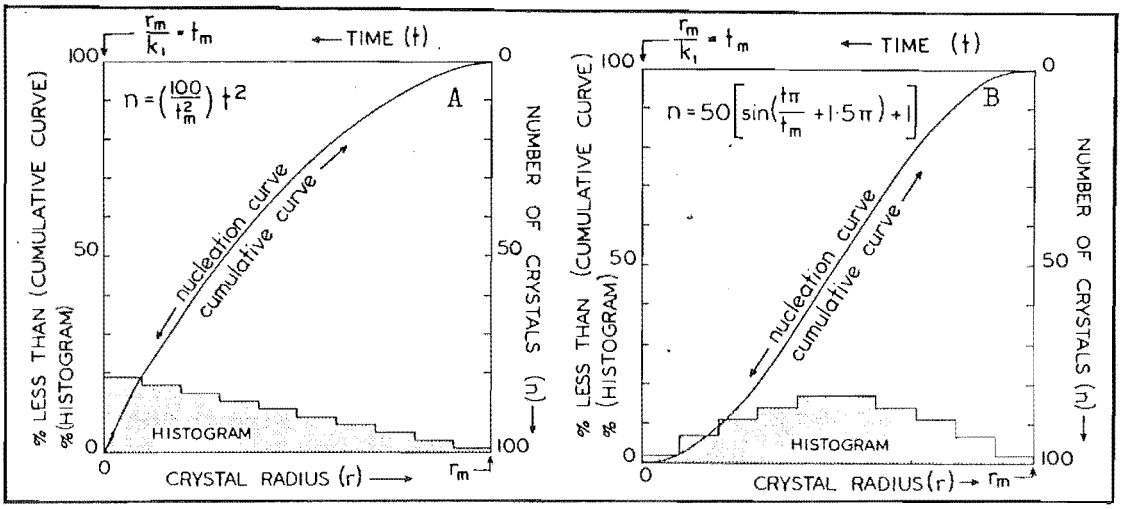

FIG. 16 Diagram (after Kretz 1974) shows the two nucleation models - A & B based on the hypothetical crystal-size distributions .

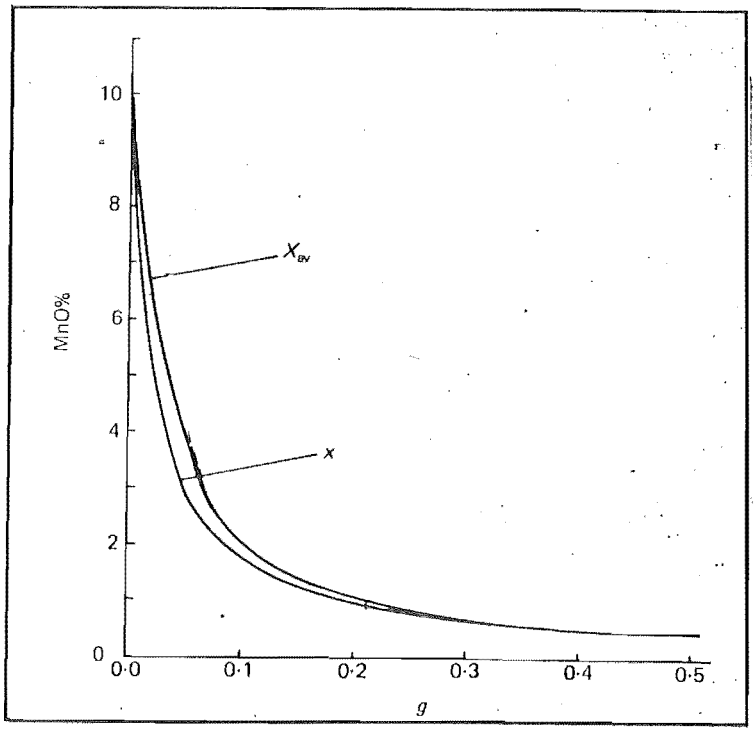

FIG. 17 Diagram (after Miyashiro 1973) shows that as g (i.e. the wt. fraction of all the already crystallized garnet in all the ferromagnesian minerals of the rock) increases, the MnO content in garnets decreases . X_{av} graph belongs to the complete fractionation model, and X graph belongs to the complete equilibrium model .

surfaces. Under this condition, P_{H_2O} within the rock becomes lower than that which existed in the presence of an aqueous fluid phase. In this model, $P_s > P_{H_2O}$.

Although the first model is not preferred by the writer, it cannot be completely ruled out because of the lack of outcrop to indicate positively the absence of nearby calcareous deposits.

The higher Mn and Ca contents in the garnet cores, and the absence of metamorphic chlorite in the schist suggest that the mineral was formed by the reaction of chlorite and quartz in the system at low metamorphic temperature. Three reactions may be envisaged.

i) $2(Mg, Fe, Mn)_{4.5}Al_3Si_{2.5}O_{10}(OH)_8 + 4SiO_2$
(CHLORITE) (QUARTZ)

$= 3(Mg, Fe, Mn)_3Al_2Si_3O_{12} + 8H_2O$
(GARNET) (WATER)

.....(Miyashiro 1973)

ii) $3(Mg, Fe, Mn)_5Al(AlSi_3)O_{10}(OH)_8 + KAl_2(AlSi_3)O_{10}(OH)_2$
(CHLORITE) (MUSCOVITE)

$+ 3SiO_2$
(QUARTZ)

$= 4(Mg, Fe, Mn)_3Al_2Si_3O_{12} + K(Mg, Fe, Mn)_3(AlSi_3)O_{10}(OH)_2$
(GARNET) (BIOTITE)

$+ 12H_2O$
(WATER)

.....(Kretz 1966)

iii) $38.5(Fe_{3.25}Mn_{1.56}Al_{2.34}Si_{2.85}O_{10}(OH)_8$ +
(CHLORITE)

$45(Ca_2Al_{2.45}Fe_{0.55}Si_3O_{12}(OH)$ + $55.3(SiO_2)$
(EPIDOTE) (QUARTZ)

$= 100(Fe_{1.5}Ca_{0.9}Mn_{0.6}Al_2Si_3O_{12})$ + $6.0(O_2)$ + $176.5(H_2O)$
(GARNET) (OXYGEN) (WATER)

.....(Brown 1969)

Fig. (10b)shows that Fe^{2+} and Mg are nearly homogeneously distributed in section 'a' of the garnet. Such a distribution pattern is best accounted for in terms of accelerating growth because water - a catalyst in most chemical reactions, is generated by reactions i), ii), and iii), and generally abundant in pelitic sediments.

Also in section 'a' of the garnet, Figs.(10a and 10b) show that Mn and Ca are heterogeneously distributed. Such distribution patterns imply that although the factors governing nucleation, growth, and elemental distribution during accelerating growth are generally unchanged, they nevertheless experienced minor variations. Since water is known to have a tendency of migrating to zones of lower temperature and pressure, it is likely that the amount of water in the system will vary with time during accelerating growth. In such a case it is not inconceivable that the scattered Mn plots with decreasing concentration towards section 'b' of the garnet are caused by decreasing water content in the system as P_{H_2O} is known to influence the Mn content in garnets (see section II/9 v). The drop

in water content in the system need not be drastic. It is likely that the observed distribution of Mn in section 'a' is a reflection of the element's sensitivity to variations in water content. It is also possible that the scatter of Mn plots are enhanced by Mn substituting for Ca in the crystal lattice at low metamorphic temperature (Saxena 1968). But more detail microprobe analyses is required before this suggestion is accepted as valid.

The irregular distribution of Ca is harder to account for. However, it is conceivable that Ca is more sensitive to variations in P_{O_2}, P_{CO_2}, and pH because such factors control the amount of Ca available to the growing garnet.

The suggestion that the garnet in section 'a' was rapidly grown is supported by textural observation. The garnet cores display abundant inclusions, and the S-surfaces formed from such inclusions are undeformed (Fig. 6).

Sections 'b' and 'c' of Figs. (10a and 10b) show an antipathetic relationship between Mn & Ca, and Fe & Mg. Such a distribution pattern may be explained as follows.

i) Effects of rising temperature on garnet structure. Miyashiro (1953) has pointed out that the interstices in the Si-Al network are smaller at higher temperatures. Since large ions like Ca and Mn are less suitable for such interstices, garnets formed at progressively higher temperatures are therefore enriched in Mg and Fe^{2+}, and impoverished in Ca and Mn. Increasing temperature will not only cause preference for smaller ions but also create an effect of Ca dilution. Saxena (1968) explained that Ca is 'immisible' in the mixture (Mg,

Fe^{2+}, Mn, Ca)$Al_{2/3}SiO_4$ at high temperatures. Hence the decrease in Ca in garnets is the combined effects of elemental dilution and structural unsuitability.

ii) Depletion of element(s) in the system.

Hollister (1966) suggested that the progressive decrease of Mn in garnets is due to depletion of the element in the system during crystallization. Miyashiro and Shido (1973) provided a complete fractionation model and a complete equilibrium model to quantitatively account for such element depletion in the system.

In the complete fractionation model, MnO is highly concentrated in the early formed garnet, which is then removed from the active diffusional system, with a resultant decrease in the MnO content of the system. Hence, the subsequently formed garnet becomes rapidly poorer in MnO. The following equation describes the relationship between the MnO contents in the system and garnet.

$$x + SC(1-g)^{S-1} \quad \text{.....(Miyashiro 1973, p. 219),}$$

Where

x = Wt. % of MnO in the outermost layer of garnet,

g = Wt. fraction of all the already crystallised garnet in all the ferromagnesian minerals of the rock,

S = (Wt. % of MnO in a garnet rim)/(average Wt. % of MnO in the associated ferromagnesian minerals), and

C = average Wt % of MnO in all the ferromagnesian minerals of the rock (including garnet).

According to Miyashiro, the average MnO content (X_{av}) of zoned garnet crystals when S is greater than 10 and constant

is approximately C/g in the range of g is greater than 0.2. The change of X_{av} with g i. e. the change of MnO in garnet with increasing wt. of the mineral is clearly illustrated in Fig. (17).

In the complete equilibrium model, the garnet crystals are assumed to be homogeneous and to have been in equilibrium with the associated minerals during their growth. The following equations describe the relationship between the MnO contents in the diffusional system and garnet.

$g + a = 1.00$; $x/y = S'$; $gx + ay = C$ (Miyashiro 1973, p. 220)

where

x = Wt. % of MnO in garnet,

y = average Wt % of MnO in the associated ferromagnesian minerals,

g = Wt. fraction of garnet in all the ferromagnesian minerals,

S'= fractionation factor, and

C = average Wt. % of MnO in all the ferromagnesian minerals of the rock (including garnet).

According to Miyashiro, the above relationships may be re-expressed as

$$x = \frac{CS'}{1 + g(S'-1)} \quad \text{and} \quad y = \frac{C}{1 + g(S'-1)}$$

For S' greater than unity, the value of $1 + g(S'-1)$ increases rapidly with increasing amount of garnet. As a result, both x and y decrease progressively. The change of x with g is illustrated in Fig. (17) .

Of the two models given by Miyashiro and Shido, the writer prefers the complete equilibrium model because it does not require the removal of previously crystallized garnets from the active diffusional system, and the fractionation factor need not be constant.

iii) Effects of rising temperature on the conversion of ferromagnesium minerals to garnets: As ferromagnesian minerals are progressively destroyed during metamorphism, new and additional elements are introduced into the diffusional system. Miyashiro and Shido (1973) showed that the increase of Mg in garnets is directly related to the introduction of additional Mg in the diffusional system by the breakdown of biotite. Like Mn, the increase of Mg in garnets is quantitatively explained in Miyashiro's and Shido's equilibrium model.

The progressive increase of Fe^{2+} content in garnets may also be explained in this way.

iv) Effects of increasing rock pressure on the breakdown of ferromagnesium minerals: The increase of total rock pressure alone will not greatly affect the rate of biotite breakdown. However, if the increase of total rock pressure is accompanied by an increase of temperature, and decrease of f_{O_2}, f_{H_2O}, & P_{H_2O}, then the speed of decomposition of biotite may be significantly increased as shown by Eugster and Wones (1962, 1965). As the increase of total rock pressure also increases the rate of growth, any subsequently formed garnets are inevitably enriched in Mg and Fe^{2+}.

The increase of growth rate with increasing rock pressure also enhances the depletion of Mn in the diffusional system.

v) Effects of water content in the system:

Variations in P_{H_2O} in the system is known to affect the distribution of MnO in garnets (see Miyashiro 1973, p. 221). Assuming that the behaviour of water in the rocks undergoing metamorphism is that of model 1 or 2 or combinations of models 1 and 2 (refer the begining of section II/9), and that the rate of water leaving the system is greater than the rate of dehydration reactions, then it is conceivable that the MnO zoning in garnets is due to the progressive expulsion of water from the system. As reduction of water content in the system is likely to be accompanied by a decrease of f_{H_2O}, one might suspect that the speed of biotite decomposition will somewhat increase. However, Eugster and Wones (1962, 1965) have shown that the decrease of P_{H_2O} and f_{H_2O} must be accompanied by changes in T, P. & f_{O_2} if the rate of biotite breakdown is to be significantly affected. Therefore, a reduction in water content in the system alone will not greatly influence the distribution patterns of Mg and Fe^{2+} in garnets. The extra steepness in the gradient of Mn in sections 'b' and 'c' (Figs. 10a and 10b) support such a suggestion, as well as the suggestion that Mn is more sensitive to variations of water content in the system (see section II/a).

vi) Effects of non-preferred substitution:

The distribution of Fe^{2+} and Mg in garnets is a function of not only T and P, but also of the concentrations of Mn and Ca in the system. If there is a depletion of Mn and Ca in the system caused by competition from growths of co-existing minerals eg. chloritoid, epidote etc., or if Mn and Ca are rendered immobile by the formation of complex ions due to changing chemical conditions, then it is possible that Mg and Fe^{2+} might be forced to occupy those sites in the garnet structure normally occupied by Mn and Ca. Such garnets are enriched in Mg and Fe^{2+}, and they do not reflect higher metamorphic temperature and pressure.

As non-preferred substitution requires there to be conditions of low metamorphic grade with unchanging T and P, the effects of non-preferred substitution might not be applicable in the case of progressive metamorphism discussed in this chapter. However, if such a phenomenon had occurred in sections 'b' and 'c' of the garnet, its effect is likely to be minimal.

Thin section examination reveals that sections 'b' and 'c' of the mineral are composed of poikiloblastic and inclusion-poor garnets. If the inclusion-rich, and inclusion-poor garnets represent two phases of mineral growth, the distribution patterns of elements shown in Figs. (10a and 10b), would display breaks in distribution trends. Figs. (10a and 10b) show that the distribution trends of elements are unaffected by garnet textural change. The lack of difference in R. I. at the boundary between the poikiloblastic and inclusion-poor garnets,

and the occasional occurrence of S-surfaces as structures traceable from the core to the rim are evidence reinforcing the suggestion that sections 'b' and 'c' were formed in a single period of growth.

Spry (1969) mentioned that crystals even when they are produced during the state of steady growth are able to capture foreign minerals to form inclusions. He suggested that the phenomenon is due to the low-energy gradient between the crystal front and the foreigh grains which cause the interface to be immobile and consequently force the crystal to build around the foreign grains to result in inclusions.

Quartz is chemically and to some extent structurally compatible with garnets. It is conceivable that the interface energy in such a case is low, and hence allows the described grain capture process to operate. The engulfment of opaques may also be explained by a similar process. The low interface energy here is not due to chemical or structural compatibility with garnets but to the special surface characteristic of the opaques. Spry (1969) has mentioned that iron oxides and carbonaceous matter have resulted as inclusions in crystals because of such special surface characteristics.

Assuming that the foreign grain capture process continues in section 'c' of the garnet the occasional quartz and opaque mineral inclusions suggest that the textural change is possibly caused by significant diffusion between the crystal front and foreign minerals resulting in the majority of quartz grains being completely assimilated

by the garnet while the opaques and carbonaceous matter are rejected and pushed outwards by the moving crystal front. The boundary marking the change from inclusion-rich to inclusion-poor garnets in such a case then represents the 'critical' temperature at which diffusion has become sufficiently intense so as to completely assimilate most of the quartz grains.

The essentially similar gradients of the Fe, Mg, Mn and Ca lines in sections 'b' and 'c' of the garnet (refer Figs.(10a, 10b, & 10c)suggest that the growth rate was unchanged at this stage.

Detailed inclusion-studies reveal that not all quartz inclusions are due to engulfment by garnet. The shapes, sizes and orientations of the quartz inclusions in Fig. (18) indicate that some of the inclusions are the results of healed microfractures in the garnet crystal.

II/10 GARNETS AS INDICATORS OF METAMORPHIC GRADES AND FACIES

The $\frac{CaO + MnO}{FeO + MgO}$ diagrams (Figs. 19a and 19b)show that the Brown Grey garnets are similar to the high grade garnets reported from the Alpine (NZ) and Dalradian (UK) Schists. According to the metamorphic grade - composition relationships shown by Sturt (1962), and Wallace (1974), the analysed garnets indicate an upper Garnet-Sillimanite metamorphic grade.

Numerous workers (Skinner 1956, Sriradamus 1958, Winchell 1958, etc.) have established that there is a

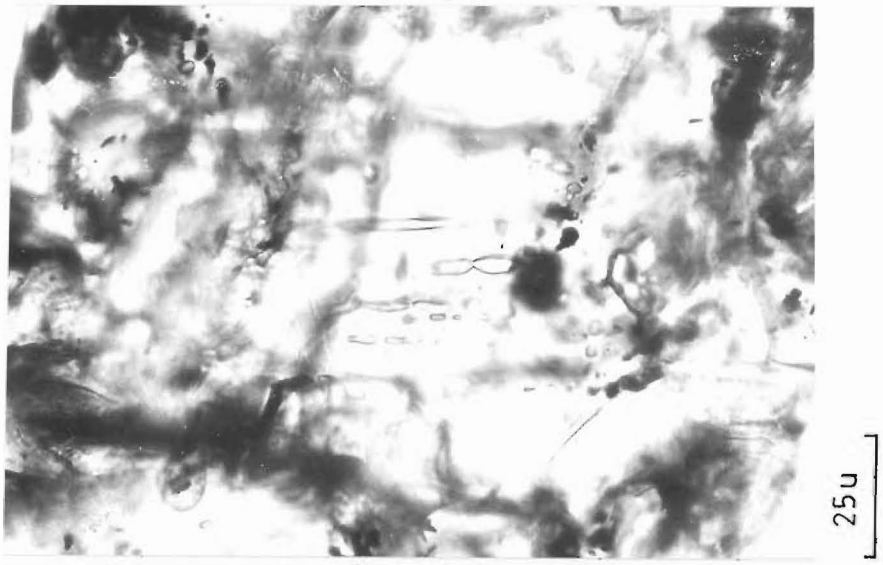

S46 557959

FIG. 18a Photograph showing the various stages of healed micro-fractures in almandine . Note the formation of inclusions from healed micro-fractures .

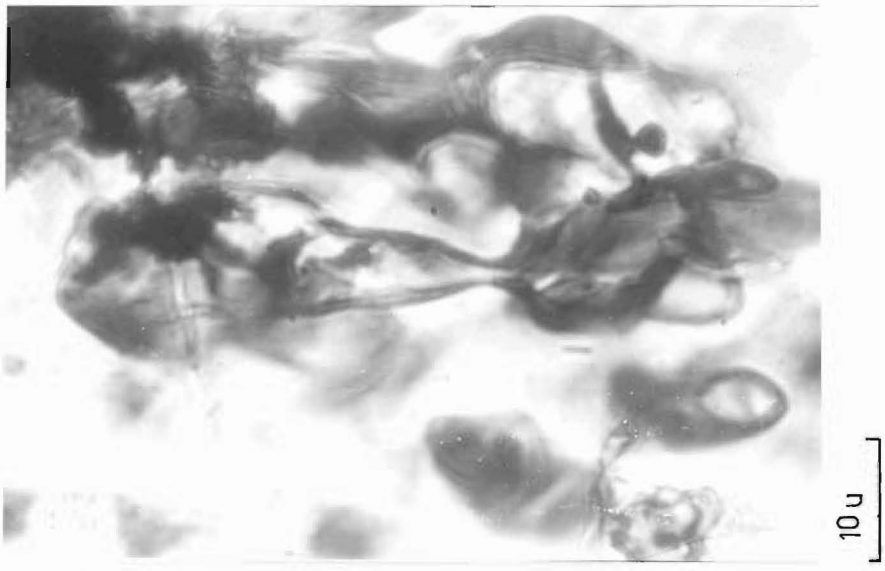

S46 557959

FIG. 18b A close-up picture showing healed micro-fractures in the process of forming discrete inclusions in almandine .

S46 557959

FIG. 18c A close-up picture showing tear drop shaped inclusions formed from healed micro-fractures in almandine .

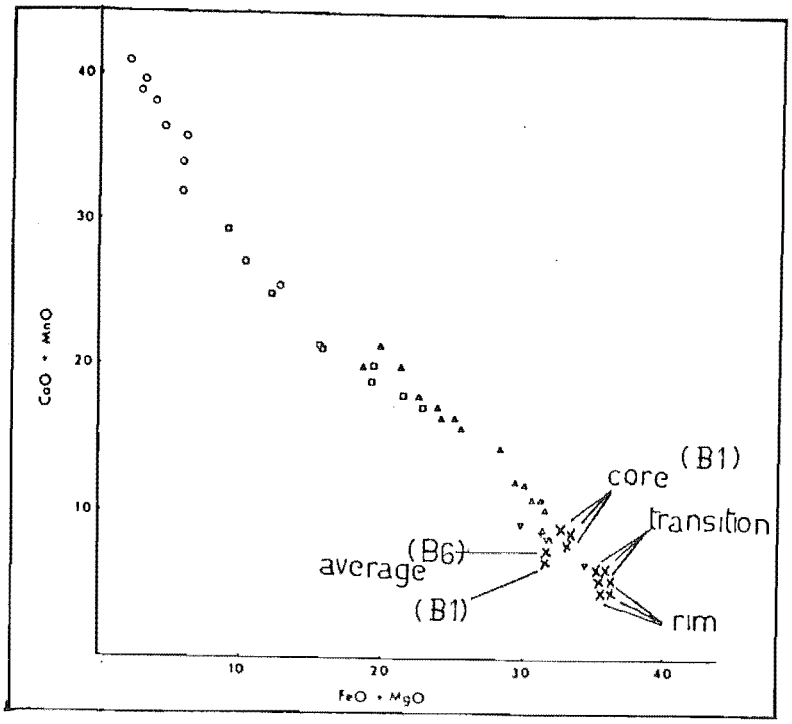

FIG. 19a Chemical parameters of almandine from the Brown Grey River compared with garnets from the Haast Schist . The above diagram is after Cooper (1970) ; Mason (1968) and Wallace (1974) . Circle - chlorite zone ; square - biotite zone ; triangle - garnet zone and inverted triangle - oligoclase zone .

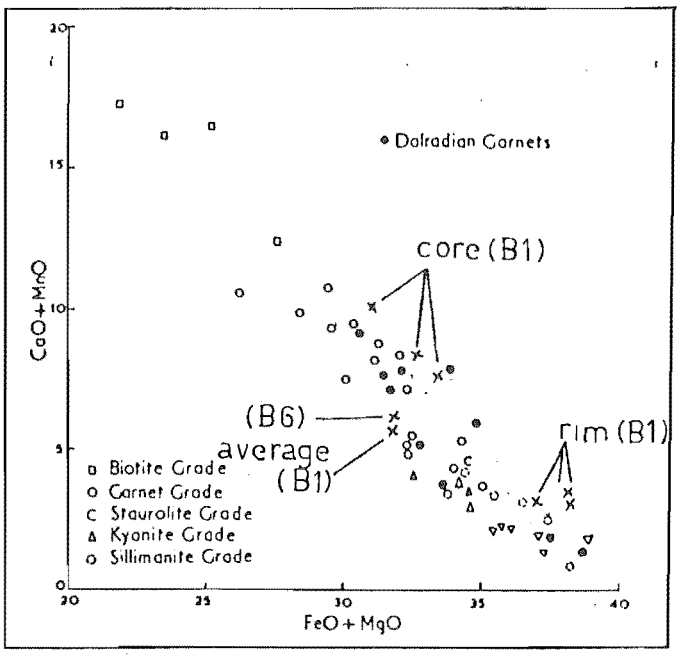

FIG. 19b Chemical parameters of almandine from the Brown Grey River compared with garnets from the Dalradian Schist (Scotland) and other schists around the world . The above diagram is after Sturt (1962) . Note that the Brown Grey almandine plots in the region of upper garnet to sillimanite zone .

regular relationship between garnet composition and various physical properties and this relationship in particular areas has been interpreted by Stuart (see Fig. 20) to reflect metamorphic grade. The writer found that the range of metamorphic grades obtained from the $\frac{CaO + MnO}{FeO + MgO}$ diagrams for Brown Grey garnets may be reduced to the Staurolite grade (Fig. 20). The metamorphic mineral assemblage consisting of staurolite, almandine, biotite, muscovite, and quartz in the rocks near locality B1 agrees with the metamorphic grade determined from garnet composition and physical properties.

According to Miyashiro (1953), the approximate metamorphic facies may be determined from end-member composition diagrams. Fig.(21) shows that the garnets are in the epidote-amphibolite, and amphibolite facies or following Winkler's 1967 classification, the upper most greenschist facies and almandine-amphibolite facies. The metamorphic mineral assemblage in the lower Brown Grey area indicates that the rocks are in the staurolite-almandine subfacies - a division of the almandine-amphibolite facies.

Hsu (1968) has shown that the temperature range for the production of almandine in the iron-magnetite buffer system is 500 to 575° C which agrees closely with Hirschberg's and Winkler's (1968) experimental results of greater than 4 kb at 500° C for the stability of almandine-rich garnets.

SPECIMEN	B6	B6	B6	B1	B1
CaO wt. %	2.18	2.45	1.82	3.38	3.38
R.I.	1.80	1.80	1.80	1.80	1.80
Unit cell edge (a)	11.554	11.554	11.555	11.557	11.555
(a)/R.I.	6.42	6.42	6.42	6.42	6.42

TABLE 5 Cao content and physical properties of almandine from the schists in the Lower Brown Grey Valley .

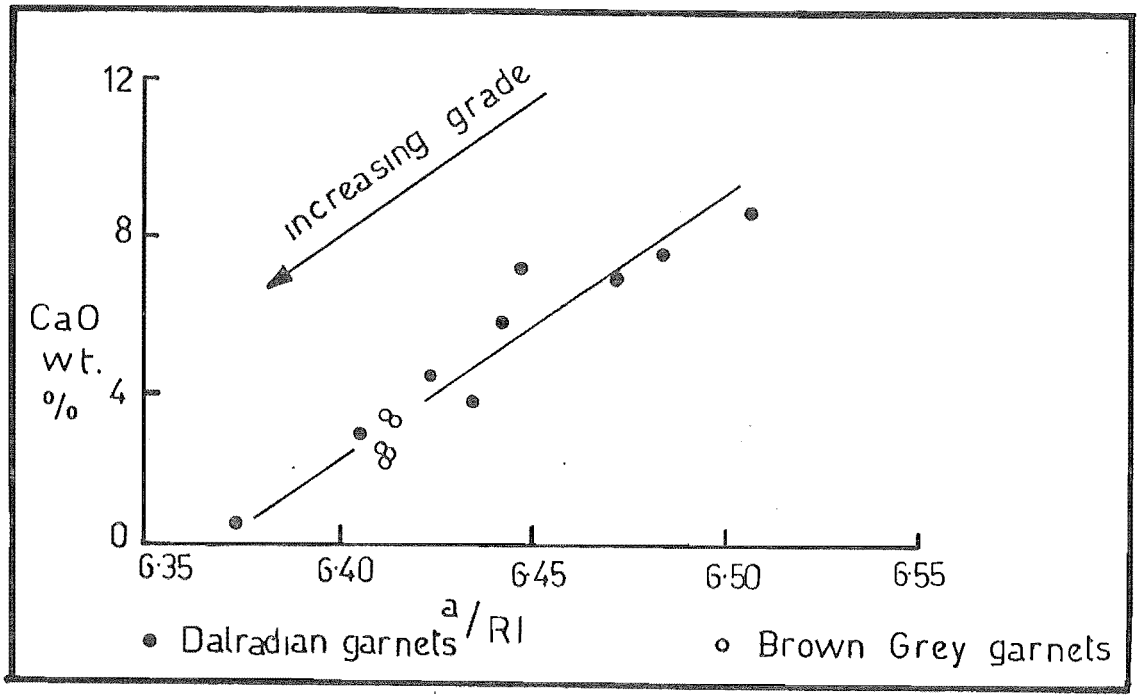

FIG. 20 Diagram shows the closeness of the plots of physical properties in relation to Cao content in the Brown Grey almandine to those of garnets from the Dalradian Schist (staurolite grade) .

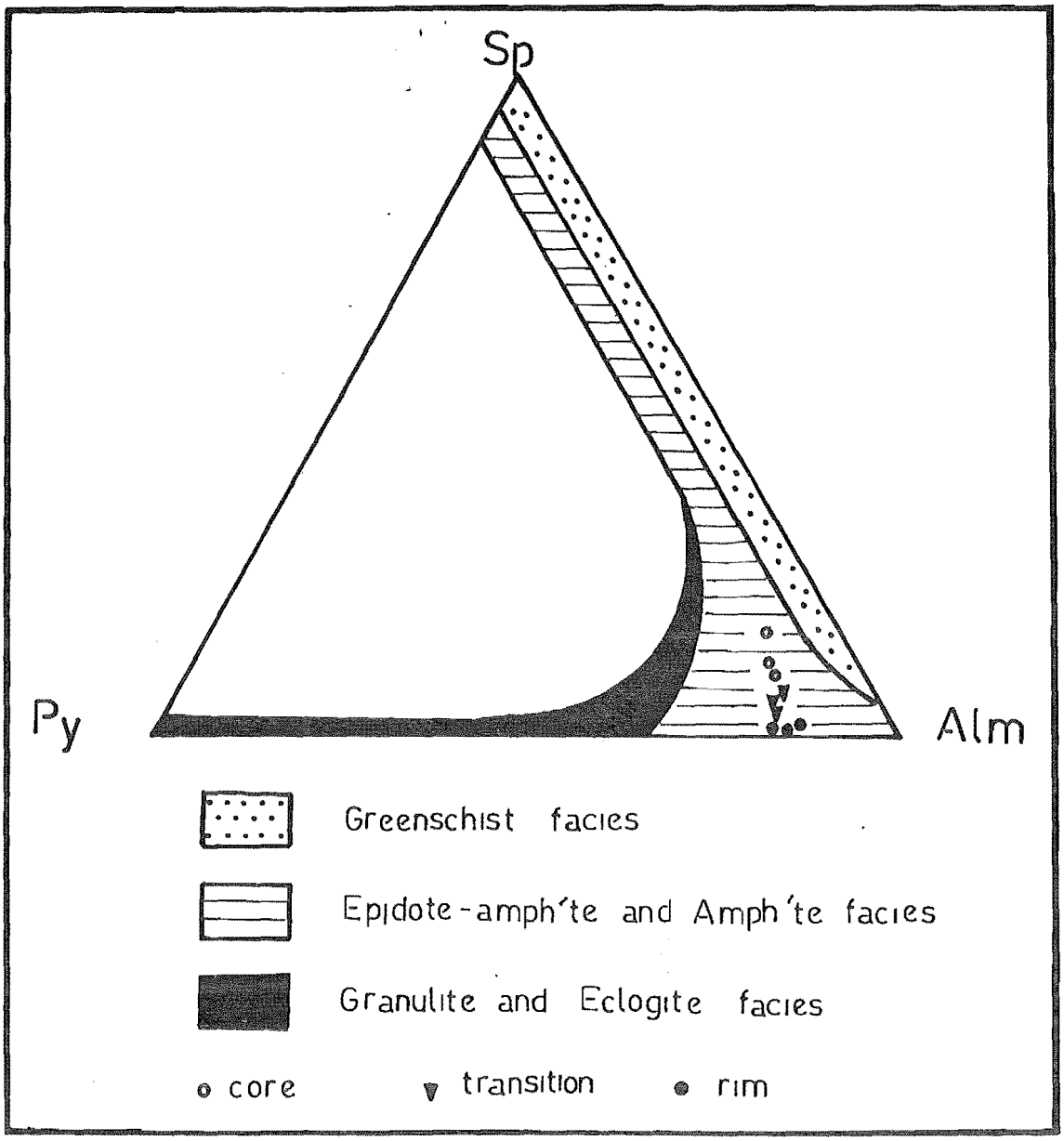

FIG. 21 The end-member composition of almandine from locality B1 shows that the mineral belongs to the epidote-amphibolite, and amphibolite facies as defined by Miyashiro (1953).

Detailed investigations of the garnets described in this chapter reveal the following:

1) Garnets are probably formed from the reaction(s) of chlorite + quartz, or/and chlorite + quartz + muscovite, or/and chlorite + quartz + epidote.

2) The rate of garnet growth is initially accelerated and later possibly regular.

3) There are three generations of garnets; the main generation in the size range of 1.5 to 2.5 mm represents the occurrence of garnet grade metamorphism, and the minor generations reflect the variations in directed pressure (stress) and bulk chemical composition in the Thompson's Flat Formation.

4) The garnets are formed in two growth stages. The first is probably accelerated, the formation reactions being catalysed by water. The second is possibly steady as T and P increase at constant rate s. Fig. 22 provides a visual summary of the factors controlling the distribution of elements in garnets.

5) Garnet is concentrically zoned and shows a chemical trend towards Almandine.

6) The concept of textural change coinciding with growth rate change normally used in the interpretation of crystallization history is shown to be unreliable in this case, because the change in texture in B1 garnets is not clearly marked by any change in growth rate.

7) The directed pressure and formation of crenulation cleavage did not begin until a late stage of garnet growth (garnet grade metamorphism). According to the

size distribution studies at localities B1 and B6, the directed pressure is not homogeneous.

8) The rate of increase of metamorphic temperature may be assumed to be constant if the predominant growth phase of garnet is indeed regular.

9) The highest metamorphic temperature reached in the thesis area is that of the staurolite grade or the almandine-staurolite subfacies. Hischberg and Winkler (1968) have shown that for almandine-rich garnets to remain stable, the metamorphic conditions during the formation of the mineral would need to be greater than 4 kb at 500° C.

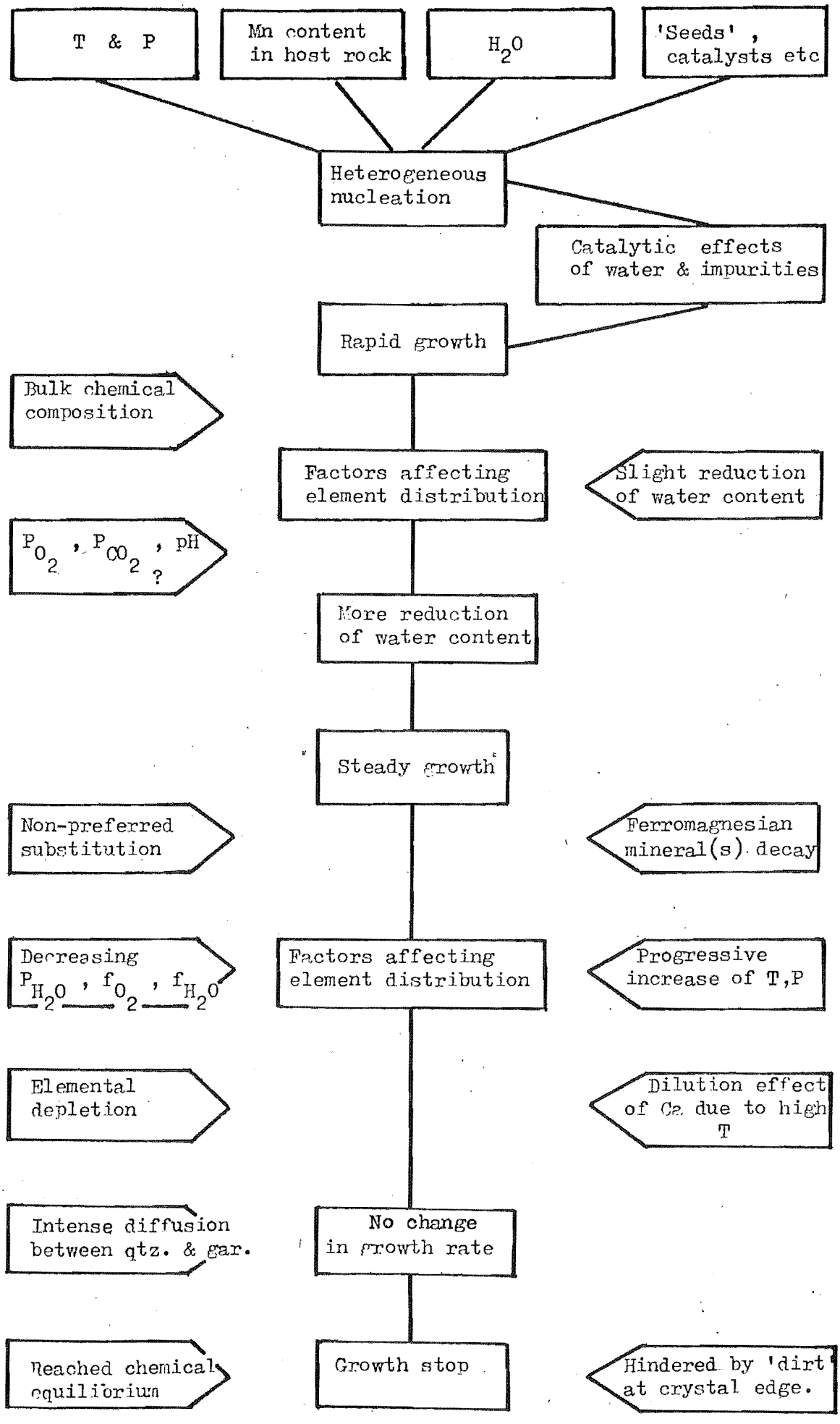

FIG. 22 Summary of growth history and factors controlling elemental distributions in garnets (B1).

CHAPTER III

REGIONAL METAMORPHISM IN THE THOMPSON'S FLAT, SLUICE BOX, AND ALFRED FORMATION IN THE SPRINGS JUNCTION DISTRICT, WEST OF THE NEW ZEALAND ALPINE FAULT.

III/1 MAPPING OF METAMORPHIC ROCKS AND PROBLEMS ASSOCIATED WITH IT

Mapping of metamorphic rocks is based on isograds in the common pelitic Paleozoic sediments of Springs Junction. This method of mapping is not completely successful because of the lack of outcrops at strategic localities, and possible bulk composition variations in pelite; the former is mainly due to Pleistocene and vegetation covers, and the latter may be caused by differences in stratigraphic levels or/and lateral facies changes. The positions of the isograds in the map are therefore approximations of the true isograds. The Barrow-like zones defined by these isograds show that the metamorphic grade of the thesis area increases along a south-westerly direction with the highest grade (i. e. the staurolite zone) located in the vicinity of Palmer's Flat.

III/2 LITHOLOGIES:

PELITE

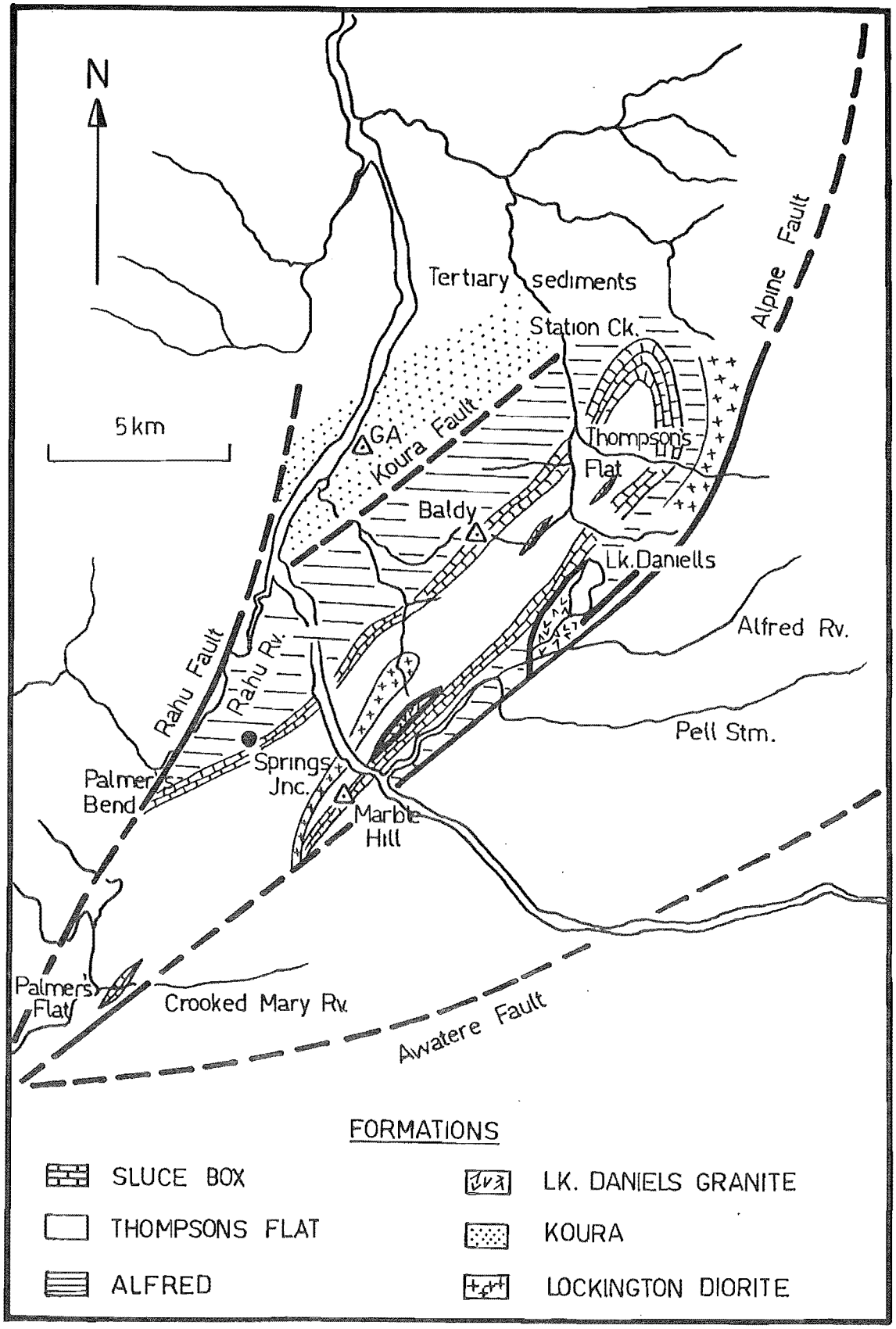

FIG. 23 Diagram shows the various localities mentioned in this chapter . The formation boundaries in the map are after Farmer (1967, unpublished M.Sc. thesis) .

This is the most common lithology in the thesis area, east of the Rahu Fault. It constitutes a major portion of the Alfred and Thompson's Flat Formations. The rock is commonly dark grey or black, laminated, and pyritic especially in the latter formation. The development of slaty-cleavage, fissility parallel to bedding, and lineations is not wide spread.

The pelite exposed in the Upper Station Creek, north-west of Lake Daniells, is calcareous, and displays microfolds, and axial plane-cleavage.

LIMESTONE

It is generally tough, dark grey, and massive. It occurs as a prominent formation known as the Sluice Box Formation throughout the entire area. Limestone also occurs as lenses near Palmer's and Thompson's Flats forming part of the Lower Thompson's Flat Formation. The latter, and the Sluice Box Formation at Marble Hill is lighter coloured, and over 95% carbonate. Elsewhere the carbonate content is more variable, and near Palmer's Bend, the limestone is interbedded with pelitic sediments.

In Farmer's map (unpublished thesis 1967), the Sluice Box Formation outlines a major north-east trending anticline. The fold limbs may be traced from Palmer's Bend, and Marble Hill to north of Thompson's Flat.

MARL

A grey or black calcareous pelite found near limestone as at Upper Station Creek, or interbedded with

limestone as seen at Palmer's Bend. Slaty-cleavage in this rock varies from well to poorly developed.

SANDSTONE

This rock is light coloured, indurated, medium-to fine-grained, and generally quartzose. It is not very common in the thesis area, and constitutes a minor portion of the Alfred and Thompson's Flat Formations.

Structural features are rare in the sandstone except at the junction of Pell and Alfred Streams where graded bedding, and/or crude cleavage have been observed.

QUARTZITE

It is worthwhile to seperately discuss the distinctly purer quartzose sandstones which are restricted to the Thompson's Flat Formation. These quartzites are light coloured, well indurated, homogeneous (i. e. without any sedimentary structures), medium-to fine-grained, and form a minor part of the Thompson's Flat Formation. Individual bed thickness near the top of the formation is variable, and is less than 4 m in the Lower Brown Grey Valley. Quartzite is also present in the Lower Thompson's Flat Formation at the Upper Station, and Crooked Mary Creeks.

VOLCANOGENIC SEDIMENT AND CONGLOMERATE

These rocks are restricted to the Lower Thompson's Flat Formation at Upper Station Creek. The volcanogenic

sediment and conglomerate are well indurated. The latter is sometimes weakly schistose, and contains numerous subangular volcanic and quartzitic pebbles. The larger pebbles are crudely aligned, reflecting preferred orientation by either current during deposition or flattening during the formation of the major north-east trending anticline.

INTRUSIVES

The rock is very well indurated, green, and medium-to fine-grained. Thin section studies reveal that it is composed of mostly andesine, quartz, occasional zircon, and mafic minerals which are usually unidentifiable because of alteration, except for the aegirine-augite phenocrysts in specimen UC 5802. In rock sample UC 5804, the high andesine content, the occurence of zoned crystals, and the random orientation of feldspar suggest that the intrusive is probably andesite. In specimen UC 5802, the porphyritic texture, and the presence of andesine and aegirine-augite phenocrysts also suggest that the intrusive is andesite.

III/3 EFFECTS OF REGIONAL METAMORPHISM:

A. MINERALOGICAL CHANGES:

i) IN PELITE

Sericite, muscovite, quartz, and less common

albite, chlorite, tourmaline, and calcite are formed in the pelite of the quartz-albite-muscovite-chlorite subfacies. With a rise in temperature to the quartz-albite-epidote-biotite, and quartz-albite-epidote-almandine subfacies, chlorite is replaced by biotite and epidote-clinozoisite, as shown by the mineral assemblage of specimens UC 5816, and UC 7811 near Palmer's Bend. With further increase of temperature to the staurolite-almandine subfacies, whilst muscovite and quartz are retained, epidote-clinozoisite is destroyed, and almandine and staurolite appear instead. Although plagioclase is observed in the pelite of the quartz-albite-muscovite-chlorite subfacies, it is conspicuously lacking in similar lithologies at higher metamorphic grades. Its absence may be attributed to the very low CaO content in pelite (Miyashiro 1973, p. 210).

ii) IN LIMESTONE

Thin section studies, and XRD analysis of the rock from Thompson's Flat, Marble Hill, Palmer's Bend, and Lower Crooked Mary Creek show that the limestone is composed of calcite. As the metamorphic temperature experienced by the limestone is not greater than that at which dolomite decomposes to calcite (Winkler 1974, p. 129), it is probable that the present calcite is recrystallised from sedimentary calcite, hence suggesting no mineralogical changes during regional metamorphism. In the impure (siliceous) limestone of the quartz-albite-muscovite-chlorite subfacies, sericite,

quartz, muscovite, calcite, and sometimes Mg-chlorite are crystallised.

iii) IN MARL

Calcite, sericite, quartz, and sometimes muscovite, albite, and Mg-chlorite are formed in the marl of the quartz-albite-muscovite-chlorite subfacies. With an increase in temperature to the quartz-albite-epidote-biotite, and quartz-albite-epidote-almandine subfacies, sericite and chlorite are replaced by tremolite-actinolite, biotite, and epidote-clinozoisite whilst plagioclase is retained as albite/sodic-oligoclase. Although no mineralogical information for marl in the staurolite-almandine subfacies is available, the anticipated mineralogical development according to Winkler (1967, p. 109) is the crystallization of hornblende, almandine, and more calcic-plagioclase.

iv) IN SANDSTONE

The mineralogical changes in this lithology are less well known as sandstone is uncommon and not homogeneously distributed in the thesis area. About 1.5 km north of Marble Hill, muscovite, sericite, quartz, Mg-chlorite, tourmaline, and albite are formed in the very fine-grained sandstone. Along the Lower Rahu River, north-west of Springs Junction, muscovite, sericite, quartz, Fe-chlorite, and sodic-plagioclase (?) are crystallised in the coarse-grained sandstone. With an increase of temperature to the staurolite-almandine

subfacies, sericite and chlorite are replaced by biotite, and occasional almandine, as shown by the mineral assemblage of specimens UC 7651b and UC 7653a in the Lower Brown Grey River Valley. The mineralogical changes in the more quartzose sandstone are less well developed.

v) IN QUARTZITE

As with the limestone, no new minerals are formed in the quartzite during regional metamorphism. The present quartzite is recrystallised and adjacent detrital grain sizes cannot be safely determined.

vi) IN VOLCANOGENIC SEDIMENT AND CONGLOMERATE

As these rocks are restricted to the Lower Thompson's Flat Formation at Upper Station Creek, the observed mineralogical changes are limited to the quartz-albite-muscovite-chlorite subfacies. Epidote-clinozoisite, quartz, Mg-chlorite, albite, and occasional zoisite and calcite are crystallised in the volcanogenic sediment and conglomerate. In similar lithologies but with a relatively lower mafic content, the mineral assemblage is sericite + Fe-chlorite + quartz $\pm$ muscovite (small amounts) $\pm$ albite (?).

vii) IN MAFIC INTRUSIVE

Like the volcanogenic sediment and conglomerate, this lithology is not found except in areas subjected to lower greenschist facies metamorphism. Thin section

studies of rock samples from the vicinity of Thompson's Flat, and Springs Junction show that the mineralogical developments in all the intrusive rocks are the same, even though the metamorphic temperature is higher at Springs Junction. The mineral assemblage is epidote-clinozoisite + chlorite + quartz + calcite ± sericite ± tremolite + plagioclase (albite ?), with epidote-clinozoisite the most abundant mineral.

B. TEXTURAL CHANGES:

Thin section studies of the Lower Paleozoic metamorphic rocks in the Springs Junction district reveal that all the rocks are texturally altered to a greater or lesser extent by the following, depending on lithology and position in the metamorphic zones.

1) The recrystallization of pre-existing minerals such as quartz and calcite. Where such effect is sufficiently extensive, the original grain shape and size are destroyed.

2) The crystallization of new minerals. Unlike the preceeding event which extensively destroys the original rock texture(s), the formation of new minerals results in new texture(s) being superimposed on pre-existing texture(s). The crystallization of platy minerals in pelitic rocks is usually structurally controlled.

3) The deformation of pre-existing structures. For example, S-surfaces, Schistosity, and bedding are

frequently distorted. Sometimes, bedding is transposed by slip on axial plane surfaces as shown by specimen UC 5728, and pressure-shadows are formed around almandine porphyroblasts.

The detailed effects of each of the above mentioned events in a particular lithology are discussed in the following section.

i) IN PELITE

In the quartz-albite-muscovite-chlorite subfacies, sericite often has a preferred orientation, forming the slaty-cleavage, and less commonly a second axial plane-cleavage to folds of the slaty-cleavage. In some calcareous pelite, elongate calcite crystals are aligned parallel to the axial plane cleavage as shown by specimen UC 5728. Bedding here is distorted by folding, and slippage on axial planes.

Near Thompson's Flat, quartz is recrystallised, forming aggregates of finer-grained quartz with irregular or/and sutured boundaries; the original grain shape and size are usually preserved. The mineral is often replaced at grain boundaries by sericite. Albite, chlorite, tourmaline, muscovite, and calcite are also present.

Southwards, with increasing metamorphic grade towards Springs Junction, quartz develops a granoblastic elongate texture. The long axis of the quartz grains are oriented parallel to schistosity as seen in specimen UC 7764c. The original clastic texture is destroyed.

In the same rock, calcite occurs as pseudomorphs after an unknown mineral. The porphyroblasts are crudely hexagonal, nearly 0.5 mm diameter, and poikiloblastic. The tiny quartz inclusions are randomly oriented and sparsely distributed in the pseudomorphs. Considering that 1) the porphyroblasts are hexagonal-shaped, 2) the quartz-albite-muscovite-chlorite subfacies is adjacent to the lawsonite-albite facies (Fig. 26), and 3) albite porphyroblasts are known to develop in the lower greenschist facies (Harker 1932, and others), it is conceivable that the calcite pseudomorphs are after either lawsonite or albite.

Further south, near Palmer's Bend, the preferred orientation of muscovite, green biotite, together with elongate quartz define schistosity which is subsequently deformed by F2 and F3. Reddish-brown biotite is crystallised on some of the axial plane cleavages.

Still further south, in the staurolite-almandine subfacies, muscovite, reddish-brown biotite, and elongate quartz are strongly aligned, forming a schistosity which is subsequently deformed like that near Palmer's Bend. The axial planes (S2) are sometimes wrapped around staurolite and almandine porphyroblasts, creating pressure-shadows. The porphyroblasts are poikiloblastic. S1-surfaces folded by F2, are included in the porphyroblasts as shown by Fig. 6.

ii) RELATIONSHIP OF TEXTURAL FEATURES TO DEFORMATION IN PELITE:

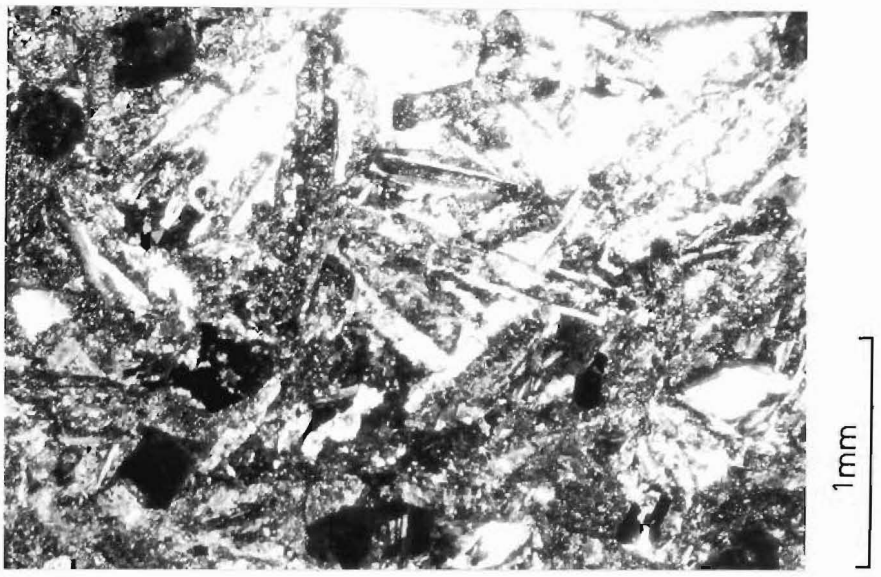

S46 722085

FIG. 24 Lath-shaped zoned plagioclase in igneous rocks near Mt. Baldy . Note the porphyritic texture and alteration of plagioclase by sericite, calcite, and chlorite .

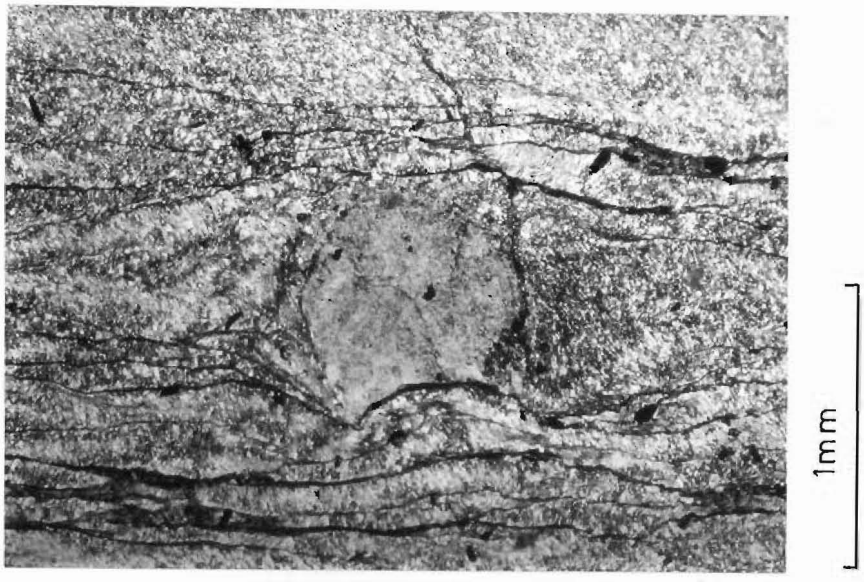

S46 617059

FIG. 25 Calcite psuedomorph after an unknown mineral (Lawsonite ?) in specimen UC 7764a . Note that the axial planes (S2) are 'wrapped' around the calcite psuedomorph .

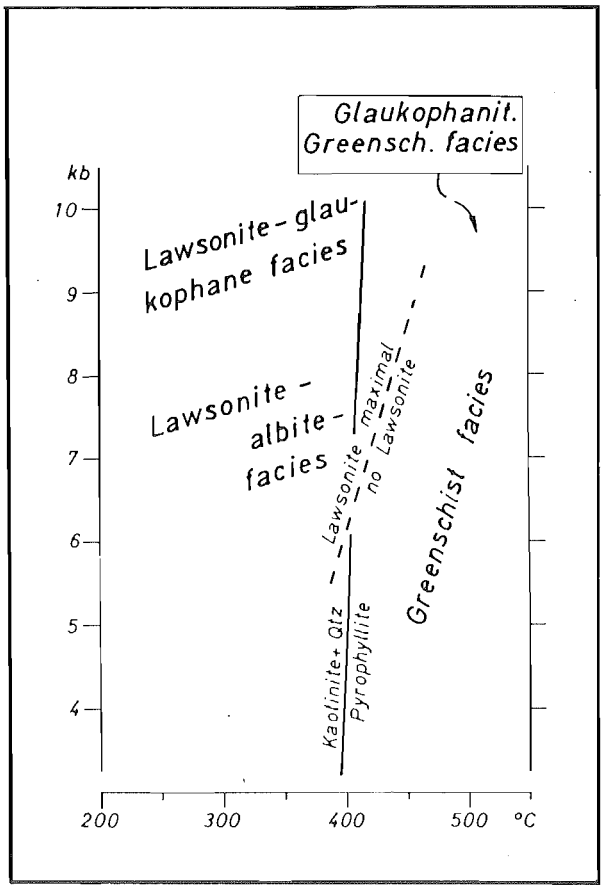

FIG. 26 Diagram (after Winkler 1967) shows the boundary between lawsonite-albite facies and greenschist facies .

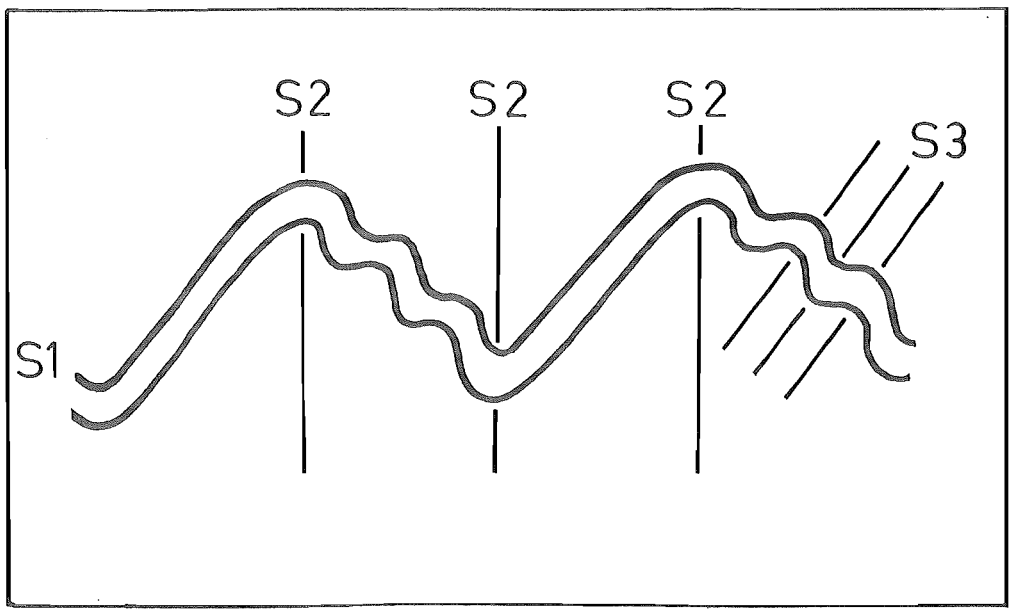

FIG. 27 Figure shows the relationships between S1 and S2, and S2 and S3 . Note that one limb of F2 is not affected by the deformation which generated F3 . For reference see specimens UC 5730 , UC 7811 and UC 7654g .

Terminology.

A mineral is said to be pre-, syn-, or post-tectonic according to whether it crystallised before, during, or after some tectonic event. In the case of a mineral which is syn-tectonic, further distinction is possible, and depending on whether the mineral crystallised at the beginning or end of deformation, the term 'early' or 'late' syn-tectonic is used. The criteria for recognising these relations are discussed in this section.

During regional deformation, various planar structures are generated, and these are assigned as 'S' with a number indicating the relative age of the feature. Explained below are some of the notations used in this section.

So = bedding.

S1 = schistosity formed by the earliest fold (F1) whose trend and style can not be observed in the field.

S2 = axial plane of the first recognisable crenulation/folding (F2); the major and obvious anticline of the area as mapped by Farmer (1967) is F2.

S3 = axial plane of the second crenulation/folding (F3).

Fig. (27) depicts the relationship of the S-surfaces seen in specimen UC 5730 and UC 7654g from the Lower Brown Grey River, and Palmer's Flat.

Staurolite and almandine.

In specimens UC 7651a and UC 7654g staurolite and almandine contain S1-surfaces which are folded by F2. The axial planes (S2) are sometimes wrapped around such porphyroblasts. These textural features indicate that staurolite and almandine are post-S1 but pre- or syn-S2. The large portion of undeformed S1-surfaces in the almandine crystals suggest that the mineral is probably early-syn-S2.

Biotite.

As shown in Fig. (30), there are many generations of biotite. The biotite folded by F2 and deformed by F3 in thin sections UC 5730, UC 5816, and UC 7654g is pre-S2. The mineral that is poikiloblastic, aligned parallel to the limbs of F2 crenulations, and wrapped by S2, is post-S1 but pre- or syn-S2. In specimens UC 5730, UC 7654g and UC 7651a , the biotite with cleavage oriented parallel to S2, is considered as syn- to post-S2. The randomly oriented biotite in the pressure-shadows of almandine porphyroblasts indicates that not all the syn- to post-S2 biotite crystallization is mimetic.

Chlorite.

Those chlorite crystals oriented parallel to S1 are regarded as syn-S1. In specimens UC 5774, 5780, and 5730, the porphyroblastic chlorite aligned parallel to S2 and with kinks and wavy extinctions is dated as syn- to post-S2 but pre-S3. Chlorite pseudomorphs after pre- and syn-S1 biotite, are either post-S1 or

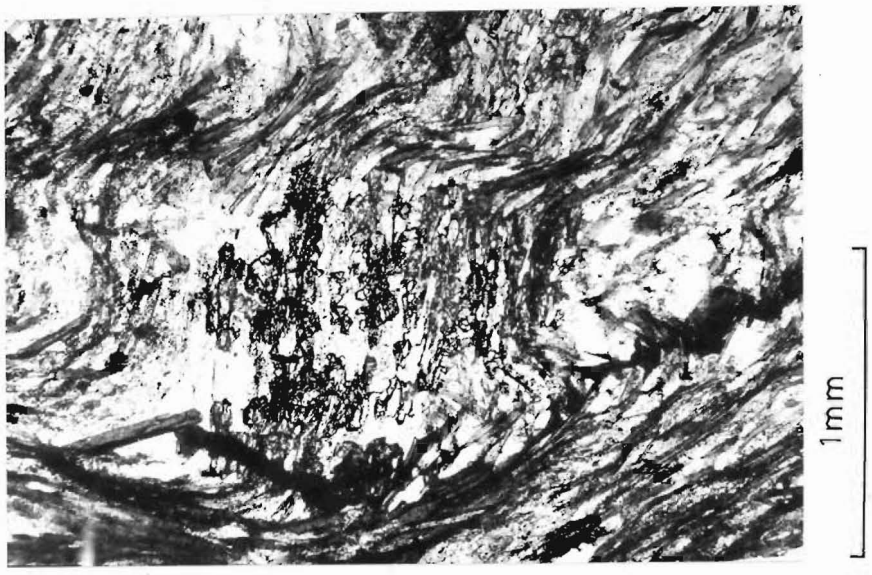

S46 557959

FIG. 28 The axial planes (S2) are deformed around the staurolite porphyroblast in specimen UC 7654g .

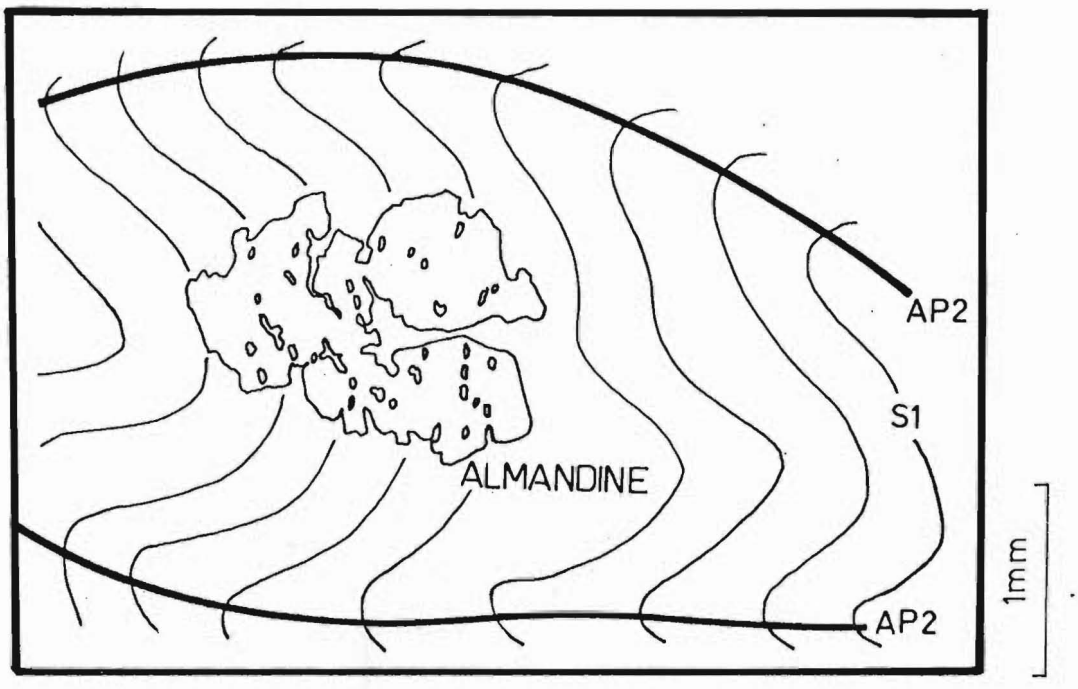

S46 557959

FIG. 29 The axial planes (S2) are deformed around the almandine porphyroblast in specimen UC 7654g . The diagram is after Fig. 7 in chapter 2 .

METAMORPHISM / MINERALS	REGIONAL			RETRO-GRADE
Staurolite		X		
Almandine		X		
Biotite	X	X	X ?	X
Chlorite	X		X ?	X
Muscovite	X		X ?	X
Quartz	X	X ?	X ?	X
Calcite	X		X ?	X
Epidote-clinozoisite	X			
Tourmaline	X			
Deformation Stage	Pre-	Early syn-	Late syn-	Post-
	TECTONIC			
S formed	S2			
S folded	So , S1			

FIG. 30 Time relations of mineral crystallization to deformation in pelite of Spring Junction district, east of the Rehu Fault.
X - Present ; X ? - inferred or suspect present ; So - bedding ; S1 - schistosity ; S2 - axial plane-cleavage

post-S2 because chlorite crystals are not oriented parallel to S2. As chlorite is unlikely to crystallise between biotite and almandine during progressive metamorphism, it is probable that the pseudomorphs are post-S2. The kink planes developed in these crystals are parallel to S3, hence suggesting that this generation of chlorite is post-S2 but pre-S3. In thin section UC 5816, chloritization of pre-S2 biotite is so intense that pre-S2 and post-S2 chlorite is not distinguishable. Some of the post-S2 but pre-S3 chlorite occurs as large, irregularly-shaped, randomly oriented crystals with wavy extinctions and included S1-surfaces which are folded by F2.

Thin section studies show that in contrast with the younger generation biotite, chlorite formed during and after S2 is coarser-grained, and relatively abundant.

Muscovite.

The muscovite that is parallel to S1, and deformed by F2 is pre-S2 as seen in specimens UC 7651a , UC 7654g UC 7764c , and UC 5730. In thin section UC 7764c, the muscovite aligned parallel to S2 but crenulated by F3, indicates that its age is syn- to post-S2 but pre-S3. The muscovite present in the pressure-shadows of almandine porphyroblasts is randomly oriented, and syn- to post-S2.

S46 567960

FIG. 31 Pre-S2 biotite (probably syn-S1) . Note that these biotite plates are affected by F2 and F3 .

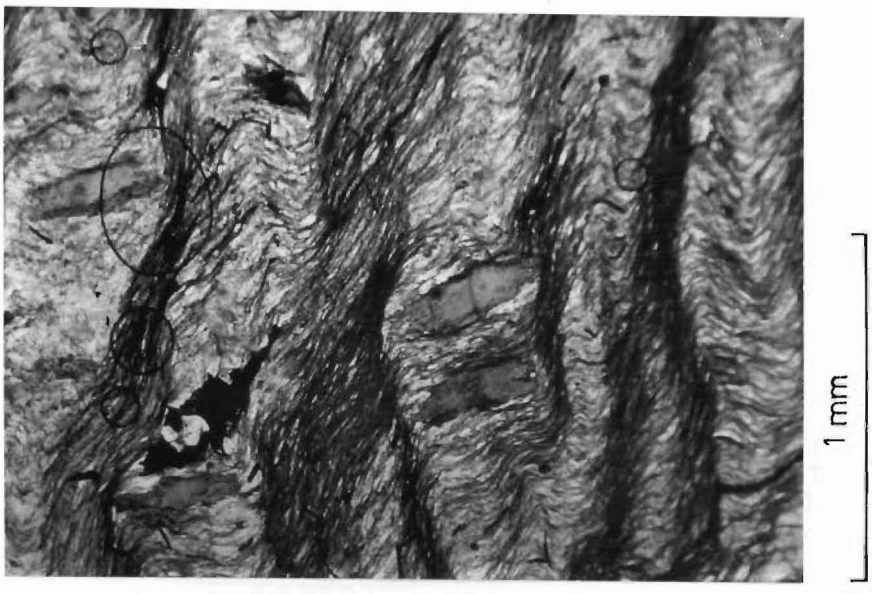

S46 591005

FIG. 32 Post-S1 but pre- to syn-S2 biotite . Note that the biotite plates contain dusty inclusions (S1), and that the axial planes (S2) are deformed around such porphyroblasts .

S46 557959

FIG. 33 Syn- to post-S2 biotite . Note that the biotite plate in the centre of the photograph contains part of the crenulated schistosity (S1) .

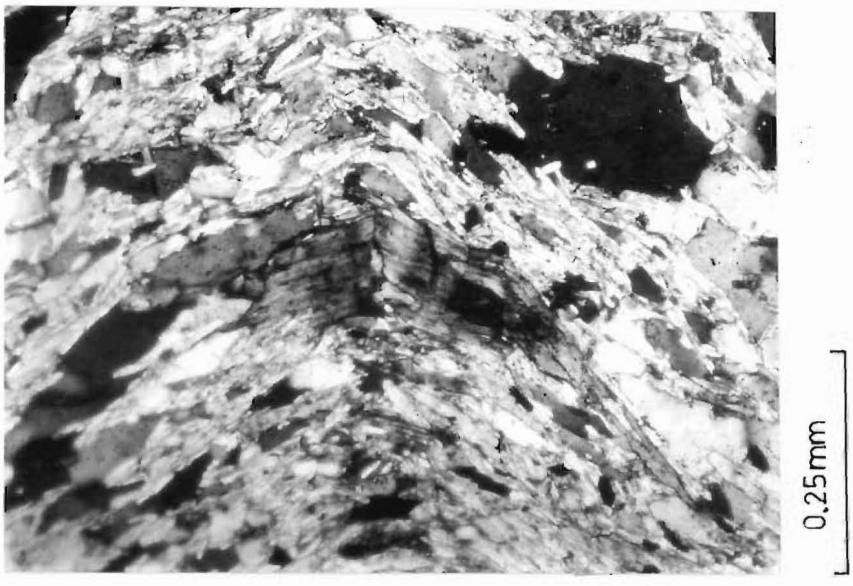

S46 567960

FIG. 34 Syn-S1 but pre-S2 chlorite . Note that the chlorite crystal is folded by F2 .

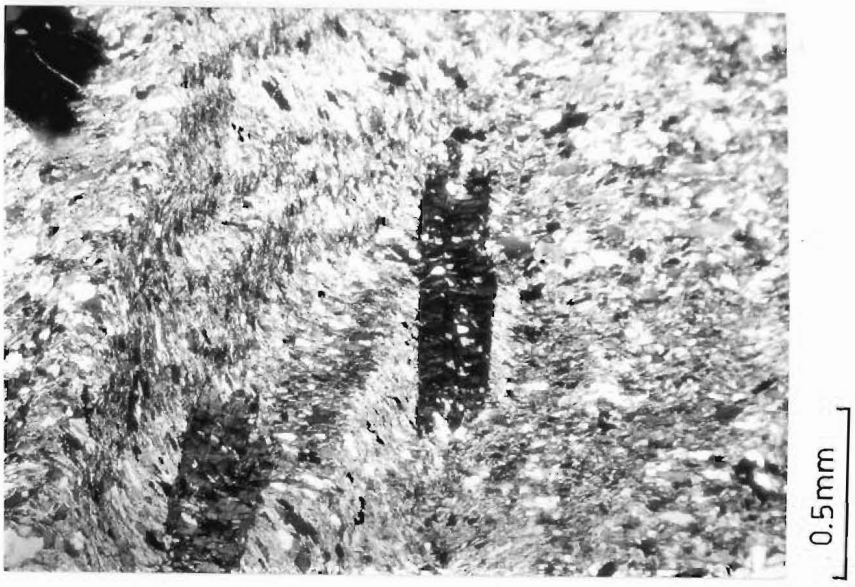

S46 567960

FIG. 35 Syn-S2 but pre-S3 chlorite . Note that the chlorite plates in the picture are kinked by F3 .

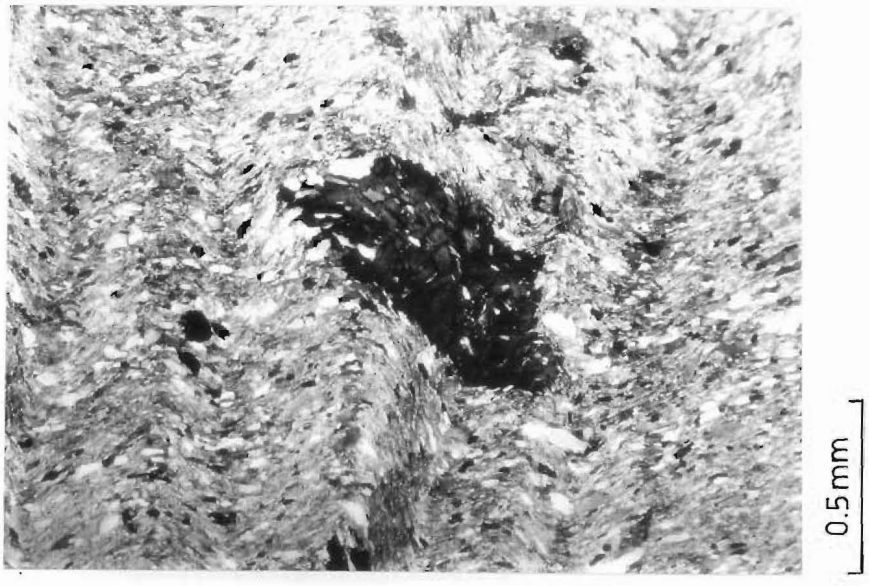

S46 567960

FIG. 36 Post-S2 but pre-S3 chlorite . Note that the chlorite crystal contains part of the crest of F2 and is kinked such that its kink planes are oriented parallel to S3 .

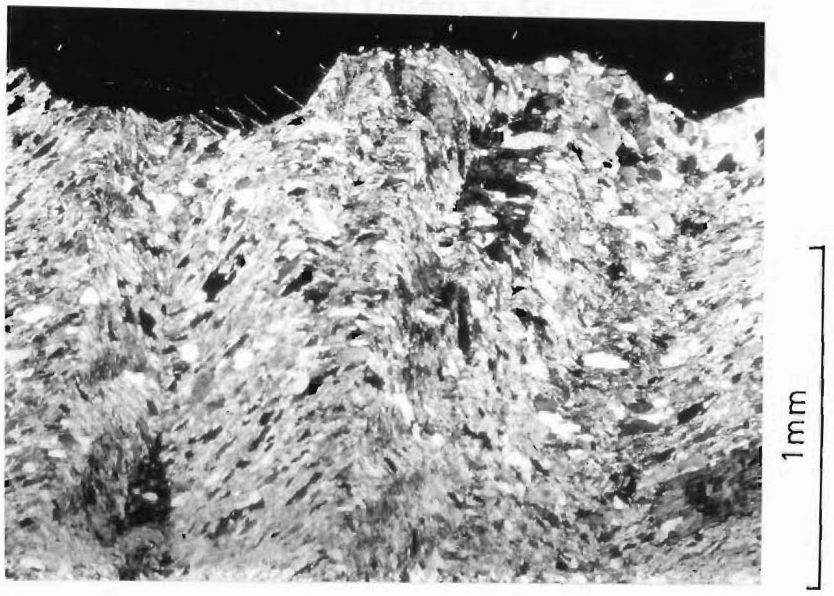

S46 567960

FIG. 37 Chlorite pseudomorphs after Syn-S1 biotite . These chlorite plates are post-S2 but pre-S3 . The relative age - post-S2 is inferred from the fact that chlorite is unlikely to be formed during the crystallization of biotite and almandine during progressive metamorphism . The pre-S3 age is inferred from the fact that the chlorite plates are affected by F3 .

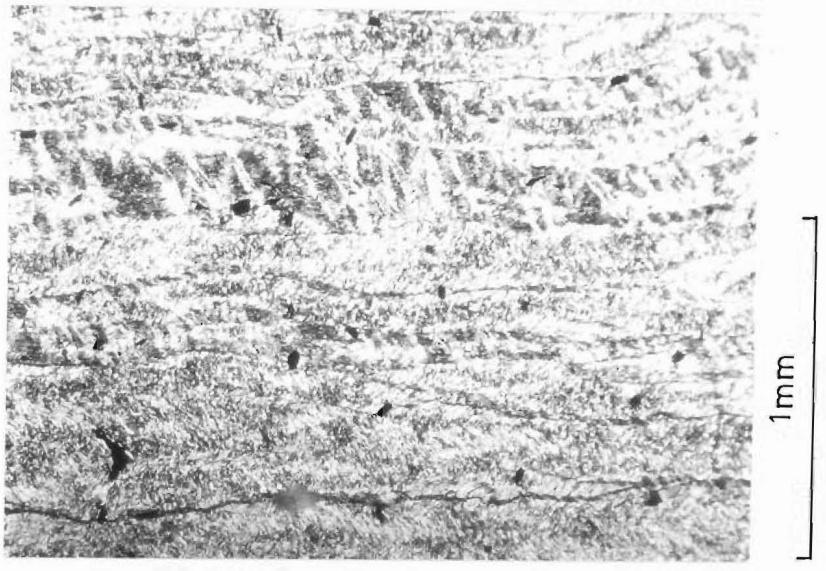

S46 617059

FIG. 38 Syn-S1 but pre-S2 muscovite, and syn- to post-S2 but pre-S3 muscovite . Note that the latter is aligned parallel to the axial plane (S2) of the crenulated schistosity (S1), and is deformed by F3 .

Epidote-clinozoisite.

The elongate epidote-clinozoisite in sample UC 5816 is folded by F2. In addition layers of elongate epidote-clinozoisite parallel to S1 are deformed by F2, hence indicating that the mineral is syn- to post-S1 but pre-S2.

Calcite.

Like the previous mineral, layers of elongate calcite aligned parallel to S1 are deformed by F2, thus suggesting that this mineral is syn- to post-S1 but pre-S2. In specimen UC 5728, elongate calcite oriented parallel to S2 indicates that this generation of calcite is syn- to post-S2. The calcite pseudomorphs wrapped by S2 in thin section UC 7764c , date this calcite as syn- to post-S2 also.

Quartz.

The elongate quartz parallel to S1 is syn-S1. The granoblastic elongate quartz parallel to S1 and folded by F2 is pre-S2. In specimen UC 7651a, the relatively unstrained and polygonal quartz in the pressure-shadows of almandine porphyroblasts is syn- to post-S2. Although only two distinct groups of quartz are recognised, i.e. pre-S2, and syn- to post-S2, it is probable that quartz is constantly formed during regional metamorphism as the mineral is susceptible to recrystallization.

Fig. (30) summarizes the time relations of mineral crystallization to deformation during regional

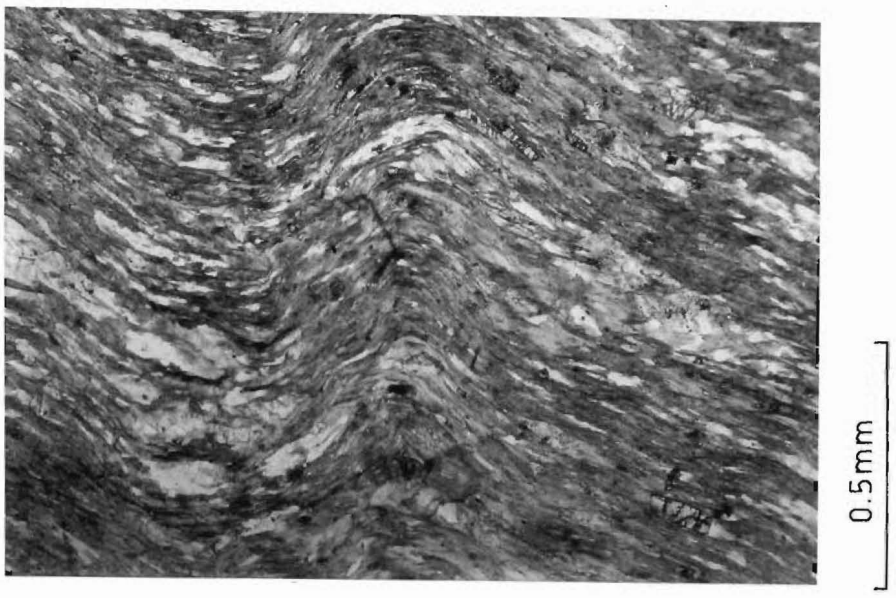

S46 648108

FIG. 39 Syn-S1 but pre-S2 epidote-clinozoisite . Note that trains of elongate epidote-clinozoisite crystals (the high relief mineral) are 'folded' by F2 .

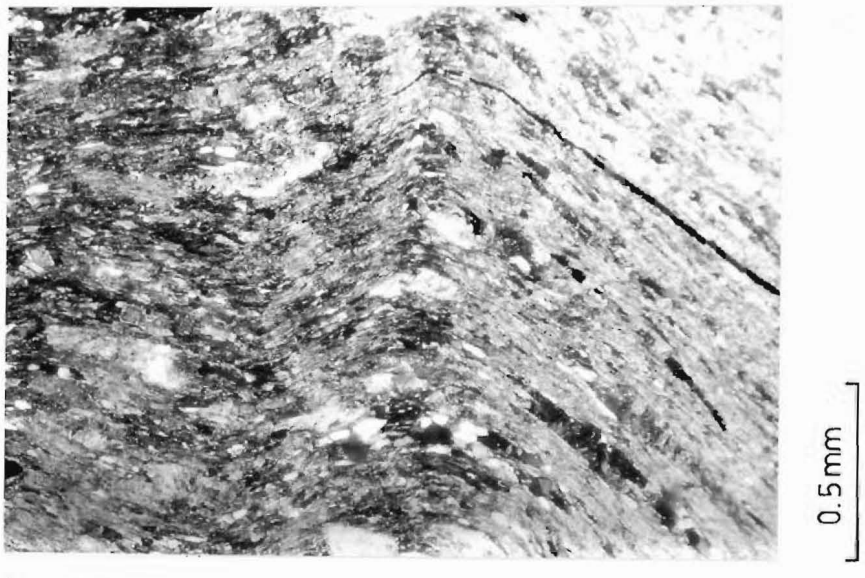

S46 648108

FIG. 40 Syn-S1 but pre-S2 calcite . Note the grain of calcite (elongate-shaped) in the centre of the picture is folded by F2 .

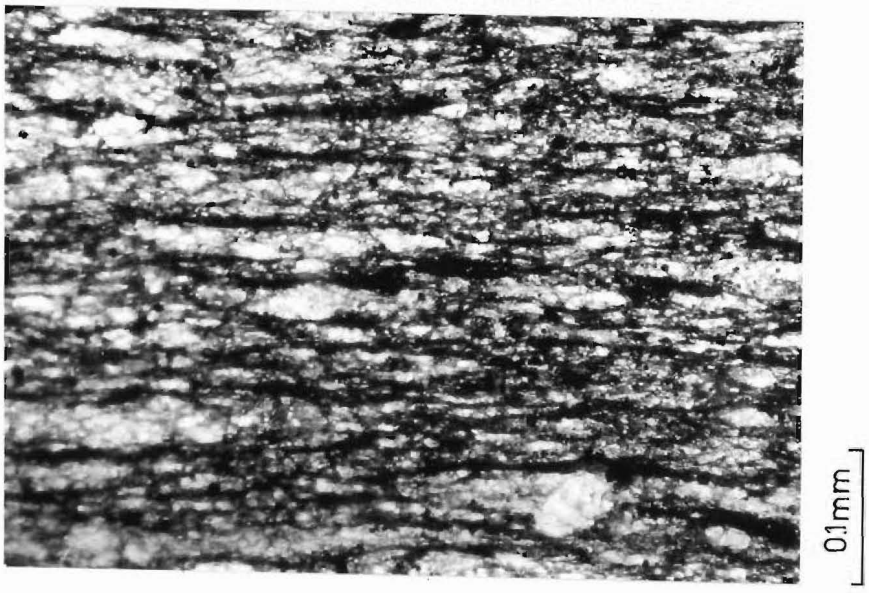

S46 702081

FIG. 41 Syn- to post-S2 calcite . The elongate calcite crystals are aligned parallel to S2 .

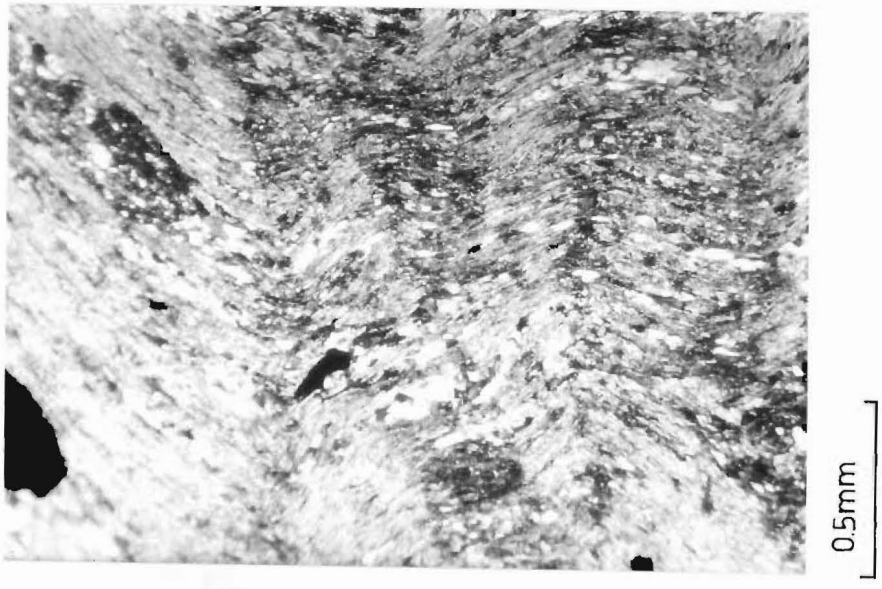

S46 648108

FIG. 42 Syn-S1 but pre-S2 quartz . Note that layers of polygonal-elongate quartz are folded by F2 .

metamorphism.

TEXTURAL CHANGES:

iii) IN LIMESTONE

Thin section examination of the rock from north of Lake Daniells, 1 km east of the Maruia Bridge, Marble Hill, and 200 m south-west of Springs Junction shows that 1) recrystallization has obliterated all the texture of sedimentary calcite, and 2) the present calcite texture varies with metamorphic grade. In the lower greenschist facies, the limestone is composed of interlocking calcite grains with irregular boundaries, whereas in the middle and upper green schist facies, the same lithology is made up of polygonal calcite. The latter observation is consistent with that seen in marble foumed in conditions of high temperature and low stress (Spry 1969, p. 267).

The recrystallised calcite is twinned (deformation origin), and displays dimensional preferred orientation, and occasional kinks as observed in specimen UC 5742 from Marble Hill. According to Spry (1969, p. 267), these textures indicate that the calcite is pre-tectonic.

iv) IN MARL

In the quartz-albite-muscovite-chlorite subfacies, the clay minerals are destroyed, forming sericite with preformed orientation very nearly parallel to bedding. Although the planar fabric is distinct in thin sections,

it is not obviously visible in hand specimens. Muscovite and chlorite crystals are also aligned, and like sericite the preferred orientation is very nearly parallel to bedding. Quartz recrystallization is not advance. Consequently, much quartz retains its original clastic texture. Calcite occurs as blebs, some of which are oriented parallel to the foliation. In specimen UC 5728, the elongate calcite is aligned parallel to axial plane-cleavage (S2), and Mg-chlorite, originally as flakes are bent and kinked, forming pseudo-porphyroblasts (see Fig. 43). Bedding here is distorted by microfolds, and slippage on axial planes.

With increased metamorphic grade to the quartz-albite-epidote-biotite, and quartz-albite-epidote-almandine subfacies, the marl is completely reconstituted. The green biotite which according to Deer, Howie, and Zussman (1965) implies a Ti/Fe^{3+} ratio less than 1, is oriented so as to form the schistosity. Tremolite-actinolite, epidote-clinozoisite, albite/sodic-oligoclase, calcite, and quartz are randomly oriented and homogeneously distributed in the marl. Except for the first two minerals which occur as columnar crystals and granular aggregates, the other minerals are anhedral and irregularly-sized. Unlike those plagioclase grains in the lower greenschist facies, the albite/sodic-oligoclase here is coarse-grained, and displays albite twins, and biotite inclusions.

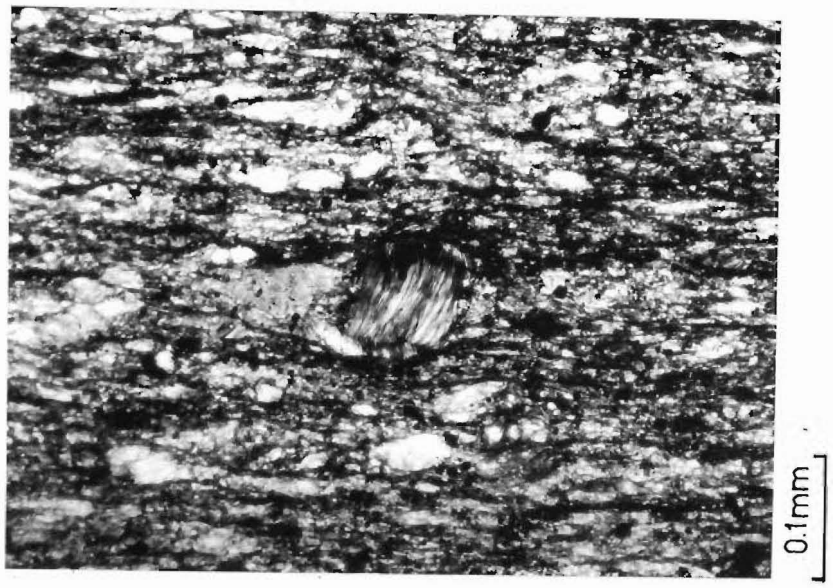

S46 702081

FIG. 43 A flake of syn-S1 chlorite which has been deformed and wrapped by S2, resulting in the appearance of a syn-tectonic mineral . Such chlorite crystals are referred to as pseudo-porphyroblasts in this chapter by the writer .

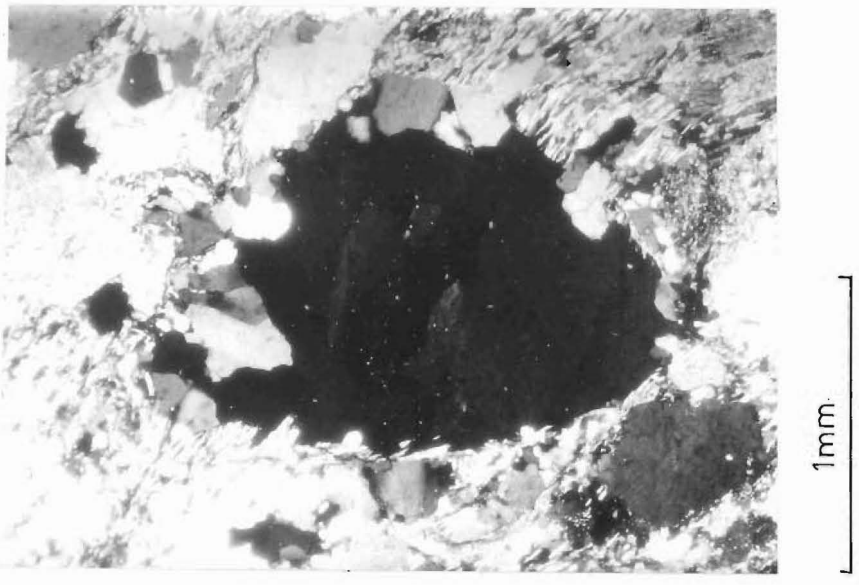

S46 608042

FIG. 44 Effects of recrystallization in quartz . Note the polygonization of the mineral at the edge of the detrital quartz grain .

v) IN SANDSTONE

In the greenschist facies, the sandstone matrix is reconstituted, and the original clastic texture is preserved to a greater or lesser extent, depending on quartz content, and grain-size of the rock. The original rock texture in fine-grained, quartzose sandstone is usually destroyed by recrystallization as shown by specimens UC 5780 and 5744. In the coarse-grained sandstone, although quartz recrystallization is somewhat advanced, the pre-existing grain texture is often partly or wholly preserved. Fig. 44 (photo) shows that the effect of quartz recrystallization is one of changes in grain-shape and reduction in grain-size. Most of the crystallised Mg-chlorite, sericite, and muscovite is oriented to form a planar fabric in the metamorphosed sandstone. This fabric is poorly developed in quartzose rocks. The albite and tourmaline associated with the platy minerals are commonly anhedral and randomly distributed in the sandstone.

With increased temperature, the original rock texture is completely destroyed as in sample UC 7653a muscovite, biotite, and elongate quartz are strongly aligned, forming or schistosity. Irregularly shaped garnets sometimes co-exist with these minerals.

vi) IN QUARTZITE

Like limestone, recrystallization has obliterated the original rock texture(s), and the new texture varies with metamorphic grade. In the greenschist facies, the

quartzite is composed of interlocking quartz with irregular grain boundaries, and aggregates/layers of polygonal quartz. With increased temperature and possibly pressure, the rock is made up of granoblastic-elongate quartz. The crystals here are dimensionally oriented parallel to schistosity, and possess irregular grain boundaries. These features together with the common occurence of strained quartz suggest that the recrystallization of the quartzite is syn-tectonic.

vii) IN VOLCANOGENIC SEDIMENT AND CONGLOMERATE

The textural changes in these lithologies are restricted to those in the quartz-albite-muscovite-chlorite subfacies. The degree of retention of recognisable relict features in these rocks is dependent on 1) grain- or pebble-size, 2) the amount of matrix, and 3) composition of matrix, and clasts/pebbles. Except for the coarse-sized and mafic poor pebbles in the conglomerate, the original textures in the volcanogenic sediment and conglomerate with mafic-rich matrix, are destroyed by recrystallization and formation of new minerals. In conglomerate with mafic-poor matrix and pebbles, the original rock texture is more or less preserved, even though most of the pebbles are sericitized. The matrix is reconstituted, with abundant sericite and chlorite. In specimen UC 5789, microcline and quartz are recrystallised to granular or polygonal aggregates.

viii) IN MAFIC INTRUSIVE

The effect of regional metamorphism on the original rock texture is basically that which is caused by crystallization of new minerals, i. e. new textures are superimposed on pre-existing textures. Epidote-clinozoisite, the most common mineral occurs as granular aggregates or/and bladed crystals. chlorite, sericite, and calcite occur in forms which are typical of replacement minerals (see fig. 45 a, b, & c). Chlorite pseudomorphs after pyroxene or amphibole are observed in specimen UC 5810, near Springs Junction, and relic aegirine-augite phenocrysts are seen in sample UC 5802, near Mt. Baldy. In the latter, many of the andesine laths are sericitized. Except in thin section UC 5804, the chlorite associated with epidote-clinozoisite is of the Mg-variety. Such a mineral association may be explained by the crystallization of epidote-clinoisite causing a depletion of iron available for other minerals in the system. The recrystallised quartz is polygonal-shaped.

With increased temperature, near Springs Junction, andesine is recrystallised to granular aggregates. The rocks here are generally more schistose than those in the vicinity of Thompson's Flat.

III/4 METAMORPHIC FACIES/GRADES-TEMPERATURE/PRESSURE OF METAMORPHISM:

A. STAUROLITE-ALMANDINE SUBFACIES

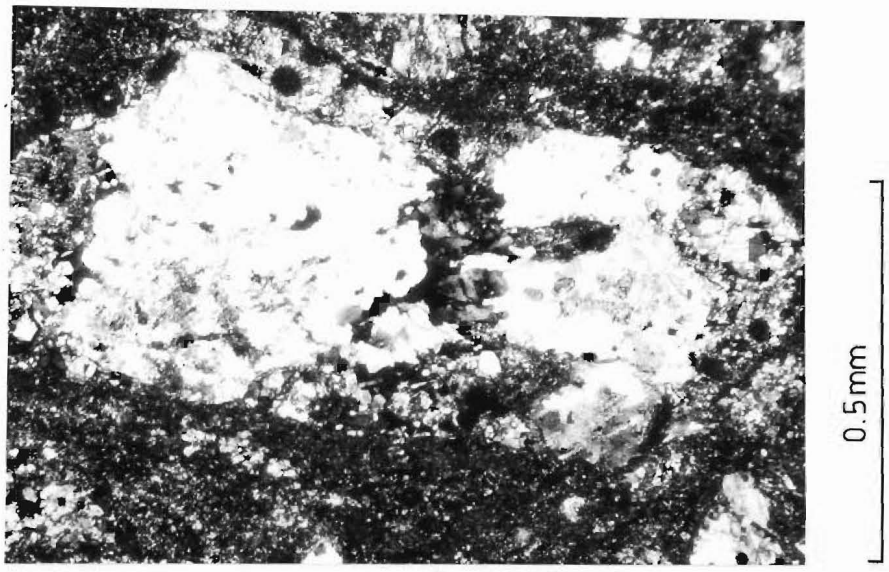

S46 613019

FIG. 45a Epidote-clinozoisite (high relief mineral), calcite (white mineral), and chlorite (light grey mineral) replacing a feldspar lath .

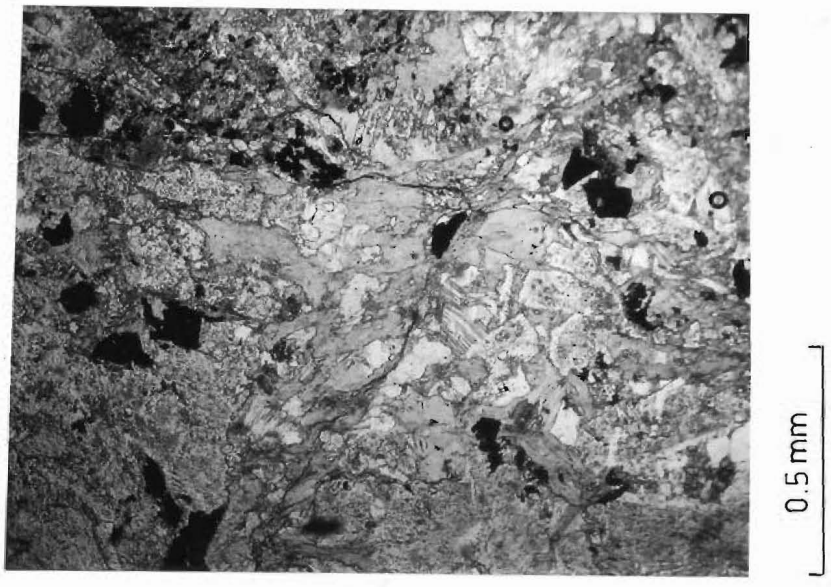

S46 722085

FIG. 45b Chlorite (light grey mineral) replacing feldspars and the matrix .

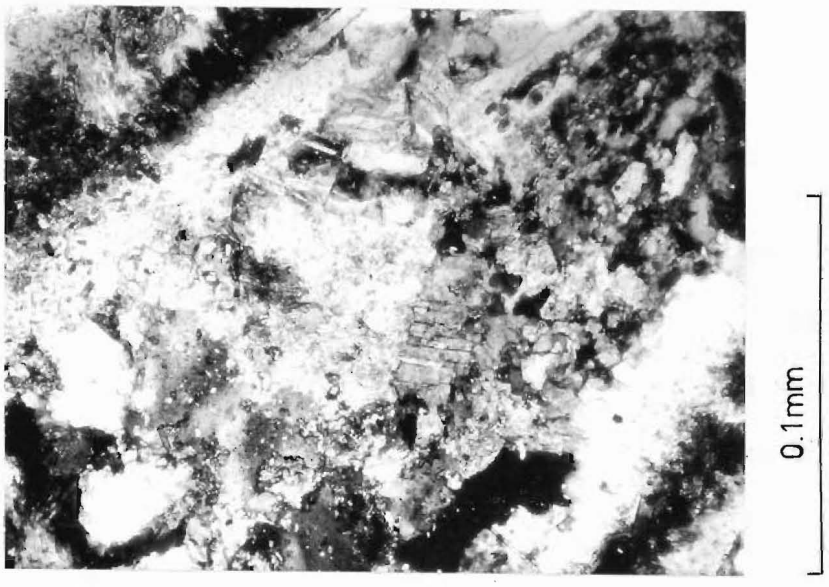

S46 613019

FIG. 45c Calcite replacing a feldspar crystal in igneous rocks .

The mineral assemblages in the pelitic schists of the Lower Brown Grey River, and Palmer's Flat are staurolite + almandine + biotite + muscovite + quartz + plagioclase (very rare), and almandine + biotite + muscovite + quartz. According to Winkler (1967, p. 107-110), these mineral assemblages unaccompanied by cordierite, andalusite, or kyanite indicate that the schists are of the Barrovian-type staurolite-almandine subfacies.

The formation of staurolite unaccompanied by cordierite restricts the minimum metamorphic temperature and pressure to not less than 550° C and 5 kb (Winkler 1974, p. 236). Garnets enriched in almandine (73%) and impoverished in spessartine (5%) also indicate that the minimum pressure is not less than 4-5 kb (Winkler and Hirschberg 1968, p. 17-42). At this pressure, the reaction of staurolite + muscovite + quartz, forming sillimanite is nearly 650° C which is also the temperature of anatexis. As staurolite is well preserved in the schist, and the co-existing muscovite is abundant, it is probable that the maximum temperature is not greater than 650° C. The absence of K-feldspar co-existing with sillimanite, and migmatitic gneisses support this suggestion. Fig. (46) shows that with increased pressure e. g. 8 kb, the maximum temperature is restricted to not greater than 620° C. According to Turner's phase diagram (1968, p. 114) showing the stability field of polymorphs of Al_2SiO_5, the intersection of the kyanite-sillimanite phase boun-

dary with curves of cordierite-staurolite formation, and anatexis also show that the minimum P-T condition is greater than 4-6 kb in the temperature range of 550° to 640° C.

The inferred temperature-pressure of metamorphism of the staurolite-almandine subfacies is shown in Fig. (46).

B. QUARTZ-ALBITE-EPIDOTE-BIOTITE, AND QUARTZ-ALBITE-EPIDOTE-ALMANDINE SUBFACIES

In the vicinity of Palmer's Bend, the mineral assemblages in the marl, and pelite are epidote-clinozoisite + biotite + tremolite-actinolite + albite/sodic-oligoclase quartz + calcite, and biotite + muscovite + quartz, respectively. In the faulted block of biotite schist near Trig. GA, the mineral assemblage is biotite (green) + epidote-clinozoisite + calcite + quartz. The nearby intrusive contains epidote-clinozoisite + biotite (green) + quartz + calcite + albite. Following Winkler's classification (1967), the occurence of biotite in the schist unaccompanied by almandine, cordierite, andalusite, and staurolite suggests that the rock belongs to either the Abukuma-type or Barrovian-type greenschist facies. However, as Palmer's Bend is only 3 km from the Barrovian-type schist known in the Lower Brown Grey Valley, and since the rocks from both localities display similar deformation texture associated with the regional metamorphism, it is likely that the schist and marl at

Palmer's Bend are members of the Barrovian-type greenschist facies. The described mineral assemblages are consistent with those found in the quartz-albite-epidote-biotite, and quartz-albite-epidote-almandine subfacies. Similarly, the body of schist near Trig. GA is classified as Barrovian-type greenschist facies. As metamorphic hornblende is absent in the nearby igneous rocks, this faulted block of schist is likely to belong to the quartz-albite-epidote-biotite subfacies.

At Palmer's Bend the mineral assemblages in the marl and pelite suggest that the metamorphic temperature is between 450° to 530° C; the lower limit is defined by the entry of biotite, and the upper limit is indicated by the absence of 1) almandine, and 2) actinolite and epidote-clinozoisite reacting to form hornblende in marl. The absence of the reaction $CaCO_3 + SiO_2 \rightleftharpoons CaSiO_3 + CO_2$, forming wollastonite in the marl is in agreement with the suggested temperature range because wollastonite is never formed in marl metamorphosed at 400° to 500° C (Winkler 1974, p. 126). Although there is no direct indication of metamorphic pressure, it may be assumed that the minimum pressure at Palmer's Bend is similar to that determined in the Lower Brown Grey Valley and Palmer's Flat; the reasons are as outlined in the preceeding paragraph. In addition, it has been well documented by Turner (1968) that in many terrains of regional metamorphism, temperature was increased, while pressure remained nearly constant. Fig. (47) shows the estimated P-T conditions during regional metamorphism.

C. QUARTZ-ALBITE-MUSCOVITE-CHLORITE SUBFACIES

North of Springs Junction and Marble Hill, the mineral assemblage in the various lithologies are as follows.

Igneous rocks (mafic)	:	epidote-clinozoisite + chlorite + quartz + calcite ± sericite ± tremolite + plagioclase (albite ?).
Pelite	:	sericite (predominant) + muscovite + quartz ± chlorite ± calcite ± plagioclase (albite) ± tourmaline.
Marl	:	sericite + calcite + quartz ± muscovite ± Mg-chlorite ± albite.
Siliceous limestone	:	calcite + sericite + quartz + muscovite ± Mg-chlorite.
Sandstone	:	muscovite + sericite + quartz + chlorite + albite ± tourmaline.
Volcanic sediment & conglomerate	:	epidote-clinozoisite + quartz + chlorite + albite ± zoisite ± calcite. sericite + chlorite + quartz ± muscovite ± albite (?).

The absence of lawsonite, jadiete, glaucophane, and aragonite in the above lithologies indicates that the rocks belong to the greenschist facies. The lack of biotite in the pelite limits the greenschist facies to that of the Barrovian-type quartz-albite-muscovite-chlorite subfacies. The breakdown of hornblende in the mafic intrusive agrees with this classification (Winkler 1974, p. 165).

The absence of laumontite, lawsonite, prehnite, and aragonite in the mafic intrusive, although providing no information on metamorphic pressure, indicates that the temperature is at least 350° C (see Fig. 47). This minimum temperature is consistent with the temperature range of 300° to 380° C suggested by the complete breakdown of clay minerals in pelite, forming sericite and other platy minerals (see Miyashiro 1973, p. 199). As biotite and stilpnomelane are lacking in pelite, the upper temperature limit may be deduced as 420° to 480° C or less. The absence of Al_2SiO_5 species forming from pyrophyllite in the pelite agrees with this suggestion (see Miyashiro 1973, p. 199). This maximum temperature is further restricted to 350° to 400° C by the absence of epidote-clinozoisite in calcareous pelite (Winkler 1974, p. 138).

Like the critical reaction curves in the middle and upper greenschist facies, the reaction curves here do not intersect, and hence information on metamorphic pressure is not available. However, assuming that metamorphic pressure is the same through the thesis

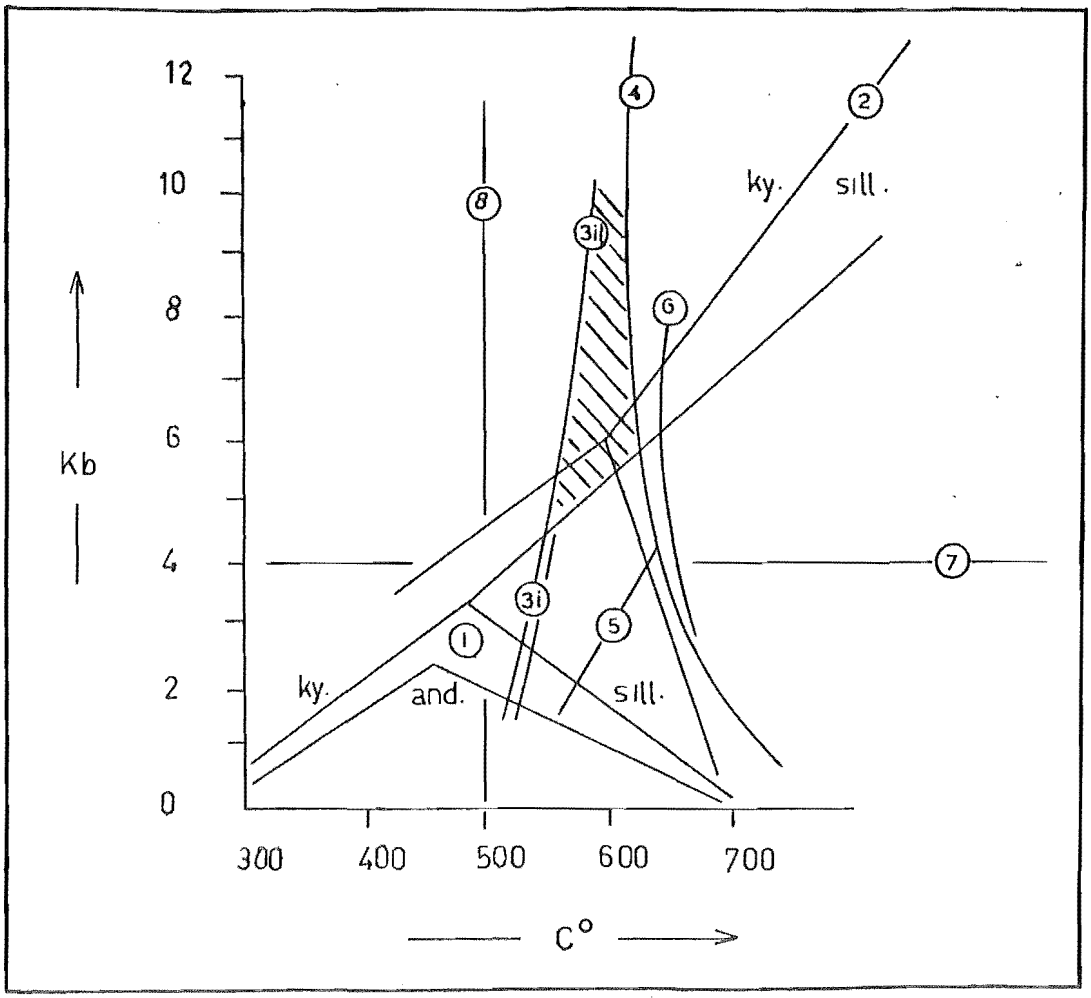

FIG. 46 1) Al_2SiO_5 diagram after Turner (1968, p.114) .

2) Al_2SiO_5 diagram after Winkler (1973, p.236) .

3i) Entry of cordierite and staurolite from the left handside .

3ii) Entry of staurolite from the left handside (Winkler 1973, p. 236) .

4) Anatexis (Tuttle & Bowen 1958 ; Merrill et al. 1970) .

5) Breakdown of staurolite on the right handside : staurolite + muscovite + quartz = Al_2SiO_5 + biotite (Winkler 1973, p.236) .

6) Breakdown of muscovite on the right handside : muscovite + albite + quartz + H_2O = Liquid + Al_2SiO_5 .

7) Minimum pressure for the stability of almandine (Winkler and Hirschberg 1968, p.17-42) .

8) Minimum temperature for the stability of almandine (Miyashiro 1973, p.215) .

The shaded area indicates the probable P-T conditions during regional metamorphism in the vicinity of the Lower Brown Grey River .

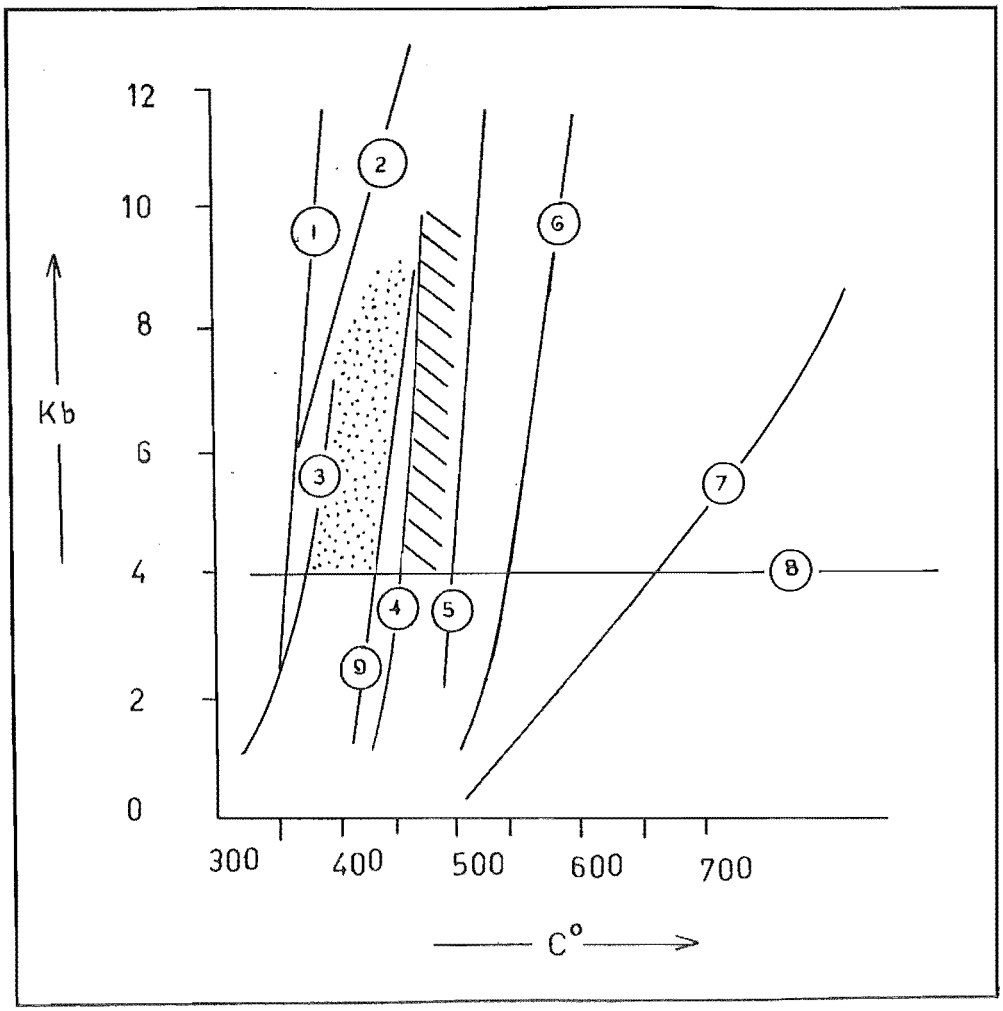

FIG. 47 1) Pumpellyite + chlorite + quartz = zoisite + actinolite on the right handside (Winkler 1973, p.232) .

2) Lawsonite-out on the right handside (Winkler 1973, p.232) .

3) Complete reconstitution of clay minerals on the right handside : Kaolinite + quartz = pyrophyllite + H_2O (Miyashiro 1973, p.199).

4) Stilpnomelane-out, and biotite-in on the right handside (Winkler 1973, p.232) .

5) Hornblende-in on the right handside (Winkler 1973, p.232) .

6) Staurolite + cordierite -in on the right handside (Winkler 1973, p.236) .

7) Wollastonite-in (in marl) (Miyashiro 1973, p.275) .

8) The minimum pressure limit established in Fig. 46 .

9) Breakdown of pyrophyllite, and entry of Al_2SiO_5 on the right handside (Miyashiro 1973, p.199) .

The stipled area indicates the probable P-T conditions of regional metamorphism in the country north of Springs Junction and Marble Hill . The shaded area shows the probable P-T conditions in the vicinity of Palmer's Bend .

area during regional metamorphism, the minimum pressure is 4 to 6 kb. The inferred P-T conditions are shown in Fig. (47).

D. CLASSIFICATION ACCORDING TO WINKLER (1974)

Fig. (48) shows the progressive mineralogical changes in the Lower Paleozoic rocks of Springs Junction district. The same diagram also shows the classification of metamorphic rocks according to the three different concepts; 1) metamorphic zones defined by the occurence of index minerals as proposed by Barrow during the turn of the 19th century, 2) metamorphic facies as outlined by Winkler in 1967, and 3) metamorphic grades as defined by Winkler in 1974. The boundaries of all these metamorphic divisions may or may not coincide as shown in the mentioned figure.

Following Winkler's scheme of metamorphic division (1974), the schists in the Lower Brown Grey Valley, and Palmer's Flat were formed in conditions of medium grade metamorphic temperature and pressure. The criteria are as follows:

1) breakdown or absence of chlorite in the presence of muscovite.

2) formation of almandine and staurolite

3) abundant muscovite co-existing with quartz and plagioclase (rare) which indicates that metamorphism is not high grade.

At Palmer's Bend, and areas further north, the rocks were metamorphosed in conditions of low grade metamorphic temperature and pressure. The indicators of this metamorphic grade are;

1) absence of laumontite, lawsonite, pumpellyite, glaucophane, and prehnite.

2) presence of epidote-clinozoisite.

1) + 2) indicate the start of low metamorphic grade.

3) absence of almandine which limits the P-T conditions to that below the medium grade metamorphism.

Such a classification of metamorphic rocks when compared to that based on the facies concept is less cumbersome and confusing. Although this scheme is preferred by the writer, the use of the facies classification is retained for the purpose of discussion and comparison with past work.

III/5 EFFECTS OF RETROGRADE METAMORPHISM

A. MINERALOGICAL CHANGES

The effect of retrograde metamorphism in very pure limestone, quartzite, and rocks of the quartz-albite-muscovite-chlorite subfacies is not significant. Where mineralogical changes associated with this metamorphism have occured, they are restricted to the pelitic rocks of the upper greenschist, and almandine-amphibolite facies. Pre-existing biotite

is partially or completely altered to Mg-chlorite. Occasionally, muscovite and chlorite are crystallised on the axial plane-cleavage (S2), as observed in specimens UC 5730 and UC 7764c from Palmer's Flat and the Lower Rahu River. Of the three minerals, chlorite is the most abundant.

B. TEXTURAL CHANGES

Where chloritization has occured, the earlier rock texture is preserved. In the schists of the upper greenschist, and almandine-amphibolite facies, the crystallization of platy minerals is structurally controlled. Sometimes, the crystallization of chlorite is not mimetic; these crystals are irregularly-shaped and randomly oriented as described in III/3Bii. The retrograde chlorite in thin section UC 5730 occurs as coarse-grained poikiloblastic plates, and/or pseudomorphs after pre-existing biotite.

III/6 CORRELATION AND AGE OF REGIONAL METAMORPHISM

The metamorphosed pelitic rocks and quartzite which underlie the Sluice Box Formation (Mt. Arthur Formation) can be correlated with the Pikikiruna Schist, east of the Takaka Valley on the basis of similar metamorphic mineral assemblages, structure and stratigraphic position. The metamorphism which

produced these schists which commonly contain almandine is considered by previous workers as related to the Cretaceous (Rangitata) granite emplacement (Ghent 1968; Grindley 1971; Wodzicki 1972). This view is currently shown to be erroneous by Shelley (1975) who pointed out that if the low pressure Cretaceous (Rangitata) metamorphism had produced the schists, andalusite should appear before almandine, which it does not. Shelley has argued that the regional metamorphism in such a case is likely to related to earlier deformation during the Tuhua Orogeny (Devonian-Carboniferous). The thermal effect (probably Cretaceous, see Chap. VI) superimposed on already existing almandine schist in the vicinity of the Lower Brown Grey River supports this suggestion. Clearly, to substantiate any opinions on the age of metamorphism, more radiometric work is needed on the schists and the intruding granites.

III/7 SUMMARY

The effects of regional metamorphism in the Lower Paleozoic rocks of Springs Junction district are as follows.

i) Pelite is metamorphosed to slate, biotite schist, or staurolite-almandine schist, depending on its location relative to the metamorphic zones.

ii) Limestone is converted to marble; the rock in the upper greenschist facies is composed of polygonal calcite.

iii) Marl or calcareous pelite is metamorphosed

to slate or calcareous biotite schist, depending on its position relative to the metamorphic zones.

iv) Sandstone is metamorphosed to weakly schistose sandstone or quartz-mica schist, depending on content of pelitic impurity and degree of metamorphism.

v) Sedimentary quartzite is recrystallised; the quartz grains are dimensionally oriented parallel to schistosity in the staurolite-almandine subfacies.

vi) Volcanogenic sediment and conglomerate are metamorphosed to weakly schistose meta-sediment and meta-rudite. These metamorphic rocks are restricted to the areas near Upper Station Creek, west of Thompson's Flat.

vii) Mafic intrusive is changed to meta-intrusive of the greenschist facies. The majority of mafic minerals are altered to chlorite or/and sericite.

The mineral assemblages in the metamorphic rocks indicate that regional metamorphism ranges from the quartz-albite-muscovite-chlorite to the staurolite-almandine subfacies, at temperature of 350° to 640° C, and pressure of not less than 4 to 6 kb. Detailed textural studies in pelite reveal three groups of minerals.

i) Biotite, chlorite, muscovite, quartz, calcite, and epidote-clinozoisite which are probably syn-S1 but definitely pre-S2,

ii) Staurolite, almandine, biotite, and possibly chlorite, muscovite, quartz, and calcite which are syn-S2,

and iii) Chlorite, muscovite, and quartz which are post-S2 but pre-S3.

The platy minerals in iii) are associated with retrograde metamorphism.

The lack of andalusite in the mineral assemblages and the later thermal effect (see Chap. VI) superimposed on already existing almandine schist suggest that the regional metamorphism is related to the Tuhua Orogeny, and its age is Devonian-Carboniferous.

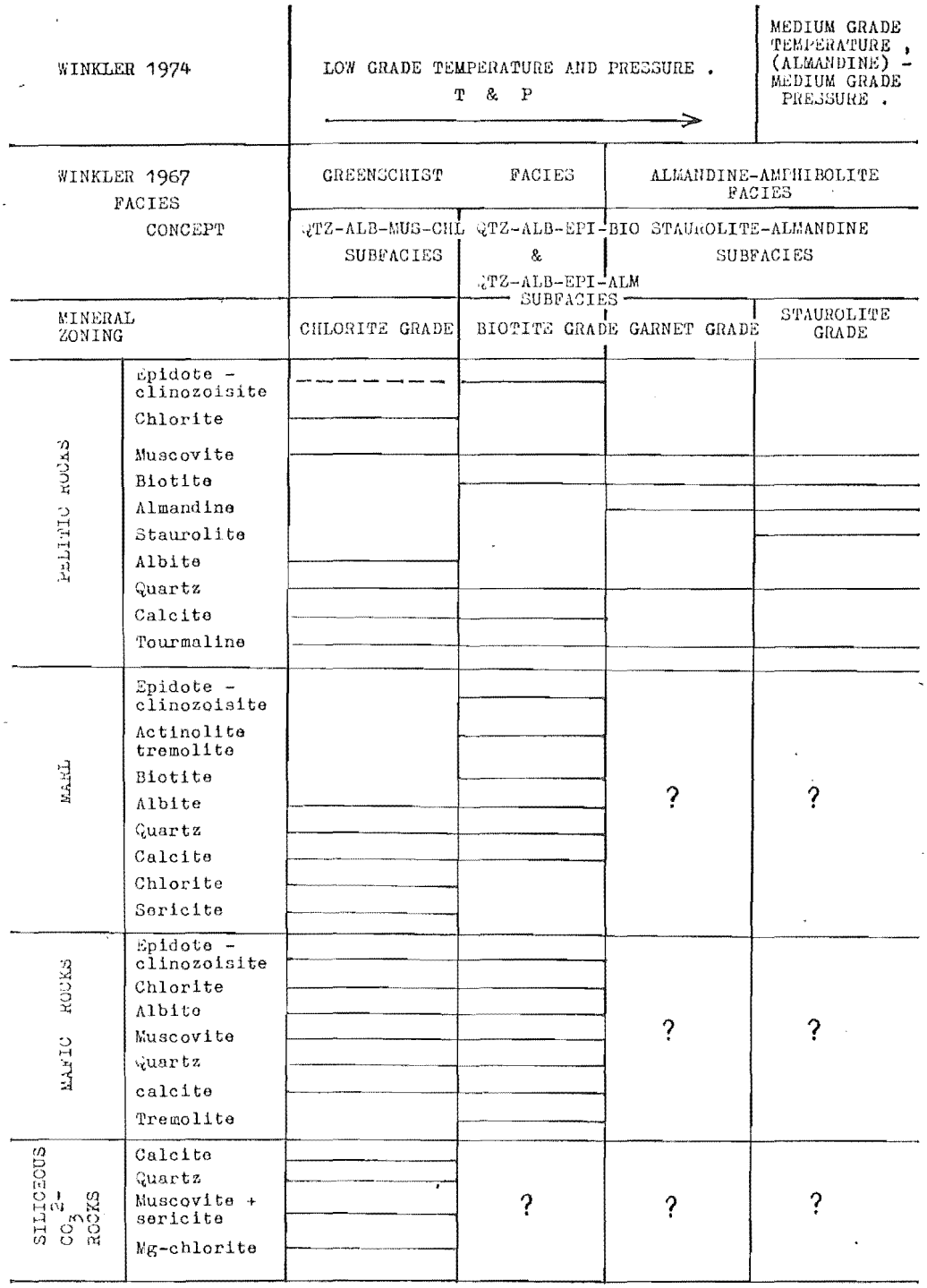

FIG. 48 Diagram shows the mineral assemblage in the different lithologies, and the progressive mineralogical changes with increased T and P in the district of Springs Junction, west of the New Zealand Alpine Fault .

CRYSTAL	1	2	3	4	5	6
SiO_2	37.46	35.20	37.77	37.21	35.30	35.20
Al_2O_3	20.03	NA	20.16	19.83	NA	NA
TiO_2	1.48	1.48	1.48	1.57	1.47	1.49
FeO	17.34	17.42	17.24	17.15	16.52	16.93
MnO	0	0	0	0	0	0
MgO	11.42	12.33	11.53	11.62	12.57	12.75
CaO	0.01	0.02	0	0.02	0.01	0.01
TOTAL wt. %	87.74		88.18	87.40		

TABLE 6 Six partial analyses (microprobe) of biotite in schist of locality B1. Na_2O , K_2O , and H_2O are not analysed.

CRYSTAL	1	2	3	4	5	6
SiO_2	44.77	48.86	45.98	39.84	39.71	41.26
Al_2O_3	25.78	34.52	35.06	NA	NA	NA
TiO_2	0.34	0.34	0.35	0.37	0.38	0.34
FeO	0.87	1.04	0.75	0.93	0.71	0.80
MnO	0	0	0	0	0	0
MgO	0.68	0.79	0.60	0.79	0.74	0.76
CaO	0.06	0.01	0.02	0.02	0.02	0
TOTAL wt. %	72.49	85.55	82.75			

TABLE 7 Six partial analyses (microprobe) of muscovite in schist of B1. Na_2O , K_2O , and H_2O are not analysed .

CRYSTAL	1	2	3
SiO_2	29.08	29.60	29.24
Al_2O_3	58.22	63.44	63.74
TiO_2	0.78	0.74	0.86
FeO	10.32	13.33	13.22
MnO	0.40	0.33	0.24
MgO	1.35	1.90	2.00
CaO	0	0	0
TOTAL wt. %	100.16	109.35	109.30

TABLE 8 Three complete analyses (microprobe) of staurolite in schist of locality B6 .

CHAPTER IV

CONTACT OR THERMAL METAMORPHISM IN THE THOMPSON'S FLAT, SLUICE BOX, AND ALFRED FORMATIONS IN THE SPRINGS JUNCTION DISTRICT, WEST OF THE NEW ZEALAND ALPINE FAULT.

IV/1 MAPPING OF THE ROCKS AFFECTED BY CONTACT METAMORPHISM

Only a few localities in the thesis area, east of the Rahu Fault show signs of contact metamorphism by the Victoria Range Granite. Because of limited exposures and thick vegetation, accurate mapping of these rocks is impossible. In the vicinity of the Lower Brown Grey River, the contact aureole is crudely mapped as parallel to the granite-metasediment contact, west of the Rahu Fault. The width of the hornfels zone is estimated as 200 m in the Lower Brown Grey River, and the zone can be mapped for at least 500 m parallel to the granite contact. As this contact aureole is fault bounded on the western side, it is conceivable that the original width of the hornfels zone is greater than 200 m.

At about 1 km south of the Brown Grey River bridge, the schist (e. g. UC 5730) is not significantly recrystallized. The effect of contact metamorphism here is the formation of biotite and chlorite parallel to S3. The mimetic crystallization of platy minerals, and the

lack of extensive recrystallization in the schist indicate that the influence of contact metamorphism is weak.

However, in the areas 1.5 km north-east of Lake Daniells, contact metamorphism similar to that in the Lower Brown Grey River is observed. Andalusite/cordierite occurs as porphyroblasts in the pelite near the Lockington Diorite (see Farmer's map, unpublished M.Sc. thesis, 1967). This thermal aureole together with those associated with the intrusion of Lake Daniells Granite, and Lockington Diorite have not been mapped due to the lack of time, and the difficult terrain.

IV/2 EFFECTS OF CONTACT METAMORPHISM

Except for pelite and some sandstones, the other lithologies of the Lower Paleozoic formations are apparently unaffected by the Victoria Range Granite. The following discussion is restricted to 1) the pelite of the staurolite-almandine subfacies in the Lower Brown Grey River, 2) the sandstone downstream from the Sluice Box bridge, and 3) the pelite of the lower greenschist facies, 2 km east of Thompson's Flat.

A. MINERALOGICAL CHANGES:

i) IN PELITE OF THE LOWER BROWN GREY RIVER

The mineralogical development during contact metamorphism is as follows. The outer part of the aureole is characterised by the mimetic crystallization of chlorite and biotite, as seen in sample UC 5730, 1 km south of the Brown Grey River bridge. The inner part of the thermal zone is marked by the formation of quartz, biotite, muscovite, and cordierite andalusite porphyroblasts; the last two minerals are distinguished on the basis of their equidimensional or diamond shapes, and alteration products consisting of quartz + muscovite + some biotite. The common occurence of equidimensional porphyroblasts suggests that cordierite is abundant in the rock. The hornfels matrix is enriched in reddish-brown biotite and 'impoverished' in muscovite and quartz.

ii) IN THE PELITE, 2 KM EAST OF THOMPSON'S FLAT

Cordierite and muscovite are crystallised in the pelite during contact metamorphism; the latter is not distinguishable from that formed during regional metamorphism. Biotite is absent, probably due to inappropriate bulk composition.

iii) IN SANDSTONE JUST DOWNSTREAM FROM THE SLUICE BOX BRIDGE

Cummingtonite and randomly oriented biotite have been found in specimens UC 5734 and 5733. The former mineral in UC 5734 suggests contact metamorphism of the hornblende-hornfels facies.

B. TEXTURAL CHANGES:

i) IN THE PELITE OF THE LOWER BROWN GREY RIVER

The schist in the cordierite/andalusite zone is recrystallised to a tough, fine-grained, spotted hornfels, consisting of quartz, randomly oriented mica, and cordierite/andalusite porphyroblasts. The pre-existing rock texture related to regional metamorphism is obliterated. Quartz occurs as granoblastic-polygonal aggregate, and together with biotite and muscovite, form the hornfels matrix. Muscovite is generally poikiloblastic, containing quartz and biotite inclusions. Although the pre-existing rock texture is extensively destroyed by contact metamorphism, the almandine, staurolite, and tourmaline associated with regional metamorphism are preserved.

In the outer part of the aureole, chlorite and biotite are crystallised on the axial plane-cleavage (S3). Biotite is interpreted as post-chlorite because biotite is scarce and not replaced by chlorite. These platy minerals are considered as syn- to post-S3.

ii) IN THE PELITE, 2 KM EAST OF THOMPSON'S FLAT

Although recrystallisation has occurred in the pelite, the lithological layerings, i. e. alternating sandy and muddy beds are preserved. Cordierite occurs as equidimensional porphyroblasts in the muddy layers.

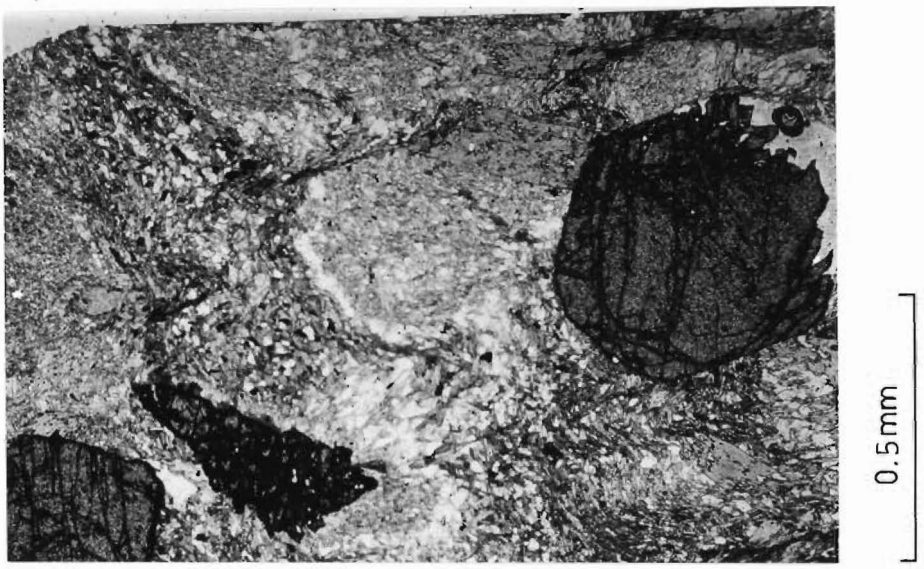

S46 557959

FIG. 49 Cordierite porphyroblasts (in the centre of the picture) replaced by fine-grained muscovite and quartz .

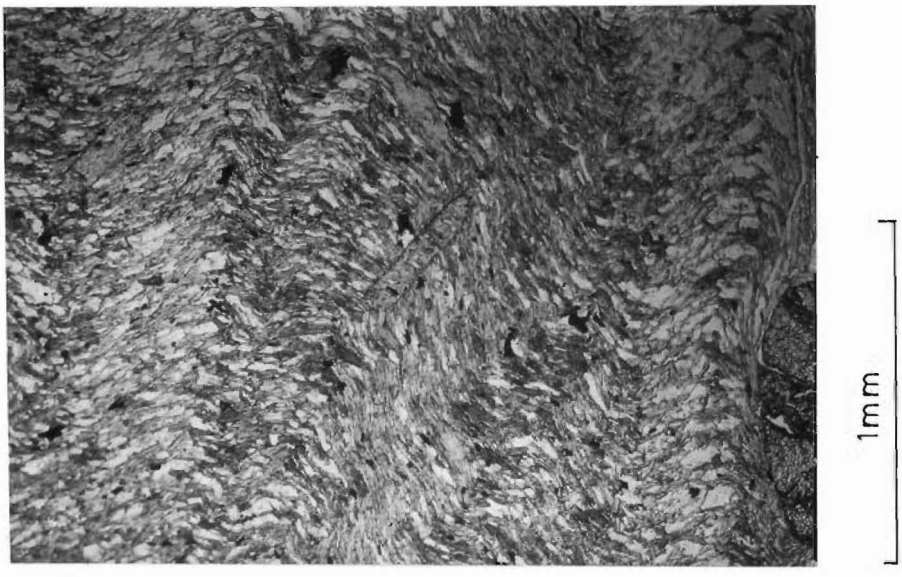

S46 567960

FIG. 50 Syn- to post-S3 chlorite . Note that the chlorite crystals are aligned parallel to S3 .

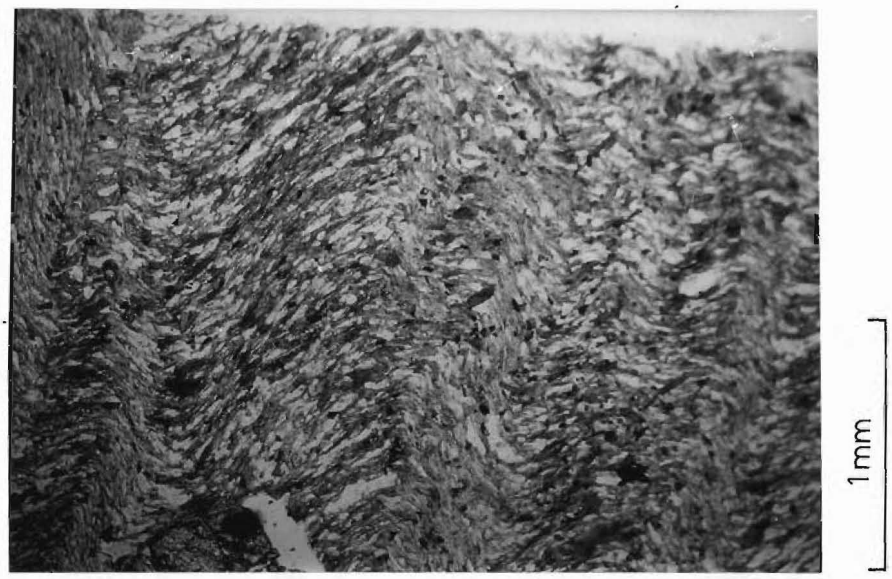

S46 567960

FIG. 51 Syn-S3 biotite . Note that the biotite plates (dark mineral) are oriented parallel to S3 .

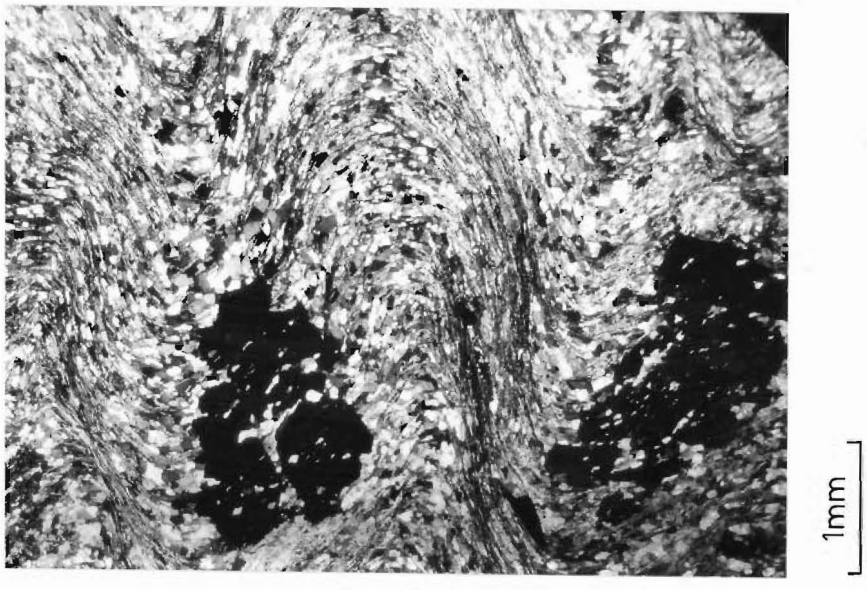

S46 557959

FIG. 52 The crenulated almandine-staurolite schist which is not hornfelsed (specimen UC 7654g) .

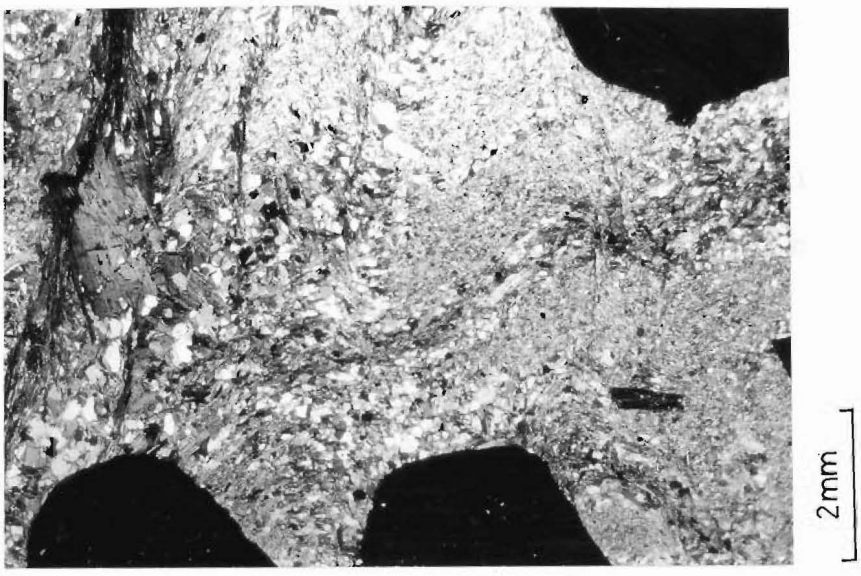

S46 557959

FIG. 53 The crenulated schist which has been hornfelsed . Note that the reconstitution of the matrix has not completely obliterated the pre-existing crenulated schistosity (S1) .

The quartz and fine-grained muscovite associated with contact metamorphism are not distinguishable from those crystallised during regional metamorphism.

iii) IN THE SANDSTONE DOWN STREAM FROM THE SLUICE BOX BRIDGE

Cummingtonite occurs as coarse-grained radiated aggregates in specimen UC 5744, and biotite occurs as randomly oriented grains in UC 5733. As with the preceeding case, quartz and muscovite formed during contact metamorphism are not distinguishable from those crystallised during regional metamorphism.

IV/3 METAMORPHIC FACIES - TEMPERATURE/ PRESSURE OF METAMORPHISM

The mineral assemblage in the hornfels of the Lower Brown Grey River is andalusite/cordierite + biotite + muscovite + quartz. According to Winkler (1967, p. 70), the disappearance of chlorite, and the entry of cordierite mark the beginning of the hornblende-hornfels facies. The occurence of cummingtonite in the sandstone near the Sluice Box bridge, and the presence of muscovite in the hornfels matrix restrict the contact metamorphism to the hornblende-hornfels facies. The mineral assemblage in the hornfels of the Lower Brown Grey River is consistent with that from the reaction of chlorite + muscovite + quartz during metamorphism of the hornblende-hornfels facies (Winkler 1967, p. 70).

The presence of cordierite in the hornfels indicates that the maximum pressure is less than 5.5 kb, and the minimum temperature is greater than 500° C. Although the co-existing muscovite is not abundant, its presence in the hornfels matrix suggests that the maximum temperature is unlikely to exceed 650° C. The absence of K-feldspar co-existing with sillimanite, and migmatitic gneisses support this suggestion.

The paragenesis, (cordierite/andalusite) -in, and (chlorite + some muscovite) -out, and the abundance of cordierite suggest that the metamorphic pressure is in the range of 1.5 to 2.5 kb (Winkler 1974, p. 242). The occurence of andalusite in the hornfels whilst suggesting a maximum pressure of less than 2 kb and hence agreeing with the inferred pressure above, restricts the maximum temperature to not greater than 580° C. However, according to Winkler's Al_2SiO_5 diagram (1974) which is derived from Althaus (1967, 1969), and Richardson et. al (1968, 1969), the presence of andalusite indicates that the maximum temperature and pressure is less than 650° C and 5.5 kb. The writer prefers the P-T conditions deduced from Turner's Al_2SiO_5 diagram (1968) because as shown by Turner, the extension of the andalusite stability field to 6.5 kb by Althaus (1967) is based on less convincing reported incipient reactions, and the material used in Althaus experiment is pre-strained which significantly raises the free energy before Al_2SiO_5 inversion is effected and so the data thus obtained are suspect.

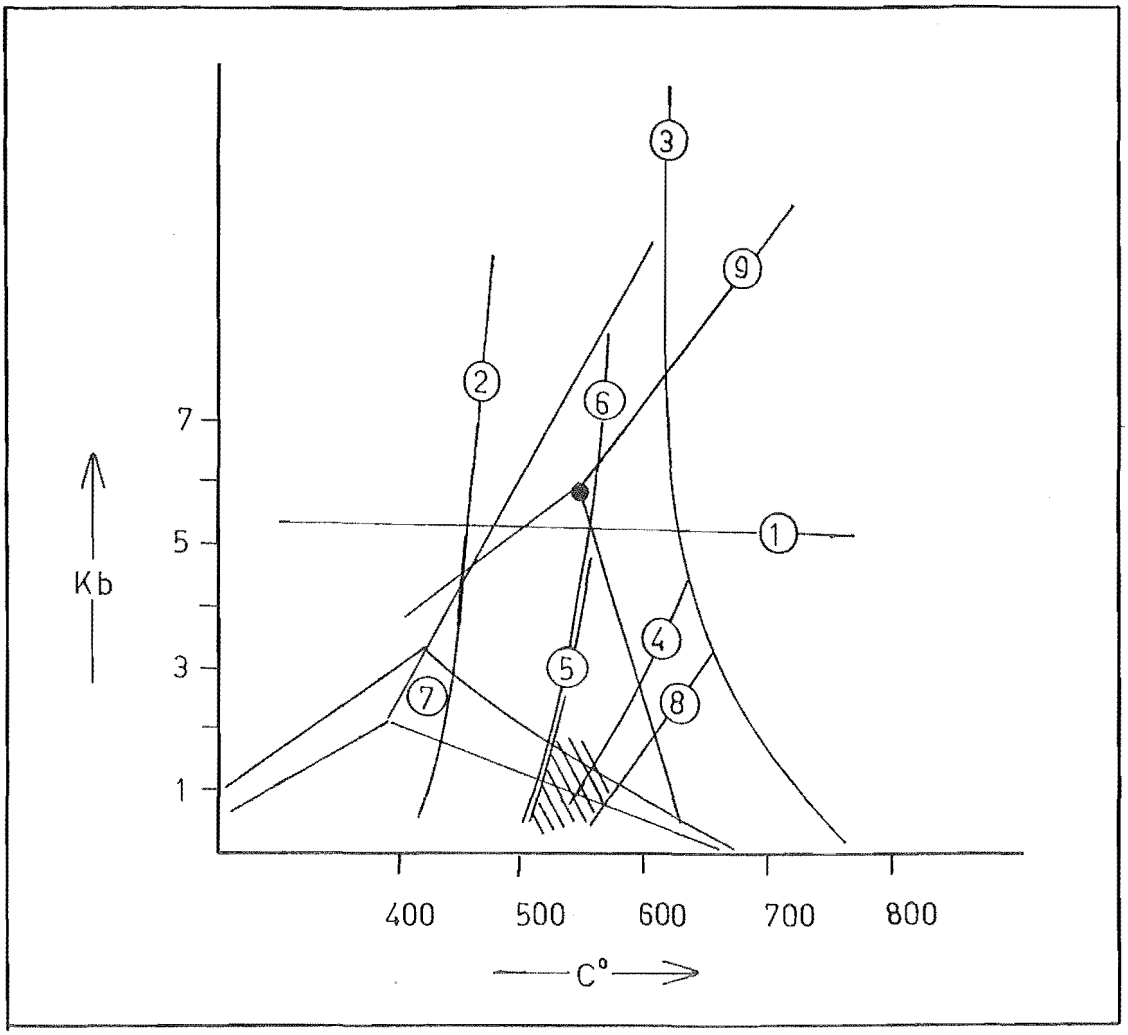

FIG. 54 1) Greater than 5.5 kb, cordierite-out (Winkler 1973) .

2) Greater than 400° C, biotite-in and muscovite-in .

3) Anatexis on the right handside .

4) Greater than 600° C, (quartz + muscovite + staurolite)-out (Winkler 1973) .

5) Greater than 550° C, (staurolite, cordierite)-in

6) Greater than 5 kb and 550° C, staurolite-in

7) Al_2SiO_5 phase diagram after Turner (1968, p.114) .

8) Muscovite- out on the right handside .

The shaded portion of the diagram indicates the probable P-T environment of thermal metamorphism in the vicinity of the Brown Grey River .

9) Al_2SiO_5 phase diagram after Winkler (1973, p.236) .

Moreover, the phase diagram provided by Turner (1968, p. 114) is deduced from five independent sets of data, and is less likely to be biased.

Fig. (54) shows the inferred P-T conditions during contact metamorphism of the Lower Paleozoic rocks in Springs Junction district.

IV/4 EFFECTS OF RETROGRADE METAMORPHISM

A. MINERALOGICAL CHANGES

The retrograde metamorphism which followed the thermal event has caused 1) the breakdown of cordierite/andalusite to aggregates of quartz, muscovite, and some biotite and chlorite, 2) the crystallization of chlorite, and sometimes 3) the partial alteration of biotite to chlorite in the hornfels of the Lower Brown Grey River. Except for the absence of biotite and chlorite, the breakdown product of cordierite/andalusite in the spotted hornfels, 2 km east of the Thompson's Flat is similar to that described above. However, at the outer part of the aureole, the effect of retrograde metamorphism is the formation of post-S3 chlorite.

B. TEXTURAL CHANGES

The quartz from the breakdown of cordierite/andalusite occurs as granoblastic-polygonal grains, and the platy minerals occur as randomly oriented

crystals. Except in specimen UC 5796, no relict structures are preserved in these pseudomorphs, indicating significant homogenization in the rock during contact metamorphism. Some of the coarser-grained muscovite is poikiloblastic, containing small quartz inclusions.

The formation of chlorite is sometimes mimetic. Such crystals are platy, coarse-grained, often poikiloblastic, and aligned parallel to S2 or/and S3. The chlorite crystals which are not structurally controlled are always irregularly-shaped, occasionally poikiloblastic, containing F3 crenulations as in specimen UC 5730, and sometimes occur as radial aggregates as in specimen

The quartz, muscovite, biotite, and chlorite associated with the retrograde metamorphism are considered as post-S3.

IV/5 CORRELATION AND AGE OF CONTACT METAMORPHISM

Granites in Westland, Buller and north-west Nelson are generally of Devonian-Carboniferous or Cretaceous age (Aronson 1968). In this area, the regional metamorphism is the earlier event (suggested by the superimposition of thermal effects on almandine schist), and clearly of different character to the contact metamorphism. Shelley (1975) has proposed a model in which the regional metamorphism is Devonian-Carboniferous and the contact metamorphism is Cretaceous. According to this

model, a paired metamorphic belt was formed during the Tuhuan Orogeny and the Tuhuan granites are restricted to the areas west of the Tuhuan median boundary. In the thesis area, the Rahu Fault seperating the low pressure metamorphism in the Victoria Range sediments from the higher pressure metamorphism in the Thompson's Flat, Sluice Box, and Alfred Formations is recognised as the fossil Tuhuan median boundary. The granites and thermal effects in the area east of the Rahu Fault are post-Tuhuan Orogeny according to Shelley's model. Recent radiometric data on the schist from the Lower Brown Grey River reveal the cooling age of the schist as 85-87 $\pm$ 1 m. y. (pers. com. C. J. Adams) which is consistent with the age of thermal event inferred from Shelley's model.

IV/6 SUMMARY:

The effects of contact metamorphism in the Lower Paleozoic rocks of Springs Junction district, east of the Rahu Fault are as follows:

i) Schist is metamorphosed to spotted hornfels in the inner part of the contact aureole. At the outer part of the aureole, mimetic crystallization of biotite and chlorite occurs in the schist.

ii) Sandstone of the lower greenschist facies is converted to quartz-hornfels containing cummingtonite crystals.

The mineral assemblage in the hornfels indicates that the contact metamorphism in the aureole is hornblende-hornfels facies. The inferred P-T conditions are 500° to 580°C and 1.5 to 2.5 kb. Textural studies reveal that:

i) Cordierite/andalusite, biotite, muscovite, and quartz in the inner part of the aureole are probably syn-S3, as this structure has been shown to be related to the Victoria Range granitic intrusion (see V/)

ii) Biotite and chlorite in the outer part of the aureole are syn- to post-S3. Although these minerals are related to the same metamorphism as in i), it is conceivable that they are crystallized after the minerals in i) because of the time lag in temperature effect of contact metamorphism in the inner and outer part of the aureole (See Winkler 1973, p. 99, 100). According to this author, deformation is instantaneous whereas temperature increase in the outer aureole is delayed.

iii) Quartz, muscovite, biotite, and chlorite associated with the retrograde metamorphism are considered as post-S3. The time relationship between ii) and iii) is unknown.

Textural studies also reveal that the contact metamorphism is post - regional metamorphism, probably Cretaceous age.

METAMORPHISM / MINERALS	THERMAL		RETROGRADE
Andalusite	X		
Cordierite	X		
Biotite	X O	O	X
Chlorite	O	O	X O?
Muscovite	X		X
Quartz	X	X? O?	X
Deformation Stage	Syn-	Post-	Post-
S formed	TECTONIC I		
S folded	S3		
	So, S1, S2		

FIG. 55 Time relations of mineral crystallization to deformation in pelitic rocks of Spring Junction district.

X - present in inner aureole .

X ? - inferred present in inner aureole .

O - present in the outer part of aureole .

O ? - inferred present in the outer part of aureole .

So - bedding ; S1 - schistosity ; S2 - axial plane-cleavage of F2 ; S3 - axial plane-cleavage of F3 .

CHAPTER V

FOLD STRUCTURES IN THE LOWER PALEOZOIC ROCKS BETWEEN THE ALPINE AND RAHU FAULTS

Thin section studies indicate that the Lower Paleozoic sediments between the Rahu and Alpine Fracture Systems have been affected by multiphase folding. The various episodes of folding previously discussed in Chapter III/3 Bii is mentioned in greater detail, arranged in chronological order, and correlated with the major New Zealand orogenies in this section of the thesis.

V1 TERMINOLOGY

D1 or F1 = The earliest deformation. If there are associated folds, they have not been observed.

D2 or F2 = The second deformation and related folds.

D3 or F3 = The third deformation and related folds.

D4 or F4 = The fourth deformation (tentative). Folds are inferred from stereographic-plots

S0 = Bedding.

S1 = Slaty cleavage/schistosity formed by the earliest deformation.

S2 = Axial plane cleavage of F2 crenulation.

S3 = Axial plane cleavage of F3 crenulation.

S4 = Axial plane cleavage of F4 fold (tentative).

FA2 = Fold axis of F2 fold.

FA3 = Fold axis of F3 crenulation.

FA4 = Fold axis belonging to F4 (tentative). This has not been observed directly in the field.

L_{S1}^{S2} = Lineation generated by the intersection of S1 and S2.

NB. All the stereographic diagrams in the thesis are lower hemisphere projections on an equal area (Schmidt) net.

V/2 STRUCTURAL ELEMENTS:

A. S0 STRUCTURES

The criteria used to define bedding are grain-size distribution and contrasting lithologies. This planar structure is most affected by F2 folding, and it is intersected by S1, S2, and less obviously, by S3 and S4. In most localities, apart from that in the vicinity of Thompson's Flat, the bedding attitude is NE-SW and steeply dipping SE.

B. S1 STRUCTURES

There are no megascopic and microscopic F1 structures associated with S1. The major regional post-bedding S-surface in the low metamorphic grade pelitic rocks is a slaty-cleavage eg. in the areas north of Springs Junction and Marble Hill. With increasing metamorphic temperature,

the major S-surface is a well developed schistosity. Both slaty-cleavage and schistosity are classified as S1 because of the following.

1) The fabric cross-cuts the pre-existing surface S0 (bedding) at a low angle.

2) The attitude of the fabric is variable in the thesis area, indicating that the slaty-cleavage/ schistosity is deformed by F2 and subsequent folding(s).

3) The fabric is crenulated by F2 and subsequently intersected by S2 planar structures.

As F1 folds have not been observed in the field, and S0 is significantly folded only by F2, it is conceivable that S1 is the result of plastic flattening during regional metamorphism.

C. F2 MEGASCOPIC STRUCTURE

A north-east trending major anticline is outlined by the Sluice Box Formation. The highly fractured hinge-zone, and the approximately similar bedding attitude (NE-SW/60°-70° SE) in both fold limbs suggest that this structure is a tight fold with an inclined axial plane dipping SE steeply. A stereographic-plot of poles to bedding shows that the distribution pattern approximates that of an ideal symmetrical fold with a plunging fold axis, and inclined axial plane. Thus, the stereographic-analysis is consistent with field observations.

The orientation of the fold axis as determined in Fig. (56) is 040°-045°/10°-15° NE, and the axial plane is

040°-045°/60° SE. As the latter is consistent with the attitude of S2 (refer section V/2 C), the major anticline in the thesis area is classified as a F2 feature. The orientation of the maximum stress axis (direction perpendicular to axial plane) which formed the F2 anticline is NW-SE.

D. F2 MESOSCOPIC STRUCTURES

Mesoscopic folds are formed as the result of folding of S0 and S1 surfaces. These features are not commonly seen in the Lower Paleozoic rocks. In the vicinity of Trig. GA (100 m south), a mesoscopic fold observed is upright, open and symmetrical. In addition there are small crenulations. The axes of the crenulations are oriented parallel to the axis of the mesoscopic fold; both the major fold axis and crenulation axes trend NE-SW with a gentle plunge towards the NE. As S0 and S1 form the mesoscopic fold surfaces, and the trend of the mesoscopic fold axis is consistent with that of the major anticline, the mesoscopic structure here is considered to be an F2 feature.

E. F2 AND S2 MICROSCOPIC STRUCTURES

The development of these features is widespread. They are formed as the result of crenulation of slaty-cleavage/schistosity (S1), and bedding (S0). The microscopic folds are symmetrical, and have very sharp hinges

(Fig. 62). Observations of thin sections perpendicular to the fold axes reveal that the apical angles do not exceed 80^{o}. In some places eg. specimens UC 5730, UC 5816, and UC 7811 one limb of this generation of crenulations is itself crenulated (Fig. 62).

The axial planes of the F2 crenulations form a set of finely spaced fracture cleavages. This planar fabric usually intersects the S0 and S1 surfaces at a high angle in the hinge-zone. However, in intensely deformed rocks, the axial plane cleavage may coincide with S1 or S0, thus enhancing the pre-existing fabric eg. in specimens UC 7651a and UC 7764a. The attitude of the axial plane cleavage strikes nearly NE-SW and dips steeply SE (i. e. parallel to the axial plane of the F2 anticline). Where this planar fabric is developed, its intersection with S1 produces a prominent lineation-L_{S1}^{S2}. Mimetic crystallization of biotite and chlorite on the axial plane cleavage is known in the rocks of the Lower Brown Grey River, Palmer's Flat, and Palmer's Bend. At the junction of Pell Stream and Alfred River, and at Upper Station Creek, axial plane slippage has resulted in transposition of bedding (Fig. 64). As mentioned previously, because one limb of the F2 microscopic folds is itself crenulated, the axial plane cleavage here is intersected by S3 fabric.

F. F3 AND S3 MICROSCOPIC STRUCTURES

Unlike the S2 and F2 structures, F3 and S3 microscopic features are less well developed, and are not as

widespread. They are apparently restricted to the areas near or metamorphosed by the Cretaceous granites. The microscopic folds are formed as the result of post-F2 crenulation on one limb of the F2 microscopic folds. The S-surface most affected is S1. S2 is deformed in places where the F2 crenulation is isoclinal (Fig. 38). S0 (bedding) like S2 is not significantly affected as shown by the stereographic-plots in Figs. (56 & 58). Because the inter-relationship of this generation of crenulation and F2 requires the maximum stress axis of this phase of deformation to be perpendicular to the undeformed F2 crenulation limb (Fig. 63), the lineation belonging to D2 is not affected by this generation of folding.

The axial plane of the F3 crenulations form a set of crude fracture cleavages. This structure is seen as an incipient fracture cleavage which intersects S2 at a low angle in the schist at the first outcrop in the Lower Brown Grey River, and is consistent with the angular relationship of S2 and S3 depicted in Fig. (63). Rare mimetic growth of biotite and chlorite on S3 is observed in the schist of Palmer's Flat, Lower Brown Grey River, and Palmer's bend.

The unique inter-relationship of the F2 and F3 crenulations shown in Fig. (62) indicates that the F3 maximum stress axis has retained the trend of the earlier (F2) maximum stress axis but with a different plunge. Specimen UC 5730 perpendicular to the Fold axes of F2 and F3 suggests that the increased plunge of the new

maximum stress axis is of the order of 40^{o} to the F2 maximum stress axis.

G. F4 AND S4 STRUCTURES

The scatter of the L_{S1}^{S2} lineation about a new fold axis implies a further phase of folding (tentatively labelled as F4). The axial plane cleavage related to this generation of folds is not well developed. Its attitude measured in the field is NNW-SSE and dipping east which is consistent with that reconstructed in the stereographic-plot in Fig. (60). The axial plane cleavage (tentatively labelled as S4) is known to intersect the deformed S3 fabric at a high angle in the schist at the first outcrop in the Lower Brown Grey River.

H. RECONSTRUCTION OF THE F4 MEGASCOPIC STRUCTURE

Besides outlining the major anticline, the outcrop pattern of the Sluice Box Formation is also affected by another set of folds whose fold axes are at an angle to FA2. Unlike the earlier major structure, these folds are less well developed, and they are only inferred from the outcrop pattern of the Sluice Box Formation. Because of insufficient structural data, the relationship of these folds to the microscopic F3 crenulations is somewhat obscure. However, according to the discussion in section V/3, it is conceivable that they belong to the fourth phase of deformation.

The following section outlines the attempt to reconstruct the attitude of the F4 axial plane, as well as the maximum stress axis which produced the structure.

The distribution of the Sluice Box Formation in Farmer's map (1967, unpublished thesis) suggests that the interference pattern created by two successive major fold episodes is essentially type 1 (Ramsay 1967, p. 252; see Fig. 66). In such a case, β is greater than 70°, and a4 is 90° to FA4 measured along the F4 axial plane (see Fig. 57 after Ramsay 1967, p. 251). This information together with the known positions of poles to S2, and FA4 (refer Figs. 58 & 59) permits the reconstruction of the F4 axial plane and the maximum stress axis which generated the structure. The steps involved in the reconstruction are described in Fig. (60).

The shaded portion in the diagram contains the F4 axial plane. The attitude of this structure is approximately $10^{\circ}/70^{\circ}$-90° E, and the orientation of the maximum stress axis is nearly east-west. Stereographic-plot of the fracture cleavage intersecting S2 at a high angle in the schist of the Lower Brown Grey River shows that the attitude of this planar fabric is similar to the reconstructed F4 axial plane, thus implying that the method used in the reconstruction of F4 axial plane is supported by the occurence of a corresponding surface (Fig. 61). The small circle distribution of the L_{S1}^{S2} lineation about a new fold axis (FA4) suggests that F4 is a flexural fold (Fig. 59). The diagram also shows that FA4 is

gently plunging north, and at an angle of 50° to FA2.

Although the orientation of the F4 axial plane, and the maximum stress axis have been successfully estimated using the stereographic-plot technique, they are not conclusive because of the following.

1) The number of lineations used in the plot in Fig. (59) is not statistically reliable.

2) The method assumes that the Lower Paleozoic rocks have undergone two major phases of folding and that they are not significantly affected by later folding and faulting.

3) The method also assumes that F3 has no appreciable effect on the redistribution of the L_{S1}^{S2} lineation.

4) The outcrop pattern of the Sluice Box Formation is not seriously affected by F3.

The assumption in 2) may be considered as reasonable because the lineation plots in Fig. (59) display no scatter tendency. Instead, the plots are distributed along a plunging small circle, indicating that F4 fold is not significantly affected by subsequent deformation and faulting. The writer suspects that this may be due to the ability of the pre-existing Rahu Fault to relieve the stress induced by post-F4 deformation. F4 has been dated as not older than Cretaceous (refer section V/3), and the Rahu Fault is known to be active during the Cretaceous and Tertiary period (Chap. VI). The assumption in 3) is also reasonable because the F3 maximum stress axis is at 90° to the L_{S1}^{S2} lineation. The linear structure

in such a case is not affected by F3. Like the others, this last assumption is also reasonable because F3 is considered to be related to the Cretaceous granites. Deformation associated with intrusions is not commonly widespread and intense.

Clearly, more field work on structures is needed in the thesis area before the reconstructed attitude of the F4 axial plane, and the maximum stress axis can be accepted with confidence.

I. LINEATIONS

The most prominent lineations are those generated by the intersection of S1 and S2. They are known to be redistributed about the F4 fold axis (Fig. 59). As mentioned earlier, this generation of lineation is not affected by F3 because the F3 maximum stress axis is at 90° to the L_{S1}^{S2} lineation.

The other sets of lineations produced by the intersection of various S-surfaces are not apparent in the field.

V/3 TIME RELATIONSHIP OF DEFORMATION AND REGIONAL METAMORPHISM

The writer has used the overprinting relationship of microscopic structures to delineate deformation phases. By this method four phases of deformation have been recognised; two syn-metamorphic and two post-metamorphic.

The first syn-metamorphic deformation resulted in the regional development of slaty-cleavage/schistosity. Folds associated with this deformation have not been observed in the field. This, together with the fact that S0 (bedding) is only significantly affected by F2 (or more strictly deformation two) suggests that deformation at this stage is probably predominantly plastic flattening. The possibility that schistosity/slaty-cleavage is due to thrusting or sliding movement is ruled out by the observations below.

1) The non-mylonitic nature of the S1 fabric.

2) The fact that the replacement of slaty-cleavage by schistosity is closely related to the regional isograds. Schistosity occurs only in metamorphic zones of biotite and almandine grades.

The age of this syn-metamorphic deformation is probably Devonian-Carboniferous (see chap. III/6).

The second syn-metamorphic phase of folding resulted in the mimetic growth of biotite on the axial plane S2, and the syn-tectonic crystallization of almandine (chap. III/3B). As mentioned in section V/2 (A, B, C), three orders of folds are generated during this folding episode; 1) an inclined, gently plunging, tight, major anticline, 2) open, symmetrical, mesoscopic folds, and 3) microscopic chevron folds. The age of this phase of deformation is probably Devonian-Carboniferous also (see chap. III/6).

The post-metamorphic F3 deformation is represented by the microscopic crenulation on one limb of the F2 crenulations. Unlike the development of F1 (or more

strictly S1) and F2, the formation of F3 is not accompanied by the crystallization of almandine and biotite. Where mimetic growth of biotite and chlorite on the axial plane S3 has occured, it is restricted to the areas affected by the Cretaceous granites (refer chap. IV). This, together with the apparent restriction of F3 crenulations to the areas near or metamorphosed by granites suggest that this phase of deformation is related to the Cretaceous granite emplacement.

Because the F3 maximum stress axis is at 90° to the L_{S1}^{S2} lineation, the third phase of folding does not affect the L_{S1}^{S2} linear structure. The redistribution of L_{S1}^{S2} lineation about a new fold axis must therefore reflect another phase of deformation post-F3. Like F3, F4 is post-regional metamorphism, and its age is not older than Cretaceous.

H. Cutten (1976, unpublished thesis) has suggested that the zig-zag en echelon folding of the Tertiary sediments in the region north of the thesis area is caused by plastic deformation or parallel 'micro-faulting' in the basement as a response to movement along the Alpine Fault. The compressional axis according to his proposed mechanism is oriented E-W (45° to the Alpine Fault) and some of the folds (referring to synclines) generated, initially have N-S trending fold axes. As the reconstructed compressional axis, and FA4 are consistent with those in Cutten's model, it is conceivable that F4 here is also a response to the movement along the nearby Alpine Fault during the Tertiary period. Any

difference in the behaviour of basement rocks to the stress induced by the Alpine Fault in the thesis area and in the region north of the Koura Village may be accounted for by the suggestion that the rocks are more schistose or fissile in the former and are therefore more responsive to folding.

As mentioned before, clearly more structural data from the thesis area is required before the F4 structure and its correlative can be accepted with confidence.

Fig. (65) summarizes the time relationship of deformation and regional metamorphism.

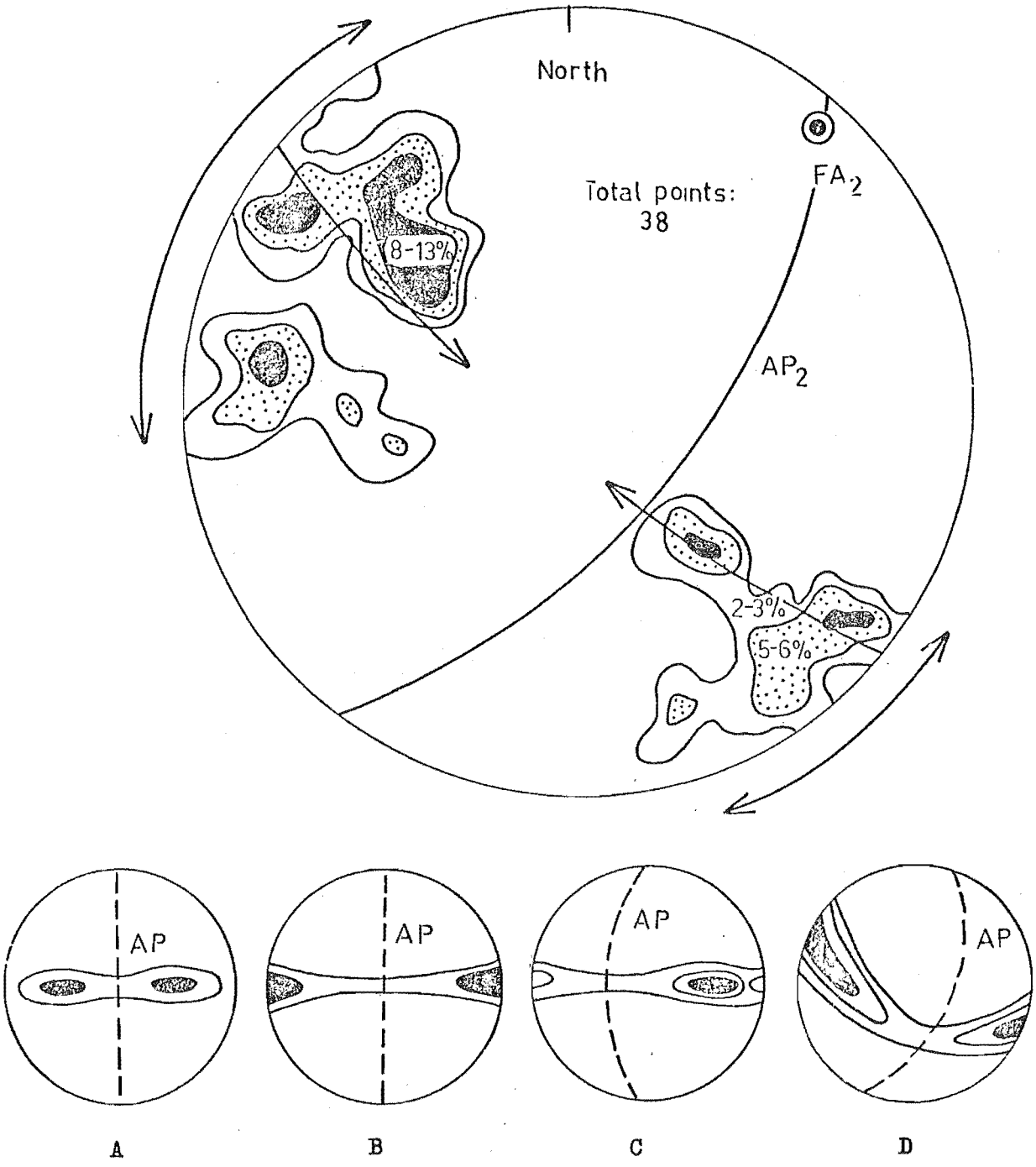

FIG. 56 Plot of poles to bedding (SO) . The arrows indicate the scatter tendency of poles to SO . Note that the distribution pattern is somewhat similar to that of plot D .

A - Open, symmetrical fold .

B - Symmetrical fold with limbs approaching parallelism .

C - Asymmetrical, plunging and inclined axial plane .

D - Symmetrical, plunging and inclined fold .

Diagrams A,B,C,&D are after Ragan (1973) .

FA2 is about 042°/010° N .

AP2 is about 42° / 60° SE .

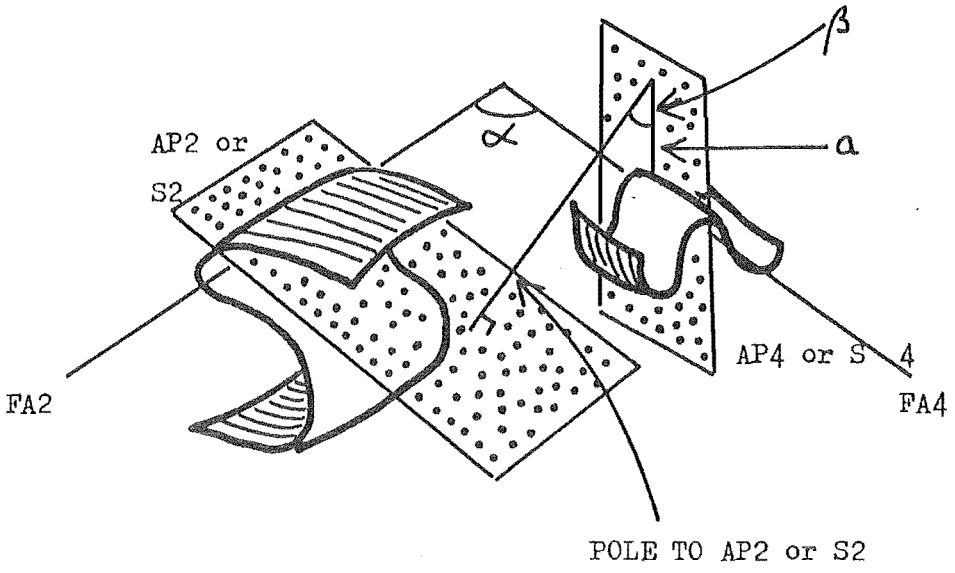

FIG. 57 Interference fold : the angular relationships of S2 & S4 ; FA2 & FA4 ; etc . Diagram is after Ramsay (1967, p.521) .

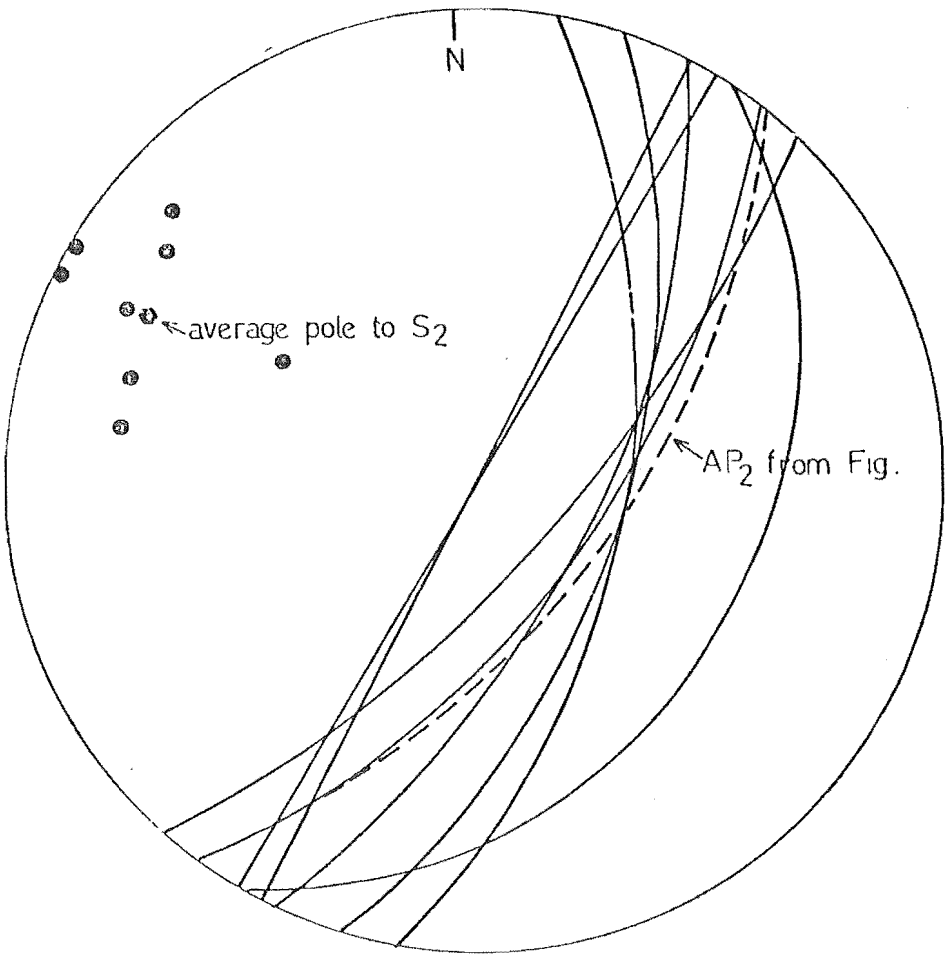

FIG. 58 Plot of axial plane cleavage (S2) , and poles to S2 . Note that the axial plane determined in Fig. 56 is very similar in attitude to the axial plane cleavage here .

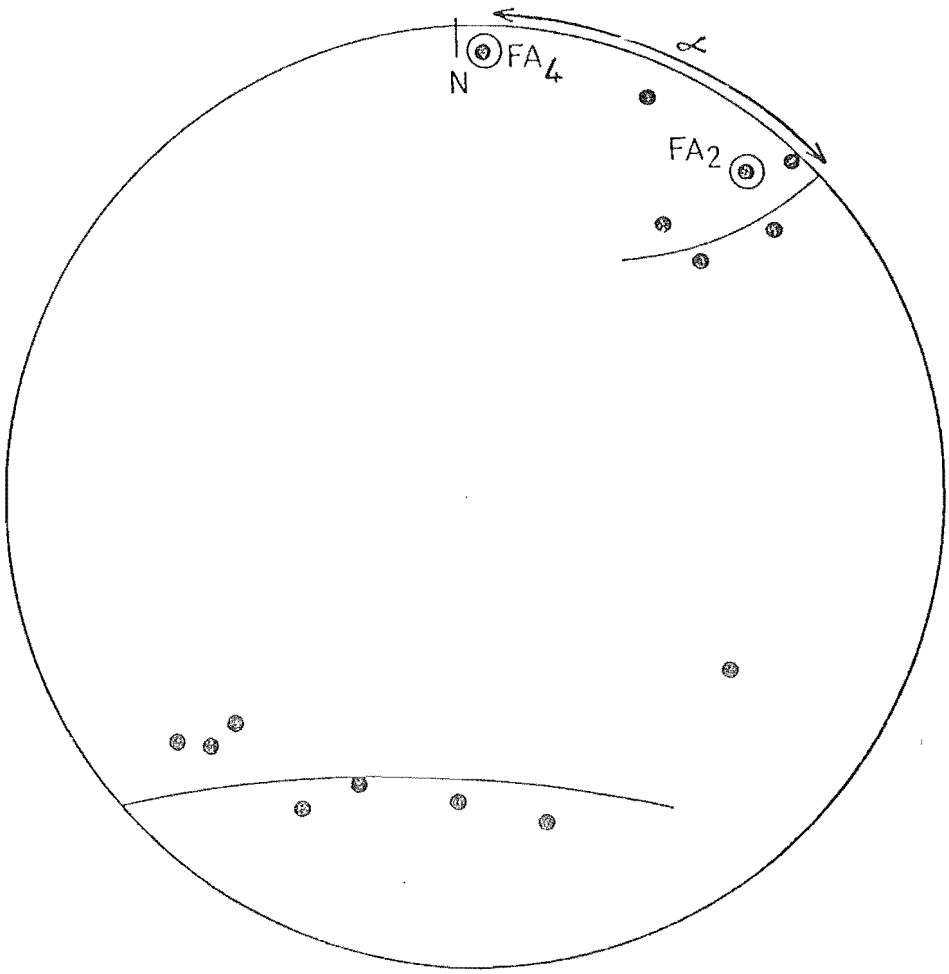

FIG. 59 Plot of the lineation L_{S1}^{S2} . Note that the lineations are redistributed about an axis FA4 . The angle α is the angle FA2 makes with FA4 , and it is about 50^{o} . The reason that L_{S1}^{S2} is affected by F4 and not F3 is because the maximum stress axis of the latter deformation is oriented perpendicular to the L_{S1}^{S2} lineation . Refer Fig. 63 .

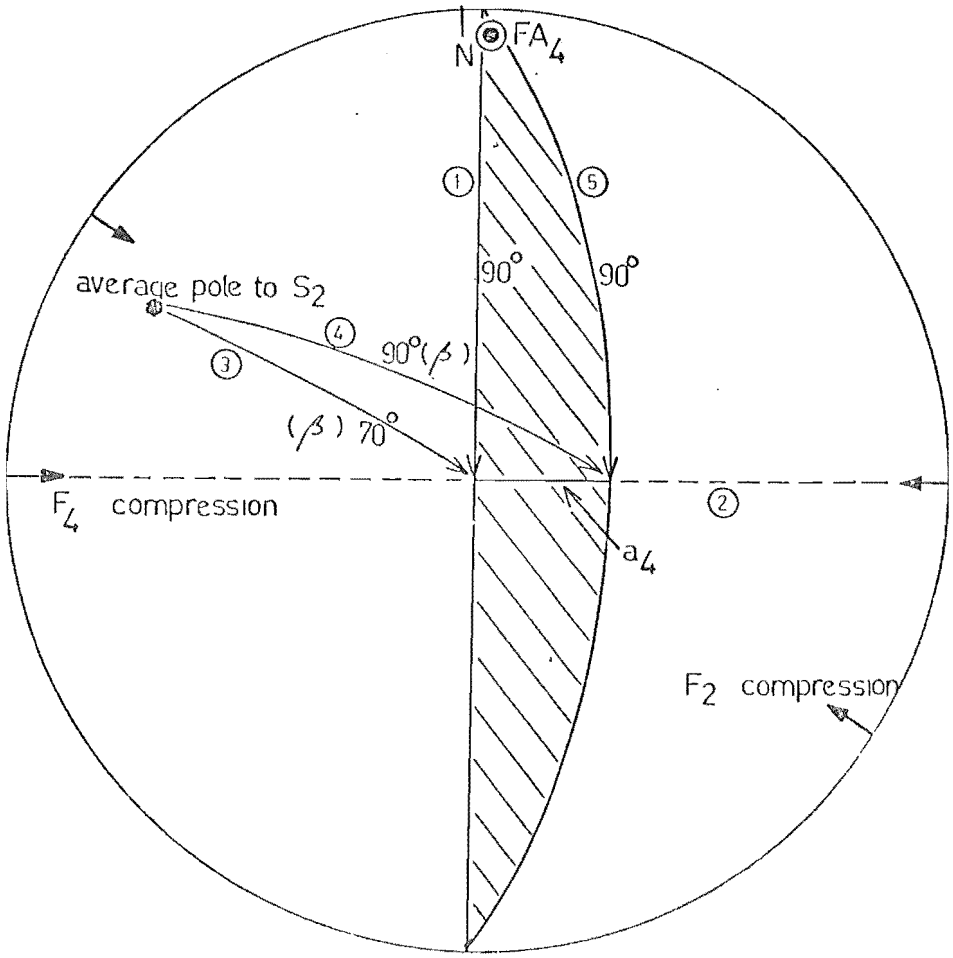

FIG. 60 The above figure shows the steps involved in the reconstruction of the axial plane (S4) , and compares the orientation of the F2 and F4 compressional axes .

Steps in the reconstruction of S4 or AP4, and the reason(s) for each step taken .

1) because FA4 and a4 are at 90° to each other (Fig. 57) .
2)
3) because β is the angle made by a4 and pole to S2
4) (see Fig. 57), and β is greater than 70° .
5) because β is not greater than 90° .

The shaded portion of the diagram contains the axial plane (S4) . The new compressional axis orientation is nearly east-west .

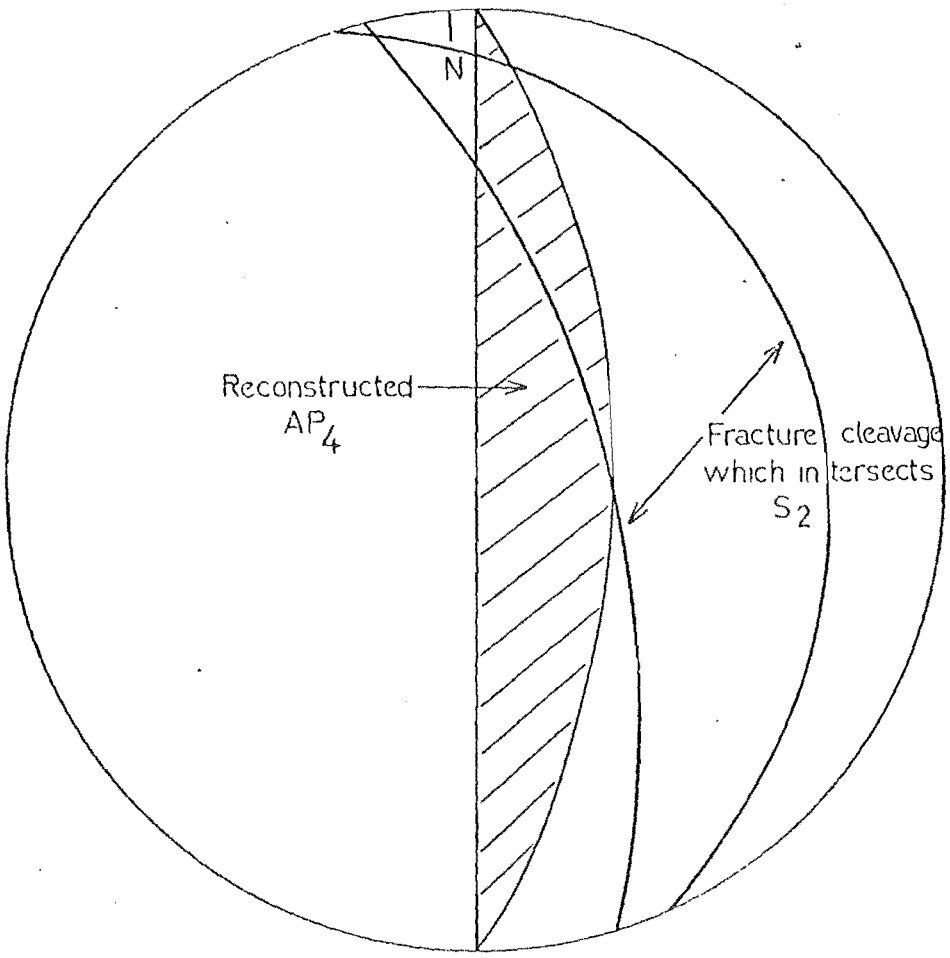

FIG. 61 Plot of the fracture cleavage which intersects S2 . Note that their attitudes lie very close to the shaded portion of the diagram containing the reconstructed axial plane (S4) .

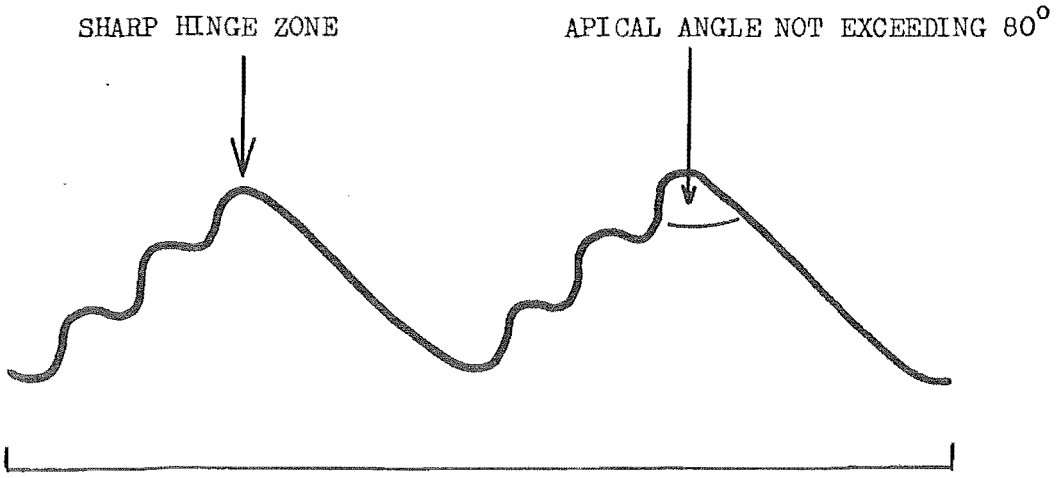

FIG. 62 A schematic diagram showing the crenulations observed in UC 5730 . Note that one limb of F2 crenulations is itself crenulated . The unique relationship of F2 and F3 requires FA2 and FA3 to be parallel to each other, and that the younger maximum stress axis to be parallel to the earlier maximum stress axis .

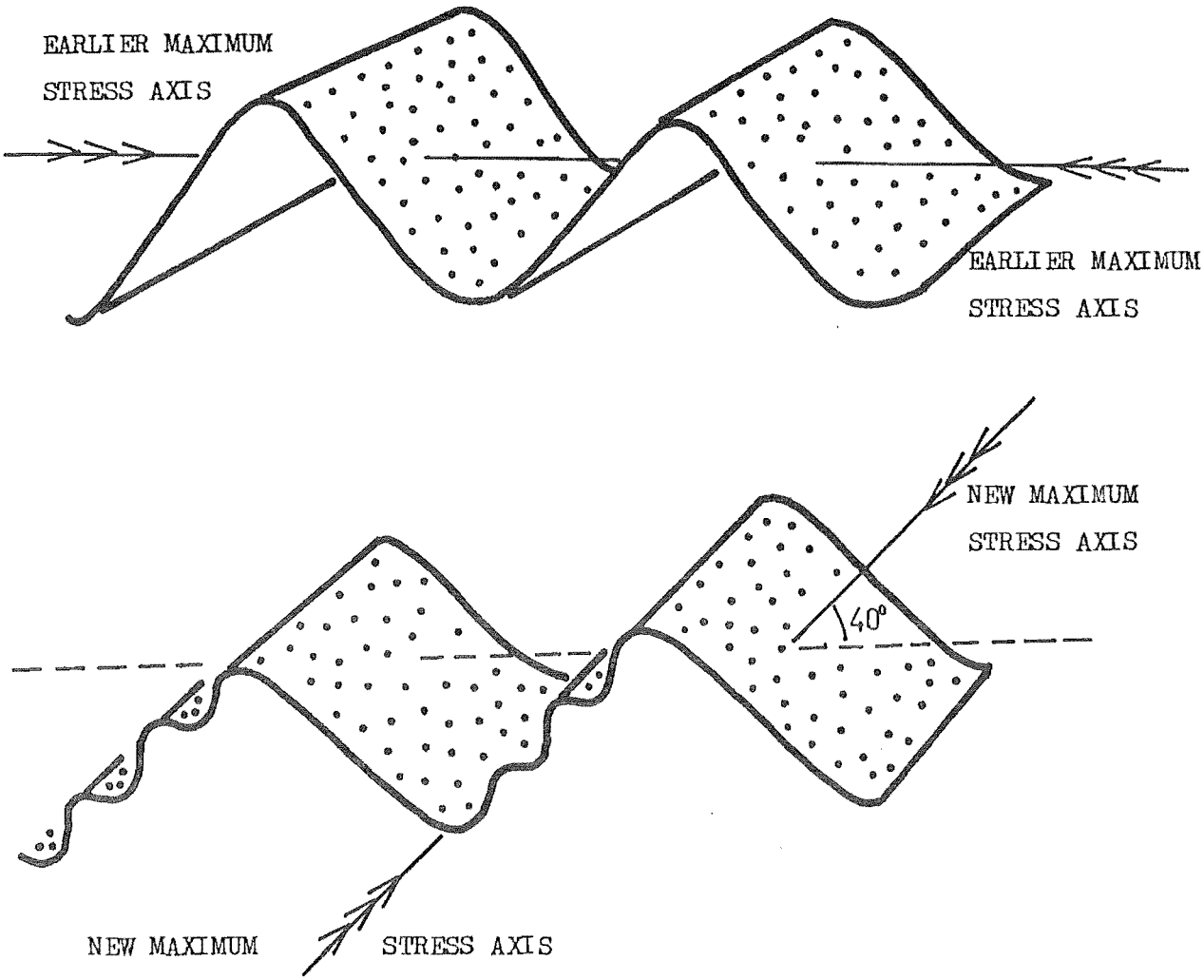

FIG. 63 The above diagram shows that for one limb of the fold to be crenulated, the earlier and the later fold axes must be parallel to each other . Note that the trend of the new maximum stress axis is similar to that of the earlier stress axis but with increased plunge .

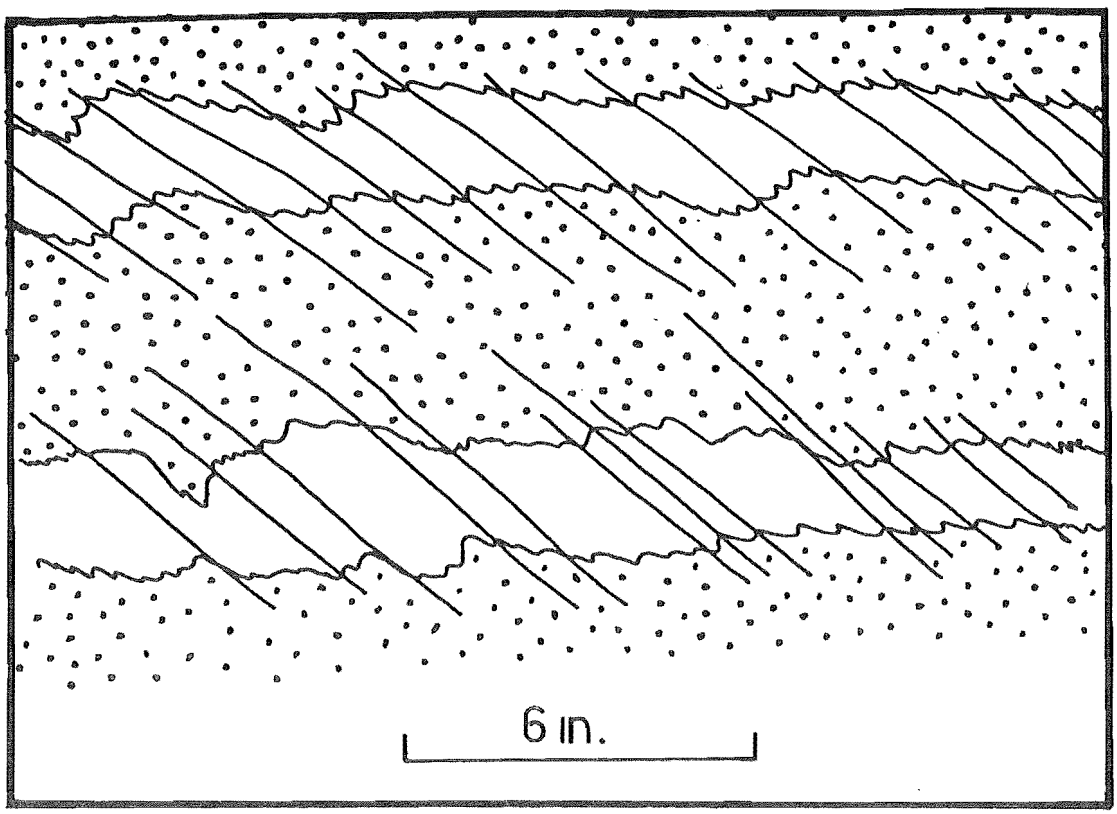

FIG. 64 Axial plane slippage which has resulted in transposition of graded bedding . Diagram after the exposure near the junction of Pell and Alfred Rivers .

PHASES OF DEFORMATION	PRE-TECTONIC PRE-METAMORPHIC	FIRST SYN-METAMORPHIC (DEV-CARB)	SECOND SYN-METAMORPHIC (DEV-CARB)	THIRD POST-METAMORPHIC (CRET)	FOURTH POST-METAMORPHIC (TERTIARY)
FOLD(S)	——	F1	F2	F3	F4
MEGAFOLD(S)	——	NOT APPARENT IN THE FIELD .	A MAJOR NE-TRENDING, TIGHT, ANTICLINE WITH AXIAL PLANE DIPPING E.	——	A SERIES OF FOLDS SMALLER SCALE THAN THE MAJOR ANTICLINE . FOLD STYLE AND TREND ARE OBSCURE IN THE FIELD . RECONSTRUCTED FOLD TREND IS NORTH-SOUTH .
MESOSCOPIC FOLDS	——	NOT APPARENT IN THE FIELD .	OPEN, SYMMETRICAL, NE-TRENDING FOLD WITH KINKS ON FOLD SURFACE .	——	
MICROSCOPIC FOLDS	——	NOT APPARENT IN THE FIELD .	CRENULATIONS WHOSE AXIAL PLANE HAS AN ATTITUDE SIMILAR TO THAT OF THE MEGAFOLD.	CRENULATIONS WHOSE AXIAL PLANE IS AT A LOW ANGLE TO S2.	
S-SURFACE FORMED	BEDDING (So)	SLATY-CLEAVAGE / SCHISTOSITY (S1)	AXIAL PLANE CLEAVAGE (S2), GENERALLY 40-45°/60° E .	AXIAL PLANE CLEAVAGE (S3), GENERALLY AT A LOW ANGLE TO S2.	AXIAL PLANE CLEAVAGE (S4), GENERALLY NNW-SSE/DIPPING E .
S-SURFACE FOLDED	——	So	So, S1	So, S1, S2	So, S1, S2, S3

FIG. Summary of the time relationship of deformation and regional metamorphism .

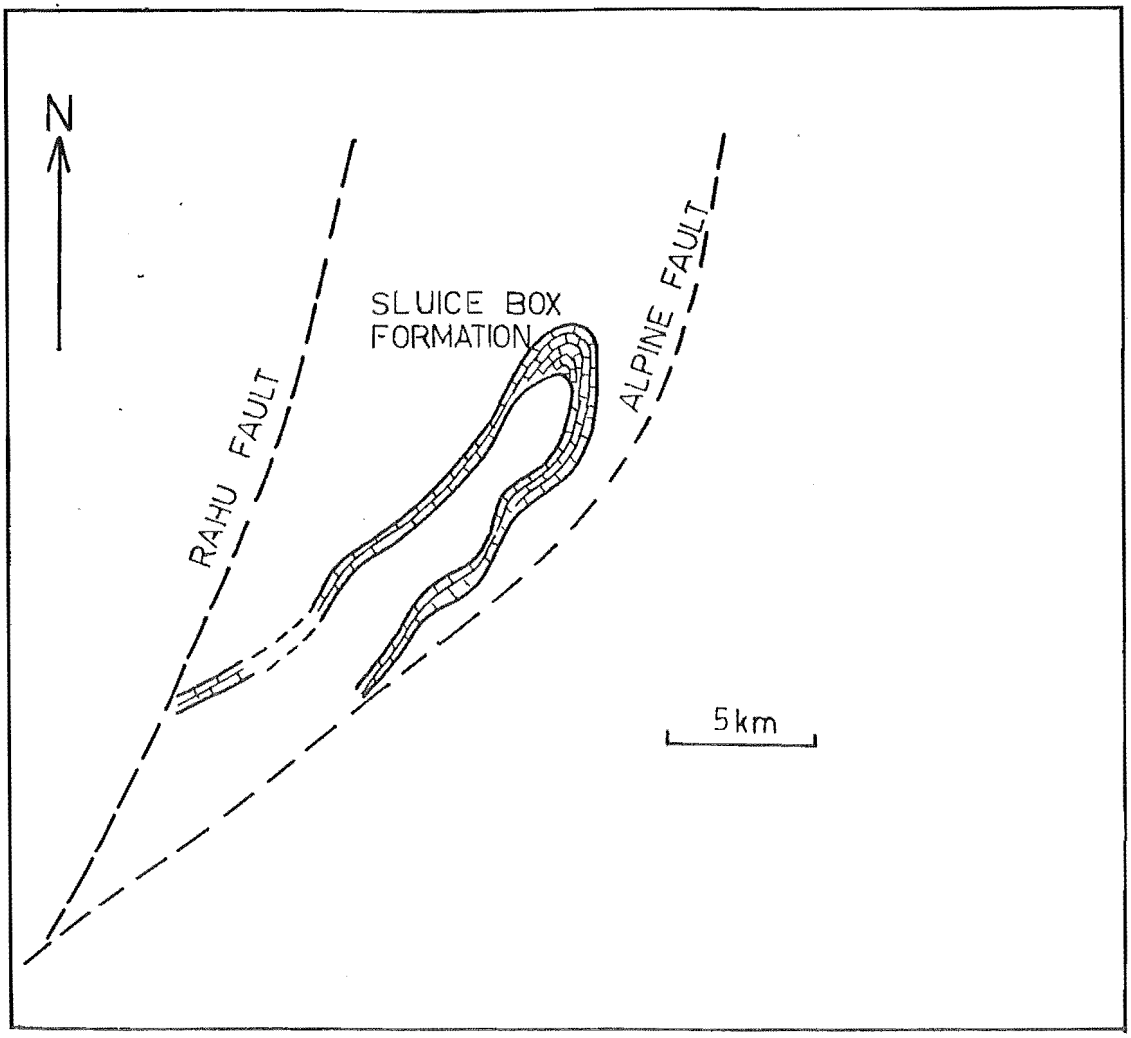

FIG. 66 Map showing the outcrop pattern of the Sluice Box Formation as outlined by Farmer (1967, unpublished M.Sc. thesis) . According to Ramsay (1967), the Sluice Box Formation outcrop pattern may be interpreted as type 1 interference fold pattern .

CHAPTER VI

THE KOURA AND RAHU FAULT ZONES

VI/1 INTRODUCTION

Generally, the Koura Fault Zone trends north-east near Trig. GA but south of the junction of the Maruia and Rahu Rivers, the structure merges with the younger Rahu Fault Zone and roughly trends north-northeast, closely following the course of the Rahu River and Palmer's road until it is truncated by the younger Alpine Fault. The Rahu Fault Zone--the later structural feature, trends north-northeast from west of Trig. GA to Palmer's Bend. Southwards from the latter locality, the structure splays into three major secondary faults; two of them trend southwest and the other trends north-northeast. The trace of this major fault is marked by 1) lineaments in air photos, 2) truncated slope and ridges, 3) breccia and shear zones, and 4) sudden changes in the courses of the Rahu, May, and Brown Grey Rivers. The splay pattern of the Rahu Fault is somewhat similar to that generated by a uniaxial compression described by Chinnery (1966 a, 1966 b).

VI/2 THE PROPOSED KOURA FAULT ZONE

The proposed Koura Fault Zone is nearly 1 km wide. Although no fault trace is visible on the ground,

the structure may be considered to be present because of the following observations.

1) The occurence of a chain of quartz-talc-carbonate intrusive bodies near Trig. GA hinting that their emplacement is structurally controlled--possibly by a fault (refer Farmer's map 1967, unpublished thesis).

2) The presence of lenses of the Koura Formation within the Alfred Formation. These bodies of Koura Formation rocks are aligned like those intrusives in 1).

3) The isolated occurence of a body of biotite schist in the general area of chlorite grade schist. The mineral assemblage and deformation texture in the schist here have been recognised as similar to those in the vicinity of Palmer's Bend.

4) The discordance in bedding attitudes of the Koura and Alfred Formations 1.5 km NE of Trig. GA.

5) The contrasting lithologies and bulk composition differences in the sediments to each side of the proposed structure south of Palmer's Bend (predominantly feldspathic sandstone in the west and mostly mudstone and limestone in the east).

The exact age of the proposed Rahu Fault Zone is not known. However, the allochthonous block of biotite schist containing F2 and F3 crenulations suggests that the last transcurrent movement is post-regional metamorphism and is not older than Cretaceous. The strike slip along the Koura Fault is dextral and the apparent displacement is of the order of 6 km or more.

VI/3 THE RAHU FAULT ZONE

This major structure first recognised by Fyfe (1926-1930) is also about 1 km wide. Its age like that of the Koura Fault Zone is uncertain. The sinistral transcurrent movement--at least 1 km apparent displacement--is suggested by the displaced granite-metasediment contact in May Creek. The age of this faulting is post-granite emplacement, i. e. it is not pre-Devonian (see chap. IX/7). The fact that Carboniferous-Jurassic sediments and Tertiary rocks are displaced by this fault suggests that the Rahu Fault was active in post-Tertiary times (possibly not before the Eocene) or was active in post-Carboniferous and post-Tertiary times. Although there is no conclusive evidence against or for any one of the possibilities, the writer prefers the latter because it is not inconceivable that the reverse movement along the pre-existing Koura Fault during the Rangitata Orogeny had given rise to the formation of the Rahu Fault system, and that activity along the latter fault was renewed during the Kaikoura Orogeny (refer VI/6).

VI/4 THE UPTHROWN SIDE ON THE KOURA AND RAHU FAULTS

The amount of throw on the two major structures is uncertain. The upthrown side on the Koura Fracture System may be inferred as being to the east of the major structure from the occurence of almandine schist on the

east, and andalusite hornfels on the west (the situation may be considered to be analogous to that of the Alpine Fault). As for the Rahu Fault, the direction of throw is not determinable. The approach used for inferring the upthrown side in the case of the Koura Fault is not applicable here because the metamorphic rocks on both sides of the major structure suffered low-pressure metamorphism before or during the formation of the Rahu Fault.

Although the dip of the Rahu Fault is not directly determinable, the steep fault planes observed in the associated minor faults suggest that the fault plane of the major structure is possibly also steeply dipping. Unlike the attitude of the Rahu Fault plane which can be inferred from the attitudes of the minor associated faults, the dip of the Koura Fault plane is unknown.

VI/5 THE RELATIVE AGE OF THE KOURA AND RAHU FAULTS

The relative age of the two major structures is hard to establish. However, according to the most recent interpretation of the New Zealand Lower Paleozoic sediments in Buller, Westland, and NW-Nelson, the Koura Fault may be considered to be the older structural feature as discussed in the following.

Shelley (1975) in his discussion on the Tuhuan paired metamorphic belts, pointed out that the Eastern Belt described by Cooper (1975) is characterised by relatively high pressure metamorphism, and is seperated from the relatively low-pressure metamorphosed Western and Central Belts by a median boundary. This Tuhuan

median boundary has been recognised in the thesis area, and is known to coincide with the Koura Fault System. As the median boundary is also the fundamental contact zone of two bodies of rocks of contrasting rigidity it is a natural weak site. In such circumstances, it is not inconceivable that during the Tuhua Orogeny, the Tuhuan median boundary became at least in parts a significant fracture zone just like the major portion of the Rangitatan median boundary which became the Alpine Fault (see Fig. 3 of Shelley 1975). This would make the Koura Fracture System the older feature because the Rahu Fault is not pre-Carboniferous.

The relative age of the Koura and Rahu Faults may also be determined by the relationship of the two structures and their directions of transcurrent movement. The fault relationship depicted in Fig. (67) may be viewed as due to 1) secondary faults of a single system or 2) faults belonging to two systems; the older structure is intersected by the younger ones. The directions of transcurrent movements along the Koura and Rahu Faults are not the same whereas similar directions of movement are commonly observed in the case of secondary faulting as shown by Chinnery (1966 a, 1966 b), and Anderson (1951). It is probable therefore that the Koura and Rahu Faults are two discrete systems. The fault trace pattern shown in Fig. (68) suggests that the Koura Fault is the older structure and it is intersected by the younger Rahu Fault.

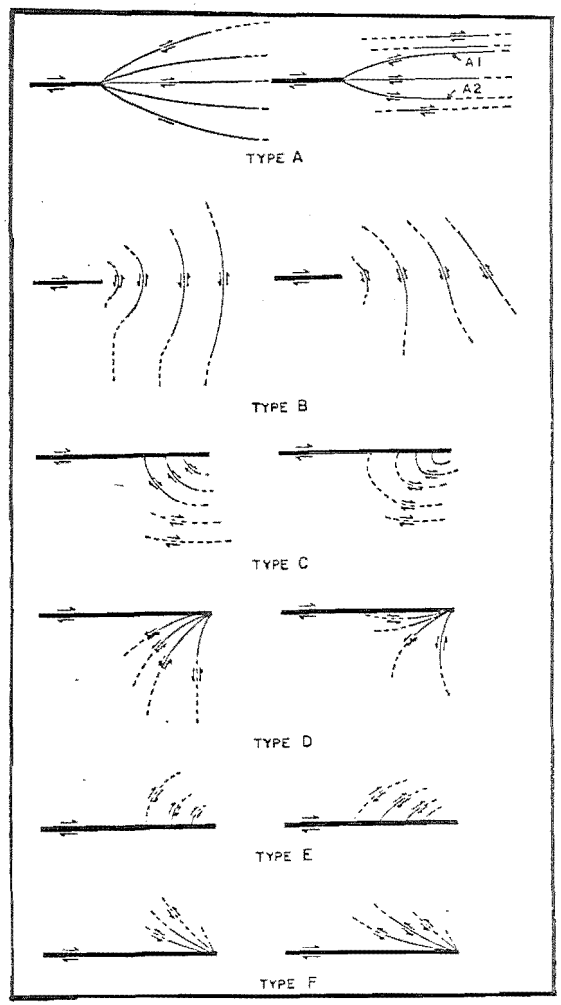

pure shear uniaxial compression

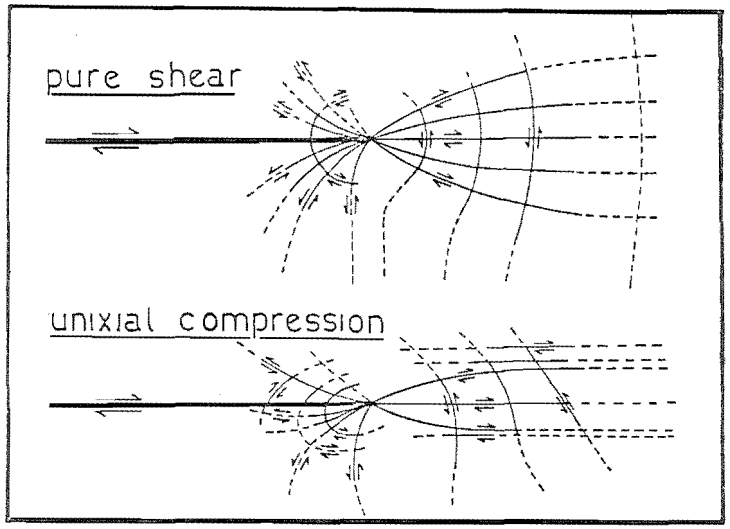

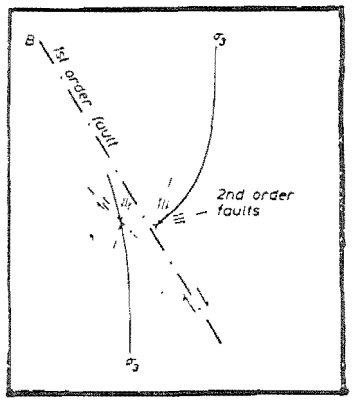

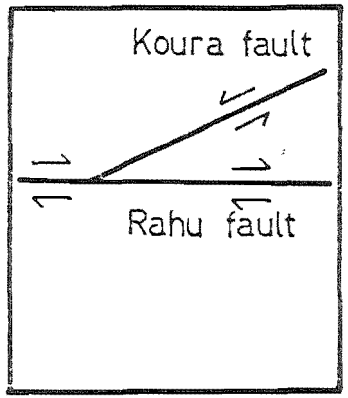

schematic diagram

Modes of secondary faults described by Chinnery (1966) and Anderson (1951) . The schematic diagram for the Koura and Rahu Faults has been flipped over for the purpose of easy comparison with Anderson's and Chinnery's diagrams . Note that the direction of transcurrent movement along the Koura Fault is not the same as that along the Rahu Fault . As this is unlike those of secondary faults, the Rahu and Koura Faults are features belonging to two discrete major fracture system .

FIG. 67

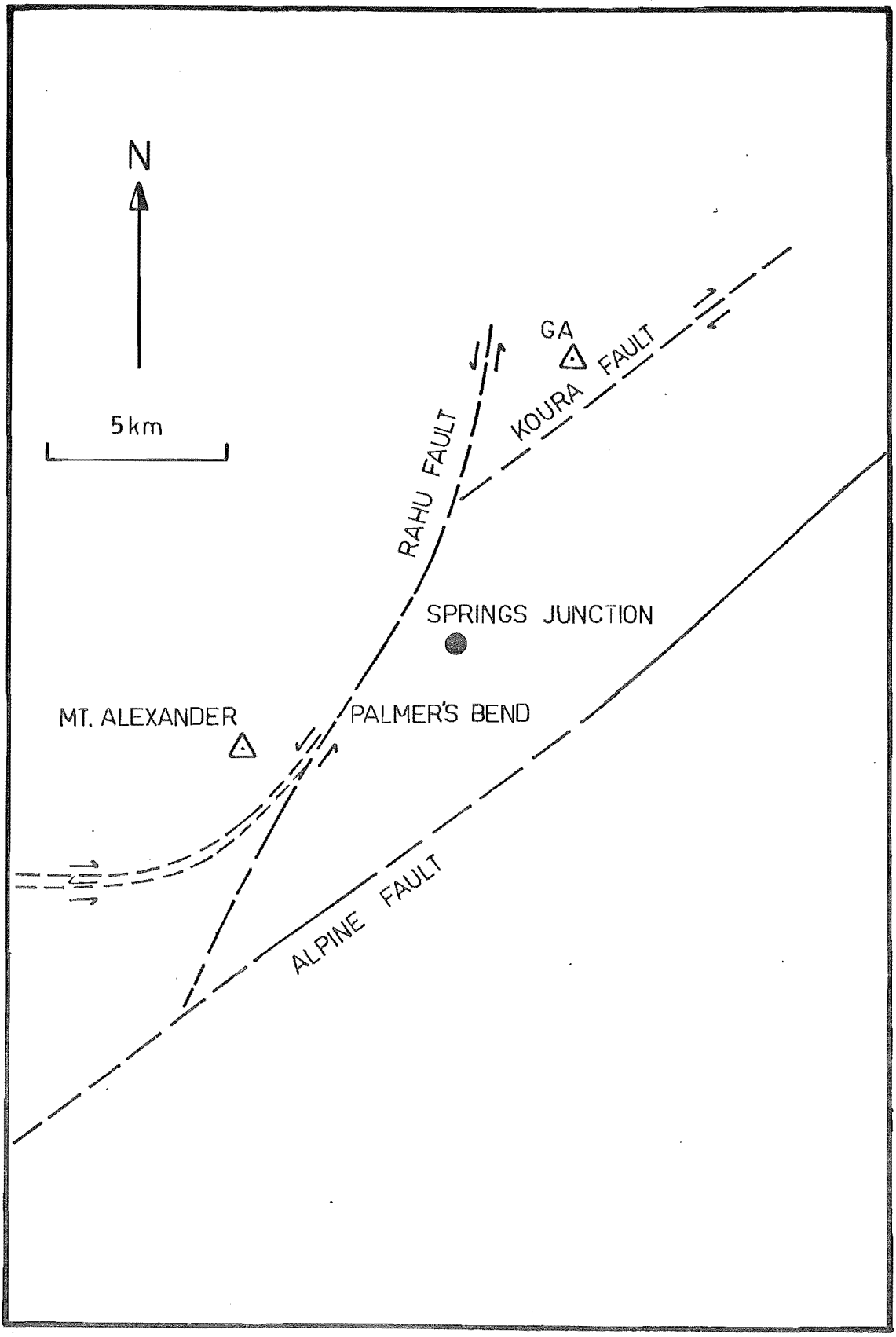

FIG. 68 A sketch map of the Koura and Rahu Fault Systems . Note that the former is dextral, and the latter is sinistral .

VI/6 HISTORY OF FAULT MOVEMENTS

As proposed in section VI/5, the Koura Fault was formed possibly during the Tuhua Orogeny (Devonian-Carboniferous). The nature of fault movement(s) during this period is unknown. The writer, however, suspects that faulting was probably very complicated. The last known transcurrent movement (dextral) on the Koura Fault is post-regional metamorphism and post-Rangitatan Granite emplacement. The date of this event is considered as not older than Cretaceous.

Unlike the preceeding case, the date of the development of the Rahu Fault can not be inferred. The last sinistral strike-slip along this structure is either post-Tertiary (i. e. possibly post-Eocene) or post-Carboniferous. It is conceivable that transcurrent movement occured both post-Carboniferous and post-Tertiary. As part of the Rahu Fault merges with the Koura Fault in the area west of Springs Junction, the latter structure may be considered to have undergone reverse transcurrent movement some time after the Cretaceous period--possibly during the late Rangitata Orogeny (see preceeding paragraph). Strike-slips in the same direction could have possibly occurred again sometime after the Tertiary period, coinciding with the Kaikoura Orogeny.

The movement on the Koura/Rahu Fault in the Lower Brown Grey River valley is post-granite emplacement as suggested by the invasion of pegmatitic and granitic

veins in the fault breccia and near-by granites. Because the Victoria Range Granite is probably a mixture of Cretaceous, and Devonian-Carboniferous intrusives, the date of this structural event is somewhat uncertain (Chap. IX). However, as the Cretaceous aureole in the almandine schist on the east is 'truncated' by this fault, and as the pegmatitic and granitic veins are not sheared, it is conceivable that the age of this episode of faulting is not older than Cretaceous--possibly related to the dextral transcurrent movement known in the vicinity of Trig. GA. The vertically folded granitic dykes exposed along the Rahu Saddle road are considered by the writer to have formed some time not earlier than Cretaceous and probably not later than Cretaceous; the latter limit is inferred from the plastic response of the dykes to folding.

VI/7 SUMMARY

Studies of the Koura and Rahu Fracture Systems reveal the following:

1) Both structures are approximately 1 km wide. The Rahu Fault south of Palmer's Bend splays into a series of secondary faults (at least two faults).

2) The upthrown side of the Koura Fault is probably on the east. As for the Rahu Fault the direction of throw is unknown.

3) Although the exact ages of the two major structures are unknown, the Koura Fracture System may

be inferred from Shelley's model of paired Tuhuan metamorphic belts to be Devonian-Carboniferous. The last known transcurrent movement (dextral) occurred some time after the Cretaceous. The sinistral strike-slip along the Rahu Fault is post-Carboniferous or post-Tertiary (possibly post-Eocene) or even both post-Carboniferous and post-Tertiary.

4) Part of the Rahu Fault which merges with the Koura Fault could have caused reverse transcurrent movement along the structure in the area west of Springs Junction.

5) The apparent displacement along the Koura and Rahu Faults is approximately 6 km, and 1 km respectively.

CHAPTER VII

METAMORPHISM IN THE ROCKS OF THE KOURA FORMATION

VII/1 LITHOLOGIES:

Most of the lithologies in the Koura Formation are green or bluish-green in colour. The rocks are generally tough, pyritic, medium- to coarse-grained, and have a distinctive smell when they are wet. Due to the nature of the lithologies described below, their alteration, and the poor exposure (and the lack of time) bedding characteristics and their interrelationships are poorly understood.

A. HORNBLENDE-BIOTITE ANDESITE

This is the most common lithology in the Koura Formation. The rock has a porphyritic texture. The phenocrysts are hornblende and strongly zoned plagioclase, and the groundmass is composed of fine-grained feldspar(s). The igneous mineral assemblage is hornblende + biotite + plagioclase (suspect within range of andesine) + quartz + alkali feldspar(s) + zircon (accessory mineral).

B. VOLCANOGENIC CONGLOMERATE

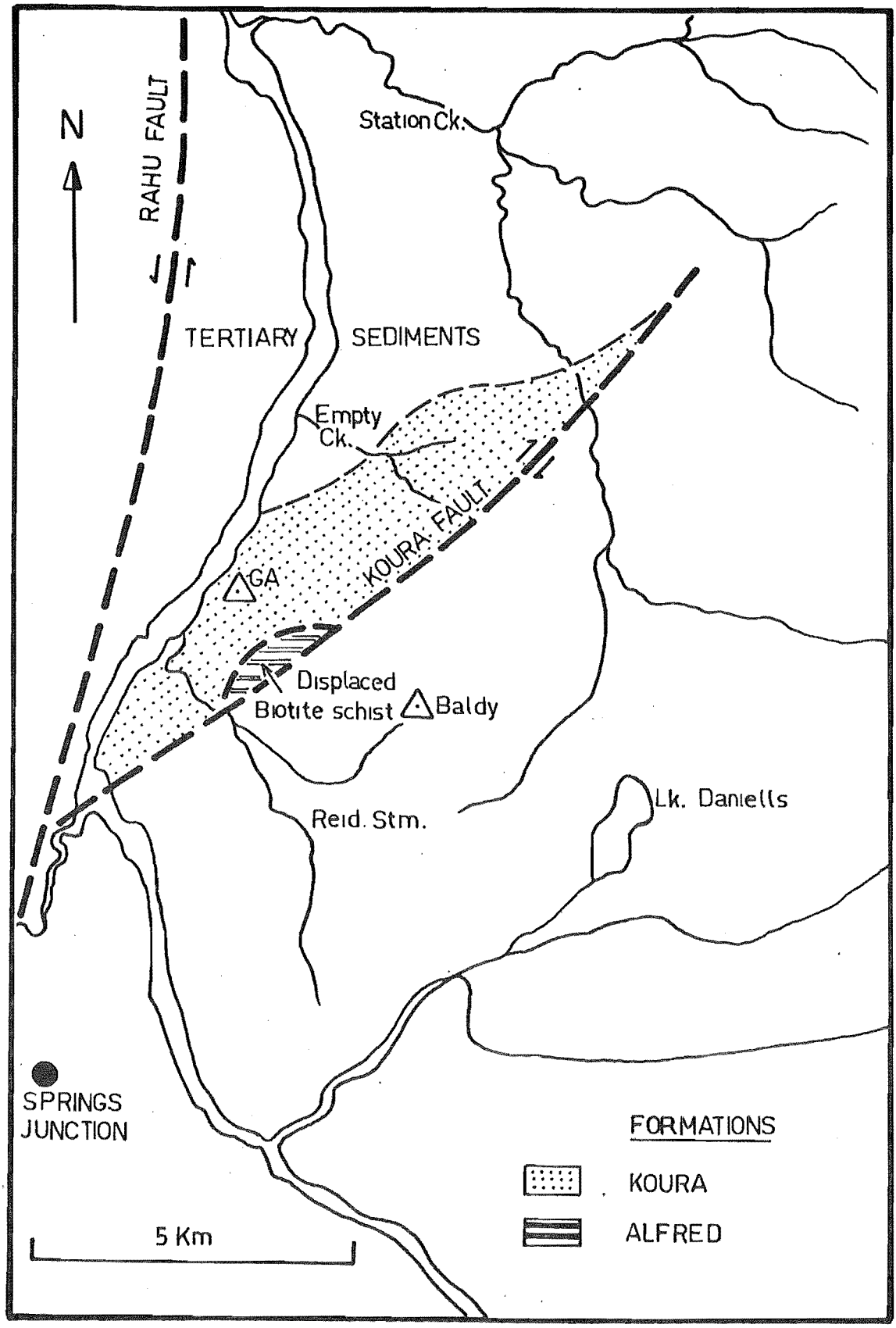

FIG. 69 Map showing the distribution of the Koura Formation, the localities mentioned in this chapter, and a sliver of biotite schist displaced from Palmer's Bend .

This rock is made up of rounded quartz and volcanogenic pebbles set in a tuffaceous matrix. Some of the latter pebbles have a similar composition to the groundmass. The conglomerate is usually extensively altered and the original clastic minerals and textures are not recognisable. However, as the metamorphic mineral assemblage is very similar to that observed in the metamorphosed andesite, one may assume that the conglomerate matrix and pebbles were originally composed of fragments of plagioclase, alkali feldspar(s), quartz, hornblende, etc.

C. TUFFACEOUS SEDIMENTS

These tuffs are generally fine grained and a weakly developed schistosity is visible in handspecimens. At Trig. GA, the rock has a well developed slaty-cleavage. This fabric is known to intersect bedding at a low angle in the rocks from Empty Creek. Subsequent crenulation of the slaty-cleavage has produced a prominent lineation in the rock.

VII/2 EFFECTS OF METAMORPHISM

A. MINERALOGICAL CHANGES:

i) IN ANDESITE

Hornblende and green biotite are altered to Mg-chlorite, and to a lesser extent, calcite and epidote. The zoned plagioclase, and fine-grained feldspar(s) are replaced by calcite, epidote, and zoisite. Some of the

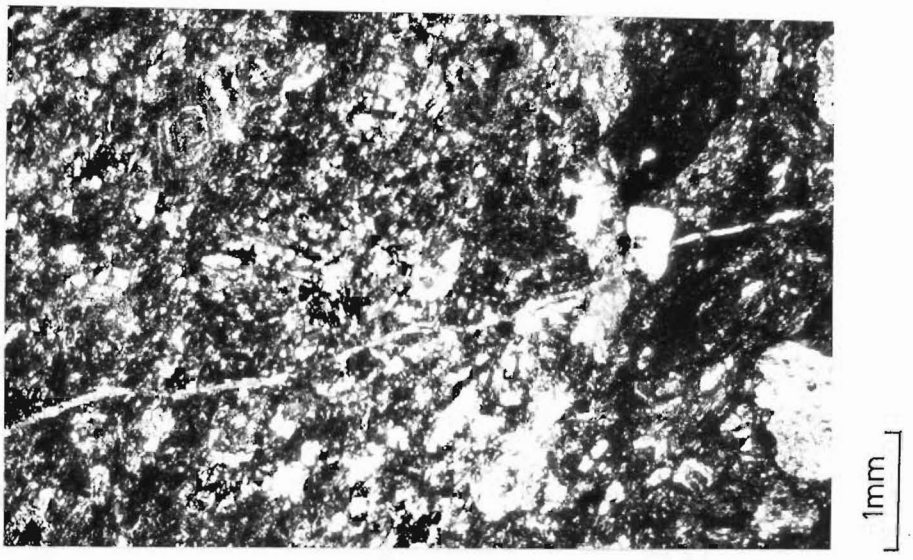

S46 646112

FIG.70 Zoned andesine in the igneous rocks from the Koura Formation . Note the porphyritic texture, and extensive alteration by chlorite and calcite .

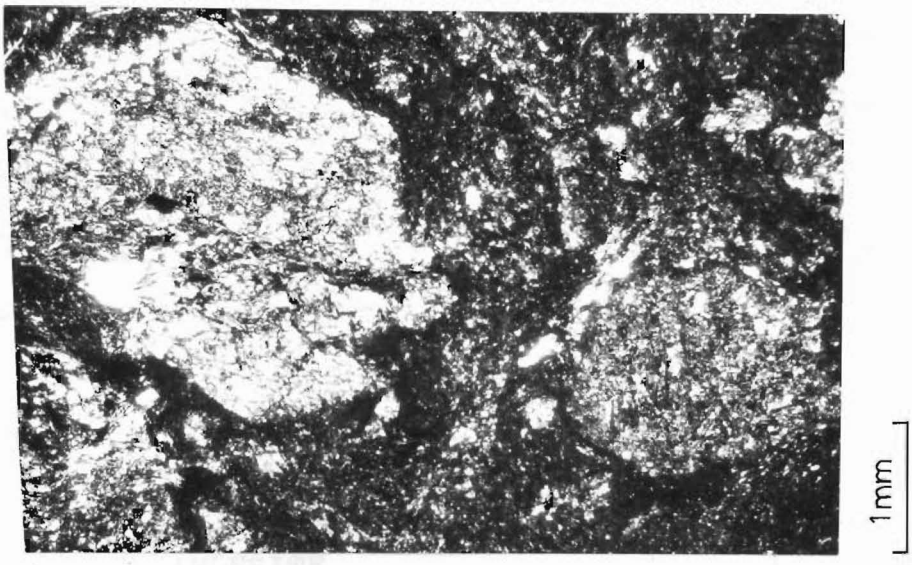

S46 648108

FIG. 71 Chlorite pseudomorphs after hornblende crystals in the igneous rocks of the Koura Formation .

plagioclase is converted to albite. Quartz is recrystallised to polygonal aggregates. The metamorphic mineral assemblage is as follows:

albite + epidote + zoisite + Mg-chlorite + calcite + quartz.

ii) IN CONGLOMERATE

Unlike andesite, this rock is so extensively altered that its clastic mineralogy is completely obscured. However, as the metamorphic mineral assemblage of the conglomerate is similar to that in the meta-andesite, one may infer that the mineralogical changes are like those described in i).

iii) IN TUFFACEOUS SEDIMENTS

Sericite/muscovite, Fe-chlorite, albite, and quartz are crystallised in the volcanogenic sediments. The platy minerals may be assumed to have formed from the clay-minerals originally present in the rock. Quartz and albite are recrystallised from pre-existing quartz and feldspar(s).

B. TEXTURAL CHANGES:

i) IN ANDESITE

Epidote - the most abundant mineral, and zoisite occur as granular aggregates and bladed crystals. Quartz is recrystallised to polygonal aggregates. Chlorite and calcite usually occur in forms which are typical of re-

placement minerals. The latter together with epidote is known to invade pre-existing feldspars. Chlorite psuedomorphs after hornblende and biotite are observed in specimen UC 5816. The newly formed albite is commonly anhedral and untwinned. In the andesite specimen UC 5816, elongate blebs of calcite, chlorite, and granoblastic-elongate quartz form an incipient schistosity in the rock.

ii) IN CONGLOMERATE

The original clastic texture is completely obliterated by the formation of new minerals. The new texture of the rock is generally similar to that seen in the meta-andesite.

iii) IN TUFFACEOUS SEDIMENTS

Like the conglomerate, this rock is completely reconstituted. Sericite/muscovite and to a lesser extent, chlorite are dimensionally oriented, forming a weak schistosity in the meta-sediment. The pre-existing feldspars and quartz are recrystallised to polygonal aggregates.

VII/3 METAMORPHIC FACIES/GRADE - TEMPERATURE/ PRESSURE OF METAMORPHISM

The mineral assemblages in andesite, volcanogenic conglomerate, and tuffaceous sediments are as follows.

Meta-andesite : albite + epidote + zoisite + Mg-chlorite + quartz + calcite

Meta-rudite : albite + epidote + Mg-chlorite + calcite + quartz ± zoisite

Meta-sediments : sericite/muscovite + Fe-chlorite + albite + quartz

According to Winkler (1967), the absence of laumontite, pumpellyite-prehnite, pumpellyite-epidote, and lawsonite in the meta-sediments indicates that metamorphism is of the greenschist facies. As metamorphic hornblende is absent in the metamorphosed andesite, it is likely that the metamorphism experienced by the rocks of the Koura Formation is not higher than the quartz-andalusite-plagioclase-chlorite, or quartz-albite-epidote-almandine subfacies. The breakdown of hornblende in the andesite, and the lack of biotite in the metamorphosed volcanogenic mudstone support this suggestion; the latter suggests that the metamorphic conditions were probably those of the quartz-albite-albite-muscovite-chlorite subfacies that is at least a moderate type metamorphism. The lack of biotite in the meta-sediments limits the maximum metamorphic temperature to not greater than 450° C, and the entry of zoisite in the meta-andesite restricts the minimum temperature to not less than 350° C. This temperature range is consistent with that suggested by the complete breakdown of clay-minerals in mudstone, forming sericite

and other platy minerals (see Miyashiro 1973, p. 199).

Although the temperature range has been successfully inferred from the crystallization of certain minerals in the metamorphic rocks, the pressure range is less certain. However, the widespread occurrence of this low grade metamorphism and the lack of granites and rapid metamorphic gradients suggest relatively low geothermal gradient. According to Shelley's (1975) model of the pre-Tuhuan paired metamorphic belt, the Koura Formation is on the eastern side of the pre-Tuhuan median boundary. In such a case, the lower greenschist facies will be of the Barrovian type.

The stilpnomelane reported by Brathwaite (1968) in the same belt of volcanics and volcanogenic sediments near Lake Boulder in NW-Nelson district suggests that the Koura Formation was probably metamorphosed in conditions of moderate to high pressure.

The above classification according to Winkler's (1974) new scheme of metamorphic division is equivalent to the low grade metamorphism (see Winkler 1974, p. 231). This newly assigned metamorphic division is defined by

i) the absence of laumontite, lawsonite, pumpellyite, glacophane, and prehnite,

ii) the presence of epidote-clinozoisite.

i) + ii) indicate the start of the mentioned metamorphic grade. The absence of almandine and metamorphic hornblende indicates that the metamorphic conditions were probably those of the beginning of low-grade-metamorphism.

VII/4 CORRELATION AND AGE OF METAMORPHISM

The rocks of the Koura Formation have previously been correlated with the Anatoki Formation (Haupiri Group - Cambrian) of NW-Nelson by Bowen in 1964. This correlation was rejected by Farmer in 1967 who tentatively assigned them to the Lee River Group (Permian). In light of the most recent interpretation of the Lower Paleozoic geology of Westland, Buller, and NW-Nelson, Farmer's correlative is now considered by the writer to be erroneous. The metamorphosed volcanogenic rocks of the Koura Formation can be correlated with the Haupiri Group of NW-Nelson as originally suggested by Bowen (1964) on the basis of 1) lithology, 2) Cooper's model (1975) of the New Zealand Lower Paleozoic sedimentary belts, and 3) Shelley's (1975) model of paired metamorphic belts.

According to the latter model, the Koura Formation being on the eastern side of the pre-Tuhuan median boundary is in the higher-pressure part of the pre-Tuhuan metamorphic belt. The metamorphism in the Koura Formation has been noted as probably the Barrovian-type lower greenschist facies and in such a case is likely to be related to the pre-Tuhua Orogeny (pre-Devonian).

VII/5 SUMMARY

The effects of metamorphism in the rocks of the Koura Formation are as follows:

i) Andesite is metamorphosed to meta-andesite (sometimes weakly schistose) of the lower greenschist facies.

ii) Conglomerate is metamorphosed to meta-rudite of similar metamorphic grade as in i).

iii) Tuffaceous sediments are metamorphosed to schistose meta-sediments of the lower greenschist facies.

The mineral assemblages indicate that metamorphism is at temperatures of 350° - 450° C, and pressures typical of the Barrovian-type facies (medium to high).

According to the most recent studies and interpretation of the Lower Paleozoic geology of the NW part of the South Island of New Zealand, the rocks of the Koura Formation can be correlated with the Haupiri Group (Cambrian), and the age of metamorphism is conceivably pre-Tuhuan--possibly older than 450 my.

CHAPTER VIII

RE-APPRAISAL OF THE LOWER PALEOZOIC SEQUENCE IN SPRINGS JUNCTION DISTRICT

The lithologies in the Koura Formation described by R. T. Farmer (1967, unpublished thesis) are: tuffaceous sandstones, well indurated red and green volcanogenic roundstone conglomerates, carbonate rocks, quartzites, and minor intrusives. Although this Formation has previously been correlated with the Anatoki Formation by Bowen (1964), it was rejected by Farmer on the grounds of 1) the Anatoki Formation is too distant from the Koura Formation (75 km away), and 2) the age of the quartz-talc-magnesite intrusives in the Koura Formation is different from that of the Cobb Intrusives; the former is post-Upper Ordovician and the latter is Cambrian. Farmer considers that the Koura Formation is a member of the Lee River Group (Permian).

Examination of Farmer's approach of correlation by the writer reveal several defects. The proximity of the Permian sediments suggested by him as 30 km north of the Koura Formation is in doubt because the Permian rocks in the Matakitaki district belong to a transported block post the formation of the Rotorua Complex. The nearest Permian sediments known in place are at least 75 km away. The rejection of Bowen's correlative - the Anatoki Formation on the basis of distance is therefore unjustified. Furthermore, the

second criteria used by Farmer in his objection to Bowen's correlation is not valid because the difference in age of the Koura and Cobb Intrusives does not preclude membership of the host rocks of the Koura Formation in the Haupiri Group.

Cooper (1975) has pointed out that the Cambrian - Ordovician volcanics and volcanogenic sediments in the NW part of the South Island of New Zealand are always located west of the Flora, Arthur Marble, Wangepeka, Ellis, and Hailes Knob Formations. Considering that the geographic position of the Koura Formation is in line with the belt of Cambrian - Ordovician volcanics and volcanogenic sediments described by Cooper, and that the formation is located west of the Arthur Marble in the thesis area, it is probable that the Koura Formation is Cambrian - Ordovician in age. Although no fossils are available for a positive correlation, the lithologies of the Koura Formation suggest that it is possibly a member of the Haupiri Group (Cambrian). According to Shelley's (1975) model, the Koura Formation being to the east of the pre-Tuhuan median boundary in the thesis area was affected by pressure metamorphism during the pre-Tuhuan Orogeny. This part of the paired metamorphic belt corresponds with the belt of Cambrian - Ordovician volcanics and volcanogenic sediments mentioned by Cooper, and it is consistent with the suggested age of the Koura Formation discussed earlier in this paragraph. The writer suggests that the unconformity between the Alfred and Koura Formations proposed by Farmer (1967)

be removed, and the latter formation assigned to the Haupiri Group as previously suggested by Bowen (1964).

The Thompson's Flat Formation situated on the eastern side of the Tuhuan Median boundary belongs to the Eastern Belt described by Cooper (1975) and the sediments have been correlated with the Anatoki Formation by Bowen in 1964, and later, with the Flora Formation by Farmer in 1967.

The recent discovery of agnostid trilobites in a marble lense below the Sluice Box Formation in Upper Station Creek by Cooper (1975, pers. com.) suggests that the base of the Thompson's Flat Formation is conceivably Cambrian in age. The striking similarity of lithologies in the Haupiri Group and the Lower Thompson's Flat Formation noted by Cooper and the writer supports the suggested age. If the lower Thompson's Flat Formation is indeed Cambrian, then the important implication in the thesis area is the presence of a condensed sequence below the Sluice Box Formation (Mt. Arthur Marble).

It is worthwhile to note that although both the Koura and Lower Thompson's Flat Formations have been correlated with the Haupiri Group, they were deposited in completely different depositional environments according to Cooper's (1975) sedimentary model during the Lower Paleozoic period. The juxtaposition of the Koura and the Lower Thompson's Flat Formations is brought about by movement of the Koura Fault.

Fig. (72) shows the stratigraphic columns drawn by R. T. Farmer (1967) and the writer (1976).

FARMER'S COLUMN (1967)

Top not recognised

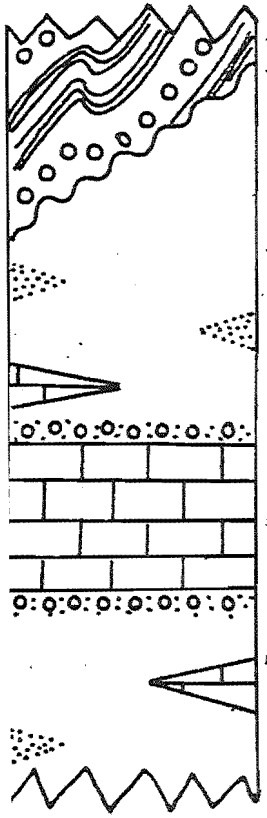

KOURA FORMATION (?UPPER ORDOVICIAN-PERMIAN?)

UNCONFORMITY

ALFRED FORMATION (UPPER ORDOVICIAN)

SLUICE BOX FORMATION (MID-UPPER ORDOVICIAN)

THOMPSON'S FLAT FORMATION (MID-ORDOVICIAN?)

Bottom not recognised

Top not recognised

KOURA FORMATION
(CAMBRIAN?)

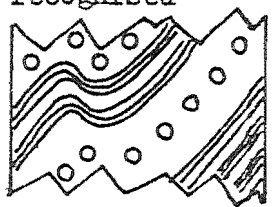

Bottom not recognised

JUXTAPOSED BY MOVEMENT(S) OF THE KOURA FAULT (TUHUAN MEDIAN BOUNDARY)

THE WRITER'S COLUMN (1976)

Top not recognised

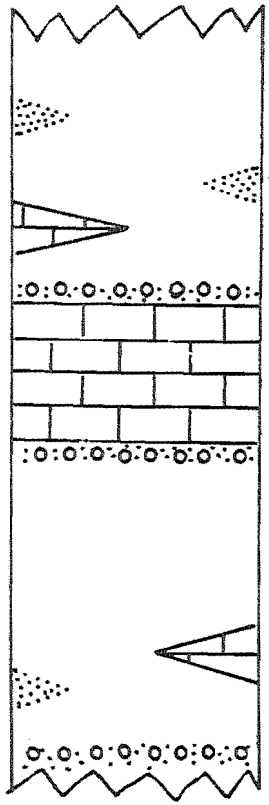

ALFRED FORMATION (UPPER ORDOVICIAN)

SLUICE BOX FORMATION (MID-UPPER ORDOVICIAN?)

THOMPSON'S FLAT FORMATION (?CAMBRIAN-ORDO
(?CAMBRIAN-ORDOVICIAN)

Bottom not recognised

FIG. 72

CHAPTER IX

CONTACT METAMORPHISM IN THE SEDIMENTS, WEST OF THE RAHU FAULT.

IX/1 MAPPING OF THE ROCKS AFFECTED BY CONTACT METAMORPHISM AND THE PROBLEMS ASSOCIATED WITH IT

Mapping of metamorphic rocks is based on mineral paragenesis. This method of mapping is not completely successful because of the following factors.

1) The lack of outcrops at strategic localities. This is due to the thick vegetation cover which prevents rock sampling in the areas where improvement in the siting of the facies boundary, as well as the granite-metasediment contact is required.

2) Sandstone - the predominant lithology is not a sensitive indicator of changes in metamorphic facies. Unless pelite is present, sandstone of the albite-epidote-hornfels facies is usually not mineralogically distinguishable from sandstone of the hornblende-hornfels facies. In some instances, this problem is partially overcome by the use of textural evidence and other minor criteria. The assigned metamorphic classification in such a case carries an element of uncertainty.

3) The heterogeneous distribution of mudstone.

This prevents a full view of the progressive metamorphic changes in pelitic rocks on any one east-west or north-south traverse. The same problem but somewhat enhanced by the vertical facies changes, i. e. sandstone grading into mudstone is encountered by the non-pelitic sediments. The heterogeneous distribution also prevents verification of the assigned metamorphic facies based on textural evidence and other minor criteria.

Despite the fact that the mapping of metamorphic rocks in the Victoria Range is 'plagued' by the above problems, some idea of the facies zonation can be deduced from the distribution of rocks of the albite-epidote-hornfels and hornblende-hornfels facies in the areas north of the Rahu Saddle road. The enclosed map shows that the latter facies can be crudely mapped as a zone parallel to the granite-metasediment contact. Two such zones are present, striking nearly north-south, with the albite-epidote-hornfels facies sandwiched between them. This unusual contact aureole is due to the metasediments being enveloped by the Victoria Range Granite.

IX/2 LITHOLOGIES

Field investigation and thin section studies have revealed only two rock-types, i. e, sandstone and mudstone. The latter is distinguished from the former in the field by the following features.

1) The occurence of andalusite porphyroblasts in rocks near the granite-metasediment contact.

2) The finer grain-size.

3) The better development of schistosity and cleavage.

4) The darker rock colour.

5) Association with pegmatitic/granitic bodies (the intrusives occur almost exclusively in mudstone beds in the Rahu Saddle area).

When examined under a microscope, mudstone is further distinguished from sandstone by the preferred orientation and higher content of muscovite.

SEDIMENTARY STRUCTURES

Although the sediments have suffered extensive recrystallization during contact metamorphism, the primary lithological layerings are preserved. Bedding is distinct and common in the vicinity of the Rocky and Anti-Rocky Creeks. The beds strike nearly north-south, and are generally steeply dipping. The thickness of each layer is variable, ranging from less than 10 cm to just over a metre (Fig. 73). Cross-bedding and laminae are also present. However, these features are rare, and have only been found at two localities in the May and Rocky Creeks (Grid. Ref. 541947 and 572023).

DISTRIBUTION OF LITHOLOGIES

S46 577027

FIG. 73 Bedding in Anti-Rocky Creek . Note the occurence of alternating sandstone and mudstone . This has been interpreted by the writer as Flysh-like deposit .

Sandstone is the predominant lithology in the thesis area, west of the Rahu Fault. It is commonly found in the May Creek section, and along the eastern margin of the metasediment. The rock is progressively finer-grained, and enriched in muscovite towards the western granite-metasediment contact, and north of the Brown Grey River. Along the western margin of the metasediment, sandstone is interbedded with mudstone. The latter becomes the main rock-type in the vicinity of the Rocky and Anti-Rocky Creeks. Although there are no abundant sedimentary structures to indicate that the sediment in this area is Flysch-type, the common occurrence of alternating sandstone and mudstone in these two Creeks suggests that here at least the sequence is probably Flysch-like (Fig. 73).

Fig. (74) gives an impression of the distribution of sandstone and mudstone in the thesis area, west of the Rahu Fault.

IX /3 EFFECTS OF CONTACT METAMORPHISM:

A. MINERALOGICAL CHANGES IN SANDSTONE

In the areas north of the Rahu Saddle road, and 2.5 km southwest of the Brown Grey River bridge, muscovite, albite, quartz, tourmaline, apatite, zircon, and less commonly, biotite are formed in the sandstone of the albite-epidote-hornfels facies. With higher temperature in the hornblende-hornfels facies, calcic-

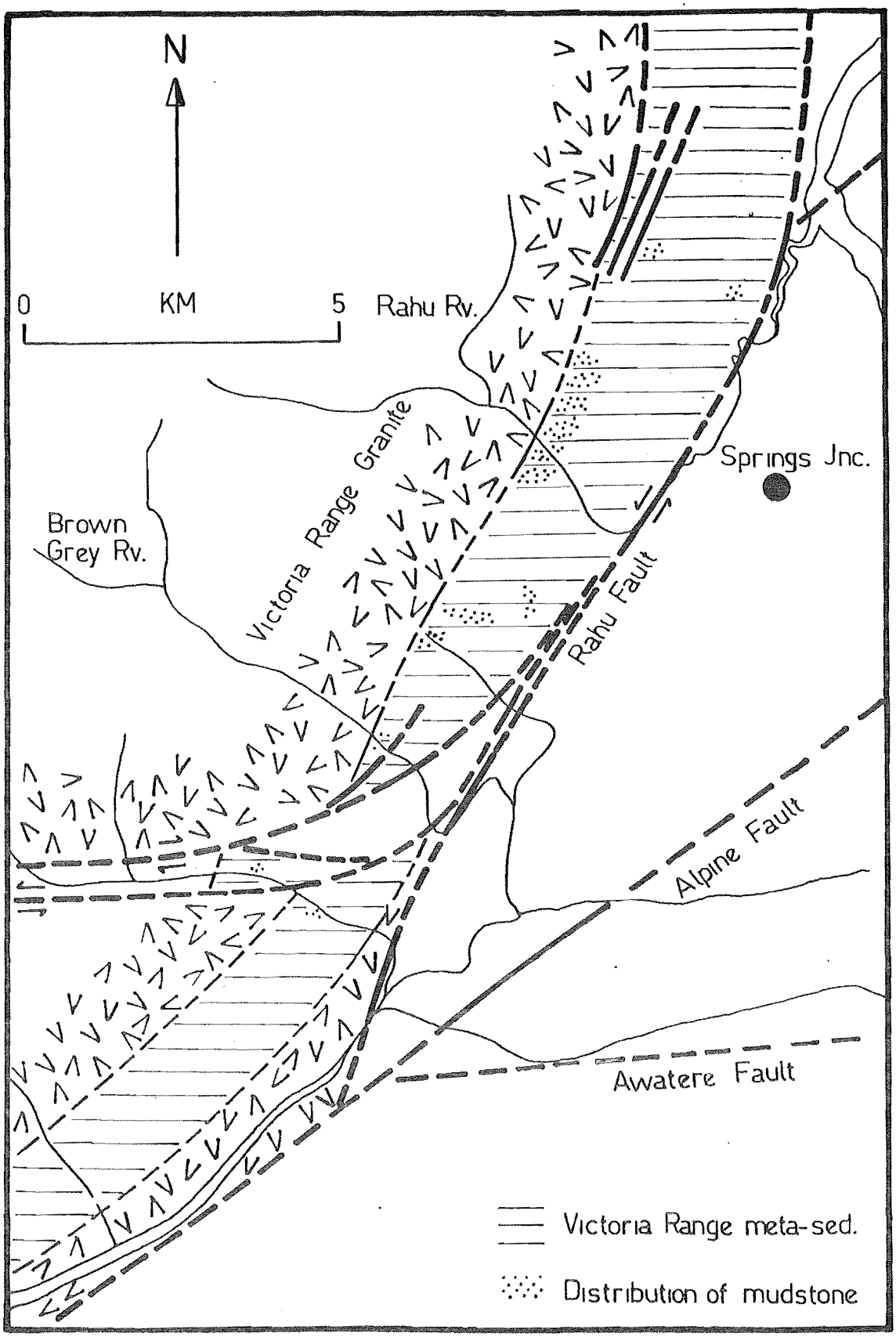

FIG. 74 Map showing the distribution of sandstone and mudstone in the Victoria Range meta-sediments . Note that mudstone is the predominant lithology in the vicinity of the Rahu Saddle .

oligoclase ± K-feldspars ± hornblende are introduced into the mineral assemblage, and the amount of biotite and feldspar is markedly increased.

With further rise in metamorphic temperature, sillimanite is formed in the metasediment. This mineral is rare, and has only been positively identified in the hornfels at Palmer's Bend (pers. com. A. Tulloch). Very fine needles which are probably Sillimanite (although they are too fine grained to identify with certainty) are present in the hornfels at the source of Timpson Stream, 1 km southeast of Trig. A, and 3.5 km northeast of Pinnacle Peak (see map no. 2).

B. MINERALOGICAL CHANGES IN MUDSTONE

Muscovite, quartz, biotite, apatite, tourmaline and zircon are crystallised in the pelite of the albite-epidote-hornfels facies. In the more advanced state of contact metamorphism, andalusite ± calcic-oligoclase ± albite ± K-feldspars are formed in addition to those minerals found in the albite-epidote-hornfels facies and as in the sandstone of the hornblende-hornfels facies, the amount of biotite and feldspar is markedly increased.

C. TEXTURAL CHANGES IN SANDSTONE

The original clastic texture in the rock has been obliterated by widespread and advanced recrystallization

during contact metamorphism. In the albite-epidote-hornfels facies, quartz and albite occur as granular-polygonal aggregates. Muscovite is fine-grained, and it has a poor preferred orientation. Together with the coarser-grained elongate quartz, it forms an incipient cleavage in the rock. Biotite, tourmaline, apatite, and zircon occur as anhedral to euhedral grains. These minerals are randomly oriented, and nearly homogeneously distributed in the hornfels.

With increased temperature, the platy minerals are coarser-grained, and less aligned. The incipient cleavage in the rock is less visible and often not detectable in the handspecimen. The coarser-grained biotite is sometimes poikiloblastic, and occurs as knots as in specimen UC 7744b (Fig. 75). Albite has a very low An content. Like the calcic-oligoclase, it is randomly oriented, twinned, and occasionally contained inclusions of fine-grained quartz and biotite. K-feldspars are commonly observed as untwinned anhedral grains. Quartz occurs as granoblastic-polygonal crystals, and displays a reduction in grain-size range when compared to the same mineral in the sandstone of the albite-epidote-hornfels facies, i. e. the quartz grain size distribution has a tendency to be uni-modal with increased temperature. Myrmekites are very rare, and have been observed in the rocks near the granite-metasediment contact just west of Rocky Creek bridge (Fig. 76). The effect of quartz recrystallization in specimen UC 7807b is one of grain-size reduction,

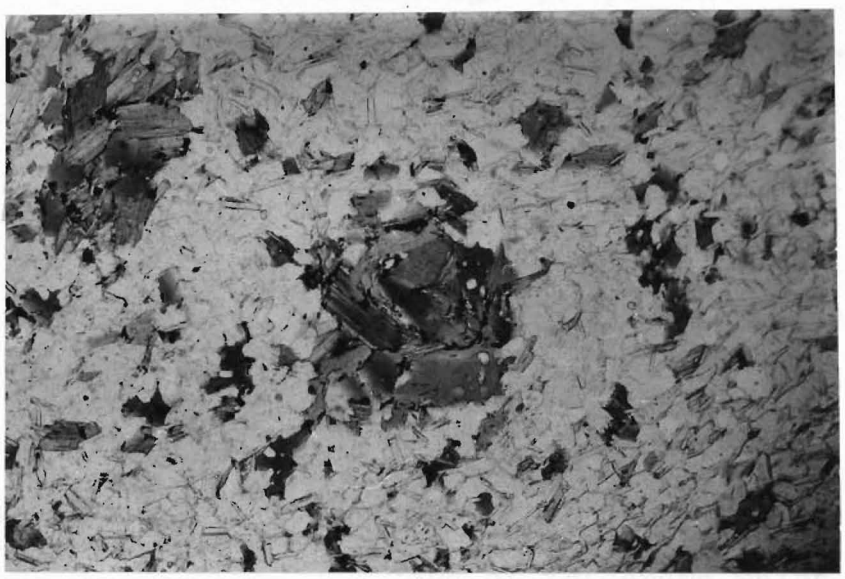

S46 526952

FIG. 75 Biotite knots in the meta-sediment in middle May Creek . Note the poikiloblastic texture of the mineral .

S46 574026

FIG. 76 Myrmekite in the sandstone of the Hornblende-hornfels facies (specimen UC 7731d) .

and grain-shape modification (Fig. 77). The wide spread occurrence of elongate quartz in the hornfels of the thesis area is probably due to the plastic deformation suffered by the metasediment during contact metamorphism.

The plagioclase in the hornfels just west of the Rocky Creek bridge is often zoned (Fig. 78). Detailed thin section studies show that the zoned mineral is composed of a calcic-plagioclase core (max. An = 30), rimmed by layers of feldspars which are progressively impoverished in Anorthite content. The estimated An difference between any two zones is less than 5%. The outer most layer is usually calcic-oligoclase.

The common occurence of oscillatory zonation, and the euhedral nature of the plagioclase within the zoned mineral suggest that zonation in feldspar is not associated with contact metamorphism. In other words, the zonation is inherited from an earlier rock. However, it would be expected that in detrital grains, grain boundaries would cut across zone boundaries. This is not observed. On the contrary, there are large numbers of fine-grained, centrally zoned feldspars. Furthermore, many feldspar grains are poikiloblastic, and it is a fact that zoned plagioclase crystals are known to develop in similar sediments which are xenoliths in the nearby granite, suggesting the opposite situation, i. e. zonation in feldspar is associated with the contact metamorphism. Although there is no strong evidence

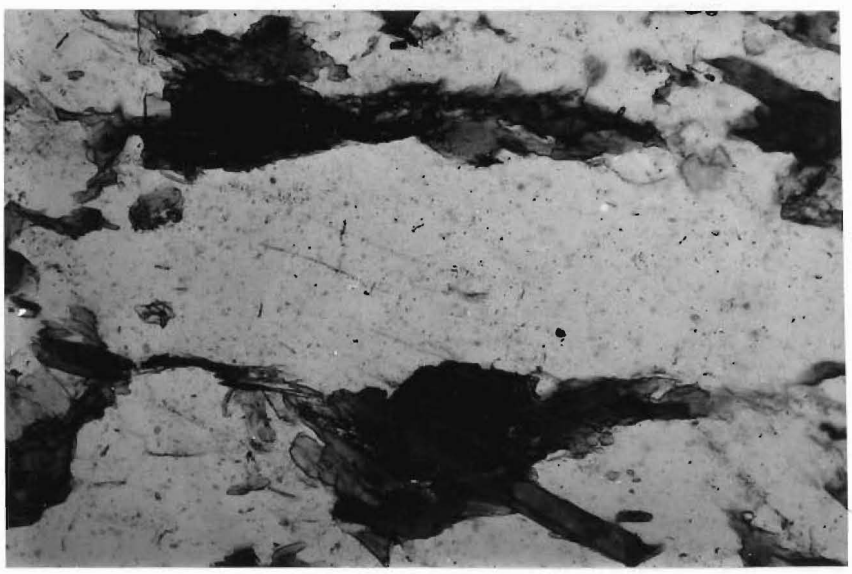

S46 586046

FIG. 77a An elongate grain of quartz photographed in plain polarised light . Compare this with the Fig. below .

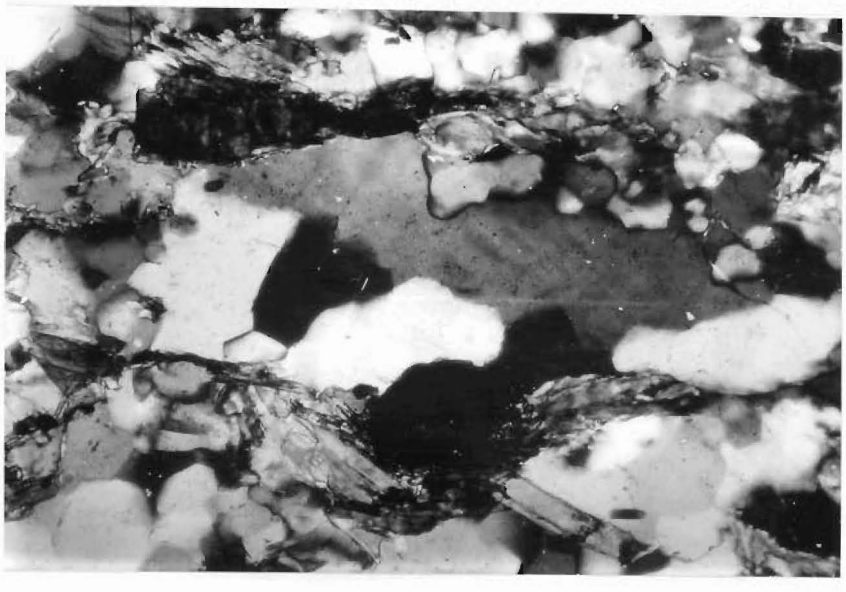

S46 586046

FIG. 77b Same quartz grain as above but photographed in cross-polarised light . Note the effects of recrystallization in quartz are grain-size reduction and grain-shape modification .

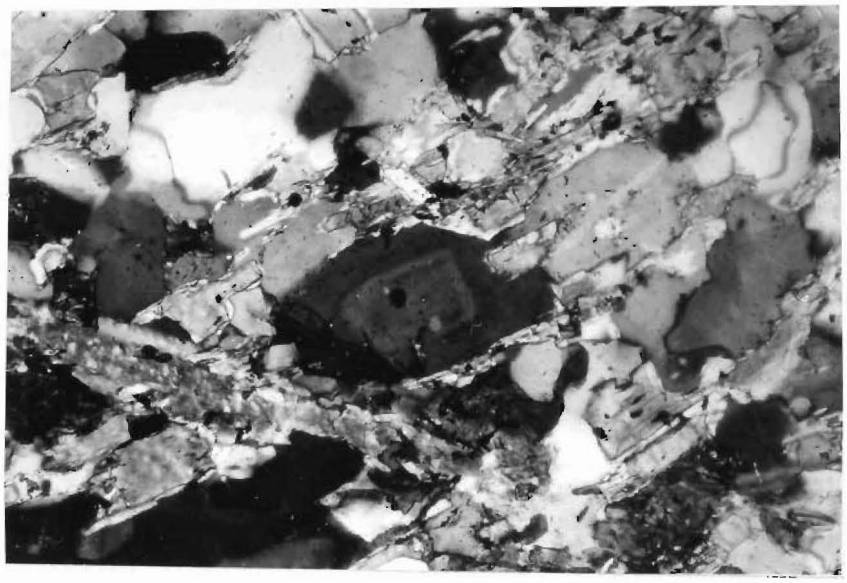

S46 574026

FIG. 78a Zoned feldspar in the sandstone of hornblende-hornfels facies (e.g. specimen UC 7731d) . Note the euhedral grain-shape, and that the zonation is centered in the plagioclase crystal .

S46 574026

FIG. 78b A grain of zoned (normal zonation) plagioclase . Note the occurence of oscillatory zonation .

against the first suggestion, the writer prefers the second possibility. It is conceivable that zonation in the plagioclase is due to any one or more of the following:

1) Introduction of sodium by the granite during contact metamorphism. The localities of zoned plagioclase being restricted to near the granite-metasediment contact support this suggestion. In addition, it helps to account for the occurence of normal zonation instead of reversed zonation usually observed in metamorphic rocks.

2) Influence of temperature, i. e. the plagioclase's ability to incorporate anorthite molecule changes with temperature.

The references for 1) and 2) are in Smith (1974, p. 225).

Sillimanite occurs as robust crystals or as fine needles. The mineral is rarely observed in the metasediment. The coarser-grained tourmaline contains inclusions of quartz.

D. TEXTURAL CHANGES IN MUDSTONE

In the albite-epidote-hornfels facies, the fine-grained muscovite has a strong preferred orientation. Together with the fine-grained granoblastic-elongate quartz, they form a distinct slaty cleavage in the rock. Biotite is not common. When the mineral is present, it is found as fine- to coarse-grained, irregularly shaped porphyroblasts, aligned parallel to the slaty

cleavage (Fig. 79). Some of such crystals contain tiny quartz inclusions. Biotite is sometimes kinked, and wrapped by the slaty cleavage as seen in specimens UC 7800 and UC 7803a (Fig. 80).

Nearer the Victoria Range Granite, in the hornblende-hornfels facies, the grain-size of muscovite increases from less than 0.04 mm to greater than 0.12 mm. The mineral occurs as discrete plates instead of a 'mass' of very fine-grained muscovite with preferred orientation as commonly seen in the pelite of lower metamorphic grade (see Fig. 81). This mica together with biotite and granoblastic-elongate quartz forms a schistosity in the rock which is later crenulated. The amount of biotite is greatly increased. The coarse-grained biotite is often poikiloblastic, containing inclusions of quartz and zircon. Quartz occurs as granoblastic-polygonal crystals. The grain-size distribution like that in the lower grade pelite is uni-modal. Andalusite crystals are seen as diamond- or square-shaped sections, ranging from 2 to 10 mm, and often contain undeformed relict schistosity (Fig. 81). The longer axis of the crystals together with the relict schistosity are sometimes aligned parallel to the schistosity in the rock. In specimens UC 7681 , UC 7839 , and UC 2833, the porphyroblasts are wrapped by the axial planes of the crenulated schistosity. These observations indicate that andalusite is pre-tectonic. Like biotite, the feldspar content is markedly increased. Albite has a very low An content,

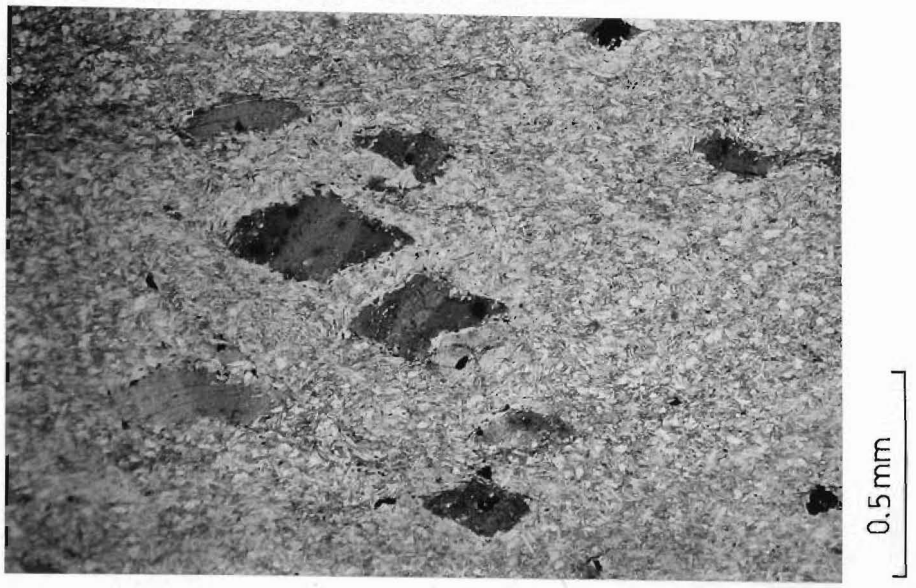

S46 590046

FIG. 79 Irregularly shaped biotite porphyroblasts in mudstone of the albite-epidote hornfels facies . Note that the porphyroblasts are aligned parallel to schistosity / slaty-cleavage . Also, note that the slaty-cleavage is deformed the biotite porphyroblasts .

S46 590046

FIG. 80 Kinked biotite . Examination of this thin section under a microscope reveals that the kink-planes in the biotite are parallel to one of the kink-planes belonging the set of conjugate kink folds (refer specimen UC 7800a) . These features are interpreted as structures generated by compression along the layerings i.e. slaty-cleavage .

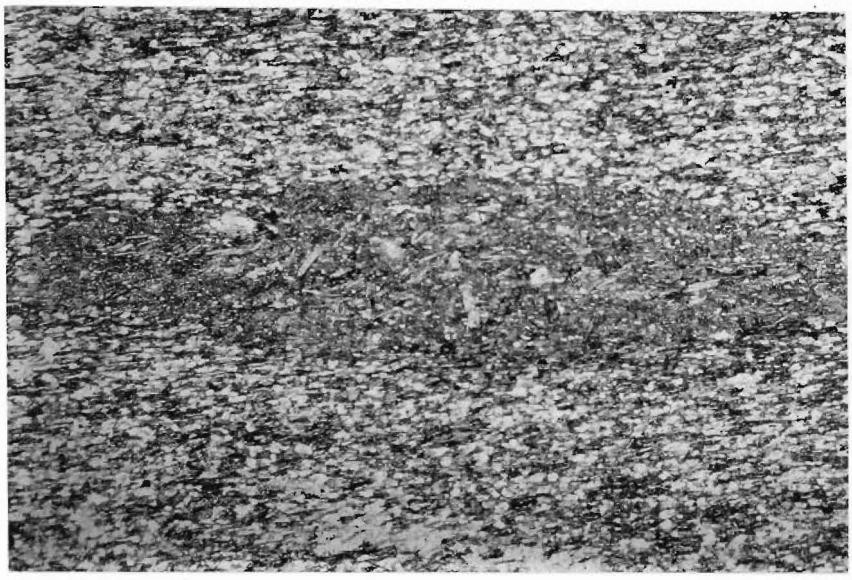

S46 573027

FIG. 81 Mudstone of the hornblende-hornfels facies containing andalusite porphyroblasts . Note that compared with the mudstone in Fig. 79, the muscovite is coarser-grained and occurs as discrete plate . Also note that schistosity is better developed and undeformed both within and around the andalusite crystal . The longer axis of the andalusite is aligned parallel to schistosity .

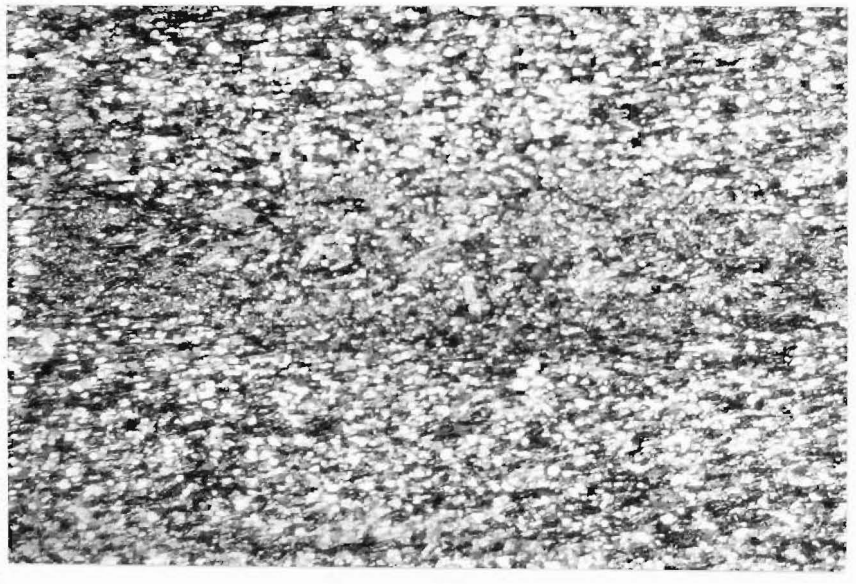

S46 573027

FIG. 82 Undeformed schistosity within the andalusite porphyroblast. The schistosity surrounding the andalusite is also undeformed . Such texture suggest that andalusite is probably not syn-tectonic i.e. pre-microscopic crenulation in chapter X 3/E .

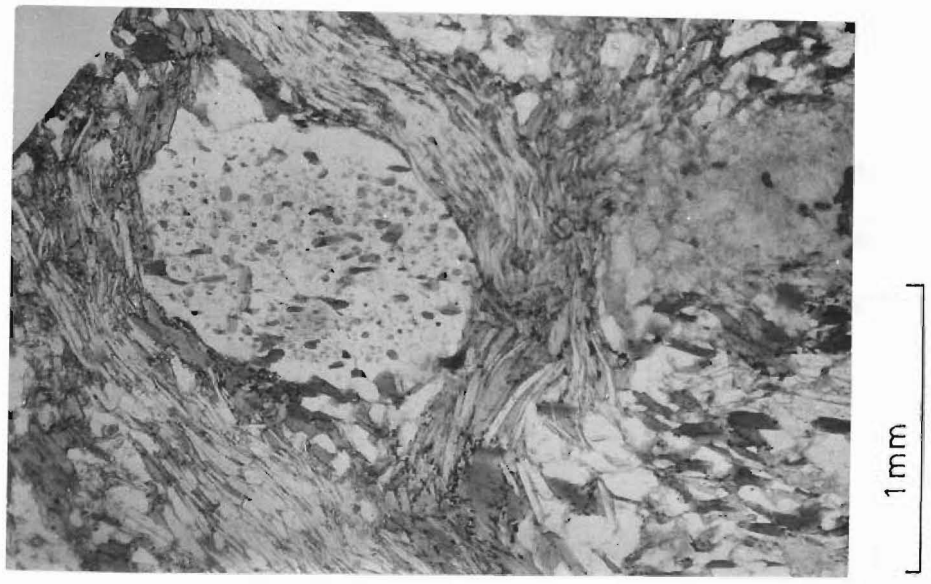

S46 568007

FIG. 83a Andalusite porphyroblast containing undeformed schistosity in specimen UC 7839 . Note that the crystal is wrapped by the surrounding schistosity, suggesting that andalusite is pre-tectonic . Such texture also indicate that the schistosity is unrelated to the contact metamorphism which produced the andalusite . If schistosity is related to granitic intrusion then one would expect schistosity to be deformed around the andalusite porphyroblasts which is not the observed case .

S46 568007

FIG. 83b Same field of view but photographed in cross-polarised light . Note that andalusite has been replaced by quartz and mica .

and like calcic-oligoclase, it is sometimes twinned and poikiloblastic. Some of the plagioclase are zoned. But the zoning is not as developed as that seen in the sandstone of similar facies. Tourmaline, apatite, and zircon are usually anhedral to subhedral, and vary from fine- to coarse-grain. Some of the larger sized tourmaline crystals contain inclusions of quartz.

IX/4 METAMORPHIC FACIES - TEMPERATURE/ PRESSURE OF METAMORPHISM:

A. ALBITE-EPIDOTE-HORNFELS FACIES

In the areas north of the Rahu Saddle road, and 2.5 km southwest of the Brown Grey River bridge, the mineral assemblage in the sandstone and mudstone are muscovite + quartz + tourmaline + apatite + zircon ± albite ± biotite, and muscovite + quartz + biotite + tourmaline + apatite + zircon, respectively. According to Winkler (1967, p. 69), the beginning of the albite-epidote-hornfels facies is marked by the formation of pyrophyllite from kaolinite and quartz at temperature of 400° C. According to Miyashiro (1973, p. 199), the same reaction occurs at 300° to 400° C depending on pressure conditions. Although pyrophyllite is not shown in the mineral assemblages above, it is possible that the mineral is present but unidentified because pyrophyllite is optically similar to muscovite. Even if the mineral is absent, the wide spread occurence

of muscovite in pelite is sufficient evidence to suggest that the temperature is about 400° C (Miyashiro 1973, p. 90 & 201). The presence of biotite supports this suggestion. The upper limit of the albite-epidote-hornfels facies is defined by the destruction of pyrophyllite and the entry of andalusite.

$$1 \text{ pyrophyllite} \rightleftharpoons 1 \text{ andalusite} + 3 \text{ quartz} + H_2O$$

According to Winkler (1967, p. 70), the reaction occurs at about 500° C. Miyashiro (1973, p. 199), however, gave a temperature range of 400° to 500° C depending on pressure conditions. As andalusite is absent, and the amount of biotite in the pelite is very small, it is probable that the metamorphic temperature experienced by the pelite of this facies is not significantly greater than 400° C.

Although there is no direct indication of metamorphic pressure, it may be considered that the pressure conditions in this facies are similar to that determined in the hornblende- hornfels facies.

B. HORNBLENDE-HORNFELS FACIES

The mineral assemblages in the sandstone and mudstone are muscovite + quartz + biotite + calcic-oligoclase + tourmaline + apatite + zircon ± albite ± K-feldspars ± hornblende, and muscovite + quartz + andalusite + biotite + tourmaline + apatite + zircon ±

albite ± calcic-oligoclase ± K-feldspars. According to Winkler (1967, p. 70-72), the beginning of the hornblende-hornfels facies is marked by the disappearance of chlorite in the presence of quartz, and the first appearance of andalusite and hornblende. The wide spread occurence of muscovite + quartz in the metapelite, and the unaltered hornblende in the rock agree with this classification.

The absence of cordierite in the pelitic hornfels indicates that the maximum metamorphic temperature is not greater than 500° to 550° C (Winkler 1973, p. 236). The abundance of muscovite, and the absence of K-feldspar co-existing with sillimanite are consistent with this suggestion. The presence of biotite restricts the minimum metamorphic temperature to not less than 400° C. Using the Al_2SiO_5 phase diagram drawn by Turner (1968, p. 114), the maximum pressure may be deduced as not exceeding 2 to 3 kb.

Fig. (84) shows the inferred P-T conditions of contact metamorphism in the thesis area, west of the Rahu Fault.

IX/5 EFFECTS OF RETROGRADE METAMORPHISM:

A. MINERALOGICAL CHANGES IN THE SANDSTONE HORNFELS

The effects of retrograde metamorphism in this lithology are as follows:

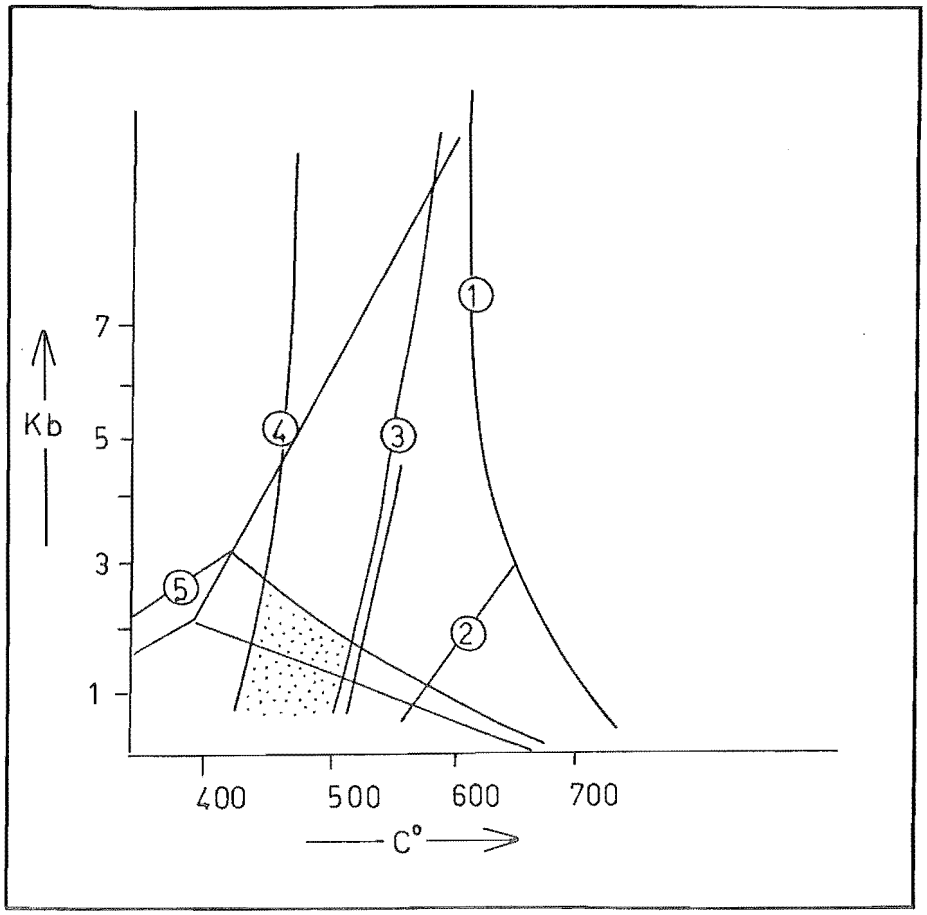

FIG. 84 1) Anatexis on the right handside (Winkler 1973, p.236) .
2) Breakdown of muscovite on the right handside :
muscovite + quartz = K-feldspar + sillimanite (Winkler 1973) .
3) (Staurolite, cordierite)-in on the right handside .
4) (Muscovite + biotite)-in on the right handside .
5) Al_2SiO_5 phase diagram after Turner (1968, p.114) .

The stipled area indicates the probable P-T conditions of contact metamorphism suffered by the Victoria Range sediments .

1) Biotite is partially or completely altered to Mg- or/and Fe-chlorite. Thin section studies show that the Fe-chlorite is the younger mineral, and its occurence and abundance is characterised by a) the distance from pegmatitic/granitic bodies; b) the distance from sheared zones; c) the distance from the granite-metasediment contact; d) an association with limonitic veins, and e) the quantity of minerals which compete for Fe in the system, e. g. zoisite and epidote-clinozoisite. These factors might suggest that Fe-chlorite is formed as the result of metasomatism around pegmatite or granite. In other words the Mg- and Fe-content of chlorites in the hornfels can not be taken as an indication of metamorphic zonation, as suggested by Albee (1962) for other areas.

2) Feldspars and some quartz are replaced by sericite. The degree of alteration in each case is dependant on factors a), b), and c) discussed in 1). It has been observed that intense chloritization of biotite is nearly always accompanied by strong sericitization of feldspars. The altered feldspars are frequently dusty looking. The mineral is commonly altered on the grain-surface, and cleavage planes. Sericitization in the feldspar core is not common.

3) Quartz besides being replaced by sericite, is also very rarely replaced by calcite.

4) Formation of zoisite and epidote-clinozoisite. These minerals are not wide spread in the hornfels, and they tend to occur near pegmatitic bodies or sheared zones. Where epidote-clinozoisite and zoisite

are abundant, the associated chlorite is always of the Mg-variety even when conditions are favourable for the crystallization of Fe-chlorite (see factors a), b), etc. mentioned in 1)).

5) Formation of muscovite due to the introduction of potassium in the hornfels during retrograde metamorphism. Its occurence is restricted to the metasediments of the hornblende-hornfels facies. The mineral displays increased grain-size and abundance with decreased distance from the pegmatitic/granitic bodies. Such a phenomenon is common in the section along the May Creek.

6) Crystallization of adularia. This mineral is frequently found in the hornfels south of the Rahu Saddle road. Its occurence and abundance is apparently related to the presence and the number of pegmatitic/granitic veins.

B. MINERALOGICAL CHANGES IN THE PELITIC HORNFELS

Retrograde metamorphism is not significant in the metasediments of the albite-epidote-hornfels facies, north of the Rahu Saddle road. However, in the hornfels of higher facies, the pre-existing minerals are replaced, and new minerals are formed in the same manner described in the preceeding section IX/5 A. In addition, andalusite is altered to sericite; (muscovite + sericite + quartz + biotite); and less common, (pinnite or kaolinite + muscovite + sericite).

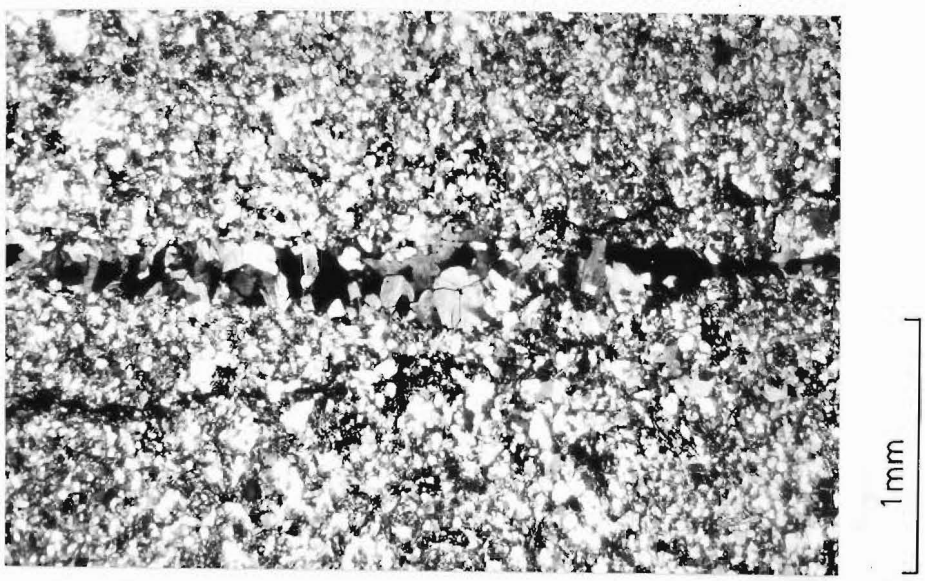

S46 543945

FIG. 85 Adularia vein (centre of picture) in sandstone hornfels .

S46 575025

FIG. 86 Retrograde muscovite in the mudstone hornfels just west of Rocky Creek . Note the coarse-grained and poikilitic nature of the mineral . The inclusions in these muscovite plates are aligned parallel to the pre-existing schistosity .

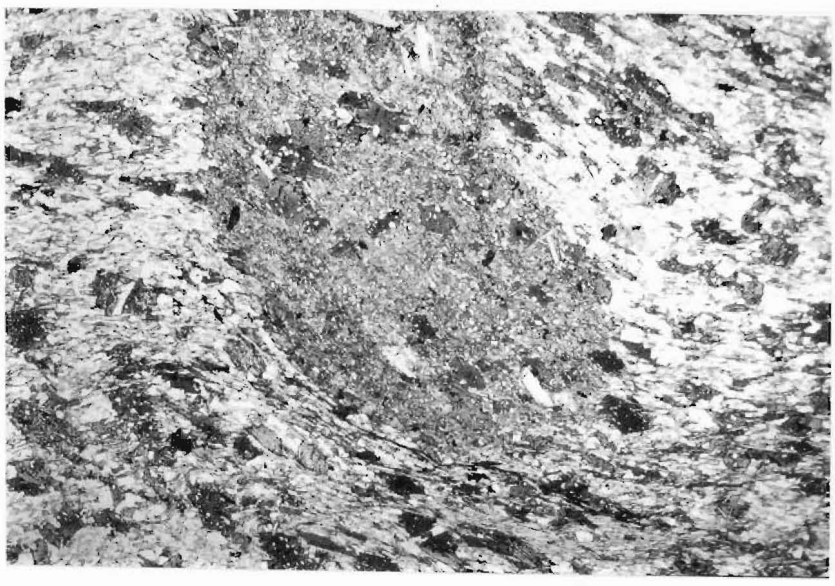

S46 557993

FIG. 87a Zoned alteration of andalusite porphyroblast . Note that a core of quartz + muscovite ± biotite is rimmed by a mica-enriched layer . The above figure is a photograph of andalusite in specimen UC 7792 .

S46 571012

FIG. 87b Zoned alteration of andalusite porphyroblast in specimen UC 7710a . The included schistosity is somewhat obscured by such alteration .

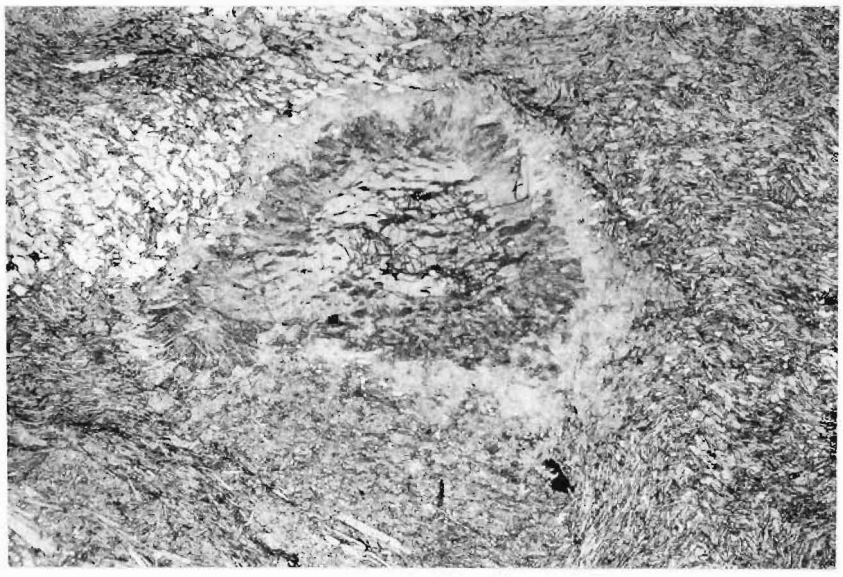

S46 573025

FIG. 88a Zoned alteration of andalusite porphyroblast in specimen UC 2833 . Note that a relict core of andalusite is surrounded by three layers of alteration product ; 1) an inner rim of pinnite or kaolinite, 2) an intermediate layer of radially arranged muscovite, and 3) an outer rim of sericite . Also note that the relict schistosity within the andalusite (defined by biotite) is undeformed .

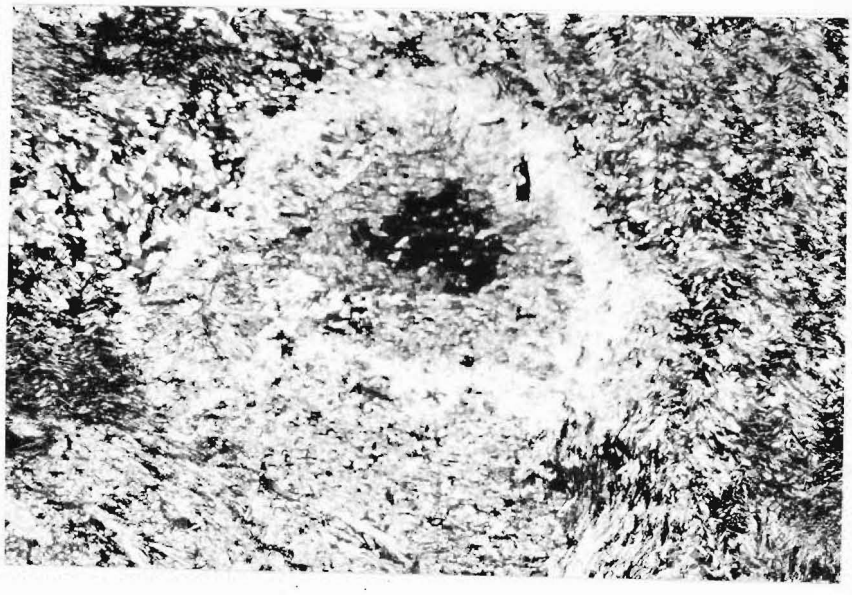

S46 573025

FIG. 88b The same field view as in Fig. above but photographed in cross-polarised light .

The wide spread occurence of retrograde muscovite, sericite, chlorite, and adularia in the Victoria Range metasediments indicates that hydration and K-metasomatism accompanying the retrograde metamorphism are significant. The restricted occurence of zoisite and epidote-clinozoisite suggests that Ca-metasomatism is local.

C. TEXTURAL CHANGES IN THE SANDSTONE HORNFELS

Fe- or/and Mg-chlorite occur as partial or/and complete psuedomorphs after biotite. Sericite occurs as fine-grained flakes, randomly oriented, and scattered in the feldspars. In feldspar sections which display developed cleavage, sericite is 'aligned' parallel to the planar structure. Zoisite and epidote-clinozoisite are found as granules or/and as bladed crystals. These minerals display no preferred orientation. Muscovite is coarse-grained, poikiloblastic, and randomly oriented. The inclusions in the mineral are composed of quartz $\pm$ biotite $\pm$ tourmaline $\pm$ opaques. Although the earlier rock texture is usually preserved during sericitization and chloritization, it is somewhat modified during the formation of muscovite, zoisite, and epidote-clinozoisite.

Adularia occurs as fine-grained polygonal aggregates in veins found in the metasediments (Fig. 85).

D. TEXTURAL CHANGES IN THE PELITIC HORNFELS

As in the sandstone hornfels, the chloritization of biotite, and sericitization of feldspars in the pelitic hornfels do not modify the pre-existing rock texture. However, as new minerals like muscovite, zoisite, etc., are formed, the hornfels texture is altered. Zoisite and epidote-clinozoisite occur as granular aggregates, and muscovite, as coarse-grained, poikiloblastic plates. The inclusions in the latter mineral are sometimes aligned parallel to the surrounding schistosity (Fig. 86). Except for a few mimetically crystallised muscovite as in specimen UC 7724c, all the mentioned minerals are randomly oriented.

Andalusite in specimens UC 7710 , UC 7792 , and UC 2833, is altered in a zoned-fashion. In the first two thin sections, the pseudomorph is made up of a core of (fine-grained quartz + muscovite ± biotite) surrounded by a mica-enriched rim (Fig. 87). Partially altered andalusite is observed in specimen UC 2833. Fig. (88) shows that the relict andalusite is rimmed by three zones of different minerals; 1) an inner rim of pinnite or kaolinite; 2) an intermediate rim of radially arranged muscovite; and 3) an outer rim of sericite.

Zoned alteration of andalusite is not very common. In most hornfels, the porphyroblasts are altered to sericite + quartz + coarse-grained, randomly oriented, poikiloblastic muscovite ± fine-grained biotite.

Although the included schistosity in the andalusite is preserved in most cases, it is somewhat obscured by the formation of new minerals.

IX/6 CORRELATION AND AGE OF THE VICTORIA RANGE METASEDIMENTS

The sediments in the Victoria Range, west of Springs Junction have previously been tentatively correlated with the Aorere Group of north-west Nelson by Fyfe in 1926-1930, and later by Grindley et. al in 1959. This correlation was rejected by Bowen in 1964, who tentatively assigned them to the Waiuta-Greenland Group. Although there is no conclusive evidence against Bowen's correlation, the following discussion which takes into account the most recent interpretation of the lower Paleozoic geology of Westland, Buller, and northwest Nelson, indicates that the earlier correlation is preferred.

According to Cooper (1975), the lower Paleozoic sediments in the north-west part of the South Island of New Zealand can be organised into three major meridional belts; 1) The Western Belt, consisting of the Waiuta-Greenland Group on the west, and the Aorere Group and Mt. Arthur Group below the Peel Formation on the east, 2) The Central Volcanic Belt, and 3) The Eastern Belt containing the Mt. Arthur Group above the Flora Formation. In the thesis area, the Thompson's Flat, Sluice Box, and Alfred Formations have been

recognised as members of the Eastern Belt, and the Koura Formation, as the Central Belt. Following Cooper's sedimentary model, the Victoria Range sediments immediately to the west of the Koura Formation, are members of the Western Belt. Besides being in the appropriate position relative to the local Central and Eastern Belts, the rocks are also in the correct geographic location which permits the Victoria Range sediments to be included as the eastern part of the Western Belt drawn by Cooper (1975, Fig. 89).

The difference in lithologies between the sedimentary belts 1) and 3) mentioned by Cooper, is identical to that observed between the Eastern Belt, and the proposed Western Belt in this area. For example, the predominant lithology to the west of the Rahu Fault is sandstone; limestone, conglomerate, and volcanic are absent, and mudstone occurs in minor amounts. In contrast, the main rock-types to the east of the Rahu Fault are mudstone and limestone; volcanics and conglomerate are present in minor quantities, and detrital feldspar is conspicuously lacking. These lithological differences reflect the contrasting sedimentary environments of the Eastern and Western Belts, and is consistent with the lower Paleozoic sedimentary situation as outlined by Cooper.

Shelley (1975) in his discussion on the Tuhuan paired metamorphic belt, pointed out that the Eastern Belt described by Cooper is characterised by higher pressure metamorphism, and is separated from the low-

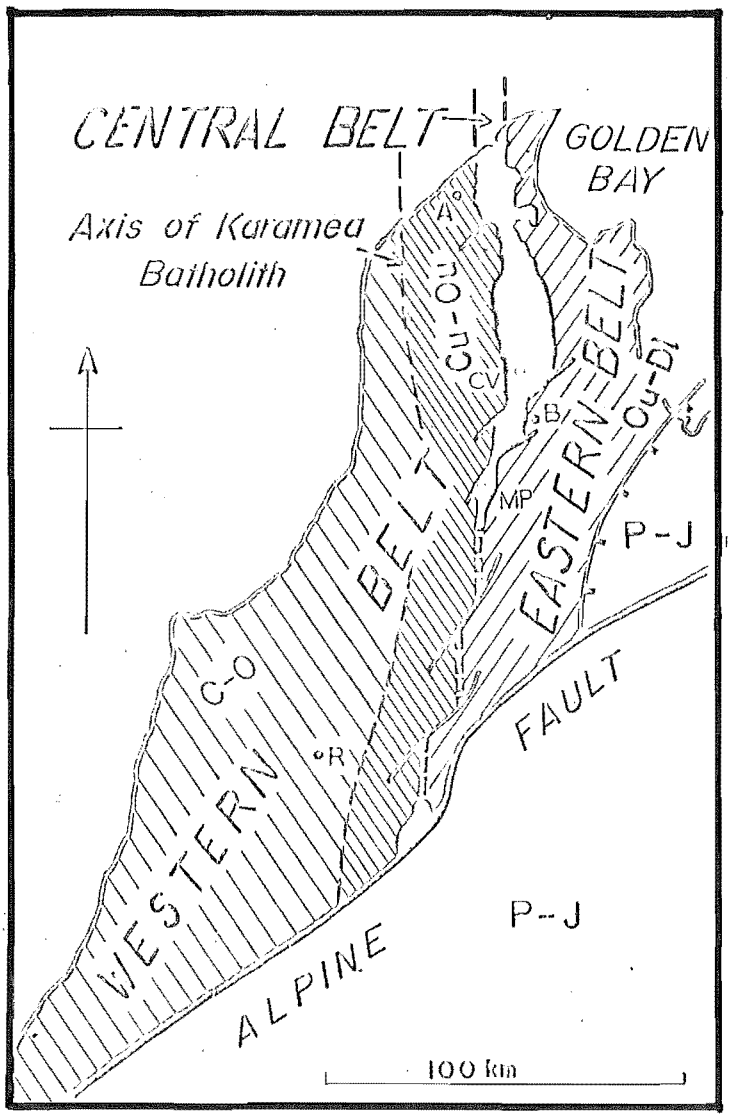

North-west part of South Island of New Zealand showing the distribution of the Eastern and Western Belts of early Paleozoic non-volcanic trough sediments and the Central Belt of Cambro-Ordovician volcanics and volcanogenic sediments. Granite, other intrusives, and covering strata are omitted. R = Reefton, B = Baton River, A = Aorangi Mine, CV = Cobb Valley, MP = Mount Patriarch, P–J = Permian–Jurassic.

FIG. 89 Diagram of the New Zealand Lower Paleozoic sedimentary belts in Westland, Buller, and NW-Nelson (after R.A. Cooper 1975) .

pressure metamorphosed Western Belt by a median boundary. The metamorphism in the Eastern Belt of this area is characterised by pressures greater than 4-6 kb, and is accompanied by the formation of almandine and staurolite. In contrast, the metamorphism in the Victoria Range sediments was achieved at pressures not exceeding 2-3 kb, and is accompanied by the crystallization of andalusite, and less commonly sillimanite at the immediate contacts of the granite. The evidence from metamorphic studies therefore supports Shelley's suggestion of a Tuhuan paired metamorphic belt with the Victoria Range sediments to the west of the median boundary.

Although the age and correlative of the metasediments have been successfully inferred from the sedimentary and metamorphic models outlined by Cooper and Shelley, they are not conclusive. The two models are yet to be proved valid by future investigations. The assumption in Cooper's model is that deposition in the Eastern Belt begins when sedimentation ceases in the Western and Central Belts in upper Ordovician times. However, it is now known that sediments older than upper Ordivician do in fact occur in the Eastern belt (discovery of middle Cambrian-Ordovician trilobites in the lower Thompson's Flat Formation--pers. com. Cooper). These sediments appear to form a condensed sequence and can possibly be accounted for in terms of the models of Cooper and Shelley, by the proposition that the Eastern Belt rocks were deposited over a distant off-

shore Cambrian sedimentary veneer. The assumption in Shelley's model is that the granites associated with the Tuhua Orogeny are never found in the areas east of the Tuhuan median boundary. The model would be invalidated in the event of a discovery of Tuhuan intrusives in the areas occupied by the Eastern Belt.

IX /7 AGE OF CONTACT METAMORPHISM

Like the Victoria Range sediments, there is no direct evidence for the age of contact metamorphism in the thesis area. However, according to the model of paired metamorphic belt proposed by Shelley, the contact metamorphism may be the result of granite intrusion during either the Tuhua or Rangitata Orogeny. The adamellite near the Rahu Saddle metamorphosed about 110 my ago or afterwards (Aronson 1968) suggest that the rocks here have suffered 2 phases of metamorphism. Further north in the Mt. Mantell district, the contact metamorphism caused by similar granites in the same belt of sediments has been dated as Carboniferous (333 $\pm$ 9 my, Aronson, 1968). Both Devonian-Carboniferous, and Cretaceous granite dates are widespread in the whole Victoria Range. Clearly detailed dating of each granite in every area will be necessary to distinguish them.

IX /8 SUMMARY:

The effects of contact metamorphism in the Victoria Range sediments are as follows:

i) Pelite is metamorphosed to spotted hornfels near the granite-metasediment contact. At the outer part of the aureole, the same lithology is metamorphosed to hornfels of the albite-epidote-hornfels facies.

ii) Sandstone is converted to hornfels of the albite-epidote-hornfels, and hornblende-hornfels facies, depending on its position relative to the granite-metasediment contact.

The mineral assemblages in the hornfels indicate that contact metamorphism ranges from the albite-epidote-hornfels facies to the hornblende-hornfels facies. The inferred P-T conditions are 400° to 550° C and less than 2-3 kb.

According to the most recent interpretation of the lower Paleozoic geology in Westland, Buller, and northwest Nelson, the metasediments can be correlated with the Aorere Group and Mt. Arthur Group below the Peel Formation, and the age of contact metamorphism is conceivably Devonian-Carboniferous.

CHAPTER X

DEFORMATION STRUCTURES IN THE VICTORIA RANGE META-SEDIMENTS

X/1 TERMINOLOGY

Foliation = laminated structure resulting from the segregation of different minerals into layers.

Schistosity = planar structure resulting from the parallel arrangement of platy minerals and ellipsoidal quartz grains.

Slaty-cleavage = closely spaced, penetrative, planar structure in very low metamorphic grade pelitic rocks. This fabric is sometimes enhanced by the parallel arrangement of platy and ellipsoidal minerals.

Fracture-cleavage = less closely spaced, non-penetrative, planar structure in coarser-grained rocks. Unlike the slaty-cleavage, this feature is independant of the parallel alignment of platy and ellipsoidal minerals.

D1/F1 = The earliest deformation. No F1 structures have been observed in the field.

D2/F2 = The second deformation and related folds.

D3/F3 = The third deformation (tentative). Folds are inferred from stereo-plots.

S0 = Bedding.

S1 = Slaty-cleavage/schistosity/foliation.

S2 = Axial plane cleavage of F2.

S3 = Axial plane cleavage of F3 (tentative).

FA2 = Fold axis of F2.

FA3 = Fold axis of F3 (tentative). This has not been observed in the field.

L_{S1}^{S2} = Lineation generated by the intersection of S2 and S1.

L_{S2}^{S3} = Lineation produced by the intersection of S3 and S2.

X/2 STEREO-ANALYSIS

The minor folds and their orientations observed in the field indicate that there are at least two phases of folding after the formation of the main cleavage/schistosity/foliation. However, due to the absence of megascopic fold structures in this part of the thesis area, the original attitudes of fold axes cannot be determined easily. The writer has used the stereo-plot technique to delineate deformation phases and their associated fold structures.

Figs. (90 ; 91 ; & 92) show the stereo-plots of poles to the prominent cleavage/foliation; poles to the axial plane produced by F2; and the lineations generated by the intersection of the F2 axial plane and the prominent cleavage/foliation. The distribution patterns in the three diagrams may be interpreted as the result of deformations in two ways.

Model 1: D1 generates the prominent cleavage/foliation (S1) such that the attitude of the fabric is sub-horizontal. D2 subsequently tightly folds the predominent cleavage/

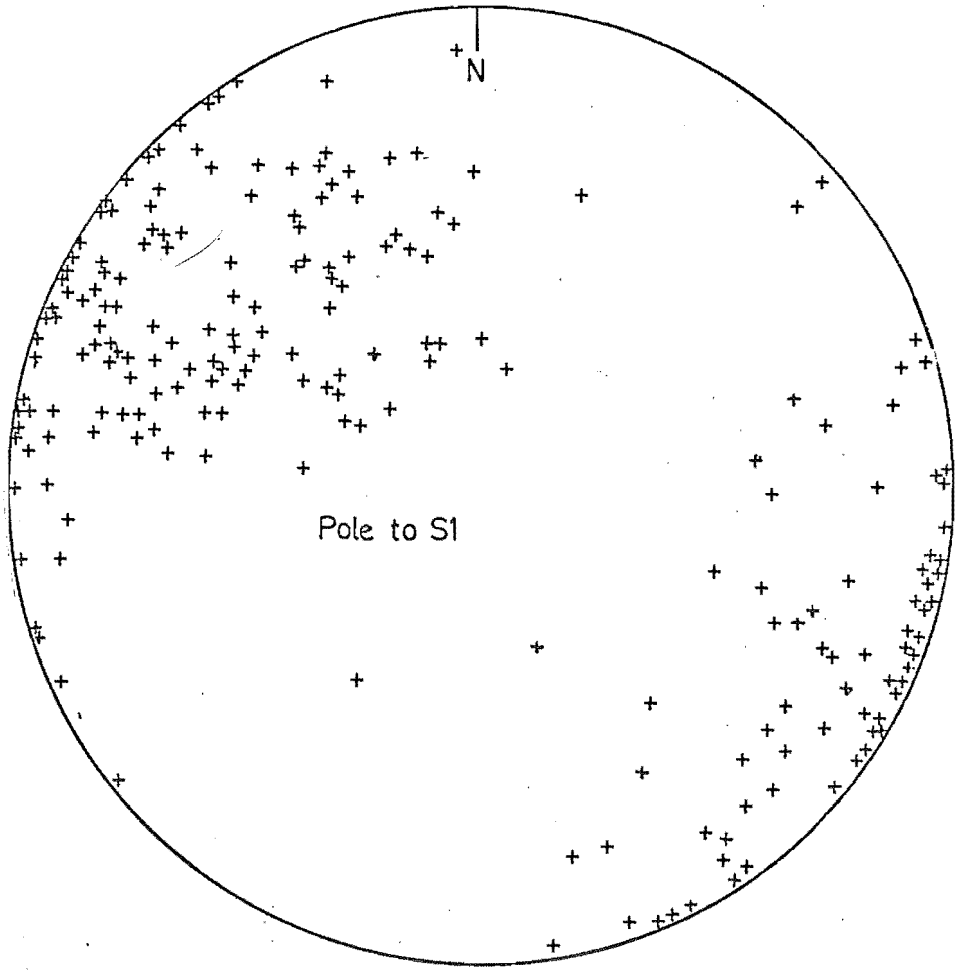

FIG.90 Stereo-plots of poles to the predominent cleavage / foliation . Note that the distribution pattern is somewhat butterfly-shaped .

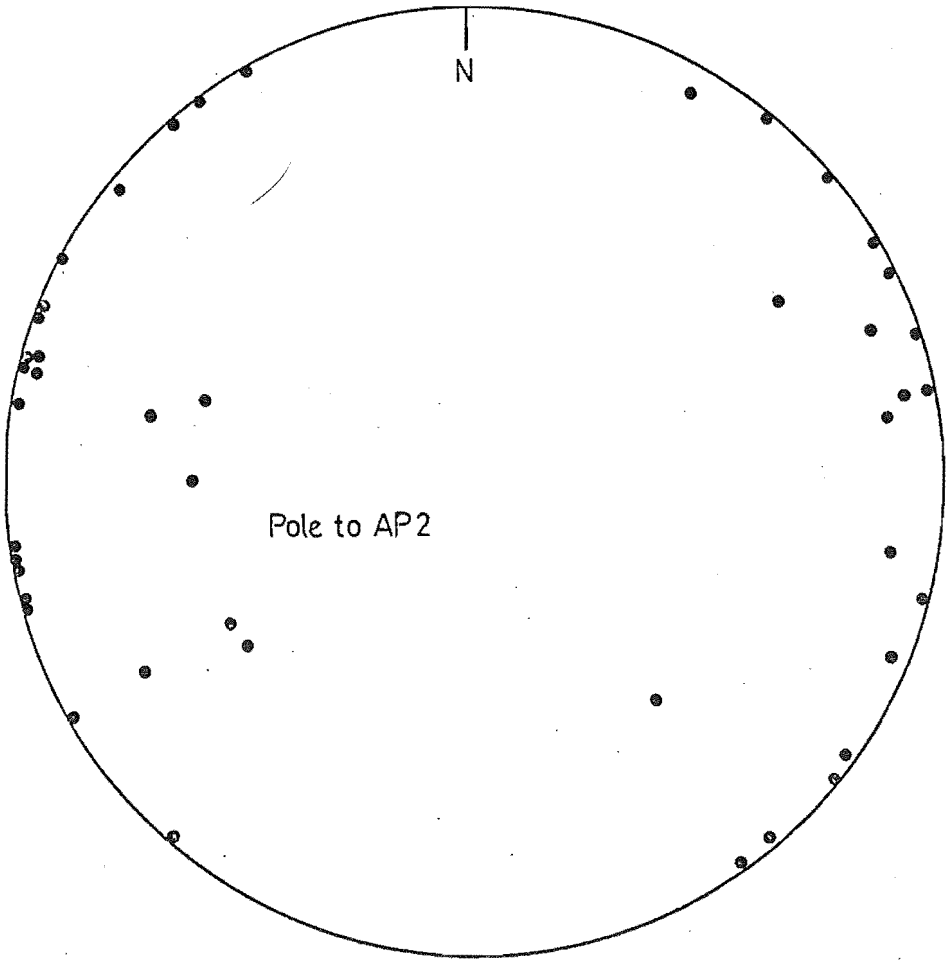

FIG. 91 Stereo-plots of poles to the axial plane cleavage (AP2). Note that some of the points plot towards the centre of the stereo-diagram.

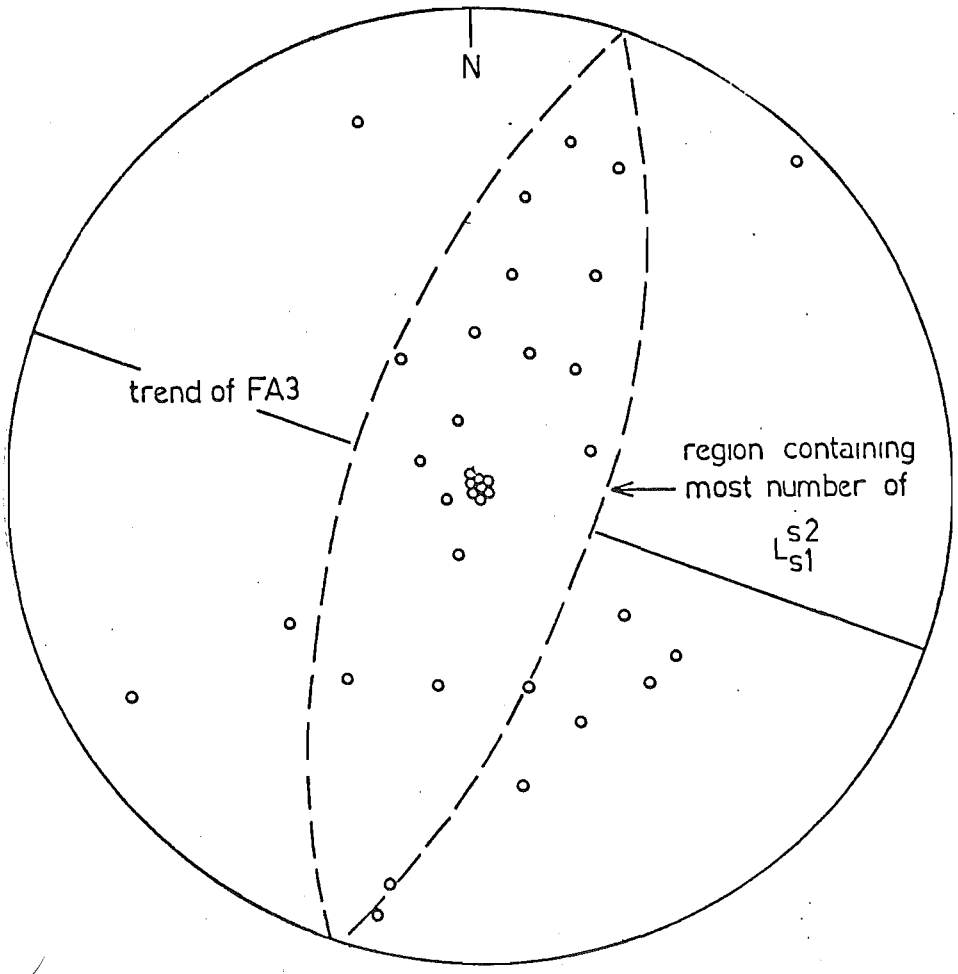

FIG. 92 Plots of L_{S1}^{S2} lineations . Note that the points are distributed in a zone trending N-NE . The trend of FA3 according to model 2 is E-SE .

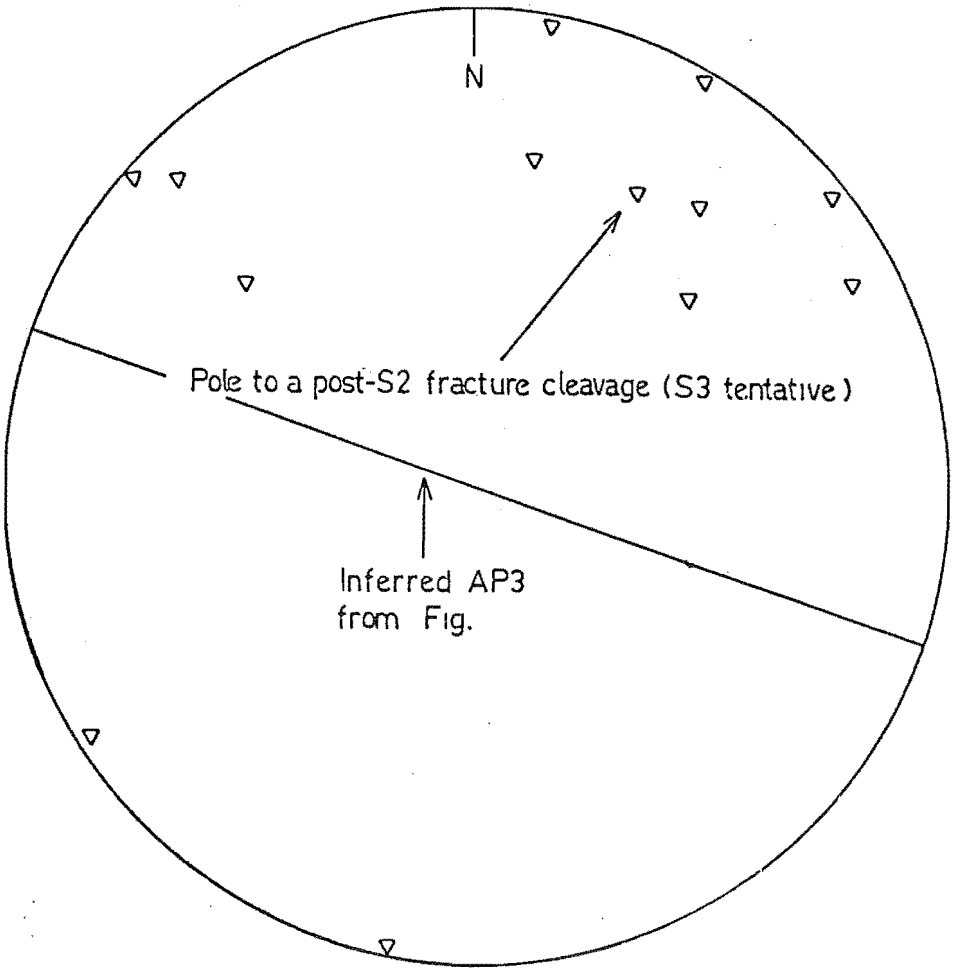

FIG. 93 Stereo-plots of poles to the axial plane cleavage (AP3 or S3 tentative) . Note that the plots are consistent with inferred strike of AP3 mentioned in the text (see section X/2) .

foliation about a gently plunging or horizontal axis. S1 is intersected by the axial plane of F2 to generate a set of gently plunging or horizontal L_{S1}^{S2} lineations. After D2, the L_{S1}^{S2} lineations and the deformed S1 are folded about a steeply plunging or vertical axis. The sequence of fold events described above is pictorially summarised in Fig. (94).

Model 2: D1 generates the predominent cleavage/foliation (S1) such that the attitude of the fabric is steeply dipping. D2 subsequently folds the predominent cleavage/foliation about a steeply plunging or vertical axis. S1 is intersected by the axial plane of F2 to produce a set of steeply plunging or vertical L_{S1}^{S2} lineations. Following D2, the L_{S1}^{S2} lineations, and the deformed S1 are folded about a gently plunging or horizontal axis. The sequence of fold events described above is pictorially summarised in Fig. (95).

The ideal stereo-plots in model 1 are as follows.

During D2, folding about a gently plunging or horizontal axis results in:

i) Poles to the predominent cleavage/foliation (S1) are scattered along a great circle at 90° to the axial plane of F2.

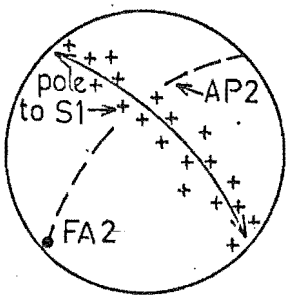

Fig. 96

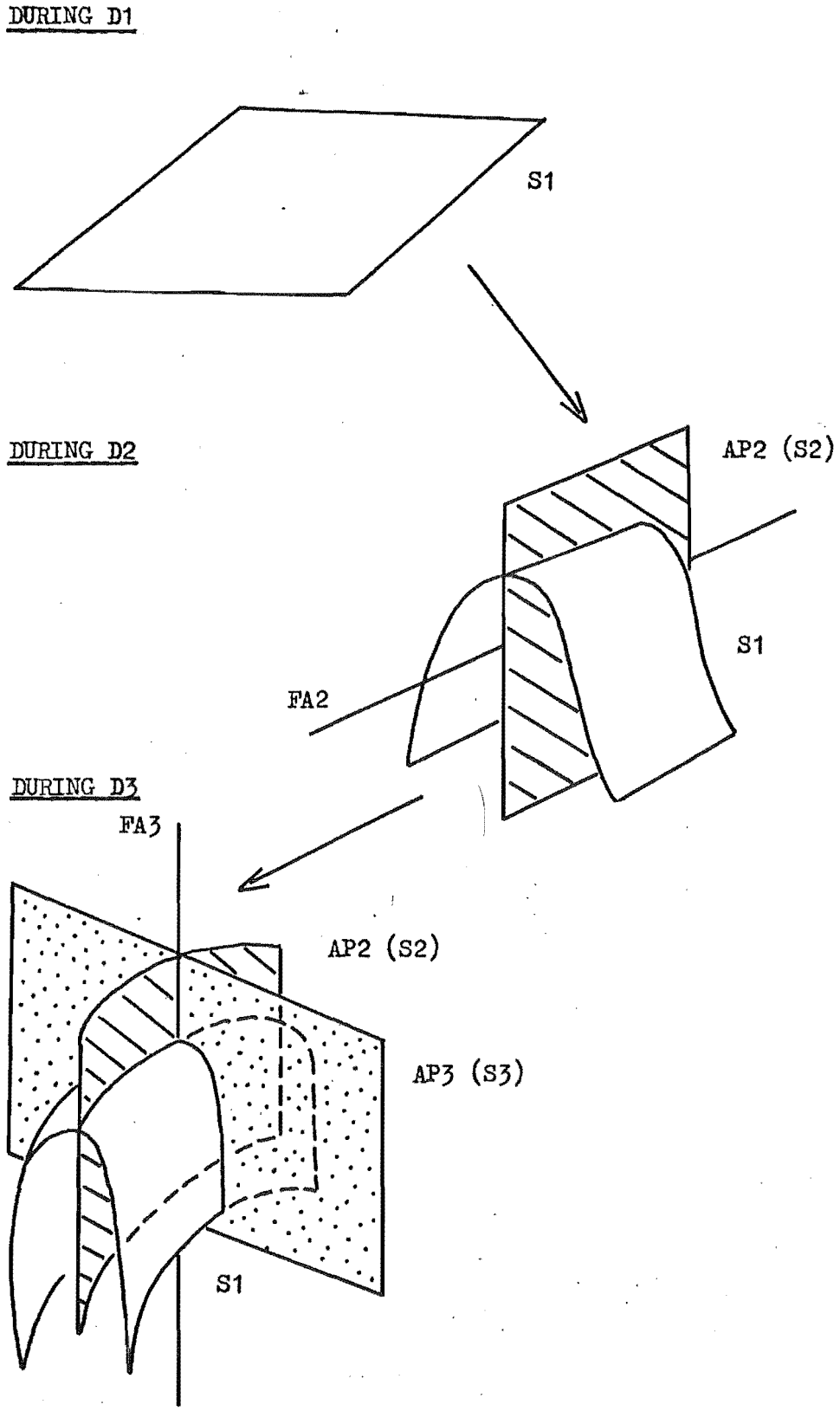

FIG. 94 A pictorial summary of model 1.

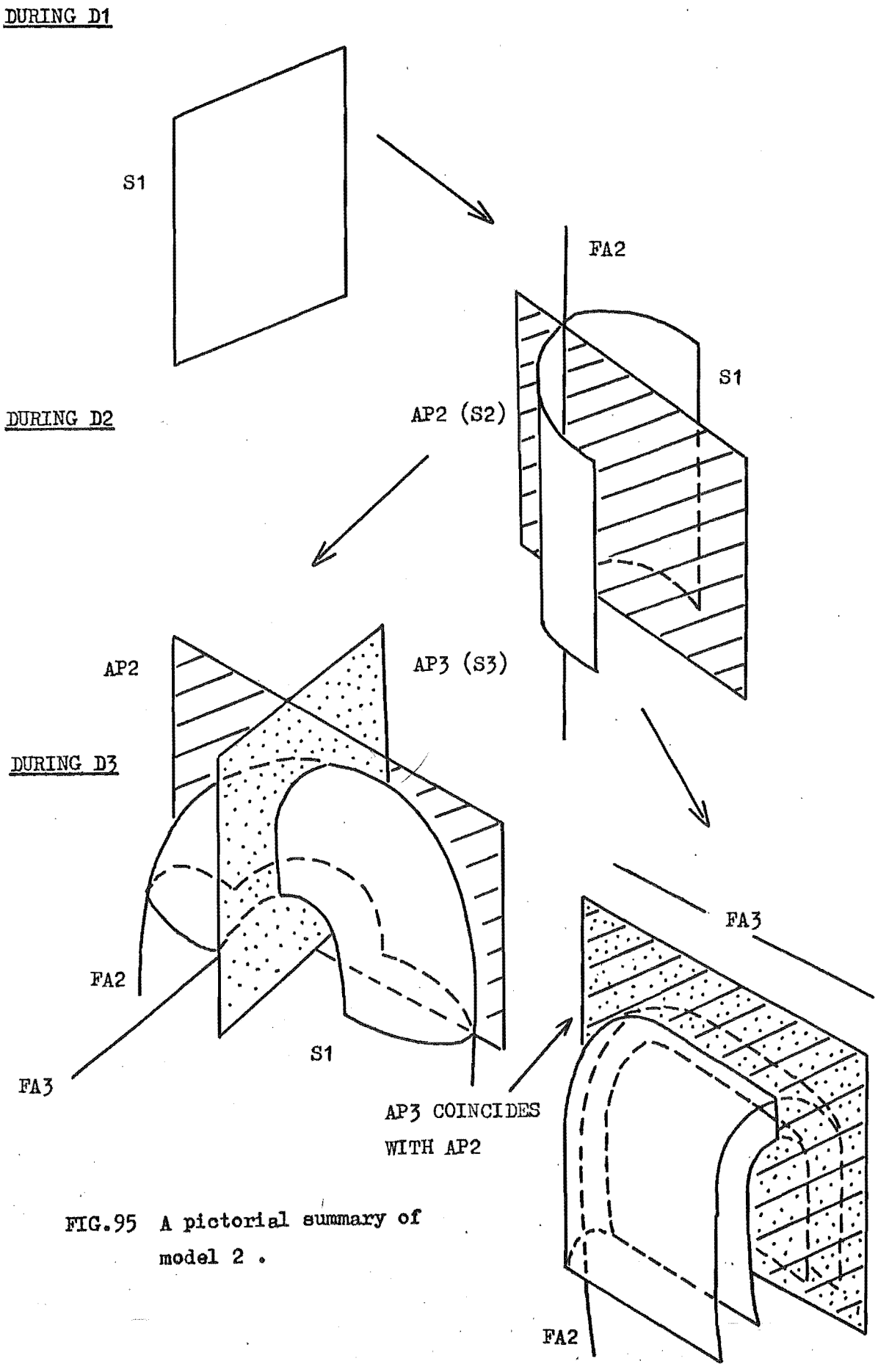

FIG.95 A pictorial summary of model 2 .

ii) The set of L_{S1}^{S2} lineations is concentrated at each end of the axial plane of F2 near the periphery of the plot.

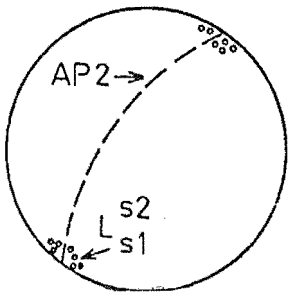

Fig. 97

iii) The poles to the axial plane of F2 are concentrated at the periphery, coinciding with each end of the great circle distribution of poles to S1.

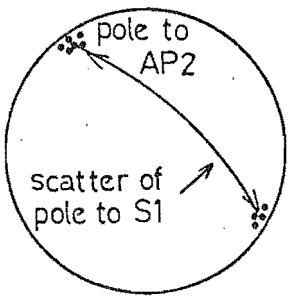

Fig. 98

During D3, refolding of pre-existing structures about a steeply plunging or vertical axis results in:

i) Poles to S1 are redistributed along small circles centered about FA3. The resultant distribution pattern is butterfly-shaped.

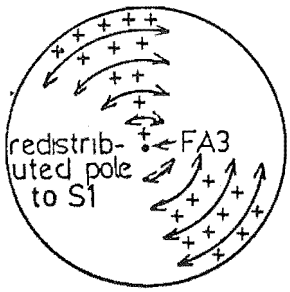

Fig. 99

ii) The set of L_{S1}^{S2} lineations is scattered at the periphery of the stereo-plot.

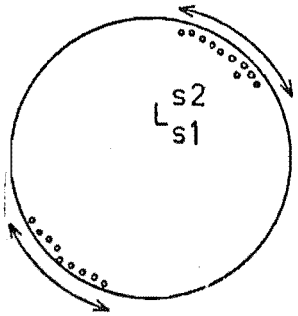

Fig. 100

iii) The poles to F2 axial plane like the set of L^{S2}_{S1} lineations are scattered at the periphery of the stereo-diagram.

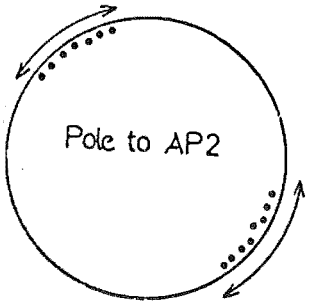

Fig. 101

iv) In addition, 2 sets of lineations - L^{S3}_{S1} and L^{S3}_{S2} are generated. The latter set is concentrated at the centre of the stereo-diagram whereas the former set is scattered in a zone along a great circle which contains the F3 axial plane because of the intersection of AP3 with a twice-folded S1 surface.

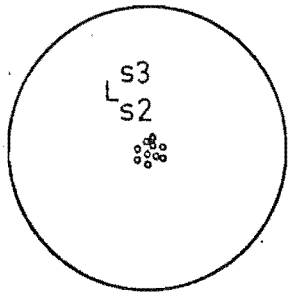

Fig. 102

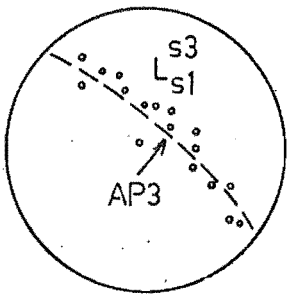

Fig. 103

Figs. (90) and (99) are somewhat identical in their distribution patterns. Fig. (91) is dissimilar to Fig. (101). Although the distribution pattern of Fig. (103) is apparently similar to that of Fig. (92),

the latter is oriented incorrectly. The incompatibilities of the stereo-plot patterns in Figs. (91 & 101) and Figs. (92 & 103) suggest that the order of deformation proposed in model 1 is not representative of that in the Victoria Range meta-sediments.

The ideal stereo-plots in model 2 are as follows.

During D2, folding about a steeply plunging or vertical axis results in:

i) Poles to the predominent cleavage/foliation (S1) are scattered at the periphery of the stereo-diagram.

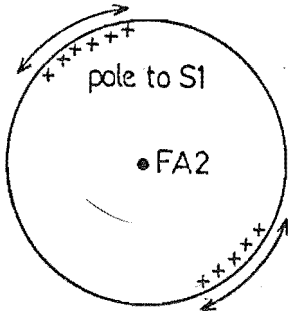

Fig. 104

ii) The set of L_{S1}^{S2} lineations is concentrated at the centre of the stereo-plot, coinciding with the fold axis of F2.

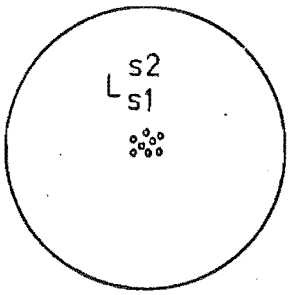

Fig. 105

iii) Poles to the F2 axial planes are concentrated at the periphery of the stereo-plot. It is conceivable that the plots are sometimes scattered at the periphery because of the fanning nature of AP2.

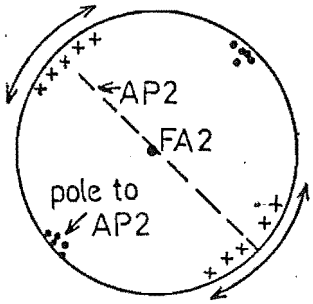

Fig. 106

During D3, refolding of earlier structures about a gently plunging or horizontal axis results in:

i) When FA3 is oriented at 90° to FA2 and is contained in the F2 axial plane, the poles to S1 are redistributed such that the points originally at the periphery are 'dragged' towards the centre of the stereo-diagram. The resultant distribution pattern is somewhat butterfly-shaped as shown below.

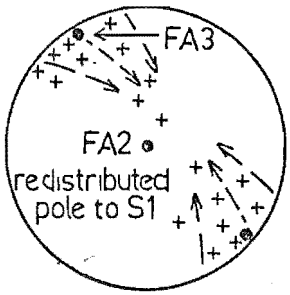

Fig. 107

The same distribution pattern in Fig. (107) may also be produced during D3 when FA3 is at 90° to both FA2 and F2 axial plane (AP2) (see fig. below).

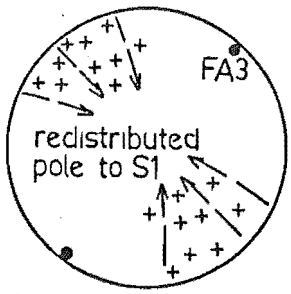

Fig. 108

ii) When FA3 is oriented perpendicular to FA2 and is contained in AP2, the poles to the F2 axial plane

are redistributed such that the plots initially at the periphery are 'dragged' towards the centre of the stereo-diagram. The resultant distribution pattern may or may not be butterfly-shaped depending on the initial scatter of poles to AP2 at the periphery.

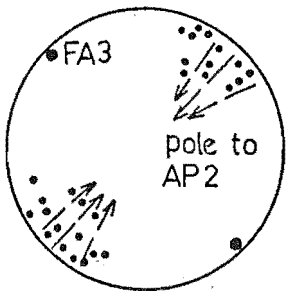

Fig. 109

When FA3 is oriented at 90^{o} to both FA2 and AP2, then poles to the F2 axial planes are strictly unaffected by D3. However, if FA3 is oriented at an angle less than 90^{o} to FA2 and AP2, then the poles to the F2 axial plane would plot along a circle but if the angle is close to 90^{o} the difference between a great circle and small circle may not be discernable in practice.

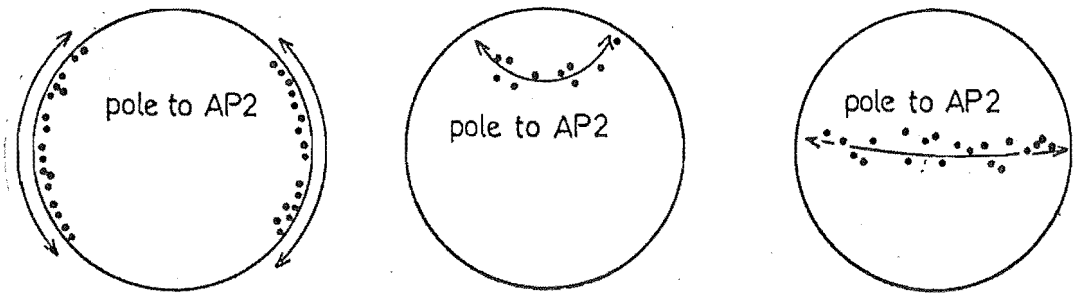

Fig. 110

Poles to AP2 are scattered along a great circle in Fig. (110 a). Poles to AP2 are distributed along a small circle in Fig. (110 b). Poles to AP2 are distributed along a small circle which in practise is close to a great circle as in Fig. (110 c).

iii) The L_{S1}^{S2} lineations in the situation where

FA3 is at 90° to FA2 and is contained in AP2 are scattered along a great circle at 90° to AP3.

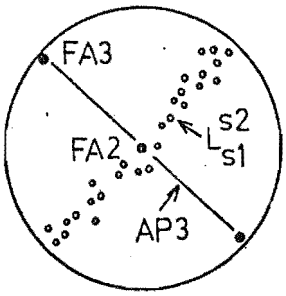

Fig. 111

However, when FA3 is oriented at 90° to both FA2 and AP2, the redistribution of the L_{S1}^{S2} lineations is such that it defines a zone which contains AP2 and overlaps with the distribution of poles to S1 in Fig. (107).

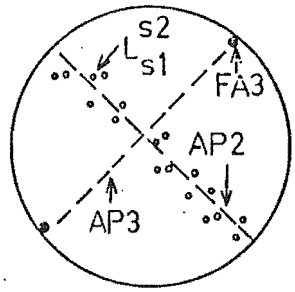

Fig. 112

The similarity in the distribution patterns of stereo-plots in the sets of Figs. (90, 91 & 92) and Figs. (107, 109 & 111) suggests that the sequence of folding outlined in model 2 is the same as that in the Victoria Range meta-sediments. Although the distribution pattern in Fig. (91) also resembles that in Fig. (110a), it does not invalidate the correlation just mentioned because it can be accounted for by 1) the insufficient number of points of poles to AP2 in Fig. (91), and 2) the fanning nature of AP2 (refer section X/3 C).

Besides the above reasons, model 2 is preferred by the writer because the spread of poles to AP2 towards

the centre of the stereo-plots in Fig. (91) is automatically accounted for by D3 and there is no need to invoke another phase of folding about a horizontal axis as in model 1.

According to model 2, the following may be inferred.

i) FA3 trends approximately E-SE and gently plunges towards E-SE or W-NW (see pole to the great circle defined by the L_{S1}^{S2} distribution in Fig. (92).

ii) The strike of AP3 inferred from Fig. (90) lies approximately in the NW-Se quadrant which is consistent with the trend of FA3 mentioned in i), and the poles of AP3 in Fig. (93).

iii) FA2 is steeply plunging or vertical (see Fig. 90).

iv) AP2 strikes approximately E-SE as this surface contains FA3 and FA2, and dips steeply or vertical because FA2 is steeply plunging.

Although, the sequence of folding and the orientations of AP2, AP3, FA2, and FA3 have been successfully determined by the stereo-plot technique, they are not conclusive because of the following.

i) The number of points used in the stereo-plots in Figs. (90,91 & 92) is not statistically reliable.

ii) The method assumes that the Victoria Range meta-sediments have suffered two major phases of folding and they are not significantly affected by subsequent deformations and faulting.

iii) The reconstructed orientation of AP2, AP3, FA2, and FA3 is based on the assumption that FA3 is

perpendicular to FA2 and is contained in AP2.

iv) The lack of megascopic structures in the field means that the suggested sequence of folding and the orientation of AP2, AP3, FA2, and FA3 cannot be directly verified.

Except for the last problem, the others could be overcome by more and improved structural data from the Victoria Range meta-sediments.

X/3 STRUCTURAL ELEMENTS:

A. S0 STRUCTURE

Except in the vicinity of Rocky and Anti-Rocky Creeks, bedding (S0) is not commonly observed in the meta-sediments. This planar structure generally strikes N-S, and dips steeply to the east or west. Bedding (S0) is intersected by the predominent cleavage/foliation (S1), the cross-cutting cleavage (S2), and other younger planar structures. The angular relationship between S1 and S0 is variable; the former may be sub-parallel or at a moderate angle to the latter. The detailed effects of D1, D2, and D3 on bedding are not clearly understood.

B. S1 STRUCTURES

There are no F1 folds associated with S1 observed in the field. The major regional post-bedding S-surface in the Victoria Range meta-sediments is a slaty-cleavage.

The regional development of S1 (i. e. not directly related to minor intrusives or faults etc.) implies a regional metamorphism. The attitude of S1 is variable because of subsequent deformation by F2 and F3. However, according to the stereo-plots in Fig. (90), the original attitude of S1 may be approximated as NE-SW/90°. S1 is intersected by S2 and younger planar structures. The angular relationship between S1 and S2 is variable and this may be explained by the fanning nature of S2. Textural studies of andalusite in the pelitic rocks near the Rahu Saddle reveal that S1 is pre-thermal metamorphism (see Figs. 81 , 83 & 88). The age of this fabric in such a case may be considered to be older than either the Tuhua or Rangitata Orogeny, depending on which orogeny the granite intrusions can be ascribed to. If the age of S1 is indeed the former, then S1 and its metamorphism would be the result of the pre-Tuhuan Orogeny and lends support to Shelley's (1975) model of paired metamorphic belts in Westland, Buller, and NW-Nelson. Clearly, a radiometric dating programme on the Victoria Range Granite in this part of the thesis area is desirable as the age of the intrusives would help to indicate more realistically the date of S1 formation and metamorphism.

The effect of contact metamorphism on S1 is not clearly understood. However, it is not inconceivable that mimetic crystallization of biotite, chlorite, and muscovite have occurred on the S1 surfaces, resulting in enhancement of the slaty-cleavage/schistosity.

C. S2 AND F2 STRUCTURES

The writer has used the sequence of folding deduced from stereoanalyses to delineate D2 and D3 structures in the field. According to model 2 (refer section X/2), F2 has a steeply plunging fold axis and S2 is steeply dipping whereas F3 has a gently plunging fold axis and S3 strikes approximately NW-SE. In the case where F2 structures have been significantly affected by D3, they are distinguished from F3 features by their N to NE trending fold axes or/and lineations.

F2 structures are formed as the result of folding of S0 and S1 surfaces about a steeply plunging or vertical axis. They are commonly observed in the meta-sediments in the area north of Trig. A. The folds are generally curvilinear, with wavelengths ranging from 1 to 5 m, and amplitudes varying from 0.5 to 2 m. In the more cleaved rocks, the folds tend to be chevron type. Small scale crenulations are observed on these fold surfaces. The fold styles of the crenulations vary from curvilinear to chevron type with wavelengths ranging from 5 to 10 cm, and amplitudes, from 1 to 5 cm. The axes of these crenulations are oriented parallel to the large fold axis but the axial planes of the crenulations are oriented such that they intersect each other in the axial plane of the large fold. In the more cleaved or schistose meta-sediments, kink bands are frequently developed in place of curvilinear crenulations. The width of these features varies from 2 to 10 cm. Where deformation is sufficiently intense, slippage occurs along the kink-planes.

The attitude of the majority of F2 observed is steeply plunging. However, according to model 2 (see section X/2) there are F2 axes which sometimes trend north to north-east and plunge in a northly or southerly direction.

S2 - the axial plane cleavage is generated by F2. Although this fabric is observed to intersect S1 in most outcrops, it is not well developed. S2 occurs as a non-penetrative cleavage. Its strike is variable because of the fanning nature of the fabric. Unlike S1, this planar structure is not accompanied by the crystallization of metamorphic minerals (both regional and thermal). This together with the fact that the pegmatitic and granitic bodies were folded about a vertical axis like the nearby meta-sediments suggest that F2 and S2 were formed sometime after the intrusion of Victoria Range Granite. The plastically deformed intrusives on the Rahu Saddle indicate that D2 and its structures are just post-Victoria Range Granite emplacement.

D. S3 AND F3 STRUCTURES

Although a E-SE trending fold has been inferred from the stereoplots in Fig. (92), F3 structures are not observed in the field. According to model 2, F3 structures if present are oriented such that their fold axes and lineations would trend E-SE and plunge gently in an easterly or westerly direction. This distinguishes F3 and S3 from the D2 structures in the field.

According to the same deformation model discussed above, S3 - the axial plane cleavage strikes approximately E-SE (refer Figs. 90 & 107). The plots of poles to a post-S2 cleavage observed in the thesis area is consistent with that of S3 just mentioned, thus implying that the post-S2 cleavage are S3 features (Fig. 93).

Like S2, this planar structure is non-penetrative, poorly developed, and post-Victoria Range Granite emplacement.

E. S2 AND F2 MICROSCOPIC STRUCTURES

These structures are restricted to the pelitic rocks. They are formed as the result of crenulation of S1 and S0 surfaces. In most of the thin sections, the microscopic structures observed are curvilinear or chevron folds. Some of the axial planes of these folds are wrapped around the andalusite porphyroblasts which contain undeformed S1 surfaces. This indicates that the microscopic structures are post-andalusite formation i. e. post-Victoria Range Granite emplacement. In specimen UC 7800a , a set of conjugate kink folds has been observed. According to Ramsay (1967) these features are generated by compression along the layerings (i. e. S1). A set of incipient cleavage related to the kink folds cross-cutting S1 has also been observed in specimen UC 7800a. Although no direct measurements have been made on the kink folds, they, together with the set of incipient cleavages have been recognised as D2 structures on the basis of the

angular relationship between S1 and S2 observed elsewhere. Like the F2 and S2 mesoscopic structures, these microscopic features are unaccompanied by the crystallization of metamorphic minerals and are deformed by F3.

No F3 and S3 microscopic structures have been observed in the meta-sediments west of the Rahu Fault.

F. LINEATIONS

The most prominent lineations are those generated by the intersection of S1 and S2. Their original orientation is nearly vertical but because of D3 they are redistributed about a new fold axis. The other sets of lineations produced by the intersection of various S-surfaces are not apparent in the field.

G. PLANAR STRUCTURES FORMED AROUND LOCAL INTRUSIVE BODIES IN THE META-SEDIMENTS

The cleavage/schistosity formed around pegmatitic and granitic bodies is restricted to the aureole zones surrounding the local intrusives. This fabric cross-cuts the pre-existing surfaces - S0 and S1. Because the cleavage/schistosity is oriented such that it reflects the attitude of the intrusive-sediment contact surface, the angular relationship between this fabric and S1 or S0 is variable. Where the pegmatitic and granitic bodies are aligned parallel to S1, the pre-existing fabric is enhanced by the development of this generation of planar

S46 598042

FIG. 113 Cleavage is very nearly parallel to bedding in middle Timpson's Stream . Note the development of kink bands in the cleaved beds .

S46 570020

FIG. 114 Water expulsion cleavage developed at an angle to bedding in middle Rocky Creek .

S46 564030

FIG. 115 Cleavage development related to intrusive bodies . Note the manner of cleavage 'wrapping' the granitic body .

structure. Although local intrusives are common in the meta-sediments, not all of them are accompanied by the formation of cleavage/schistosity. In the areas where sandstone is predominant, the cleavage/schistosity generated by pegmatitic and granitic bodies is barely developed or absent.

The effects of D2 and D3 on this generation of fabric are not known.

H. DEFORMATION OF S1 BY THE INTRUSIVES

The plastic deformation of S1 by local intrusives is not commonly observed in the thesis area. Where such deformation has occurred, it is apparently restricted to that part of the aureole that is less than 10 cm from the local intrusive-sediment contact. In Lock Creek, plastic deformation of S1 in the meta-sediments is widespread. This is because the rocks have been intensely metamorphosed by the surrounding Victoria Range Granite. The fold style and attitude are highly variable. The influences of D2 and D3 on these structures are not known. The writer expects them to be very complicated.

X/4 THE PROBABLE CAUSE(S) OF S1, S2, F2, S3, AND F3 STRUCTURES AND AGE

As mentioned previously in section X/3 B, the regional development of schistosity/foliation in the meta-sediments suggests that S1 is probably related to a regional meta-

morphism. The relative age of S1 is pre-Victoria Range Granite. If these intrusives are predominently Tuhuan, then it is conceivable that the metamorphism which produced S1 is that of the pre-Tuhua Orogeny proposed by Shelley (1975). This dates S1 and the metamorphism as Upper Ordovician.

Vertical foldings are commonly caused by transcurrent movement along a major fault. As the Koura/Rahu Fault is a strike-slip feature, it is possible that the vertical folds in the meta-sediments were generated by lateral displacements along the Koura/Rahu Fracture System. The similarly folded Lower Paleozoic and Tertiary sediments along the Koura/Rahu Fault at locality (grid. ref. 569985) and Lower Campbell Creek support this suggestion. The vertically folded (plastic response) granitic bodies on the Rahu Saddle dates S2 and F2 as just post-Victoria Range Granite emplacement. D2 and its structures would be related to either the Tuhua Orogeny or the Rangitata Orogeny. It is the writer's hope that future radiometric data on the Victoria Range Granite will yield a more positive age and correlation for D2.

The age of F3 and S3 structures is not directly determinable. However, if D2 is related to the Tuhua Orogeny then it is not inconceivable that D3 generated F3 and S3 structures some time during the Rangitata Orogeny.

CHAPTER XI

TERTIARY SEDIMENTS

XI/1 INTRODUCTION

The oldest Tertiary sequence known near the thesis area is that of the Wanganui Series which according to Bowen (1964) is non-marine, and not older than Pliocene. A fault bounded block of pre-Upper Miocene (Waiauan) marine sediments has been discovered near Springs Junction by the writer. These sediments are described below. Clearly, the pre-Wanganui Maruia-Murchison sedimentary basin is more extensive than was originally thought.

XI/2 LITHOLOGIES

Field investigation and thin section studies revealed only three rock-types; 1) well indurated calcareous medium- to fine-grained sandstone, 2) silty limestone, and 3) poorly indurated calcareous medium- to fine-grained sandstone. Due to the discontinuous exposures of these lithologies, bedding characteristics and their inter-relationships are poorly understood.

A. WELL INDURATED CALCAREOUS MEDIUM- TO FINE-GRAINED SANDSTONE

This brownish rock is composed of Foraminifera tests, quartz, chert fragments, feldspars, micas, glauconite, and black organic matter/opaques. The Foraminifera tests account for about 50% of the rock. Although most of the microscopic shells have been recrystallised, their shapes are generally well-preserved, enabling identification to the genus level. Quartz, chert, and feldspar detritus are angular, poorly sorted, and medium- to fine-grained. Their abundance ratio is crudely in the order of 2:2:1. Together the three minerals account for about 50% of the sandstone. In specimen UC 7814c , the clastic textures of quartz, chert, and feldspar have been modified by pressure solution and post-lithification fracturing. However, the effects are not significant enough to destroy the original grain shape or drastically modify grain dimensions. Glauconite and micas are rarely observed. The fine-grained black organic matter/opaque which makes up less than 5% of the rock occurs as partial infillings in microfossils, and as interstitial material in the sandstone. The presence of microcline and cherty fragments suggests that the source rocks are either metamorphic or both metamorphic and igneous. Although it has not been positively established yet, the occurrence of glauconite in the interstitials of the silicate detritus suggests that glauconite is authigenic.

B. SILTY LIMESTONE

This rock is greyish, fine-grained, well indurated, and cross-cut by numerous calcite veins. Its mineral

components are $CaCO_3$, quartz, biotite, muscovite, feldspars, glauconite, and black organic matter/opaques. The fine-grained $CaCO_3$ and calcareous microfossils constitute more than 80% of the rock. Thin section studies reveal that it is not easy to distinguish the orthochemical and allochemical carbonates. Silt-size quartz whose original texture has been altered by calcite makes up about 10-15% of the limestone. Biotite and muscovite occur as minute flakes which are less than 1% of the rock. Feldspars and glauconite-like micas are corroded by calcite and are present in small quantities. The dark organic matter/opaques which constitute less than 5% of the limestone are very fine-grained. They are nearly homogeneously distributed, and sometimes occur as infillings in the cavities of microfossils. Although the presence of clastic microcline suggests that the source rocks are igneous (granite), it is not conclusive.

C. POORLY INDURATED CALCAREOUS MEDIUM- TO FINE-GRAINED SANDSTONE

In the Lower Campbell Creek, this lithology is known to interbed with the thinner steeply dipping layers of well indurated coarser-grained sandstone. The rock is made up of the same components described in the sandstone in section XI/2 A. Glauconite and micas are moderately abundant whereas cherty fragments and Foraminifera tests are not as common as in the well indurated calcareous

sandstone. The quantity of tests may vary from 1 to 20% of the rock, and depending on the amount of cementing agent, these microfossils and the cement may account for 1 to 40% of the carbonate content in sandstone. As with the earlier sandstone, most of the Foraminifera tests have been recrystallised. Quartz and feldspars make up 50 to 80% of the rock. In the less calcareous sandstone, the detritus is well sorted, angular, and medium- to fine-grained. The fine-grained black organic matter/opaques, and glauconite constitute less than 5% and 1% of the sandstone respectively. The latter is authigenic because of its 1) occurence in the interstitials of the silicate detritus, 2) partial infilling of Foraminifera chambers, and 3) partial replacement of Foraminifera tests.

Generally, the two described sandstones are different from the limestone by the following features.

1) Coarser-grained, and angular detritus.

2) Higher glauconite content although it is still not greater than 1%.

3) Significantly higher quantities of feldspars and micas.

4) Abundant benthonics. These microfossils are larger size.

XI/3 FAUNAS

Except for a few specimens of Foraminifera, the fossils are generally too fragmentary and poorly preserved

for positive identification. The test morphology of most genera of planktonics and benthonics have been obscured by silicification or replacement by calcite.

A. IN THE SANDSTONES

The following is a faunal list for the sandstone:

1) Fish teeth and cartilage. These phosphatic fossils are less than 1mm and are seldom found in the rock.

2) Siliceous sponge spicules.

3) Bryozoa fragments.

4) Foraminifera. There are at least six genera known; siliceous spherical Radiolaria, Globigirina sp., Amphistegina sp., Anomalinoides sp., Gyroidinoides cf allani, Cibicides sp., Marginulinopsis cf allani, and Robulus sp.. Benthonics are diverse and abundant.

B. IN SILTY LIMESTONE

Given below is a faunal list for the limestone.

1) Fish teeth and cartilage. These are rarely found in the rock.

2) Bivalves. Like 1) they are also seldom observed in limestone.

3) Siliceous sponge spicules.

4) Bryozoa fragments. These are more abundant than in sandstones.

5) Foraminifera. The microfossil population is

predominantly planktonic. The number of genera here is nearly the same as that in sandstones. Siliceous spherical Radiolaria, Globigirina sp., Amphistegina sp., and three other minor benthonics have been observed. Other benthonics eg. Karreriella cf bradyi Cushman, Globigirina cf euapertura, and Bolivinopsis Cubensis are also present.

XI/4 AGE AND CORRELATION

Although microfossils are abundant and diverse in the Tertiary rocks of the thesis area, they do not indicate the exact age of the sediments because most of the specimens of Foraminifera are poorly preserved and positive identification is frequently not possible. The presence of Bolivinopsis Cubensis together with the occurence of non-marine deposits of the Wanganui Series to the north of Springs Junction restrict the age range to Tertiary. The writer found that using the distribution of Amphistegina in the South Island during the Tertiary period, the age range could be shortened to Upper Eocene-Upper Miocene i. e. Kaiatan to Waiauan Stage (refer Hornibrook 1968).

According to Hornibrook (1968), the sediments of the Arnold Series in the South Island contained abundant Amphistegina and spherical Radiolaria. As both these microfossils are abundant in the Tertiary rocks of the thesis area, it is not inconceivable that the Tertiary sandstones and limestone are Upper Eocene. The striking

similarity in the Foraminifera assemblage and clastic content of the rocks here and those of the Arnold Series near Murchison, together with the occurence of Upper Eocene-Oligocene sediments near Mt. Rutland and Reefton support this suggestion.

XI/5 INFERRED PALEO-ENVIRONMENT

Spherical Radiolaria are floating organisms. Their abundance in the limestone together with the presence of silt-size detritus, and the low population of benthonics suggest that the rock was formed in a distant shore environment. Although it cannot be positively established, the abundance of Radiolaria generally indicates that the sea water was warm and its salinity moderate.

The high benthonic-planktonic ratio, the medium-grained angular detritus, and the abundance of Amphistegina in the sandstone suggest that the rock was formed in a near shore environment. Present day observation of Amphistegina reveal that the organism thrives in warm water of depths ranging from 20 to 200m (Phleger 1952). The presence of numerous large size benthonics in the rock indicates that the habitat was favourable i. e. warm shallow water which is non-toxic, with plentiful nutrients, and minimum number of predators. The small quantity of authigenic glauconite and organic matter suggest that the environment was slightly reducing at or just below the sediment-water interface. In addition, the occurrence of authigenic glauconite also indicates that the salinity of the sea water was normal.

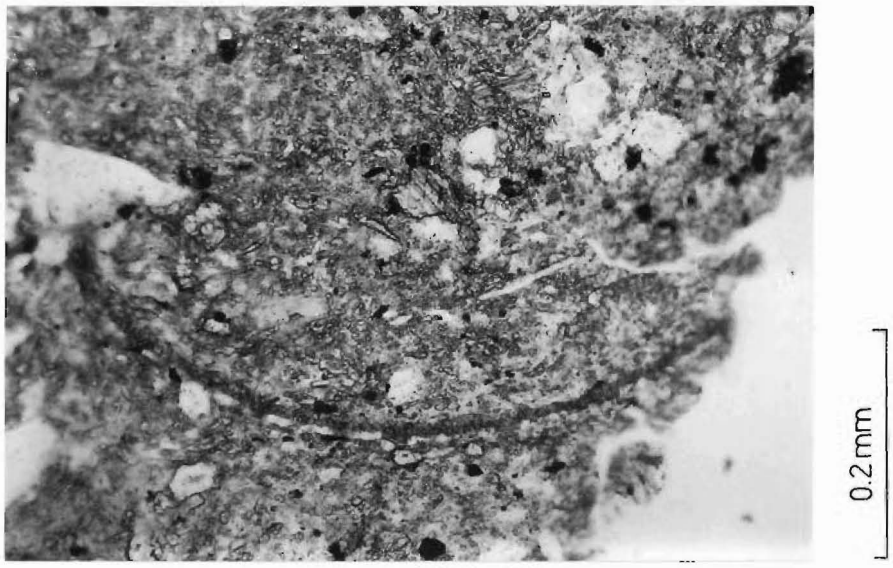

S46 607042

FIG. 116 Bivalve observed in thin section of silty limestone

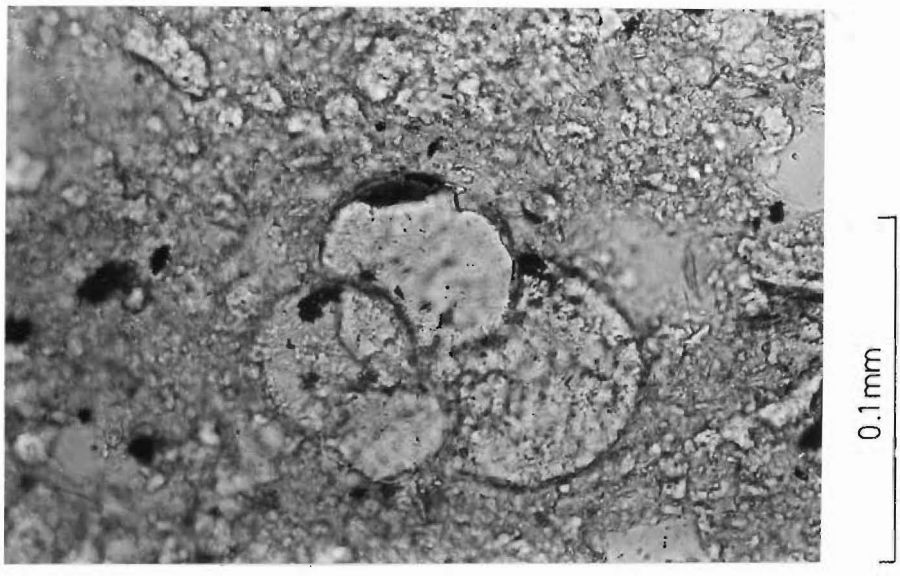

S46 607042

FIG. 117 A Globigirina test in silty limestone

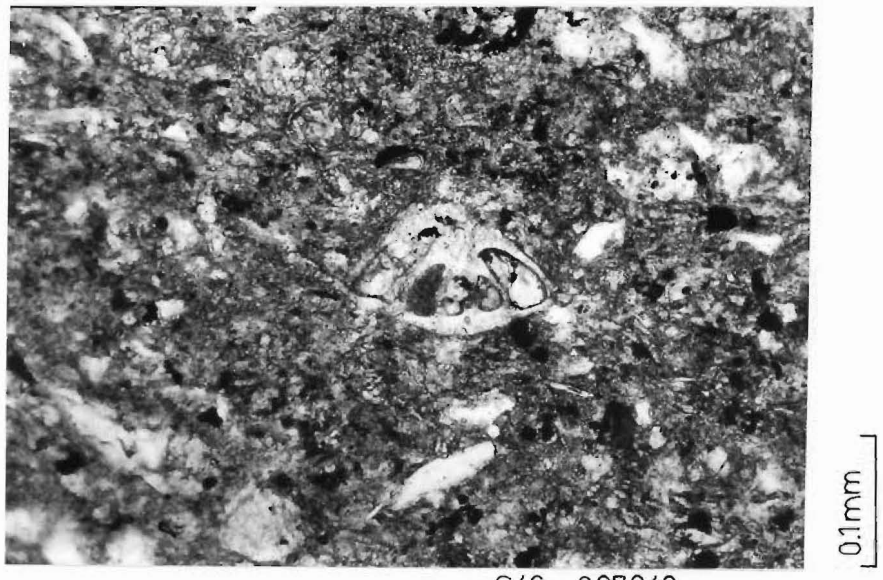

S46 607042

FIG. 118 Benthonic not recognised in silty limestone

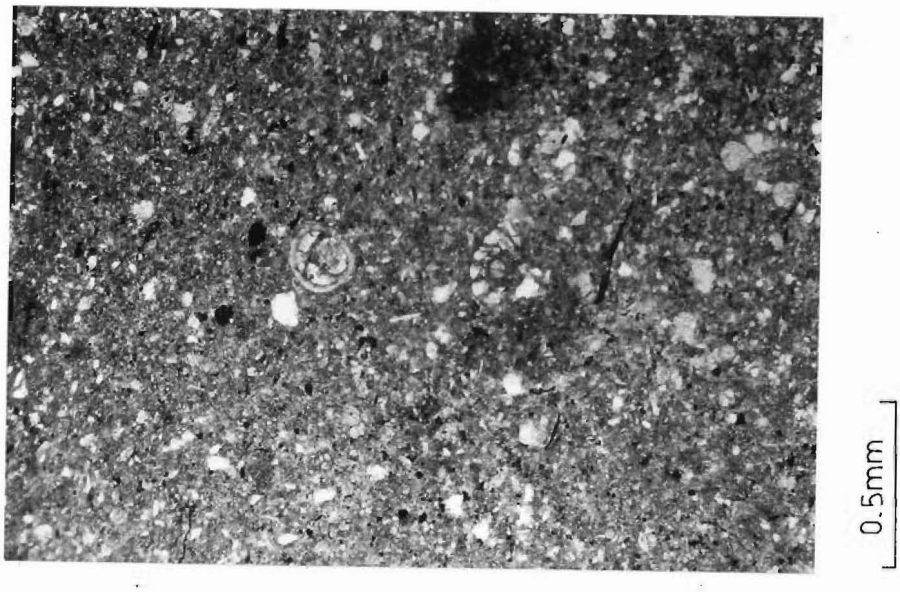

S46 607042

FIG. 119 Two variety of benthonic (centre of photograph) not recognised in silty limestone .

S46 613054

FIG. 120 Amphistegina sp. in foraminifera-rich sandstone .

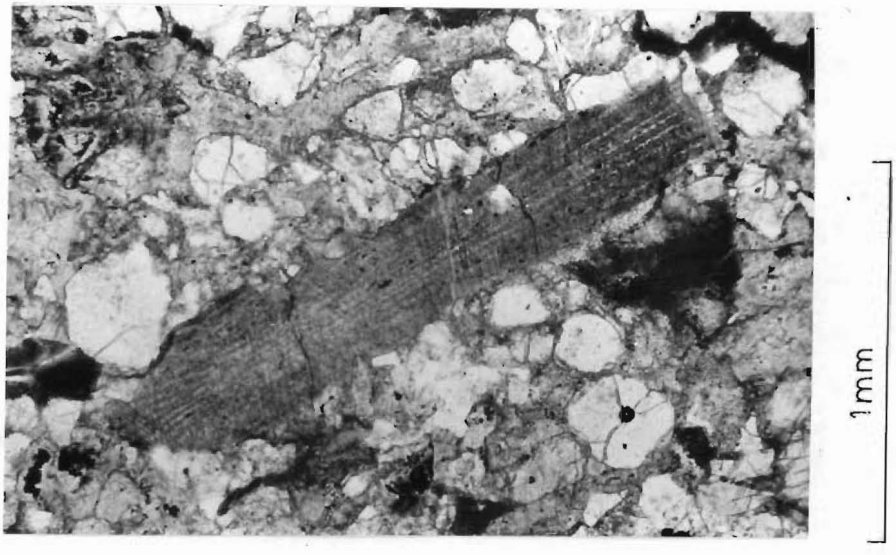

S46 613054

FIG. 121 Echinoid spine in sandstone .

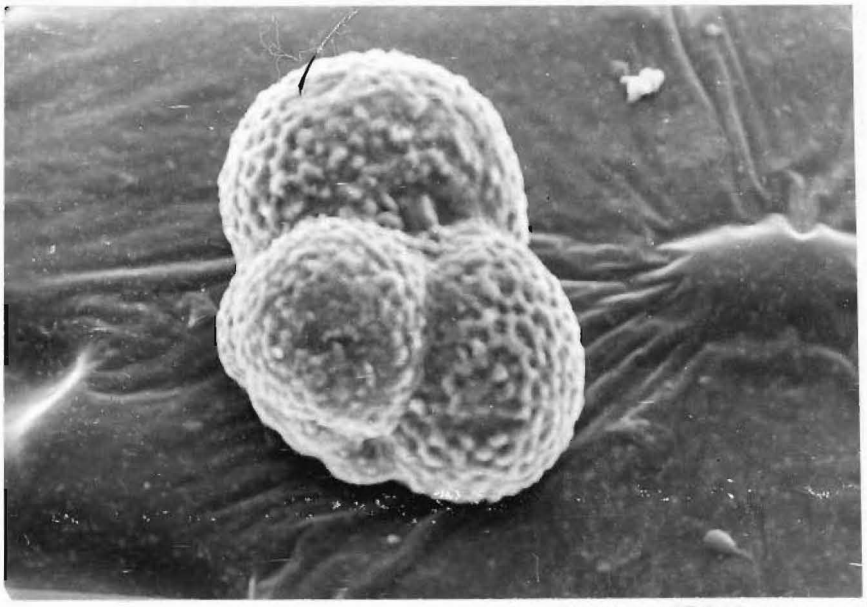

S46 607042

FIG. 122 Scanning electron picture of Globigirina cf euapertu from sample UC 7768a .

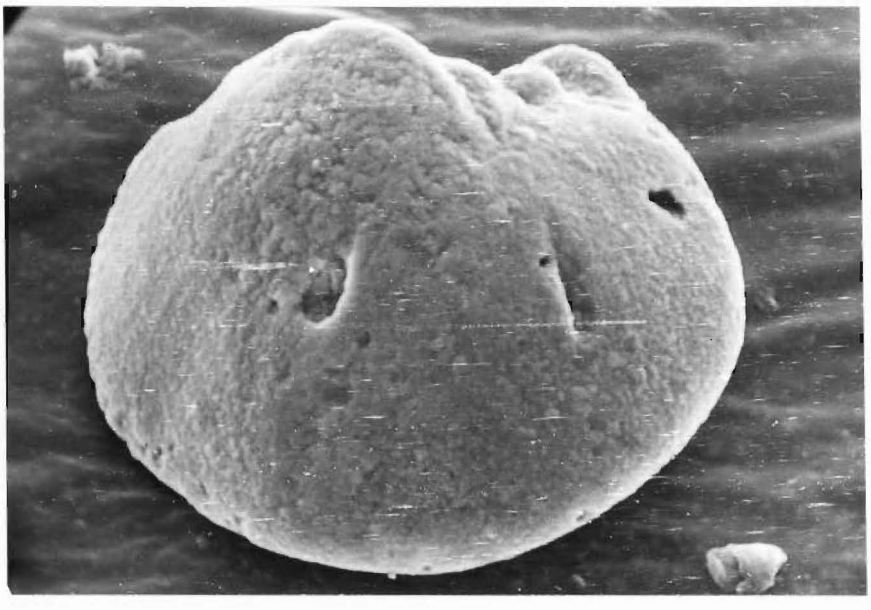

S46 613054

FIG. 123 A unknown organism in sample UC 7814b

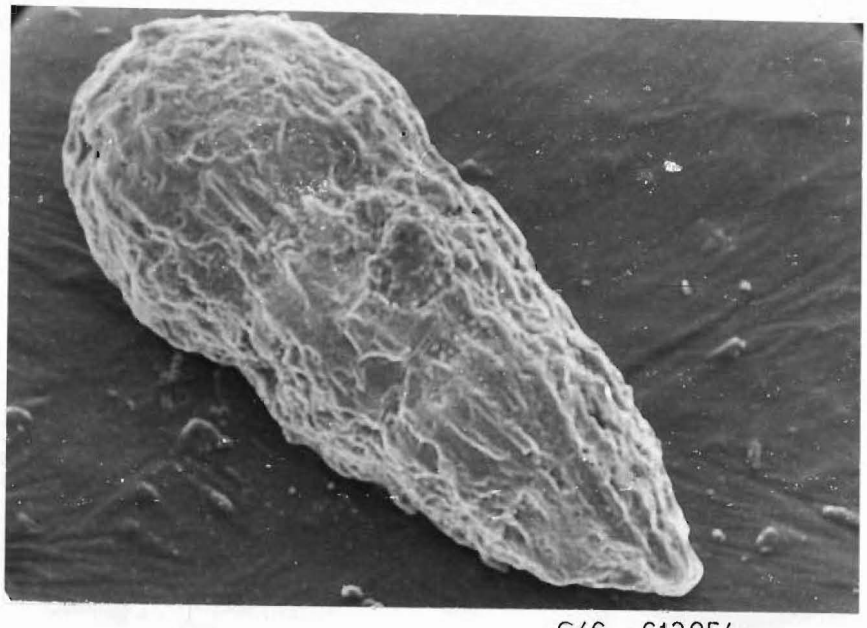

FIG. 124 Scanning electron microscopy picture of Marginulinopsis cf allani from sample UC 7814a

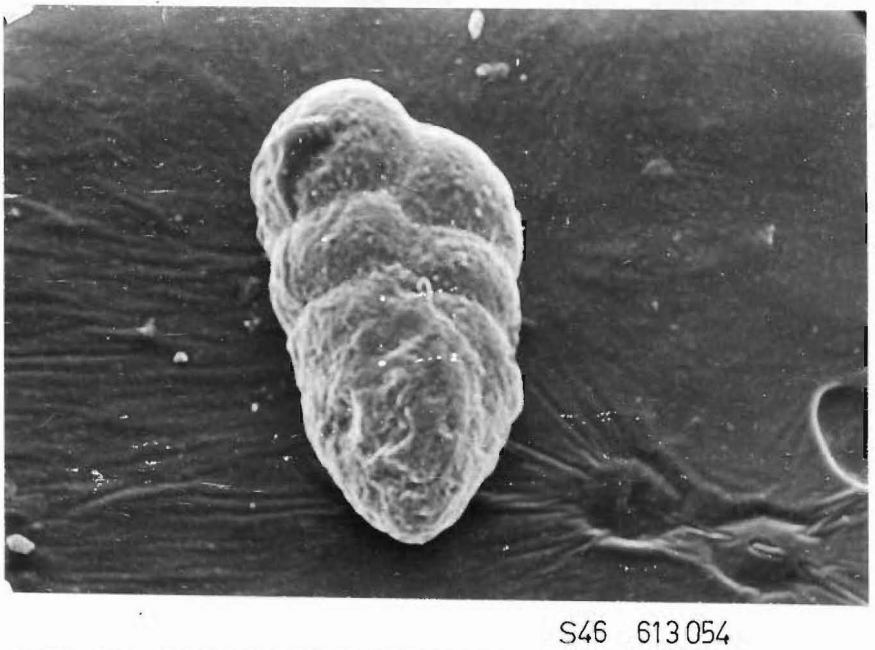

FIG. 125 Scanning electron microscopy picture of Karreriella cf bradyi Cushman from sample UC 7814a .

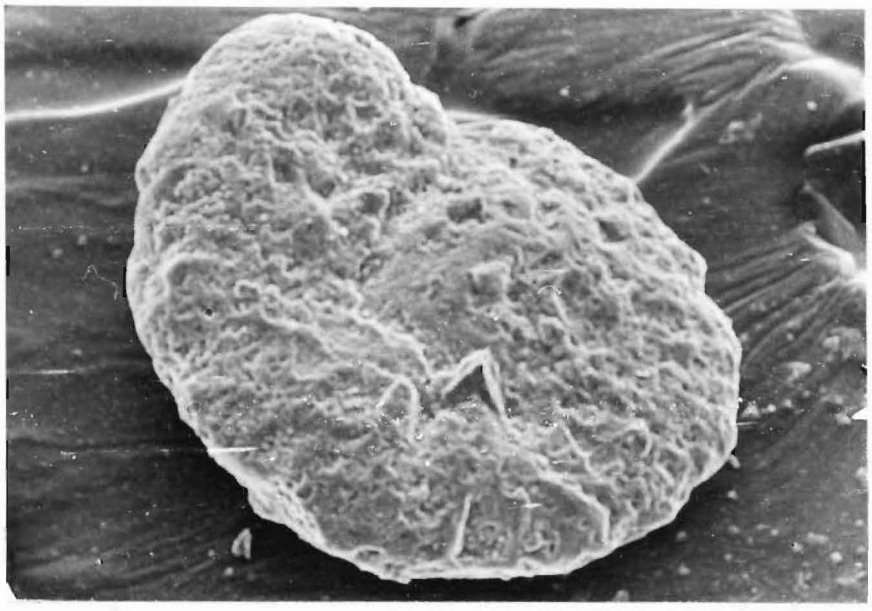

S46 613054

FIG. 126 Scanning electron microscopy picture of Cibicides sp. from sample UC 7814a .

CHAPTER XII

MESOZOIC SEDIMENTS

XII/1 INTRODUCTION

The nearest Mesozoic sediments known on the eastern side of the Victoria Range are those located about 90 km away, near the headwaters of the Wangapeka and Matiri Rivers. These rocks were first reported and correlated with the Hawks Crag Breccia by Fyfe in 1928. The lithologies described are angular and subangular fragments of greywacke, argillite, quartz, and sub-schistose rocks ranging from small sizes up to as much as 1m across, set in a gritty matrix. The mass of these roughly stratified conglomerates is cemented by a ferruginous cement, and interbedded with minor water sorted grit lenses and carbonaceous/coaly layers. The ferruginous cement has imparted a brownish red to purplish colour to the deposits. At the source of the Matiri River, sandstone with carbonaceous shale and impure bituminous coal rests with no marked unconformity on the conglomerate just described, but a conglomerate consisting of angular and subangular greywacke, argillite and quartz pebbles apparently intervenes locally between the earlier conglomerate and the sandstone of the coal measures. The latter conglomerate contains no granite pebbles and is not cemented by a ferruginous cement. This deposit is consi-

dered by Suggate (1968) to be a local facies of the main ferruginous cemented conglomerate.

According to both Fyfe (1928) and Suggate (1968), the Mesozoic conglomerates in the Matiri basin are unconformable to the slightly metamorphosed greywacke and argillite of the Aorere Formation; the surface on which they rest truncates the highly folded basement rocks. On the basis of 1) the stratigraphic position - the conglomerates overlie the Paleozoic basement rocks with a marked unconformity, and occur beneath the early Tertiary sequence, and 2) the peculiar nature and mode of origin of the deposits, the Mesozoic sediments have been correlated with the Hawks Crag Breccia in the Westport and Reefton districts. Suggate (1968) has tentatively assigned a Jurassic age to these conglomerates. This age is now considered to be erroneous because recent investigation of the Hawks Crag Breccia in the Westport and Reefton districts indicates that the conglomerates in the Matin basin if they are related to the Mesozoic deposits on the West Coast are Cretaceous.

Besides being found near the headwaters of the Matiri and Wangapeka Rivers, Mesozoic rocks are present in the Reefton district (25km NW), and Hokitika region (80km SW). The lithologies are summarised in NZ Geological Map (1:250,000) sheets 15 and 17.

XII/2 NOMENCLATURE

Although exposure of Mesozoic sediments in the thesis area is restricted to parts of the Brown Grey,

and Upper Grey Rivers, the sediments have been assigned the status of a formation because of their distinctive lithologies. Its name-the Brown Grey Red Green Formation is derived from a) the Brown Grey River which exposes the major portion of the Mesozoic sequence, and b) the presence of certain conspicuously coloured sandstones and mudstones. The sediments further upstream from the Mesozoic rocks are named the Palmers Formation.

XII/3 LITHOLOGIES - THE BROWN GREY RED GREEN FORMATION

The best section of the Brown Grey Red Green Formation is that along the Middle Brown Grey River. An approximately 180 m thick unit of fine-grained greyish sandstone containing carbonaceous lenses and minor laminated mudstone beds rests unconformably on a basement of biotite or higher grade schist. The bedding attitude of the former near the unconformity is $30^{\circ}/75^{\circ}$ W whereas the latter is 10°-$15^{\circ}/60^{\circ}$ W. The metamorphosed basement is somewhat mylonitic, and contains abundant quartz (30-35%), twinned plagioclase (25-30%), and biotite (30-40%). The schist is faulted against a sliver of granite approximately 20 m below the unconformity.

The sediment which overlies the metamorphosed basement is a layer of carbonaceous mudstone nearly 1.5 m thick whose bedding is intersected at a very low angle by a slaty-cleavage. This rock grades into a dark fine-grained sandstone nearly 3.5 m thick. Thin section

studies of the sandstone reveal that quartz and feldspar detritus is abundant, moderately well sorted, and angular, Biotite flakes occur in small quantities. Volcanics, cherty fragments, microcline, and myrmekite are also present in small amounts. This detritus is generally poorly sorted, and angular. Sericite occupies the matrix of the rock, and partially replaces the pre-existing detritus. In contrast to the basement schist, the sandstone has suffered no metamorphism. The only alteration observed in the rock is that caused by pressure solution or/and reconstitution of the matrix. A thin laminated mudstone overlies the sandstone, and is succeeded by 8 m of fine-grained greyish sandstone. This is overlain by another thin bed of laminated mudstone. Above this layer is a bed of medium-grained sandstone containing carbonaceous veneers which is succeeded by a 5 m thick unit of monotonous greyish fine-grained sandstone. The overlying carbonaceous lense 0.5 m thick contains numerous fragments of the plant fossil Equisetites sp. Higher up the stratigraphic column, the sequence is composed of monotonous grey sandstone occasionally interbedded with thin mudstone layers. Although the sedimentary contact between this sequence and the base of the red sandstone is not observed in the field, it may be assumed to be conformable because there is no evidence of faulting in the area where the contact is concealed.

The overlying red sandstone is medium- to coarse-grained, and occasionally conglomeratic towards the upper portion of the unit. Thin mudstone beds also

occur near the top of the red sandstone. Thin section examination shows that the detritus- chiefly feldspars, is angular and poorly sorted. The other components, quartz, volcanics, and cherty fragments also display a similar texture. Point-counting of the clasts in specimen UC 7662a reveals a modal composition of 60-70% feldspars, 10% quartz, and 25-35% rock fragments. The relatively high content of andesine and volcanic detritus suggests that the main source rock of the red sandstone is volcanic. Clastic contribution from pre-existing igneous and sedimentary/metamorphic rocks is indicated by the presence of myrmekite, microcline, and cherty fragments. The writer found that except for the similarity in clastic texture and cement material, the red sandstone here is different from that near Mt. Graham; the latter is generally quartzose. The membership of the red sandstone in the Brown Grey Red Green Formation to the Hawks Crag Breccia is not precluded by such mineralogical differences.

Towards the top of the Mesozoic sequence, the medium-grained red sandstone grades into finer-grained, greenish, faintly laminated sediments. X-Ray Diffraction analysis, and thin section studies show that the green colour is entirely due to the presence of fine-grained chlorite. The green mudstone is succeeded by green medium-grained sandstone. The rock is less abundant in feldspars and rock fragments, particularly volcanics. The detritus remain poorly sorted and angular like those in the underlying red sandstone. The coarse- to medium-grained, grey

sandstone above the green sandstone contains a thick 'coaly' lense. X-Ray Diffraction analysis of the material reveals the presence of feldspars, quartz, biotite, muscovite, and chlorite. Ignition lost determination shows a 51% reduction of dry weight of the 'coaly'matter. The high electrical conductivity of this material, together with the positive reaction of the carbon test suggest that the 'coaly' matter is predominantly graphitic mudstone.

Slaty-cleavage is developed nearly parallel to bedding in the green mudstone. A second set of finely spaced cleavages intersects the slaty-cleavage at a moderate angle. The attitude of bedding in the red sandstone, and green sandstone and mudstone is about $38^{\circ}/45^{\circ}$ W. This is somewhat different from that observed in the grey sandstone near the unconformity. The younging direction inferred from occasional cross-beddings in the red sandstone is towards the west which is consistent with that indicated by the unconformity. The presence of epidote-clinozoisite in the red and green beds indicates that the rocks have undergone very low grade metamorphism. The effects of pressure-solution and sericitization are widespread. They enhanced the angularity of the clasts in the rocks.

XII/4 LITHOLOGIES - PALMER'S FORMATION

The relationship of the red and green beds to the sediments exposed further up the Brown Grey River is not clearly understood because of the lack of outcrops.

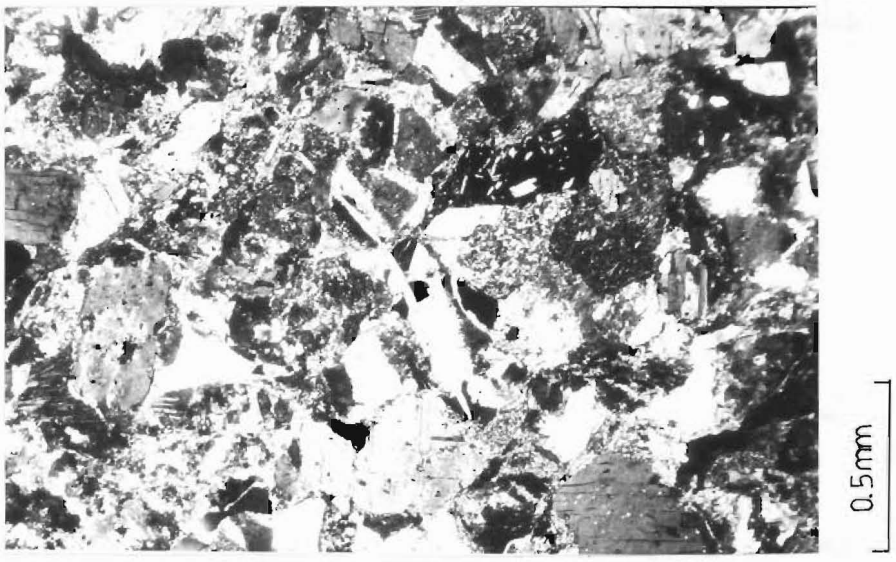

S46 549963

FIG. 127 Photograph showing volcanic & cherty fragments, and the effect of pressure solution . The former is located in the NE quadrant of the picture . The latter is best seen in the SW quadrant of the picture (Note the angular piece of quartz) . The above is a picture of UC 7662a .

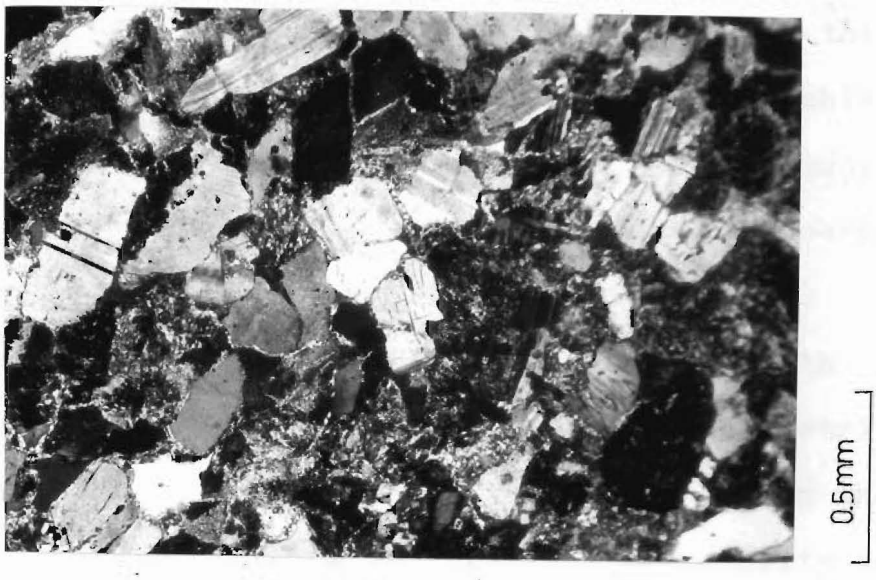

S46 549963

FIG. 128 Effect of pressure solution in specimen UC 7662a . Note the interpenetrating grain boundaries in the centre of the photograph . The solution of quartz and feldspar detrital grains along the grain margin affects (may enhance)the angularity and sorting of detritus in UC 7662a .

However, on the basis of a) change of induration, b) development of lineation and schistosity in the rocks "above" the red and green beds, and c) different mineralogical content i. e. greater abundance of microcline and perthite in the exposed sediments upstream from the red and green beds, the writer has proposed a fault contact between the two groups of sediment (see Map).

Above the proposed fault, the mudstone is grey-black, pyritic, laminated, and intersected at a low angle to bedding by a slaty-cleavage. This is succeeded by a zone of well indurated sandstone which is locally intervened by thinly bedded laminated mudstone and conglomeratic layers. The latter is composed of poorly sorted, subangular, siliceous or/and greywacke fragments ranging from pebble- to granule-size. At the top of this zone, large angular mud clasts whose texture reflect subsequent plastic deformation are present. Above these mud clasts, the rock is well indurated, slightly schistose, medium-grained, and grey coloured. Thin section studies show that the detritus is predominantly angular, poorly sorted, and set in a fine-grained micaceous matrix. Microcline and perthite are abundant. Together with quartz and volcanic fragments they form the main detrital minerals in the grey sandstone. The white micas in the matrix are aligned, forming an incipient schistosity in the rock. The schistosity and the presence of epidote-clinozoisite indicate that the sediments here have suffered low grade metamorphism. The well preserved clastic texture supports this suggestion.

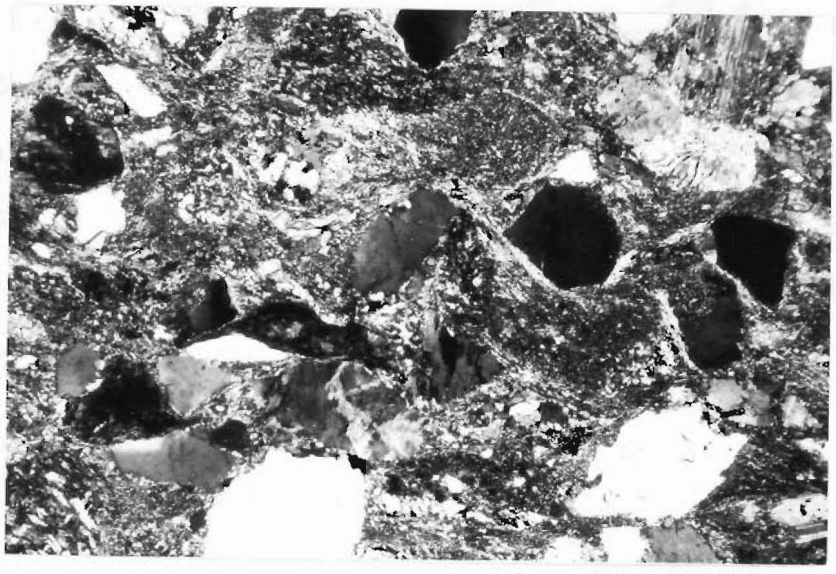

S46 549963

FIG. 129 Picture showing mymerkite and perthite fragments in the sandstone of the Palmer's Formation . The former is in the top NE quadrant of the picture . The latter is in the centre of the photograph . Note the development of'schistosity'.

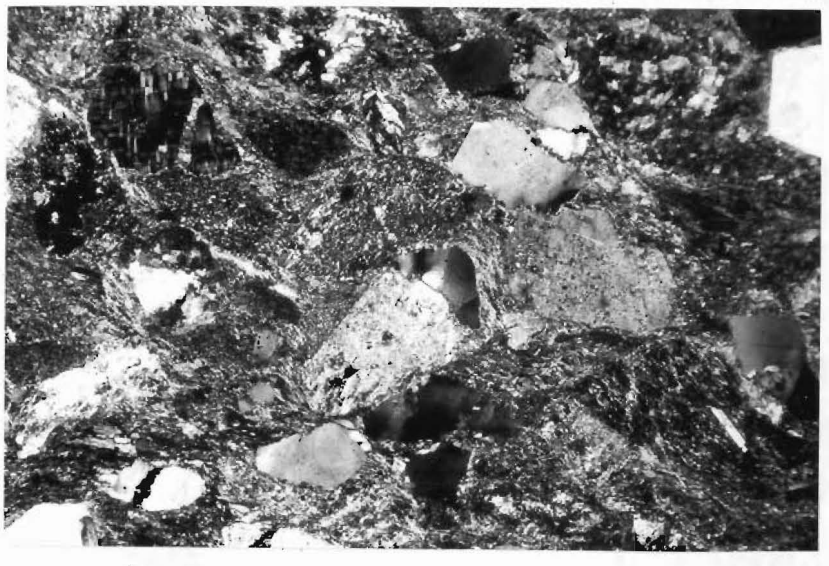

S46 549963

FIG. 130 Microcline, cherty, & perthite fragments in the NW quadrant of the picture . Also note the effect of pressure-solution . Volcanic fragment in the SE quadrant .

The mesozoic sequence observed in the Upper Grey River, 2 km SE of Trig. A is not as comprehensive as that in the Brown Grey River. The unconformity is not seen here because the red and green beds are faulted against the granites on the eastern side. Above the green sandstones, are meta-sediments. Like on the eastern side, these rocks are faulted against each other.

XII/5 AGE AND CORRELATION

Specimens of Equisetites sp. were collected from about 20 m above the unconformity. These large stemmed plants, according to D. C. Mildenhall (pers. com.) are apparently restricted to the Carboniferous-Jurassic time in New Zealand; the lower age range is based on the fact that Equisetites first appeared in abundance in the Carboniferous period and the upper age range is based on the observation that the only Equisetites previously recognised in New Zealand were from Jurassic rocks, and were small stemmed plants.

Although the Brown Grey Red Green Formation is in the appropriate stratigraphic position i. e. resting unconformably on a metamorphosed basement, and lithologically similar to the Hawks Crag Breccia (currently established as Cretaceous age), its age range precludes membership in the Pororari Group. The possibility of the Brown Grey Red Green Formation being a sliver of fault emplaced Maitai Group rocks like the Permian sediments in the Upper Matakitaki district, suggested

by the nearness of the 'bend' of the Alpine Fault together with the similarities in lithologies and rock composition (see table below), is ruled out by the fact that Maitai Group deposits do not rest unconformably over a feldsparthic schist basement.

MAITAI GROUP COMPOSITION	Quartz	Feldspar	Rock Fragments
UC 7375	3%	40%	57%
A1	0%	20%	80%
A2	5%	26%	69%
A3	20%	20%	60%
Red Sandstone from the Brown Grey Red Green Formation (UC 7662a)	10%	65%	25%

The data from the Maitai sediments were obtained from H. Cutten's (1976) M. Sc. thesis. Note the characteristic low quartz, and high feldspar and rock fragment contents in the Maitai deposits, and their similarity to the Red Bed's composition.

This leaves the Parapara Group of NW Nelson as a possible correlative. However, the lithologies in the Brown Grey Red Green Formation are dissimilar to those in the Parapara Group. Clearly more research is required, particularly in palynology for the Mesozoic sediments in the thesis area, and in the Matiri basin, previously investigated by Fyfe (1928-1929) and Suggate (1968).

Positive correlation and dating of the sediments below the unconformity are not possible because of the absence of fossils. However, as the Pikikiruna Schist in the thesis area and NW Nelson region are feldspar-impoverished, and that the schist below the unconformity are feldspathic, it is conceivable that the metamorphosed sediments below the Brown Grey Red Green Formation are members of the Aorere Group, especially that sediments in Cooper's (1975) Western Belt are known to be feldspathic.

The age and correlation of the low grade meta-sediments exposed further up stream from the Brown Grey Red Green Formation are not known. There is no conclusive evidence against or for their inclusion in the Aorere Group. All that is known is that they are unfossiliferous and more metamorphosed than the Mesozoic sequence downstream.

Top not recognised.

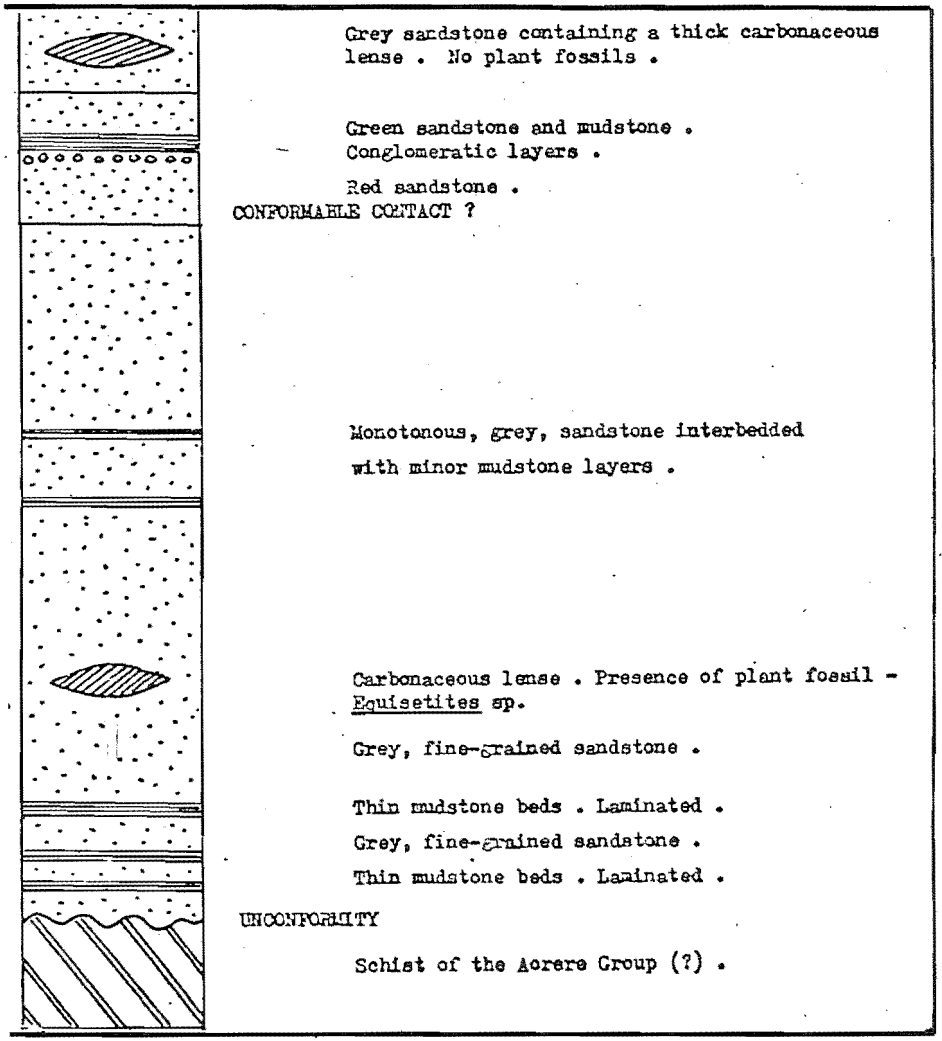

Bottom not recognised.

Top not recognised.

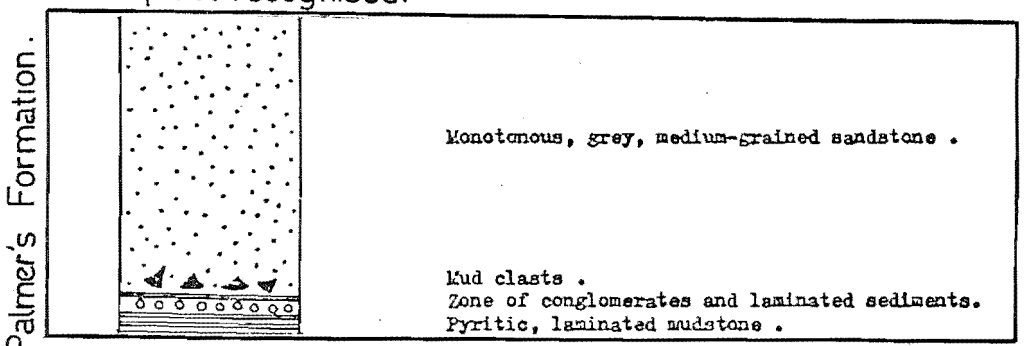

Bottom not recognised.

FIG.131 Section in the Brown Grey River.

CHAPTER XIII

SUMMARY OF CONCLUSIONS OF THE GEOLOGICAL HISTORY PRESENTED IN CHRONOLOGICAL ORDER

The writer wiches to draw the attention of the reader to the fact that the arguments for the conclusions in this section of the thesis have been presented more fully in the preceding chapters, and that queries on any particular point should be referred to the appropriate section(s).

The Lower Paleozoic period and the pre-Tuhua Orogeny

The Victoria Range Flysh-like, unfossiliferous sediments were laid down in a trough east of the Pre-Cambrian continent during the Cambrian-Ordovician period. Volcanics and unfossiliferous volcanogenic sediments of the Koura Formation were also deposited at the same time but considered to be in the area further east - in the vicinity of the seaward slope of the trough. When sedimentation ceased at the close of the Ordovician period, this belt of sediments i. e. the Victoria Range deposits plus the Koura volcanics and volcanogenic sediments was deformed and regionally metamorphosed whilst the eastern periphery of the Pre-Cambrian continent experienced low-pressure granite activity. Mineralogical development in the rocks of the Koura Formation indicates that the P-T conditions experienced by the volcanics and volcano-

genic sediments were 350° to 450° C, and perhaps moderate or high pressure. The fossil median boundary which separates the low-pressure metamorphism in the continent and the higher-pressure metamorphism in the trough sediments is located west of the thesis area.

The Lower Paleozoic period and the Tuhua Orogeny

In the areas further east of the depositional environment described in the preceeding section, the sediments considered to be Cambrian age were laid down in thin sequences on the ocean floor. Just after sedimentation ceased in the trough adjacent to the Pre-Cambrian continent, a thick, slightly fossiliferous deposit comprising predominently of mudstone and limestone accumulated above the veneer of Cambrian sediments, forming another belt of sedimentary rocks. Deposition in this second trough north of the thesis area in NW Nelson district continued to the end of Silurian or begining of Devonian times. The distinct and contrasting depositional environments in the two troughs are reflected in their lithological and mineralogical contents. As mentioned previously, the lithologies in the second trough are predominently feldspar-impoverished mudstone/sandstone and limestone whereas the rock-types in the trough adjacent to the Pre-Cambrian continent are mainly felspathic sandstone and minor mudstone. Furthermore, the latter sediments are unfossiliferous.

The sediments in the second belt were regionally deformed and metamorphosed at temperatures varying from 350° to 640° C, and pressures not less than 4 to 6 kb during the Tuhua Orogeny. So far as is known, three orders of folds were generated during this orogeny; a) a major NE-trending and gently plunging, inclined anticline, b) mesoscopic folds whose attitudes are similar to that of the major anticline, and c) microscopic crenulations whose axial planes are oriented parallel to the axial plane of the major anticline. To the west, the Victoria Range sediments in the earliest developed trough were intruded and thermally metamorphosed by the Tuhuan Granites at temperatures ranging from 400° to 550° C, and pressures not exceeding 2 to 3 kb. Unlike the higher-pressure metamorphism to the east, this thermal metamorphism was not accompanied by large scale folding.
The Tuhuan median boundary which separates the low- and higher-pressure metamorphisms is located east of the pre-Tuhuan median boundary. In the thesis area, the Tuhuan median boundary developed into a major fracture system known as the Koura Fault. The Koura volcanics and volcanogenic sediments together with with the Thompson's Flat, Sluice Box, and Alfred Formations, and the Victoria Range rocks were juxtaposed by movement(s) of this major fracture soon after the Tuhuan intrusive event. The side which contains the feldspar-impoverished mudstone/sandstone and limestone was upthrown. The Victoria Range meta-sediments and less commonly, the sediments of the Thompson's Flat and Alfred Formations bordering

the Koura Fault were folded about a steeply plunging or vertical axis during lateral displacement(s) of the major fracture system. The deformed Victoria Range meta-sediments were subsequently refolded about a gently plunging or horizontal axis. The timing of this episode of folding is not clearly understood.

The Mesozoic period

The tectonically uplifted rocks of the Victoria Range, Thompson's Flat, Sluice Box, Alfred, and Koura Formations were eroded (the extent of erosion is not clearly understood) and shallow water basins were formed. Non-fossiliferous fine- to coarse-grained sediments containing plant fossils (*Equisetites* sp.) and organic matters were deposited in these shallow depressions. The sediments of the younger Mesozoic sequence were derived from a nearby volcanic terrain.

The Rangitata Orogeny

The Lower Paleozoic sediments of the Thompson's Flat, Sluice Box and Alfred Formations were thermally metamorphosed by granites during the Rangitata Orogeny. This intrusive event is thought to have caused microscopic folding of one limb of the microscopic crenulations generated during the Tuhua Orogeny. The mineral assemblages associated with this thermal metamorphism indicate that the P-T conditions were 500° to 580° C, and 1.5 to 2.5 kb.

The rocks in the Victoria Range west of Springs Junction were also affected by the Rangitatan Granites. So far as is known, the metamorphism was not significant. Whilst the rocks in Springs Junction district were affected by low-pressure granite activity, the Torlesse Group and Hokonui facies sediments to the east were regionally metamorphosed by higher-pressure metamorphism. The Rangitatan median boundary, presently occupied by the Alpine Fault is located along the eastern margin of the thesis area.

The pre-existing Koura Fault was activated during the Rangitata Orogeny. A sliver of biotite schist was dextrally displaced from the vicinity of Palmer's Bend. Although it has not been positively established, the writer considers that the Rahu Fault was initiated during this orogeny. A wedge of Mesozoic sediments was sinistrally displaced by this major fracture.

The early Tertiary period

The Tertiary marine basin was extensive, occupying the complete length of the present Murchison-Springs Junction depression. Sediments derived predominently from the surrounding granite terrain were deposited. The shallow sedimentary environment was tropical/subtropical which supported abundant fauna, particularly foraminifera.

The Kaikoura Orogeny

H. Cutten (1976, unpublished M. Sc. thesis) has reported the occurence of zig-zag en echelon folds in the Tertiary sediments north of the thesis area as caused by movement(s) along the Alpine Fault. The two major synclinal axes are oriented north-south. Although not folded in the same fold style, the writer considers that the last episode of folding in the Thompson's Flat, Sluice Box, and Alfred Formations which is also north-south trending, was related to movement(s) along the Alpine Fault.

The Rahu Fault was activated during the Kaikoura Orogeny. Movement(s) along this major fracture displaced the early Tertiary rocks in the areas west of Springs Junction.

COMMENTS

It is worthwhile to note that the inferred geological history will be invalidated in the event of the discovery of a thick sequence of Cambrian sediments near the median axis of Cooper's (1975) Eastern Belt or finding Tuhuan Granites in the region east of Shelley's (1975) proposed Tuhuan median boundary. As both authors' models cannot be presently put to the test, the inferred geological history is regarded as tentative. It is the writer's hope that detailed investigation of the base of the Eastern Belt, and the granites east of the proposed median boundaries in Westland, Buller, and NW Nelson will be carried out by geologists in the future.

ACKNOWLEDGEMENTS

I should like to thank the following people who have provided invaluable assistance during the course of this study.

My parents who financed this research.

The Conservator of Forests (Nelson) for accomodation in the field.

Dr. D. Shelley, supervisor, for helpful discussions, suggestions, and critically reading the manuscript.

Mrs. J. K. Campbell, for discussions on structures and stereo-analyses.

Rosemary Bowell, for assistance in the field and laboratory as well as help with photography.

The people of Springs Junction, for their friendship and hospitality. Special thanks to Eric Timpson.

The staff members of the Geology Dept. and New Zealand Geological Survey, for discussions, and access to published and unpublished reports.

Mr. K. Swanson and Mr. A. Downing for advise and assistance concerning photography.

D. C. Mildenhall, for identification of plant fossils.

Dr. R. A. Cooper, for information on the recent discovery of agnostids in Upper Station Creek.

Dr. G. W. Grindley, for directing me to Dr. Adams for some unpublished radiometric data on the Brown Grey Schist.

Prof. Coombs of Otago University, for access to the microprobe analyser.

Special acknowledgement to M. Shelley for assistance in X-Ray analyses, and Dr. Y. Kawachi and 'Oli Pom' for advise and help in microprobe analyses.

N. Newman, A. Burgess, and H. Cutten for numerous discussions.

Sally German, for kindly typing this manuscript.

S. Duff and Dr. N. de B. Hornibrook for assistance in Tertiary Foraminifera identification.

APPENDIX 1

MICROPROBE-ANALYSIS

Equipment: JXA-A5 microprobe analyser (Japanese made)

Acceleration potential: 15 kV

Specimen current: 1.5×10^{-8} amp.

No. of Spectrometers in used: 3

Number of elements analysed: 7

Standards used: Haematite (Fe), Quartz (Si), Corundum (Al), Periclase (Mg), Wollastonite (Ca or Si), Rutile (Ti), Manganese oxide (Mn)

Number of specimens analysed: 5 garnet crystals from the schist at locality B1.

Procedure: Three of the five crystals were used for complete chemical analysis. For each of these garnets, a total of 15 to 20 spots were analysed at the core, the boundary between the inclusion-rich and inclusion-poor garnets, and the edge of the crystal. For the other two garnets, two traverses analysing for the same set of elements were carried out on each grain. The analysed spots were at 0.04 mm interval. Because ferric and ferrous iron cannot be distinguished and the amount of water cannot be determined by this method of analysis, the microprobe analyses in these respects are less satisfactory than the wet chemical analyses. In a few cases, the total % of the 7 elements slightly exceed 100%. This is partly due to slightly analytical error.

APPENDIX 2

CORRECTION FACTOR FOR XRF AND AA ANALYSES

Because the analysed garnet contains numerous quartz and to a lesser extent, opaque inclusions, a correction factor for the real weight of garnet was required. The correction factor was determined as follows.

1) 1 gm of garnet crystals was finely ground.

2) The powdered mineral was transferred into a test tube containing TBE whose s. g. is 2.9 at room temperature.

3) Because the s. g. of quartz is less than 2.9, the majority of the quartz inclusions were afloat. The TBE containing the powdered garnet was stirred carefully, and the resultant liquid-solid mixture was centrifuged at about 2,000 rpm for 10 minutes.

4) The tip of the tube containing 'purer' garnets was carefully dipped into liquid air.

5) The remaining liquid containing quartz was decanted into a filter funnel lined with No. 5 porosity filter paper.

6) The separated garnet and quartz grains were thoroughly washed with acetone, and dried.

7) The two portions were then carefully weighed, and their total weight was checked against the original weight of the garnet crystals to determine the amount of mineral lost during the process of separation of inclusions from garnets.

8) The separation was repeated.

The amount of quartz in 1 gram of garnet was about 3.0 to 3.2% by weight. This is surprisingly lower than the figure estimated from thin section studies. It is conceivable that 3.0 to 3.2% of quartz in garnet are conservative weights because a considerable amount of quartz in the prepared sample may have occurred as quartz-garnet fragments, and these would remain at the bottom of the test tube.

BIBLIOGRAPHY

Albee, A. L. Relationships between the mineral association chemical composition and physical properties of the chlorite series. American Mineralogist V. 47, 1962: 851-870.

Althaus, E. See Winkler 1974, p. 93. (1967, 1969a, 1969b).

Anderson, E. M. See Ramsay 1967, p. 338. (1951).

Aronson, J. L. The geochronology of the plutonic and metamorphic rocks of New Zealand. Geochem. et. Cosmochem. Acta 32 (7), 1968: 669-697.

Brathwaite, R. L. The geology of Boulder Lake Area, NW-Nelson. Part 1 - The Anatoki Formation. NZJGG V. 11, No. 3, 1968: 78-91.

Brown, E. J. Some zoned garnets from the greenschist facies. American Mineralogist V. 54, 1969: 1662-1677.

Bowen, F. E. Sheet 15 - Buller. 1st edition, 1964.

Chinnery, M. A. Secondary faults - theoretical aspect. Canadian Journal of earth science, V. 3, 1966a: 163-174.

_____. Secondary faults - geological aspect. Canadian Journal of earth science, V. 3, 1966b: 175 190.

Cooper, R. A. New Zealand and south-east Australia in the early Paleozoic. NZJGG V. 17, 1975: 955-962.

Cox, S. H. Report of geological exploration in the district between the Maruia and Buller Rivers. Report Geological Exploration V. 16, 1883.

Deer, W. A., R. A. Howie, and J. Zussman. Rock-forming minerals. 4th. ed. Longmans, Green and Co. Ltd., 1965.

Eugster, H. P. and D. R. Wones. Stability relations of the ferruginous biotite, annite. Jour. of Petrology V. 3, No. 1, 1962: 82-125.

_____. Stability of biotite: experiment, theory, and application. American Mineralogist V.50, No. 9, 1965: 1228-1272.

Farmer, R. T. Stratigraphy & structure of palaeozoic rocks near Springs Junction SW-Nelson. Unpublished thesis, M. Sc., University of Canterbury, 1967.

Fyfe, H. E. Maruia Subdivision. NZGS Annual Report, No. 23, 1929.

_____. Murchison and Maruia Subdivisions. NZGS Annual Report, No. 24, 1930.

_____. Unpublished maps to accompany NZGS Bulletin, No. 36, 1935.

Fyfe, H. E. and R. P. Suggate. Geology of Murchison subdivision. NZGS Bulletin, No. 36, 1968.

Ghent, E. D. See Trans. R. Soc. N. Z. Geol., 5, 1968: 193-213.

Grindley, G. W. NZGS Sheet S8 Takaka, 1971.

Haast, J. Report of topographic and geological exploration of the Western District of the Nelson Province. C&G Elliott Printers, 1861.

Harker, A. Metamorphism: A study of the transformations of rock-masses. London, Methuen, 1932.

Hollister, L. S. Garnet zoning: an interpretation based on the Rayleigh fractionation model. Science V. 154, 1966; 1647-1651.

Hornibrook, N. de B. A handbook of New Zealand micro-fossils (Foraminifera and Ostracoda). NZDSIR publication, 1968.

Hsu, L. C. Selected phase relationships in the system Al-Mn-Fe-Si-O; a model for garnet equilibria. Jour. of Petrology V. 9, 1968: 40-83.

Jenkins, R. and J. L. de Vries. Worked examples in X-Ray spectrometry. Philips Technical Library, 1970.

Kerr, P. F. Optical mineralogy. 3d. ed. McGraw Hill Book Company, 1959.

Kretz, R. Grain size distribution for certain metamorphic minerals in relation to nucleation and growth. J. Geol. 74, 1966: 147-173.

_____. Some models for the rate of crystallization of garnet in metamorphic rocks. Lithos V. 7, No. 3, 1974: 123-131.

Laird, M. G. Note on a major fault along the lower reaches of the Rahu River. NZGS Intermediate Report S46/ir6, 1964.

Mackay, A. Report on the geology of the SW part of Nelson and the Northern part of Westland. Reprints of Mine Reports 1865, 1896. 2d. ed., 1897.

Miyashiro, A. Calcium-poor garnet in relation to metamorphism. Geochim. Cosmochim. Acta 4, 1953: 179-208.

Miyashiro, A. and F. Shido. Progressive compositional change of garnet in metapelite. Lithos 6, 1973:, 13-20.

Nathan, S. and J. Foster. Road section west of the Rahu Saddle. NZGS Intermediate Report S46/ir5, 1968.

Phleger, F. B. Ecology and distribution of recent Foraminifera, 1952.

Ragan, D. M. Structural Geology. 2d. ed. John Wiley and Sons, 1973.

Ramsay, J. G. Folding and fracturing of rocks. McGraw Hill, 1967.

Reed, J. J. Mylonites, cataclasites and associated rocks along the Alpine Fault, South Island, N. Z. NZJGG 7, 1964: 645-684.

Richardson, S. W., et. al. See Winkler 1974, p. 94 (1968, 1969).

Saxena, S. K. Distribution of elements between co-existing minerals and the nature of solid solution in garnet. American Mineralogist V. 53, 1968: 994-1014.

Skinner. Refer Sturt 1962. (1956).

Smith, J. V. Feldspar minerals, Vol. 1. Springer-Verlag-Berlin-Heidelberg-New York, 1974, P. 224-246.

Snelling, N. J. Notes on the petrology and mineralogy of the Barrovian metamorphic zones. Geol. Mag., V. 94, 1957: 297.

Shelley, D. Metamorphic belt and volcanic arc migration in New Zealand. Nature V. 258, 1975: 668-672.

Spry, A. Metamorphic textures. Pergamon Press. 1969.

Spiradamus. Refer Sturt 1962. (1958).

Sturt, B. A. The composition of garnets from pelitic schists in relation to the grade of regional metamorphism. Jour. of Petrology V 3, 1962: 181-191.

Suggate, R. P. Examination of the geology in the Upper Grey Valley. NZGS Intermediate Report S46/ir4, 1959.

_____. Geological reconaissance in the Springs Junction District. NZGS Intermediate Report., 1959.

Suggate, R. P. and N. T. Moar, Crooked Mary Bog, Palmers Road. NZGS Intermediate Report, 1960-1966.

Suggate, R. P., H. S. Gair and D. R. Gregg. The Sw extension of the Awatere Fault. NZJGG 4, 1961: 264-269.

Suggate, R. P. The late Pleistocene geology of the northern part of the South Island of New Zealand. NZGS Bull., no. 77, 1965.

Turner, F. J. Metamorphic petrology. McGraw-Hill Book Company, 1968.

Wallace. Metamorphism of the Alpine Schist, Mataketake Range, South Westland, N. Z. NZJGG V 4, No. 3, 1974: 253-266.

Wellman, H. W. Special Examination. NZGS Annual Report, no. 35, 1941.

_____. Talc-magnesite and quartz-magnesite rocks, Cob Takaka District. NZJST 24 (3B,), 1942: 103B-127B.

_____. Talc in NW nelson and Northern Westland. NZJST 24 (5B), 1943: 227B-235B.

_____. Paleozoic in the outline of the geology of New Zealand. NZGS publication, 1948.

_____. The Alpine Fault in detail; river terrace displacement at Maruia River. NZJST 33 (5), 1952: 409-414.

_____. New graptolite localities in New Zealand. NZJGG 5, 1962: 642-645.

Winchell. Refer Sturt 1962. (1958).

Winkler, H. G. F. Petrogenesis of metamorphic rocks. Revised 2d. ed. Springer-Verlag New York Inc. 1967.

Winkler, H. G. F. and A. Hirschberg. See Contribution Mineral. Petrol. V. 18, 1968: 17-42.

Winkler, H. G. F. Petrogenesis of metamorphic rocks. Revised 3d. ed. Springer-Verlag Berlin., Heidelberg, New York. 1974.

Wodzicki, A. See NZJGG V. 17, 1974: 747-757.